SPATIALLY REGULATED β-ACTIN TRANSLATION IN EPITHELIA: ANALYSIS OF ADHERENS JUNCTION ASSEMBLY, MEMBRANE CYTOSKELETAL DYNAMICS AND TISSUE FUNCTION

By

PAVAN VEDULA

A Dissertation submitted to the

Graduate School-Newark

Rutgers, The State University of New Jersey

in partial fulfillment of the requirements

for the degree of

Doctor of Philosophy

in Biology

written under the direction of

Alexis J. Rodriguez

and approved by

_____

_____

_____

_____

_____

Newark, New Jersey

May, 2016

ABSTRACT OF THE DISSERTATION

SPATIALLY REGULATED β-ACTIN TRANSLATION IN EPITHELIA: ANALYSIS OF ADHERENS JUNCTION ASSEMBLY, MEMBRANE CYTOSKELETAL DYNAMICS AND TISSUE FUNCTION

By PAVAN VEDULA

Dissertation Director:

Alexis J. Rodriguez

The β-actin mRNA contains a 28 nucleotide sequence in the 3′UTR termed the zipcode which, along with a *trans* acting factor called the Zipcode Binding Protein-1 (ZBP-1/IMP-1), regulates the spatio-temporal expression pattern of the β-actin. This mode of post-transcriptional gene regulation is required for several cellular processes including cell migration, cell-cell adhesion, and cell-matrix adhesion. Adding to the list of signaling cascades such as RhoA and Src, work in this thesis demonstrates E-cadherin endocytosis, and plausibly gene expression pathways regulating cell proliferation, converge on spatially regulated β-actin translation. E-cadherin endocytosis and recycling has been shown to be important during the maintenance of epithelial adherens junctions. However in this thesis, endocytosis of E-cadherin is shown to negatively regulate adherens junction assembly, while spatially regulated β-actin translation balances this by promoting actin filament anchoring of cadherin complexes. Mislocalization of β-actin translation impairs adherens junction maturation in epithelial cells following *de novo* cell-cell contact. These

results have implications in development and disease where the assembly and maintenance of epithelial adherens junctions is essential. In order to quantify the extent of adherens junction assembly defects in epithelial cells following *de novo* contact, a Fluorescence Covariance Index based on calculating Pearson's Correlation Coefficients was developed and validated using several components of the adherens junction complex. In addition to quantitating the morphological effects of mislocalizing β-actin translation on adherens junctions, the FCI analysis showed correlation of these morphological defects with loss of epithelial barrier function. Lastly, inhibiting dynamin mediated endocytosis rescued adherens junction structure and epithelial barrier function in cells with partially mislocalized β-actin. Using Matrigel embedded 3D cyst cultures of MDCK cells, spatially regulated β-actin translation was shown to have an effect on cell shape, size and proliferation during epithelial morphogenesis. These defects in assembling a normal 3D epithelium along with disorganized acto-myosin and tight junctions, point to a role for compartmentalized β-actin translation in regulating a mechanosensitive module – plausibly Hippo and/or YAP/TAZ pathways. Finally, collective cell migration, an important paradigm in several biological processes such as wound repair and development, was used to determine the role of spatially regulated β-actin translation in epithelial wound repair. Spatially regulated β-actin translation is shown to regulate actin flux at cell-cell adhesions in leader-follower cell pairs to control tissue migration rates. Although cells with partially mislocalized β-actin translation have a more active leading edge, this increased protrusive activity fails to translate into increased migratory rate. These data taken together suggest that collective cell migration in epithelial sheets is an emergent property of both single cell dynamics and cell-cell interactions.

PREFACE

To curiosity and a desire to learn. After dabbling in various equally interesting projects from Anti-sense RNA to compartmentalized translation of transmembrane proteins, I saw the light at the end of the tunnel. One of the major questions that used to stump me during the initial years of my PhD was “Why do we care?”. After a long struggle with this simple yet baffling question, and lots of reading, and discussion with Alex, I realized the answer. The focus of this thesis, simply putting it, is a 28 nucleotide long sequence in the mRNA of a particular isoform of a cytoskeletal protein in epithelial cells. The reason why we should care about this: this small element in the mRNA brings about spatial and temporal control of protein translation, ultimately affecting cellular structure and function. From regulating key developmental processes such as tissue migration, to affecting the prognosis of diseases such as cancer, this process plays a fundamental role in determining how a cell behaves and hence its fate. It has most definitely not been an easy road to understanding such a basic principle in biology and how it applies to the larger context. However, through many a failed experiments and graveyards filled with good ideas buried before their time, through many fruitful and sometimes frustrating and rarely futile discussions, I hope this thesis showcases good science and helps one understand a little more than they did about the role of spatial regulation of protein translation.

ACKNOWLEDGEMENTS

First and foremost in the long list of people without whom this thesis would not have been possible are my parents. I am very thankful for all the effort they have put into making sure I remain curious, which is what precipitated my interest in science. They have been extremely supportive of my goals and encouraged my every move. Next, I would like to sincerely thank my aunt and uncle for their support in the US. Having migrated from India, they have made sure I had a comfortable transition settling down in this country. I should also thank my uncle for all the fun times and DIY projects that we did together.

Next in line, is the biology department at Rutgers-Newark. The place has provided a wonderful atmosphere for science. I have had many a fruitful discussion and argument. The faculty and colleagues have always made sure to critically evaluate all problems and experimental results. First in the list of people at this great place I would like to thank is my advisor, Alex. He has been my mentor in science and in life. I have learned how to approach a scientific problem with a calm, rational and yet always critical mind from Alex. In addition, I have learned a good deal of social skills, from networking with peers and seniors to mentoring undergraduates and fellow junior graduate students. Alex has been very patient and given me independence in his lab, which I believe has contributed to what I hope is an interesting thesis. Next, I would like to thank my co-mentor Nan. Alex and I decided we wanted to explore the role of spatial regulation of β-actin translation in mice models and colon cancer, and Nan provided us with the tools and reagents to do so. The collaboration with Nan has been a great learning experience. We have published together and I have definitely benefitted from learning *in vivo* models,

gastro-intestinal development and homeostasis. A knowledge and skill set I am sure will come in handy in my future endeavors.

Ed Bonder. He has been such an amazing inspiration, role model and mentor. I would like whole-heartedly thank Ed for all the discussions, arguments and last but not least the mountain of patience. As a department chair, mentor, and thesis committee member, this thesis would definitely not be the same without his direction. Also, I would like to thank Ed for critical comments on both the manuscripts written as a result of work presented in the thesis. Next, I would like to thank Greg, my thesis committee chair. He has taught me to be meticulous and critical at science, and I sincerely hope at least some of it has sunk in. In addition to being a critical reviewer of my science, Greg has been my mentor in home brewing. It has been great learning biology and zymology from Greg. I would like to lastly thank him for the critical reviews of the manuscripts that resulted from work presented in this thesis. I would also like to thank Ted, my external thesis committee member for making the trip all the way from Minnesota for my thesis defense. In the very short time I have known Ted, whom I met at ASCB, he has been very supportive and has been a great mentor. Thanks for all the fun times, help with the thesis, and helping me network with microscopists.

Next, I would like to thank members of the Rodriguez lab starting with Lissette. She has been a source of inspiration and an embodiment of perseverance that I admire greatly. We have co-authored two manuscripts, which would not have been fruitful if not for Lissette's efforts in quantifications. Itua, our lab tech, has been a great help with my transition into the US. He fearlessly loaned me his car so I could learn how to drive, without once discouraging my poor start behind the wheel. He and Natasha have been

great lab mates and awesome friends. I am happy I got to spend these years doing my PhD in the company of all three of you – Itua, Natasha and Lissette.

It would go amiss if I did not thank Felix, Sue, Juan, Prayush, Richard and David. Each of them have helped me with great discussions about science and made me feel at home in Rutgers Newark. They have been excellent mentors, role models, and above all great friends. In addition, a special thanks to Prayush and David who patiently taught me how to write scripts for image analysis. I would like to thank my cohort, Soumya, Chaitali, Dominic, Melissa, Ming for all the great times we have had. It was great knowing all of them and they have definitely made an impact on my life for the better. And then, Brian, Justin, Huri, Rachel, Neel and Steven, some of whom I have mentored and all of whom I have learnt a lot from. A special thanks to Brian, Justin, Rachel, Neel and Steven for help with quantifications. I would like to thank all them for help with data analysis and moral support during my thesis writing days.

The ladies of the biology department: Shandell, Neermala and Sheronda. I would like to thank all them for their great support and all their help from behind the scenes.

TABLE OF CONTENTS

LIST OF ILLUSTRATIONS

CHAPTER 1: INTRODUCTION

mRNA localization: an important regulatory mechanism controlling cell polarity and function

Physicists define polarity as having opposite poles, wherein the two poles impart different properties in a body or system. We biologists on the other h, and refer to polarity as an asymmetry in distribution of biological components: proteins, mRNA and/or lipids (Wolpert, 2013). This asymmetry plays an important role in several cellular functions: from cell migration during embryogenesis (Medioni et al., 2012), to maintaining barrier function in epithelial tissue (Nagaoka et al., 2012). Most cell types establish polarity by a series of general steps: a polarity cue causes regulation of cytoskeletal and trafficking machinery, which then acts to asymmetrically localize cellular components to establish and maintain the said polarity. One of the first cases of cells asymmetrically localizing mRNA to maintain polarity was discovered by Robert Singer and his colleagues in 1986, when they showed motile chicken embryonic fibroblasts localize β-actin mRNA to the leading edge of cells (Lawrence and Singer, 1986). For a more detailed discussion on β-actin mRNA localization, see below. The asymmetric distribution of proteins following translation occurs due to varying protein sorting codes, differential association with the cytoplasmic membrane face, and/or receptor mediated communication with the external environment. Each of these processes has been studied in quite some exquisite detail for several cellular processes (Mellman and Nelson, 2008). In contrast, localizing mRNAs sets the stage for asymmetric protein distribution by compartmentalized translation of the protein product, increasing the

protein's local concentration and polarizing the cell (Condeelis and Singer, 2005). Thus far, the known mechanisms for mRNA localization are: diffusion and local entrapment, localized degradation, and/or active transport along polarized cytoskeleton (Alberts et al., 2008; Medioni et al., 2012; Song et al., 2015). mRNA localization, rather than post-translational protein transport, provides the cell with several advantages:

1. Energetically, localizing mRNA results in reduced energy expenditure compared to localizing translated proteins. Since, translation occurs on poly-ribosomes, a few mRNA molecules are sufficient to make large quantities of protein. However, compartmentalized protein production requires protein translation machinery at the site of mRNA localization. Evidence corroborating the presence of translation machinery and/or translating mRNA has been documented in cellular compartments such as: distal dendrites of neurons, synapses (Jung et al., 2012), leading edge of migrating cells (Maizels et al., 2015; Mili and Macara, 2009; Mili et al., 2008; Mingle et al., 2005; Willett et al., 2011), and cell-cell contact sites in myoblast cells (Rodriguez et al., 2006) and epithelial cells (Gutierrez et al., 2014).

2. Localizing mRNA also prevents ectopic protein activity, which in the case of maternal determinants leads to developmental defects.

3. Nascent proteins made locally have distinct properties owing to post-translational modifications (Saha et al., 2010).

4. Compartmentalized synthesis of various sub-units of a multi-protein complex decouples formation of the complex from diffusion and/or active protein transport, resulting in faster dynamics and reduced energy expenditure by the cell (Mingle et al., 2005).

5. Similar to proteins with different sorting codes, cells can differentially localize certain mRNAs, which are either splice variants (Baj et al., 2011), or differ in their 3′ untranslated regions (UTRs) (due to alternative polyadenylation signals) (Lembo et al., 2012).

These data taken together suggest that cells localize mRNAs as quite a general rule rather than an exception. In addition to β-actin, several other mRNAs are localized to specific subcellular compartments and determine cell polarity and fate (Eliscovich et al., 2013; Martin and Ephrussi, 2009). A non-exhaustive list of such mRNAs includes: localization of *bicoid*, *gurken*, and *oskar* mRNAs regulating *Drosophila* embryogenesis, *ash1* mRNA localization inhibiting mating-type switch in budding yeast (Buxbaum et al., 2015). Considerable evidence has been gathered for several stages of localized protein translation – mRNA transport after exit from nucleus, mechanism of translational repression until the need for protein product, and the signals initiating translation at sites of localization (Shav-Tal and Singer, 2005). Transcription of a gene to mRNA, association of the transcript with RNA binding proteins, followed by nuclear export, and localization to a cellular compartment where translation is repressed, provides distinct advantages described above.

β-actin mRNA localization: an evolutionarily conserved phenomenon in embryonic development and establishment of cellular polarity

Actin message was the very first mRNA shown to have a distinct and asymmetric subcellular localization (Jeffery et al., 1983). In these seminal *in situ* hybridization experiments carried out in ascidian eggs, Jeffery and co-workers demonstrated actin

mRNA localizes to the myoplasm during early development. Members of the class *Ascidiacea* belong to the Urochordata subphylum of the Chordata phylum in the animal kingdom. They are simple invertebrates and serve as model organisms for the study of chordate evolution and are a close ancestor to vertebrates. Interestingly, mRNAs of cytoplasmic actin isoforms were found to be localized to the future muscle cell lineage in these simple invertebrates. The actin gene families in invertebrates of the Chordata phylum show a large variety of cytoplasmic and muscle isoforms with wide interspecies variations and rapid evolutionary changes as compared to the highly conserved 6 vertebrate isoforms (Bulinski, 2006; Kissinger et al., 1997). Phylogenetic analysis shows the two vertebrate cytoplasmic isoforms: β and γ, share greater similarity with each other than to the invertebrate cytoplasmic isoforms. Likewise, the four vertebrate muscle isoforms: α-cardiac, α-skeletal, α-vascular and γ-enteric, share more similarities with each other than to their invertebrate counterparts. This suggests that one ancestral gene for each of the cytoplasmic and muscle actins evolved in the vertebrates to give rise to the various isoforms through gene duplications after divergence of the vertebrates and urochordates (Kusakabe, 1997; Kusakabe et al., 1997). While the early study showed that the actin mRNA localized to the putative muscle cell lineage was non-muscle actin, further experiments with isoform specific probes, showed that an ascidian cytoplasmic actin mRNA plausibly related to the vertebrate β-actin showed differential localization to ectoplasm and subsequent ectodermal and endodermal lineages (Beach and Jeffery, 1990). In *Fucus* embryos, a model system to study simple plant embryogenesis, actin mRNA has been shown to localize to the thallus tip and the site of cell plate formation following first asymmetric cell division, where it is implicated as a spatial localizing

determinant (Bouget et al., 1996). In vertebrates, β-actin message was the first mRNA shown to be differentially localized to the leading edge of motile chicken embryonic fibroblasts (Lawrence and Singer, 1986), thus paving the way to the field of mRNA localization in higher vertebrates. These studies in simple invertebrates to vertebrates and simple plants show that actin mRNA localization is an evolutionarily conserved phenomenon determining cell polarity and fate.

Several key aspects of the molecular mechanism involved in β-actin mRNA transport, translational repression during transport, subsequent depression of translation have been worked out in vertebrate cells (Huttelmaier et al., 2005; Kislauskis et al., 1994; Latham et al., 2001; Pan et al., 2007; Shestakova et al., 2001). The *cis* acting factor in β-actin mRNA, known at the zipcode, is a 28 nucleotide sequence in the 3′UTR required for mRNA localization. Deletion, mutation or masking of the zipcode has been shown to effect mRNA localization and cell function (Cruz et al., 2015; Gutierrez et al., 2014; Rodriguez et al., 2006; Shestakova et al., 2001).

Zipcode Binding Protein-1: the *trans* acting factor required for β-actin mRNA localization in vertebrates

The first step required for asymmetrical distribution of an mRNA is recognition of a localization sequence. Such sequence(s) is (are) present in the mRNA either as sequence specific, and/or structural information. Proteins termed RNA binding proteins (RBPs), bind to these sequences. RBPs in turn bind directly/indirectly to proteins which localize the mRNA-protein complex (mRNPs) in response to specific cellular signals. This converts sequence specific information in the mRNA to spatial-temporal

information in the cell. The localization sequence is typically, but not always, present in the 3′UTR of the mRNA. Such a sequence is present in the 3′UTR of β-actin mRNA and is termed the zipcode. The RBPs that bind to zipcodes belong to members of the VICKZ family of RNA binding proteins (Yisraeli, 2005). The mRNA coding for the cytoskeletal protein, β-actin and its associated VICKZ member, Zipcode Binding Protein-1 (ZBP-1) have been extensively studied. A 28 nucleotide long zipcode in the 3′UTR of β-actin mRNA is required and sufficient for its localization (Chao et al., 2010; Mingle et al., 2005; Patel et al., 2012). The recognition is mediated by two KH domains in the proteins which bind to a bipartite sequence in the zipcode. These sequences have also been found in other mRNAs that bind ZBP-1 (Jonson et al., 2007; Patel et al., 2012). Since the sequence is characterized by the two ZBP-1 binding consensus sequences separated by a spacer that varies from one mRNA to another, it is possible to design oligonucleotides that uniquely mask the zipcode of particular mRNA without affecting other mRNAs in the cell. Given the evolutionary conservation in 3′UTR sequences, oligonucleotides designed to mask an mRNA in a particular species will mask the same mRNA's zipcode in other species as well. In fact using these oligonucleotides results in disruption of β-actin mRNA localization without any effect on the *trans* acting factor, ZBP1 (Cruz et al., 2015; Gutierrez et al., 2014; Shestakova et al., 2001).

ZBP1 associates with β-actin mRNA in the nucleus (Pan et al., 2007), accompanies the RNA during transport and is required for localizing the mRNA to protruding edge in fibroblasts (Oleynikov and Singer, 2003) and is responsible for translational repression (Huttelmaier et al., 2005). The signal for localizing β-actin mRNA to the leading edge in motile fibroblasts comes from the activation of the Rho

family GTPase – RhoA. RhoA activation is essential for the formation of integrin mediated focal adhesions, which generate traction during directional motility. RhoA effector Rho kinase (ROCK), upon activation by RhoA, mediates β-actin mRNA transport in a myosin dependent manner along polarized actin filaments (Latham et al., 2001). Recently, it has also been suggested that β-actin mRNA transport occurs on microtubules in a KIF11 mediated mechanism (Song et al., 2015). It is thus conceivable that the initial long-range transport occurs on microtubules followed by short-range transport on actin filaments, which helps fine tune the transportation of the message.

Epithelial adherens junction assembly is a multi-step process regulated by a feedforward loop initiated by E-cadherin homophilic ligation

Adherens junctions (AJs) are multi-protein complexes formed by interaction of Type 1 Cadherins on the surface of cells. E-cadherin (Epithelial-Cadherin) is typically associated with AJs which define the apico-lateral polarity in epithelial cells. The transmembrane receptor/scaffold – E-cadherin, forms a homodimer (Cailliez and Lavery, 2005). The homodimers associate in *trans* with E-cadherin on neighboring cells to form AJs. On the cytoplasmic tail, E-cadherin acts as a scaffold for a host of proteins including the catenins: α, β and p120, and c-src (McLachlan et al., 2007). This protein complex is in turn stabilized by a filamentous-actin (F-actin) ring. Specifically, β-actin knock down studies showed a disruption in adherens junction assembly indicating that β-actin is a key component of the actin anchored adherens junction complex (Baranwal et al., 2012). *De novo* cell-cell contact in epithelial cells during the formation of AJs results in RhoA activation at the expanding contact (Yamada and Nelson, 2007). The increase in RhoA

activity is required for β-actin mRNA localization to the cell-cell contact sites (Gutierrez et al., 2014). Further, active Src signaling at the assembling adherens junctions is required for β-actin translation (Huttelmaier et al., 2005). This cell-cell contact localized synthesis of β-actin provides a local pool of actin monomers resulting in linear filament polymerization and subsequent anchoring of E-cadherin to these filaments (Gutierrez et al., 2014). Briefly, epithelial adherens junction assembly occurs in three phases: contact initiation, contact expansion and junction maturation (Baum and Georgiou, 2011). The initial phase of *de novo* cell-cell contact is mediated by Rac and Arp2/3 mediated lamellipodial extension (Zegers and Friedl, 2014) to sense the environment. This is followed by a phase of RhoA activation at the expanding cell-cell contacts (Yamada and Nelson, 2007). The resulting acto-myosin contractility (Ivanov et al., 2005) leads to E-cadherin clustering at the sites of cell-cell contact. Finally during the junction maturation phase, the cells polarize and the accumulating acto-myosin tension lifts the apical plasma membrane giving epithelia their typical columnar shape (Harris et al., 2014).

Actin remodeling and adherens junction assembly are tightly coupled (Krendel and Bonder, 1999; Wu et al., 2015). In fact, deregulation of actin filament polymerization has been shown to cause adherens junction assembly defects, and conversely, actin filament polymerization is required for cadherin mediated adherens junction assembly (Vasioukhin et al., 2000). Additionally, cadherin mediated cell-cell contact has been shown to regulate actin filament dynamics at the sites of contacts (Gloushankova et al., 1997). The adherens junction complex and the cortical F-actin cytoskeleton are tightly coupled via two tension sensitive proteins – α-catenin and vinculin (Drees et al., 2005; Kobielak and Fuchs, 2004; le Duc et al., 2010; Twiss et al., 2012; Yonemura et al., 2010).

Additionally, the acto-myosin tension, mediated in epithelial cells by two non-muscle myosin II isoforms: IIA and IIB, regulates epithelial adherens junction structure and function (Ivanov et al., 2007; Smutny et al., 2010).

E-cadherin endocytosis: a key feature in epithelial adherens junction homeostasis

E-cadherin endocytosis and trafficking contribute significantly to adherens junction dynamics (Bryant and Stow, 2004; Yap et al., 2007). In addition to maintaining the turnover of adherens junction complex at steady state (de Beco et al., 2009; Kowalczyk and Nanes, 2012), E-cadherin endocytosis is deregulated in cancer and causes epithelial to mesenchymal transition and metastasis (Mosesson et al., 2008; Thiery, 2003). During *de novo* assembly of adherens junctions, endocytosis of E-cadherin that is not engaged in a homophilic interaction acts to remove cell surface E-cadherin thus contributing negatively to adherens junction assembly. The opposing positive regulator is F-actin anchoring of E-cadherin. However, a detailed analysis of how these two opposing forces balance each other to regulate adherens junction assembly has not been investigated. In order to set about the business of studying this aforementioned problem, one needs a robust quantitative tool to measure the extent of adherens junction anchoring to the actin cytoskeleton following *de novo* cell-cell contact. *De novo* cell-cell contact can be stimulated in epithelial monolayers by performing a calcium switch, whereby chelation of extracellular calcium to disassemble the calcium sensitive adherens junctions, followed by calcium repletion results in synchronous assembly of adherens junction in the monolayer (Volberg et al., 1986). However, no simple yet robust techniques exist for estimating the extent of adherens junction anchoring to F-actin. To

this end, the first chapter in this thesis introduces a method that relies on fluorescence covariance between E-cadherin and F-actin at cell-cell contacts. Utilizing Pearson's Correlation Coefficients (PCC), which are a measure of normalized covariance, between E-cadherin and F-actin fluorescence, a measure termed Fluorescence Covariance Index to estimate the extent of E-cadherin anchoring to F-actin was validated. This tool was then used to study how spatially regulated β-actin translation and E-cadherin endocytosis balance each other to control adherens junction assembly and epithelial barrier integrity.

Collective cell migration: an important biological phenomenon in development and wound repair following injury

While calcium switch assays are excellent model systems to study the assembly and disassembly dynamics of large groups of cells, they are however, poor representations of physiological conditions. A model system that is physiologically more relevant is collective cell migration in tissue culture models. Although conditions are far from physiologically relevant in several cases, they are powerful models due to the following reasons: cells can be plated on glass coverslips which can be coated with various substrates and are excellent for imaging; cells grow as a single layer making it easy to assess various properties such as traction forces on the substrate and last but not least, they are technically less challenging to handle than complex 3D matrices or embryos (Rorth, 2009). Putting collective cell migration in context, it is an important mechanism underlying several biological processes such as gastrulation, border cell migration during *Drosophila* oogenesis, neural crest migration in vertebrate development, and epithelial wound healing to name a few. Dysregulation of collective cell migration is

also detrimental to an organism in disease states such as cancer, where single cell/streaming behavior has been shown to be required for EMT and metastasis (Bravo-Cordero et al., 2012; Thiery and Sleeman, 2006). Several signaling molecules, actin binding proteins and mRNAs, including but not limited to β-actin, have been shown to differentially localize to the leading edge of a migrating cells (Maizels et al., 2015; Mingle et al., 2005). However, the role of spatially regulated β-actin translation in controlling leading edge dynamics as well as the cell-cell adhesions during epithelial sheet migration have not been subject to any studies. In this thesis, chapter 4 explores the extent to which spatially regulated β-actin translation governs actin filament dynamics at the cell-cell adhesions during epithelial sheet migration following a model wound. These experiments provide new insights into the role of compartmentalized β-actin translation in establishing dynamic equilibrium to bring about collective cell migratory behavior.

SPECIFIC AIMS

Specific Aim 1: To quantify the assembly and trafficking of the minimal cadherin-catenin complex, and maturation of the adherens junctions in epithelial cells by developing a fluorescence microscopy based covariance analysis.

Sub-aim 1A: To determine the extent to which E-cadherin and F-actin fluorescence covariance measures adherens junction maturation in epithelia.

Sub-aim 1B: To quantify the formation and trafficking of the minimal cadherin-catenin complex during adherens junction formation in epithelia.

Sub-aim 1C: To determine the extent to which α-catenin and F-actin covariance correlates with established tension profiles in epithelia during adherens junction formation.

Sub-aim 1D: To determine the extent to which E-cadherin and β-actin covariance in live cells measures adherens junction formation and maturation.

Specific Aim 2: To determine the extent to which spatially regulated β-actin translation balances E-cadherin endocytosis and anchoring to control the formation and maturation of adherens junctions in 2-dimensional, and to what extent spatially regulated β-actin translation determines 3-dimensional epithelial morphology.

Sub-aim 2A: To determine the extent to which spatially regulated β-actin translation affects adherens junction formation and maturation

Sub-aim 2B: To determine the extent to which inhibiting E-cadherin endocytosis rescues adherens junction assembly defects caused by mislocalizing β-actin translation

Sub-aim 2C: To determine the extent to which spatial regulation of endogenous β-actin translation is required to rescue adherens junction assembly by balancing E-cadherin endocytosis in cells expressing exogenous β-actin with mislocalized translation.

Sub-aim 2D: To determine the spatial localization of newly synthesized β-actin monomer in 3 dimensional epithelial cyst cultures.

Sub-aim 2E: To determine the extent to which, if any, mislocalizing β-actin translation has on 3 dimensional epithelial morphogenesis.

Specific Aim 3: To determine the extent to spatially regulated β-actin translation affects dynamics of collective cell migration in epithelial cells – an *in vitro* model for epithelial wound repair and collective cell migration during development.

Sub-aim 3A: To determine the extent to which spatially regulated β-actin translation affects protrusive activity in leader cells following model wounds in epithelial sheets.

Sub-aim 3B: To determine the extent to which spatially regulated β-actin translation affects collective epithelial sheet migration rates following model wounds in epithelial sheets.

Sub-aim 3C: To determine the extent to which spatially regulated β-actin translation affects actin dynamics at leader-follower cell pairs in epithelial sheets following model wounds.

CHAPTER 2: QUANTIFYING CADHERIN MECHANO-TRANSDUCTION MACHINERY ASSEMBLY/DISASSEMBLY DYNAMICS USING LIGHT MICROSCOPY AND FLUORESCENCE COVARIANCE ANALYSIS

INTRODUCTION

Fluorescence signal colocalization is widely used to assess protein complex assembly (Bolte and Cordelieres, 2006). A number of global pixel intensity based statistical methods provide options to quantify colocalization (Dunn et al., 2011). Two such techniques, *M*anders *O*verlap *C*oefficient (MOC) and *M*anders *C*olocalization *C*oefficients (MCC) (Manders et al., 1993), were developed to assess the degree of co-occurrence or the relative fraction of overlap of two fluorescence signals, respectively. However, both MOC and MCC analyses fail to reflect differences between bona fide protein-protein complexes and overlapping fluorescence signals due to large voxel size relative to the volume occupied by protein complexes. In addition, these coefficients are significantly affected by threshold corrections and require several processing steps to assign background values. Such corrections are especially tedious when working with low intensity signals, such as during early stages of multiprotein complex assembly (Adler and Parmryd, 2010). Protein complexes often maintain strict stoichiometry during assembly, meaning individual components vary proportionally to other components. Karl Pearson in 1896 introduced a correlation coefficient to study whether two variables covary with each other (Pearson, 1896). The coefficient now termed *P*earson's *C*orrelation *C*oefficient (PCC), has been used as a pixel-by-pixel covariance analysis

method to assess subcellular compartment specific protein complex assembly (Barlow et al., 2010; Costes et al., 2004). Since PCC is a measure of covariance between two fluorescent signals, it serves as a reliable tool to estimate whether two proteins are part of a complex (Zinchuk et al., 2007). Unlike MOC and MCC measurements, PCC values have the advantage of being insensitive to variations in the overall intensity of the two fluorescent signals being analyzed. Work presented in this thesis demonstrates PCC analysis can be applied to quantify epithelial adherens junction complex assembly/disassembly dynamics.

De novo E-cadherin homophillic contact in Madin Darby Canine Kidney (MDCK) epithelial cells triggers the formation of a multi-protein complex termed the adherens junction complex. This complex is implicated as a mechano-transduction machinery and is one of the defining features of a polarized epithelium (Ladoux et al., 2015; Nagafuchi, 2001). Utilizing extracellular calcium concentration dependence of E-cadherin function to initiate synchronized *de novo* adhesions (Volberg et al., 1986), several aspects of assembly of the multi-protein complex were quantified. These include: formation and trafficking of the minimal cadherin-catenin complex, anchoring of cadherin complexes to the actin cytoskeleton, and correlating α-catenin/F-actin anchoring dynamics to previously established tension profiles (Harris et al., 2014). Finally, this PCC based approach is used to quantitate adherens junction complex assembly dynamics in live cells with minimal computational costs and inexpensive image acquisition equipment.

RESULTS

Rational derivation of a fluorescence covariance based metric to assess cadherin mechano-transduction complex assembly/disassembly

The cadherin mechano-transduction complex functions in part by coupling tissue tension to cytoskeletal remodeling (Ladoux et al., 2015; Lecuit and Yap, 2015). E-cadherin, β-catenin and α-catenin form the "minimal cadherin-catenin complex", which directly binds the actin cytoskeleton when subject to acto-myosin generated tension (Buckley et al., 2014). Historically, multi-protein complexes thought to be important for epithelial cell-cell adhesion were studied using biochemical assays (Curtis et al., 2008; Hinck et al., 1994). Alternatively, sub-cellular localization of individual complex components has been assessed by immunofluorescence microscopy where complex assembly is indicated by co-localization of two or more components. A simplistic method to assess co-localization is to use line scan analysis, where the intensity of two or more fluorescently labelled components of the complex along a user defined line is plotted as a function of distance. For instance, line scan analysis in MDCK cells 3 hours following *de novo* epithelial cell-cell contact shows E-cadherin, β-catenin and F-actin fluorescence signal overlap at cell-cell contact sites. This is observed as a co-localization of fluorescence intensities at these sites (**Figure 1A**). The resulting intensity profiles show overlap in fluorescence peak intensities at the cell-cell contacts indicating the formation of adherens junction complexes at these sites (**Figure 1A,** line profile **I**). However, results of line scan analyses depend on the user defined position of the analysis line. Analyzing line scans across different diameters of a cell indicate absence of one or more

components of the adherens junction complex along the cell-cell interfaces (**Figure 1A,** line profile **II** and **III**). This variation stems from inherent heterogeneity in distribution of adherens junction complexes along cell-cell interfaces in any given optical section (Cavey et al., 2008). Additionally, the entire lateral interface of contacting epithelial cells is not created equal, translating to differences in distribution of adherens junction complexes along the lateral interfaces (Wu et al., 2014). This is seen as variations in peak fluorescence intensities and overlaps using line scan profiles of analogous lines across multiple optical sections (**Figure 1B** compare with optical section in **Figure 1A**). Calculating co-localization or overlap coefficients (Manders et al., 1993) using the entire volume occupied by the lateral interface circumvents most of the problems inherent to one dimensional line scans. However, overlap coefficients cannot discriminate between bona fide protein-protein interactions and overlap of two fluorescence signals in the same voxel. Given the voxel size is significantly larger than the size of a single cadherin-catenin complex (Ishiyama and Ikura, 2012), calculating *M*ander's *O*verlap *C*oefficients (MOC) (**Materials and Methods, Equation 2**) will result in erroneously overestimating complex assembly. However, quantifying fluorescence signal covariance using *P*earson's *C*orrelation *C*oefficients (PCC) (**Materials and Methods, Equation 3**) (Barlow et al., 2010) at cell-cell contacts for E-cadherin and F-actin measures the extent of their association, given the two molecules form a macromolecular complex.

MOC and PCC values were estimated for three different combinations of molecules:

1. As a negative control, Transferrin receptor (TfR) and F-actin; which have little interaction in any given sub-cellular compartment.

2. As a positive control, β-catenin immunostained by two antibodies with overlapping epitopes; which should have a near complete overlap and covariance in all sub-cellular compartments.
3. E-cadherin and F-actin; which form a complex at a specific subcellular compartment – the cell-cell interfaces.

MOC and PCC values are calculated for each cell in two regions – cytoplasm and cell-cell contact (**Figure 2A**). Negative PCC values for TfR and F-actin at cell-cell contacts indicate mutual exclusion of the two signals. This is expected due to the presence of a significant distribution of actin at cell-cell contacts, while TfR is randomly distributed throughout the cell periphery. MOC values for TfR show a small degree of co-occurrence of the two signals as would be expected for two fluorescence signals that show little overlap (**Figure 2B,** TfR:F-actin at cell-cell contacts). However, PCC values for the positive control, β-catenin stained with two antibodies, show very strong correlation at cell-cell contacts. The MOC values are also high for the two fluorescence signals as would be expected for signals from overlapping epitopes (**Figure 2B,** β-catenin:β-catenin at cell-cell contacts). E-cadherin and F-actin, which are both part of the adherens junction at cell-cell contacts show strong correlation values similar to the positive control. MOC values for E-cadherin and F-actin indicate a great degree of overlap of the two molecules at the cell-cell contacts. However, while the MOC values only indicate the degree of overlap, the PCC values indicate the nature of association. For instance, F-actin and TfR are mutually excluded at cell-cell contacts, while E-cadherin and F-actin are strongly associated with each other at cell-cell contacts (**Figure 2B**). In the cytoplasmic compartment, where TfR and F-actin are both randomly distributed, PCC

values show a “very weak” correlation and MOC values indicate weak overlap of the two signals. In contrast, β-catenin signals localized to the perinuclear ER-golgi like distribution show strong correlation and overlap, as expected from antibodies recognizing overlapping epitopes. Importantly, the PCC and MOC values for E-cadherin and F-actin in the cytoplasm are low, resembling randomly distributed signals of TfR and F-actin in this compartment (**Figure 2B,** cytoplasm). These results demonstrate the proof of principle that using PCC values reveals the nature of association between two molecules, whether they are strongly associated, very weakly associated or mutually excluded.

In order to study the behavior of the cell populations as opposed to single cells, frequency plots of PCC values for the above three combinations of molecules in multiple cells were graphed (for estimation of bin size, see **Materials and Methods, Statistical Analysis**). The distribution for E-cadherin and F-actin in cytoplasmic compartment is centered at 0, resembling that of TfR and F-actin. However, the frequency plot for the two β-catenin signals was significantly biased toward higher correlations (**Figure 3A**). Since the two β-catenin signals in the perinuclear compartment recognize the same molecule, the high correlations are expected. In contrast, frequency plot of PCC values for TfR and F-actin at cell-cell contacts shows a distribution centered at 0, while the frequency plot for E-cadherin and F-actin is biased towards high correlations resembling that of the two β-catenin signals (**Figure 3B)**. These results demonstrate a substantial proportion of cells have E-cadherin and F-actin in a complex at cell-cell contacts, while the two molecules have very little interaction in the cytoplasm.

To obtain a single metric quantifying the extent of adherens junction maturation taking into account cell-cell contact and cytoplasmic correlations (or lamellapodial

overlap containing lateral/*en face* adhesions; for a more detailed explanation of *en face* adhesions see section on α-catenin and F-actin below), the ratio of PCC values at cell-cell contacts to PCC values in the cytoplasm for E-cadherin and F-actin was logarithm transformed (**Materials and Methods, Equation 4**). This measure, termed *F*luorescence *C*ovariance *I*ndex (FCI) quantifies relative asymmetry in correlation between the two compartments: cell-cell contacts and cytoplasm. FCI values given by **Equation 4** have no bounds and are susceptible to large variations depending on the relative PCC values between the two compartments being analyzed. Since, FCI measures the asymmetry in correlations between the two compartments, PCC values lower than 0.1 were reassigned to 0.1, a value representing "very weak" correlation. Thresholding PCC values constrains FCI values to the range: -1 to +1 and eliminates undefined values due to negative PCCs. Importantly, PCC values between than 0.1 and 0 carry little biological significance justifying the thresholds applied to measure the relative asymmetry in covariance (Barlow et al., 2010; Zinchuk et al., 2013). FCI values between -1 and 0 signify higher PCCs in the cytoplasm, while values between 0 and +1 signify higher PCCs at cell-cell contacts. Thus, FCI values indicate the relative contribution of positive correlations at cell-cell contacts and in the cytoplasm, providing a single number to assess the extent of apical and lateral/*en face* adherens junctions.

To test the effects of setting a threshold on PCC values, frequency distributions of PCC values in multiple cells were re-plotted after setting thresholds for the three combinations of molecules mentioned above: TfR and F-actin, β-catenin stained with two antibodies with overlapping epitopes, and E-cadherin and F-actin. The frequency plots for PCC values in both cellular compartments for the two β-catenin signals, and E-

cadherin and F-actin remain largely unaffected after setting the threshold. However, the distribution for TfR and F-actin show a significant right shift since the two molecules were mutually excluded (large negative PCC values) in several cells (**Figure 3C, D**). The frequency distributions of FCI values for the three combinations of molecules were plotted to determine which combination show a relative asymmetry in covariance in the two sub-cellular compartments. TfR and F-actin show very weak covariance in both compartments, and the two β-catenin signals are highly correlated in both compartments (**Figure 3E**, green and red bars). The FCI distributions for these two combinations are centered at 0 representing a "null hypothesis" or no asymmetry in covariance between the two sub-cellular compartments. In contrast, E-cadherin and F-actin show a right shifted distribution, indicating a cell-cell contact biased asymmetry in E-cadherin and F-actin association owing to adherens junction maturation (**Figure 3E**, black bars). Additionally, upon chelation of extracellular calcium, E-cadherin and F-actin FCI distribution shifts to the left, resembling the null hypothesis distribution. This stems from a disassembly of adherens junction complex upon chelation of extra-cellular calcium, resulting in a loss of asymmetry in correlation between the two molecules. While steady state cells have ≈ 49% FCI values ranging between 0.5 and 1.0, only ≈ 1% of FCI values fall within this range upon calcium chelation (**Figure 3E**, grey bars). These results establish the derivation of FCI values, and the dynamic range of the metric to assess adherens junction assembly: adherens junction maturation is represented if the frequency of cells with FCI values for E-cadherin and F-actin in 0.5 – 1.0 range is ≥ 45%; and adherens junction disassembly is indicated by a frequency distribution biased towards 0.0 – 0.5 range.

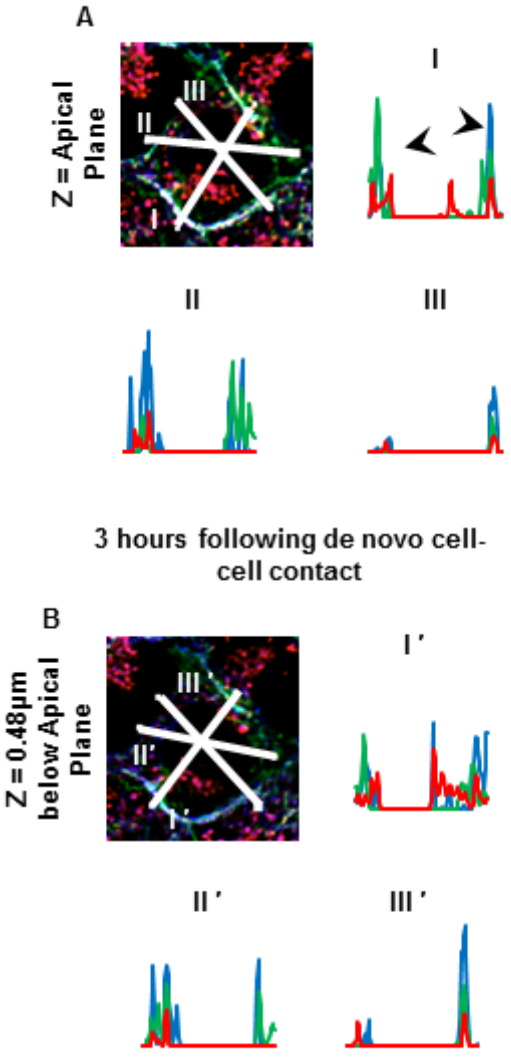
A
Z = Apical Plane
III
II
I
I
II
III
3 hours following de novo cell-cell contact
B
Z = 0.48µm below Apical Plane
III'
II'
I'
I'
II'
III'

Figure 1: Variability in assessing adherens junction assembly using fluorescence overlaps from line scans.

(**A**) Optical section of MDCK cells 3 hours after calcium repletion immunostained for E-cadherin (red), F-actin (green) and β-catenin (blue). (**B**) Optical section 0.48μm below section in **A**. Graphs show intensity plots along analysis lines **I, II, and III** in the optical section in **A** and along the analogous lines I′, II′ and III′ in the optical section in **B**. Y-axis represents Intensity (a.u.) and X-axis represents Distance (μm, values omitted from graph). I would like to acknowledge Lissette Cruz for acquiring the images shown in panel **A** and **B**.

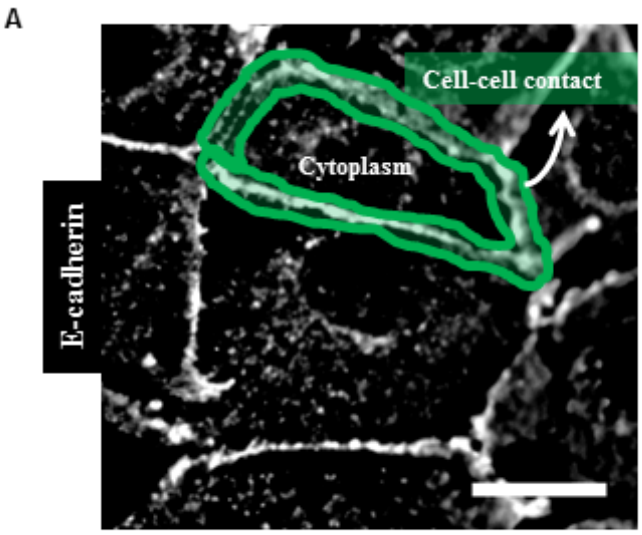

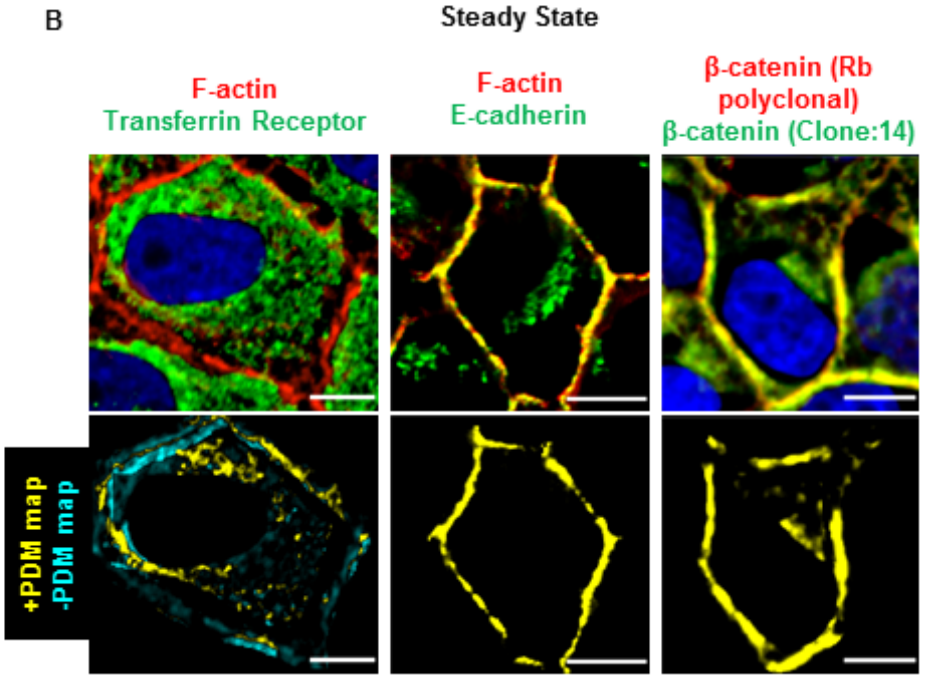

	Transferrin Receptor:F-actin		E-cadherin:F-actin		β-catenin:β-catenin	
	MOC	PCC	MOC	PCC	MOC	PCC
Cell-cell contact	0.288	-0.133	0.903	0.887	0.952	0.921
Cytoplasm	0.398	0.100	0.260	0.237	0.825	0.772

Figure 2: Defining cell-cell contact and cytoplasmic compartments to measure and compare PCC and MOC values for interacting and non-interacting protein pairs.

(**A**) Immunofluorescence image for E-cadherin in MDCK cells 2 hours after calcium repletion with ROI indicating the peripheral compartment (Green region) and the cytoplasmic compartment (Inside the cell excluding the region in the periphery and nucleus (not shown)). Scale bar = 20μm. (**B**) **Top panel:** Images representing MDCK cells in steady state immunostained for: **Left:** F-actin (Red) and transferrin receptor (Green). **Middle:** F-actin (Red) and E-cadherin (Green), and **Right:** β-catenin (Rabbit polyclonal) and β-catenin (Mouse monoclonal, Clone:14). **Bottom panel:** positive and negative *P*roduct of *D*ifference from *M*ean maps: +PDM (yellow) and –PDM (cyan) maps for the images shown in top panel. **Table:** Calculated Mander's Overlap Coefficients (MOCs) and Pearson's Correlation Coefficients (PCCs) for the cells shown in **B**. Scale bar = 10μm. I would like to acknowledge Lissette Cruz for help with making and organizing the images shown in panel **B**.

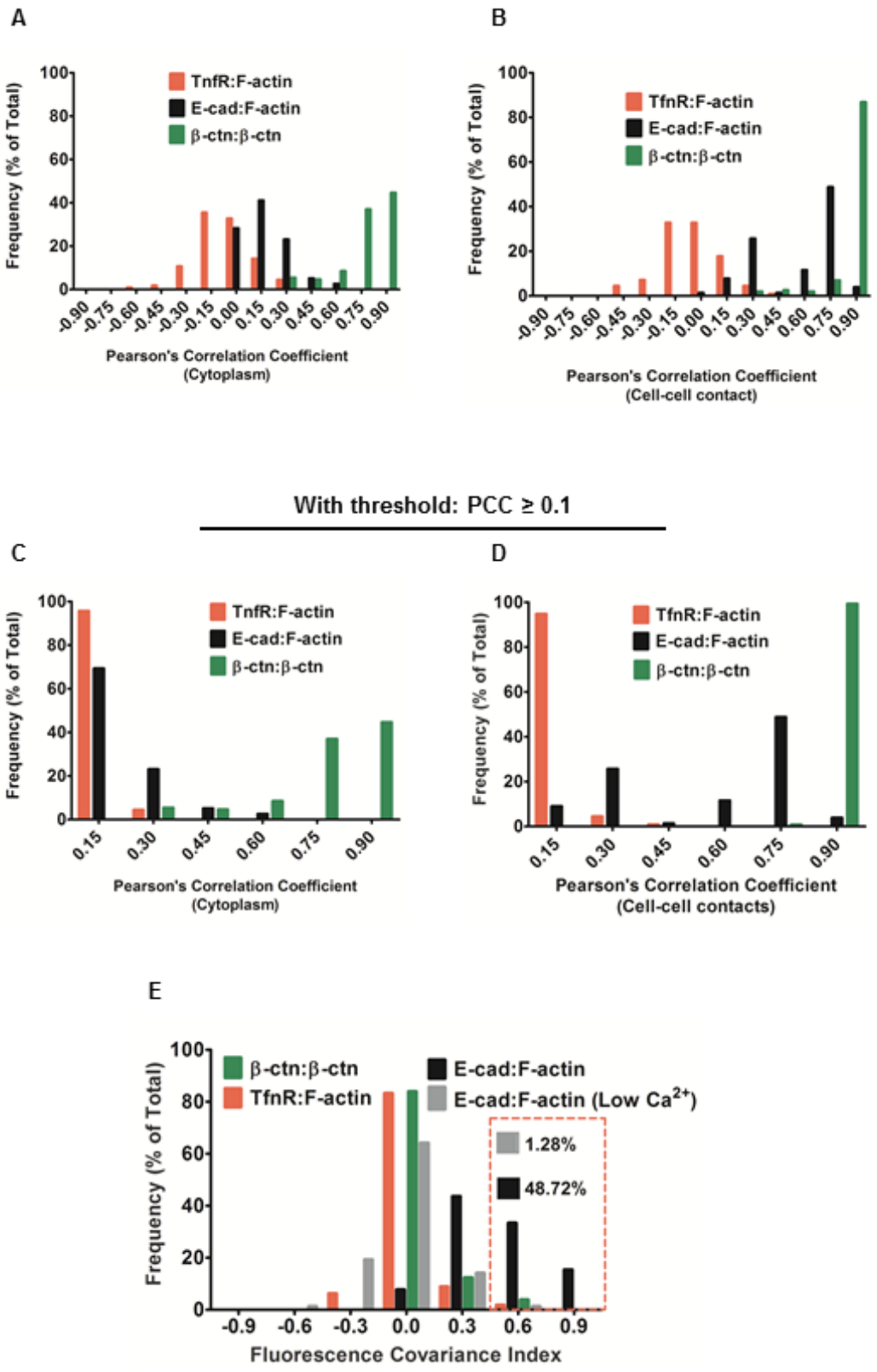
A
B
TnfR:F-actin
E-cad:F-actin
β-ctn:β-ctn
TfnR:F-actin
Frequency (% of Total)
Pearson's Correlation Coefficient (Cytoplasm)
Pearson's Correlation Coefficient (Cell-cell contact)
With threshold: PCC ≥ 0.1
C
D
Pearson's Correlation Coefficient (Cytoplasm)
Pearson's Correlation Coefficient (Cell-cell contacts)
E
E-cad:F-actin (Low Ca2+)
1.28%
48.72%
Fluorescence Covariance Index

Figure 3: Frequency distributions of PCC values at cell-cell contacts and cytoplasm and the corresponding FCI frequency distributions for interacting and non-interacting protein pairs. Frequency distributions of (**A, B**) unthresholded and (**C, D**) thresholded PCC values in: cytoplasm (**A, C**) and cell-cell contact zone (**B, D**). Values for: TfR and F-actin are shown as red bars, for β-catenin (Rabbit polyclonal) and β-catenin (Clone:14) are shown as green bars, and for E-cadherin and F-actin are shown as black bars. Bin width = 0.15. The cells were fixed and immunostained in steady state. (**E**) Frequency distributions of FCI values for: TfR and F-actin are shown as red bars, two signals for β-catenin are shown as green bars, and E-cadherin and F-actin are shown as black bars (without calcium chelator, EGTA) and grey bars (with 4mM EGTA treatment of cells at steady state for 1 hour). Bin width = 0.3. (**A-E**) N (sample size) values are as follows: Tfr:F-actin = 113, β-catenin:β-catenin = 130, E-cadherin:F-actin in steady state N = 78, and after calcium chelation for 1 hour N = 78.

Optimizing image acquisition and processing parameters for FCI measurements

In order to carry out a quantitative assessment of fluorescence covariance across multiple optical sections and include the entire 3-dimensional volume of the cell, Z-stacks were acquired using a high Quantum Efficiency CCD camera. Out-of-focus contributions due to widefield acquisition were reassigned and images were restored using the Constrained Iterative Maximum Likelihood Algorithm for deconvolution (**Figure 4**) (Bolte and Cordelieres, 2006; Schaefer et al., 2001). Since a change in absolute fluorescence intensity of either one or both of the signals does not affect PCCs, a linear normalization function was applied (**Materials and Methods, Equation 5**). However, noisy images show high PCC values due to an inability to accurately converge on a solution by the image restoration algorithm (Adler and Parmryd, 2010). Therefore, images with a low Signal-to-Noise Ratio (SNR) result in high cytoplasmic PCCs arising from signal (or more accurately, noise) overlap rather than lateral/*en face* adhesions, and ultimately underestimating the extent of complex assembly at cell-cell contacts. Exposure times were reduced up to ten fold to obtain images with low SNR and the resultant FCIs for E-cadherin and F-actin were measured (**Figure 5A**). Lowering the exposure times reduces the proportion of cells with high (0.5 – 1.0) FCI values (**Figure 5B**). Only a 10 fold reduction in exposure time shows a substantial drop in FCI values (≈ 37% in 0.5 – 1.0 range for 10 fold reduction in intensity and > 45% for all other exposure times), indicating FCI measurements can tolerate small changes in signal intensity but are sensitive to very noisy images (**Figure 5C**).

Another image processing parameter which could potentially effect FCI measurements is the degree of image restoration by deconvolution. This was tested by

varying the deconvolution "strength" parameter, thereby increasing stringency and decreasing out-of-focus contribution in the original image (Sun, 2007). Low stringency deconvolution generates images with significant out-of-focus contribution due to poor image restoration (**Figure 6A**). This results in a lower proportion of cells with high FCI values. Better image restoration correlates with an increase in the frequency of high FCI values (**Figure 6B**, ≈ 34% in 0.5 – 1.0 range for high image noise and > 45% for all other strength settings). However, there was no significant change in FCI values when images were restored with medium, high or very high stringency (**Figure 6C**). These data demonstrate FCI values exhibit minimal variation for a wide range of image restoration parameters.

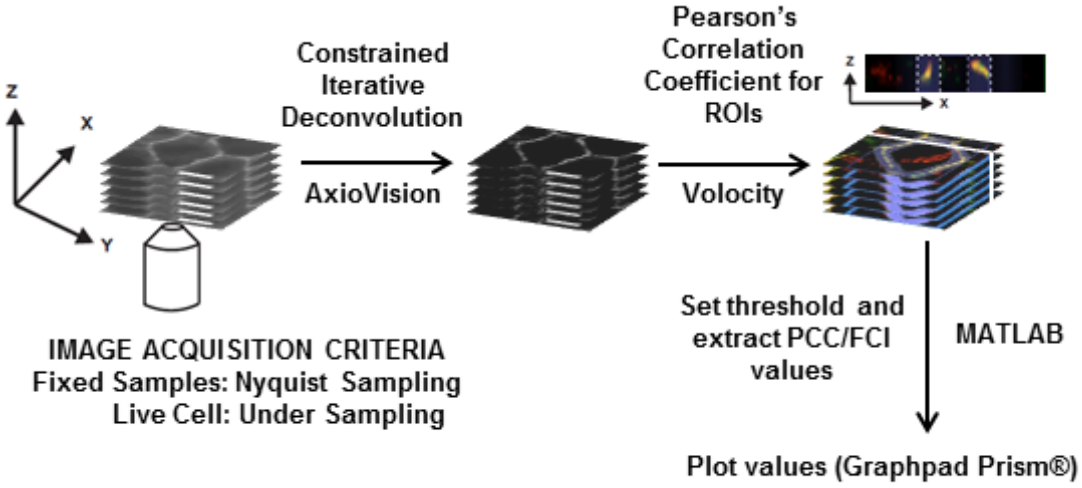
Z
X
Y
Constrained
Iterative
Deconvolution
AxioVision
Pearson's
Correlation
Coefficient for
ROIs
Z
X
Volocity
IMAGE ACQUISITION CRITERIA
Fixed Samples: Nyquist Sampling
Live Cell: Under Sampling
Set threshold and
extract PCC/FCI
values
MATLAB
Plot values (Graphpad Prism®)

Figure 4: From image acquisition to data analysis: Work flow for FCI analysis. Workflow for FCI analysis depicting: image acquisition, processing and analysis steps. Z-stacks are acquired at Nyquist sampling criteria for fixed cells (35 steps of 0.24 μm thickness each to span the entire lateral surface of the cell) and under sampling for live cells (3 steps at 3 μm interval between neighboring steps to reduce photo-toxicity). Following acquisition, image deconvolution was carried out using constrained iterative maximum likelihood algorithm. PCC values were computed for defined ROIs – cell-cell contact and cytoplasm. FCI values were extracted and plotted.

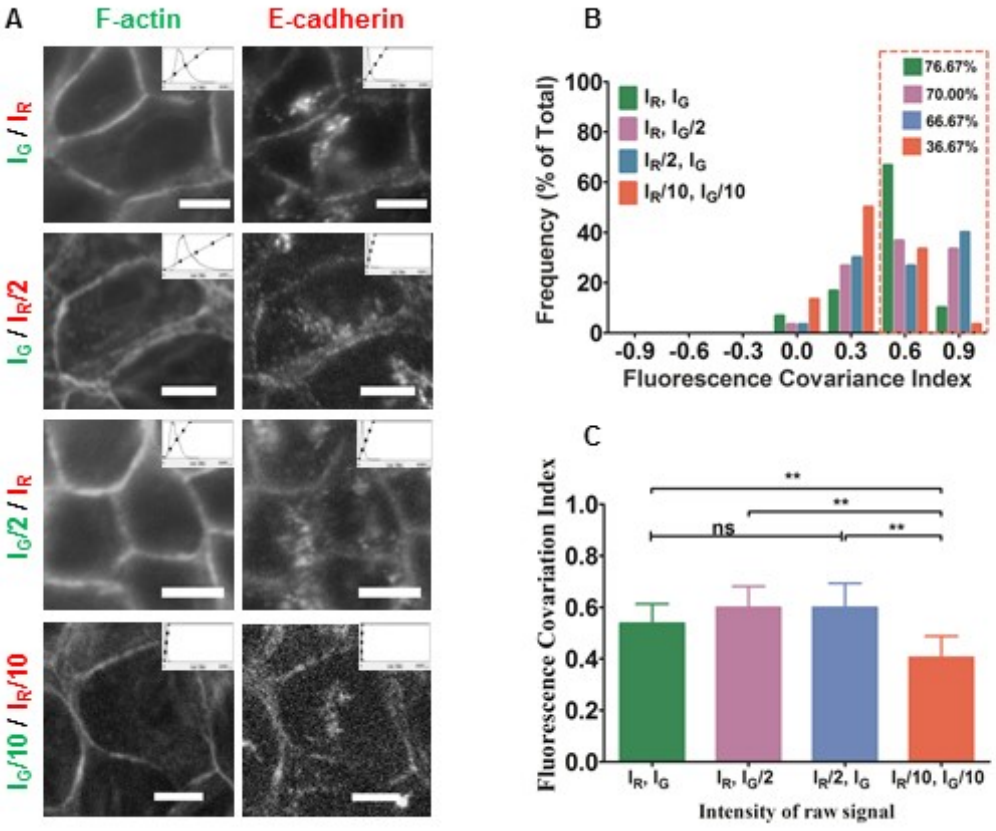
A
F-actin
E-cadherin
I_G / I_R
I_G / I_R/2
I_G/2 / I_R
I_G/10 / I_R/10
B
Frequency (% of Total)
I_R, I_G
I_R, I_G/2
I_R/2, I_G
I_R/10, I_G/10
76.67%
70.00%
66.67%
36.67%
Fluorescence Covariance Index
C
Fluorescence Covariation Index
ns
**
**
**
Intensity of raw signal

Figure 5: FCI measurements for E-cadherin and F-actin are positively correlated with image exposure times. (**A**) Optical sections of MDCK cells in steady state immunostained for E-cadherin (**Right panel**, Red) and F-actin (**Left panel**, Green). Images were acquired using the following exposure times. **Top:Bottom** – 50ms (green) and 200ms (red); 50ms (green) and 100ms (red); 25ms (green) and 200ms (red); 5ms (green) and 20ms (red). Each image was contrast adjusted such that 1% of all pixels fell to the highest value and 1% fell to the lowest value. **Insets:** Histograms for the intensity distribution and the line corresponding to the contrast adjustment's highest and lowest gray level. Scale bar = 10μm. (**B**) Frequency distributions of FCI values for E-cadherin and F-actin with images acquired using different exposure times. Red box indicates the percentage of high FCI values (0.5 – 1.0) for each case. Bin width = 0.3. (**C**) Student's t-test was performed for individual pairs of data: I_R (red intensity = E-cadherin), I_G (green intensity = F-actin). Images acquired with 10-fold reduced exposure times ($I_R/10$, $I_G/10$) had significantly lower FCI values as indicated by the t-tests (I_R, I_G: $p = 0.0087$; I_R, $I_G/2$: $p = 0.0020$; $I_R/2$, I_G: $p = 0.018$). Error bars represent mean ± 95% CI. N (sample size) = 30 cells per set of exposure times. I would like to acknowledge Lissette Cruz for acquiring the images shown in panel **A** and calculating the PCC values.

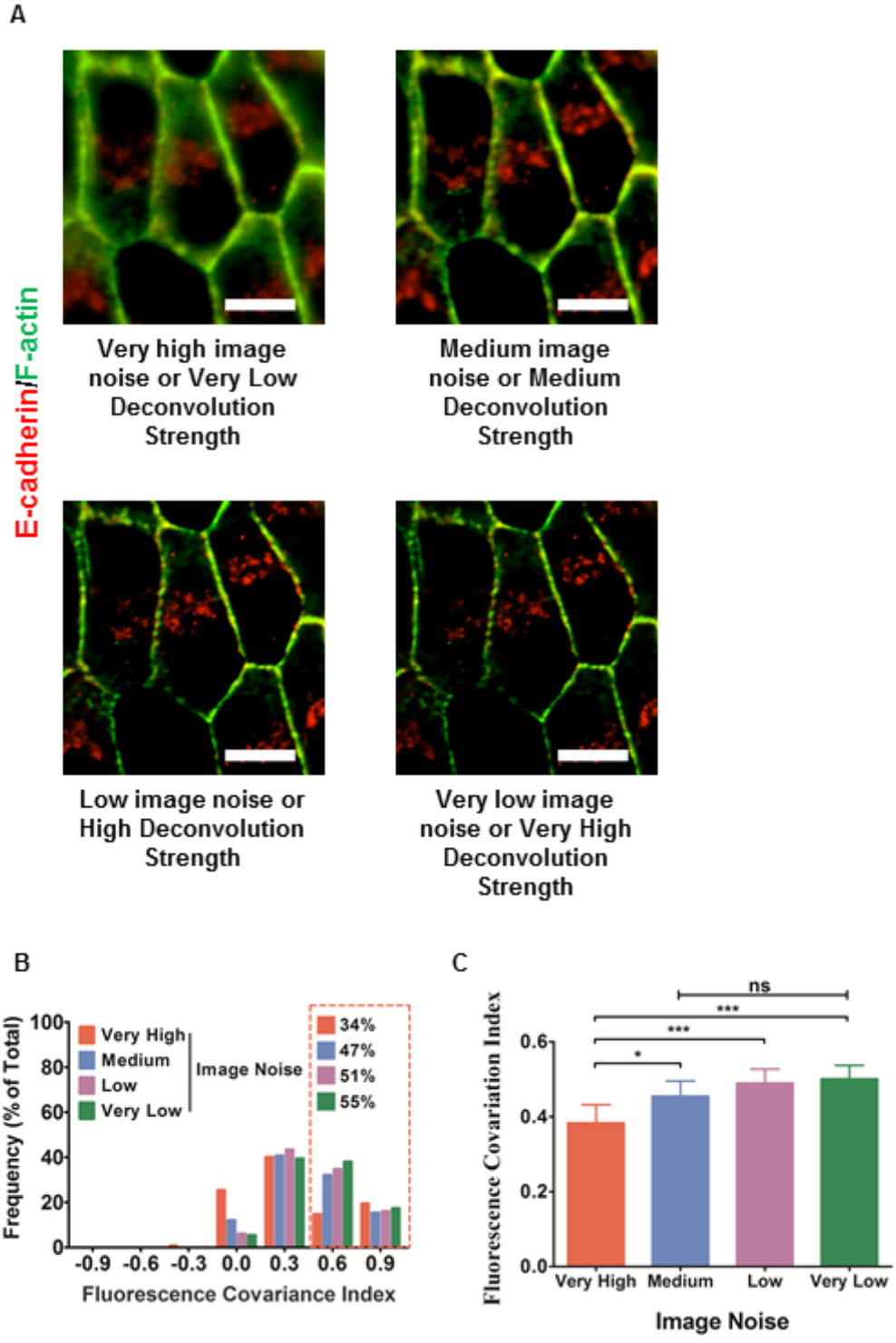
A
E-cadherin/F-actin
Very high image noise or Very Low Deconvolution Strength
Medium image noise or Medium Deconvolution Strength
Low image noise or High Deconvolution Strength
Very low image noise or Very High Deconvolution Strength
B
Frequency (% of Total)
Very High
Medium
Low
Very Low
Image Noise
34%
47%
51%
55%
Fluorescence Covariance Index
C
Fluorescence Covariation Index
ns
***
***
*
Very High
Medium
Low
Very Low
Image Noise

Figure 6: FCI values for E-cadherin and F-actin are positively correlated with the degree of image restoration. (**A**) Optical sections of MDCK cells in steady state stained for E-cadherin (red) and F-actin (green) processed with varying deconvolution "strength" parameter. Scale bar = 10μm. (**B**) Frequency distributions of FCI values for E-cadherin and F-actin with different deconvolution strength settings. Red box indicates the percentage of high FCI values (0.5 – 1.0) for each case. Bin width = 0.3. (**C**) Mean FCI values data in **B**. The result of a non-parametric Kruskal-Wallis test gives a p value < 0.0001 and the results of Dunn's post-hoc multiple comparison test are indicated on the graph (*** $p < 0.001$, *$p < 0.1$, *ns*: not significant). N (sample size) = 150 for each strength setting. I would like to acknowledge Lissette Cruz for acquiring the images shown in panel **A** and calculating the PCC values.

Adherens junction assembly/maturation occurs over a period of 3 hours following *de novo* cell-cell contact

Synchronized *de novo* cell-cell contacts were initiated using a calcium repletion assay (Volberg et al., 1986). There is a progressive increase in E-cadherin fluorescence intensity and co-localization with F-actin fluorescence intensity at cell-cell contacts as adherens junctions are assembled (**Figure 7A**). Correspondingly, frequency distribution of PCC values shows an increasing proportion of cells with higher PCCs for E-cadherin and F-actin at cell-cell contacts from 1 through 3 hours after calcium repletion indicating adherens junction assembly (**Figure 7B**). Conversely, PCC values for E-cadherin and F-actin in the cytoplasm are low following calcium repletion (**Figure 7C**), demonstrating little E-cadherin and F-actin association in the cytoplasm. To further validate the extent to which PCC values for E-cadherin and F-actin reflect adherens junction assembly, E-cadherin homophillic binding was perturbed using E-cadherin function blocking antibodies during calcium repletion (Vestweber and Kemler, 1985). Under these conditions, the cells fail to progressively accumulate E-cadherin at the cell-cell contacts and show significant intercellular overlaps following calcium repletion (**Figure 7D**). Intriguingly, PCC values at cell-cell contacts show a significant increase between 1 and 2 hours after calcium repletion with E-cadherin function blocking antibody. However, 3 hours after calcium repletion with E-cadherin function blocking antibody, the frequency distribution of PCC values shifts significantly to the left, indicating cells fail to undergo adherens junction maturation (**Figure 7E**). Additionally, significant lamellipodial overlap after calcium repletion, results in high PCC values for E-cadherin and F-actin in the cytoplasm (**Figure 7F**).

Consistent with adherens junction assembly in control conditions, there is a progressive increase in the proportion of cells with high FCI values following calcium repletion over a period of 3 hours (**Figure 8A**). 3 hours after calcium repletion, the proportion of cells with high FCI values is comparable to that at steady state (≈ 46% at 3 hours following calcium repletion compared to ≈ 49% at steady state), indicating *de novo* adherens junction assembly and maturation occurs within this time frame as supported by previous reports (Gutierrez et al., 2014) (**Figure 8B**). Finally, frequency distribution plots of FCI values for E-cadherin and F-actin during the entire course of a calcium repletion experiment were fit to Gaussian distributions and show a progressive increase in mean FCI values. The mean of the distribution at 3 hours following calcium repletion overlaps with the steady state value (**Figure 8C**). However, cells treated with E-cadherin function blocking antibody fail to reach steady state proportion of high FCI values for E-cadherin and F-actin (≈ 31% at 3 hours following calcium repletion with E-cadherin function blocking antibody compared to ≈ 49% at steady state), indicating an inability to mature adherens junctions (**Figure 8D**). These results demonstrate FCI analysis for E-cadherin and F-actin is sensitive to E-cadherin function, and the frequency of high FCI values provides a quantitative measure of adherens junction assembly/disassembly dynamics in epithelial monolayers.

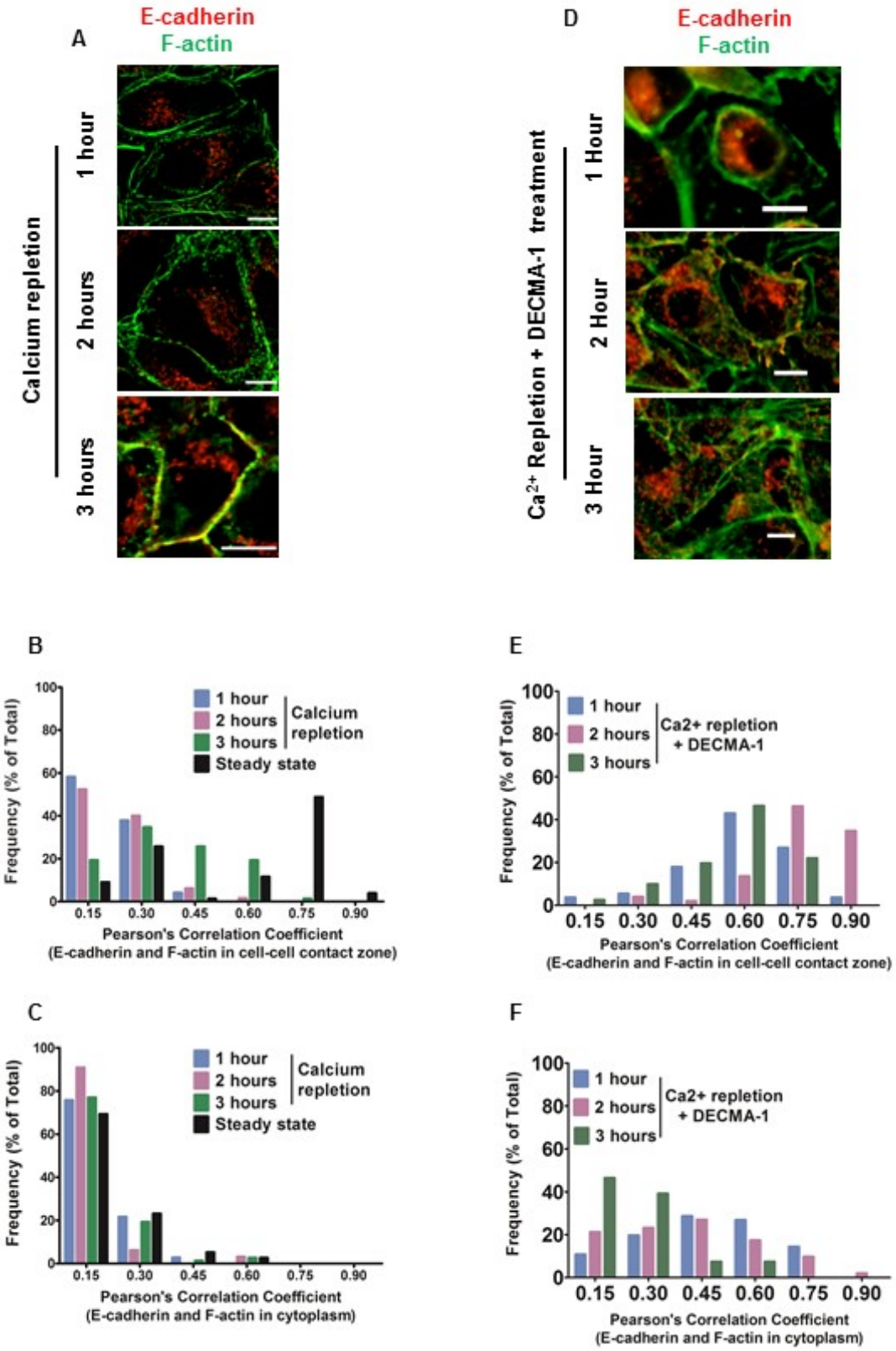
A
E-cadherin
F-actin
Calcium repletion
1 hour
2 hours
3 hours
D
E-cadherin
F-actin
Ca2+ Repletion + DECMA-1 treatment
1 Hour
2 Hour
3 Hour
B
Frequency (% of Total)
1 hour
2 hours
3 hours
Steady state
Calcium repletion
Pearson's Correlation Coefficient
(E-cadherin and F-actin in cell-cell contact zone)
E
Frequency (% of Total)
1 hour
2 hours
3 hours
Ca2+ repletion + DECMA-1
Pearson's Correlation Coefficient
(E-cadherin and F-actin in cell-cell contact zone)
C
Frequency (% of Total)
1 hour
2 hours
3 hours
Steady state
Calcium repletion
Pearson's Correlation Coefficient
(E-cadherin and F-actin in cytoplasm)
F
Frequency (% of Total)
1 hour
2 hours
3 hours
Ca2+ repletion + DECMA-1
Pearson's Correlation Coefficient
(E-cadherin and F-actin in cytoplasm)

Figure 7: E-cadherin and F-actin correlations at cell-cell contacts increase in an E-cadherin function dependent manner following *de novo* cell-cell contact. (**A**) **Top:Bottom**: Optical section of MDCK cells 1 hour, 2 hours and 3 hours after calcium repletion immunostained for E-cadherin (red) and F-actin (green). Scale bars = 10μm. (**B, C**) Frequency distributions of PCCs with bin size of 0.15 for E-cadherin and F-actin: (**B**) at cell-cell contacts, and (**C**) in the cytoplasm. N (sample size) values: 1 hour = 74, 2 hours = 65 and 3 hours = 78. (**D**) Optical sections of MDCK cells 1, 2 and 3 hours after calcium repletion with DECMA-1 (E-cadherin function blocking antibody) immunostained for E-cadherin (red) and F-actin (green). Scale bars = 10μm. (**E, F**) Frequency distributions of PCCs with bin size of 0.15 for E-cadherin and F-actin: (**E**) at cell-cell contacts and (**F**) in the cytoplasm. N (sample size) values: 1 hour = 56, 2 hours = 52 and 3 hours = 41. I would like to acknowledge Lissette Cruz for acquiring the images shown in panel **A** and calculating the PCC values.

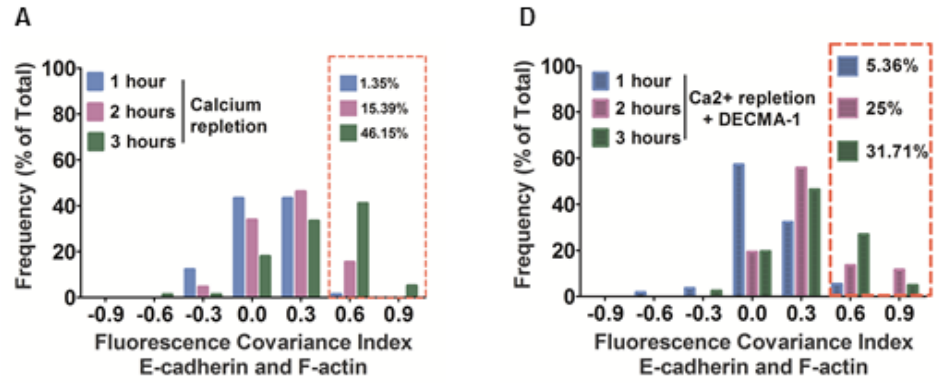
A
Frequency (% of Total)
1 hour
2 hours
3 hours
Calcium repletion
1.35%
15.39%
46.15%
Fluorescence Covariance Index
E-cadherin and F-actin
D
Frequency (% of Total)
1 hour
2 hours
3 hours
Ca2+ repletion + DECMA-1
5.36%
25%
31.71%
Fluorescence Covariance Index
E-cadherin and F-actin

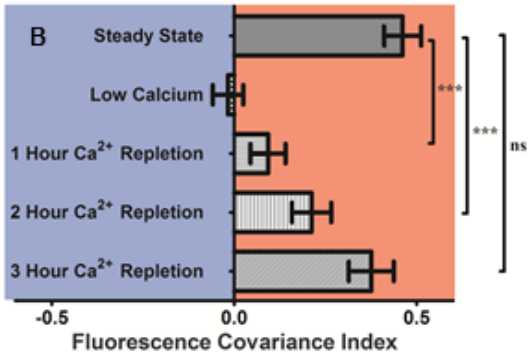
B
Steady State
Low Calcium
1 Hour Ca2+ Repletion
2 Hour Ca2+ Repletion
3 Hour Ca2+ Repletion
***
***
ns
Fluorescence Covariance Index

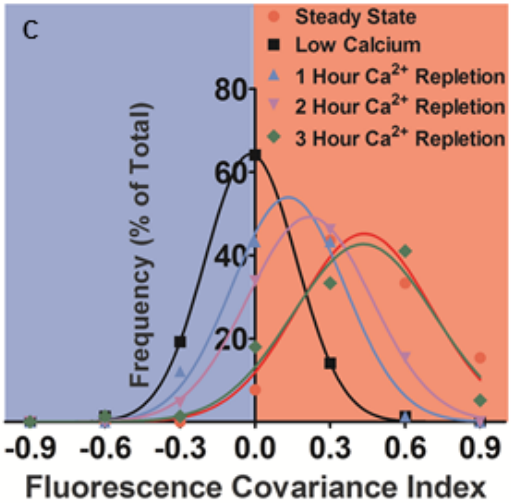
C
Steady State
Low Calcium
1 Hour Ca2+ Repletion
2 Hour Ca2+ Repletion
3 Hour Ca2+ Repletion
Frequency (% of Total)
Fluorescence Covariance Index

Figure 8: Quantifying adherens junction assembly/disassembly dynamics using FCI analysis of E-cadherin and F-actin. (**A**) Frequency distributions of FCI values for E-cadherin and F-actin in multiple cells during a calcium repletion experiment. Red box indicates percentage of cells with high FCI values (0.5 – 1.0) at 1, 2 and 3 hours after calcium repletion. (**B**) Mean FCI values for data in (**A**). Bars represent mean ± 95% CI. A Kruskal-Wallis test (excluding low calcium data set) yielded a p value < 0.0001 and Dunn's post-hoc multiple comparison test results are indicated on the graph (*** $p <$ 0.001, *ns*: not significant). (**C**) Gaussian best fits of the frequency distributions in (**A**). R^2 values: steady state: 0.9575, low calcium: 0.9994, after calcium repletion: 1 hour: 0.9808, 2 hours: 0.9988, 3 hours: 0.9371. (**D**) Frequency distributions of FCI values for E-cadherin and F-actin in multiple cells during a calcium repletion experiment with E-cadherin function blocking antibody. Red box indicates percentage of cells with high FCI values (0.5 – 1.0) at 1, 2 and 3 hours after calcium repletion.

E-cadherin at cell-cell contacts progressively switches to adhesion activated isoform during adherens junction maturation

E-cadherin exists in various conformational states, whose abundance depends on several factors including the presence of extracellular calcium, and the phosphorylation state of p120-catenin. These isoforms can be distinguished by different antibodies (Petrova et al., 2012). DECMA-1 is a rat monoclonal E-cadherin function blocking antibody that binds to an extracellular domain of the protein in the presence of calcium, while the mouse monoclonal antibody clone 36 (from BD Biosciences) detects adhesion activated E-cadherin (Chen and Chen, 2009). Activation of E-cadherin to an adhesion competent conformation exposes the cytoplasmic epitope for the clone 36 mouse monoclonal antibody (Petrova et al., 2012). In order to determine the extent of adhesion activated E-cadherin at cell-cell contacts during adherens junction assembly and maturation, E-cadherin was double labeled with DECMA-1 and clone 36 antibodies during a calcium repletion experiment. Cells in steady state show a significant proportion of E-cadherin present at the cell-cell contacts stained by DECMA-1 is in fact adhesion activated, and is co-stained by clone 36 antibody (**Figure 9A**, steady state). However, during adherens junction formation following calcium repletion, DECMA-1 staining localizes to cell-cell contacts to a greater extent than clone 36 antibody staining (**Figure 9A**, calcium repletion), Additionally, a progressive increase in clone 36 antibody staining at cell-cell contacts is observed during calcium repletion, indicating E-cadherin becomes adhesion activated during the assembly of adherens junctions. In order to determine the extent of covariance between F-actin and E-cadherin stained with either DECMA-1 or clone 36, cells were co-labelled with fluorescently tagged phalloidin. A map of the

positive *P*roduct of *D*ifferences from *M*ean (+PDM) shows higher correlations in the cell-cell contact zone between DECMA-1 and F-actin compared to clone 36 and F-actin (**Figure 9A′** arrows). Correspondingly, PCCs at the cell-cell contact sites between clone 36 and F-actin, and DECMA-1 and F-actin show a small but significant variation at all time points during calcium repletion (**Figure 9B**). Since clone 36 only recognizes adhesion activated E-cadherin, which is a subset of the E-cadherin present at cell-cell contacts, the PCC values between clone 36 and F-actin are lower than those between DECMA-1 and F-actin. Adhesion competent (or activated) E-cadherin is required to anchor adherens junctions to F-actin. Hence, clone 36 antibody was used to assess the covariance of E-cadherin and F-actin and the corresponding FCI values (**Figures 1-8**) were used as a measure of adherens junction assembly/disassembly.

As a corollary to the above results, the extent of E-cadherin that was adhesion activated at cell-cell contacts during adherens junction assembly was assessed. An increasing correlation is observed between E-cadherin fluorescence intensities detected with clone 36 and DECMA-1 during adherens junction assembly and maturation (**Figure 10**). This indicates that E-cadherin localized to the cell-cell contacts during the initial phases of adherens junction assembly is largely adhesion inactive. The gradual increase in correlation between DECMA-1 and clone 36 staining at cell-cell contacts indicates a significant proportion of E-cadherin switches to an adhesion activated from following its localization to cell-cell contacts.

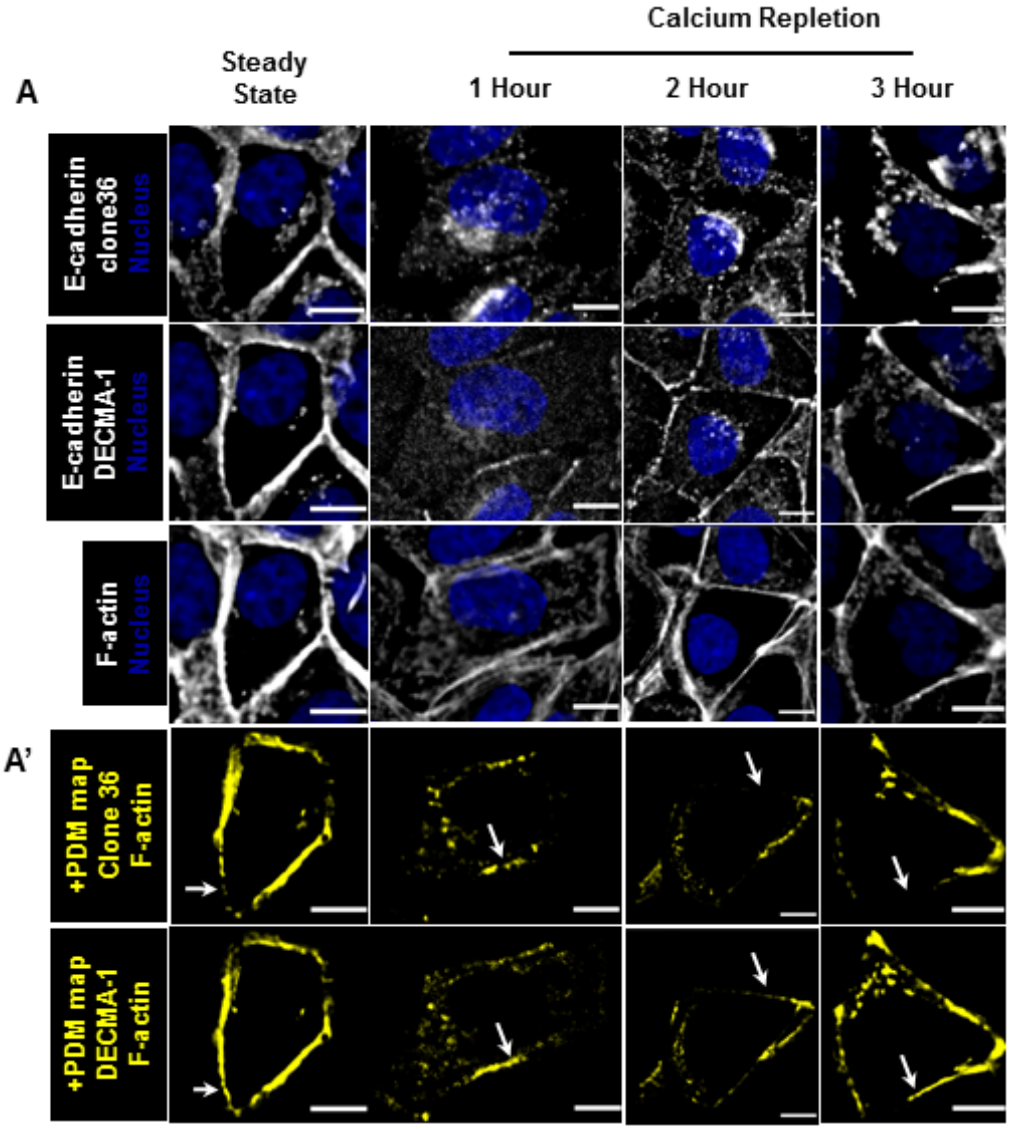
Calcium Repletion
A
Steady State
1 Hour
2 Hour
3 Hour
E-cadherin clone36 Nucleus
E-cadherin DECMA-1 Nucleus
F-actin Nucleus
A'
+PDM map Clone 36 F-actin
+PDM map DECMA-1 F-actin

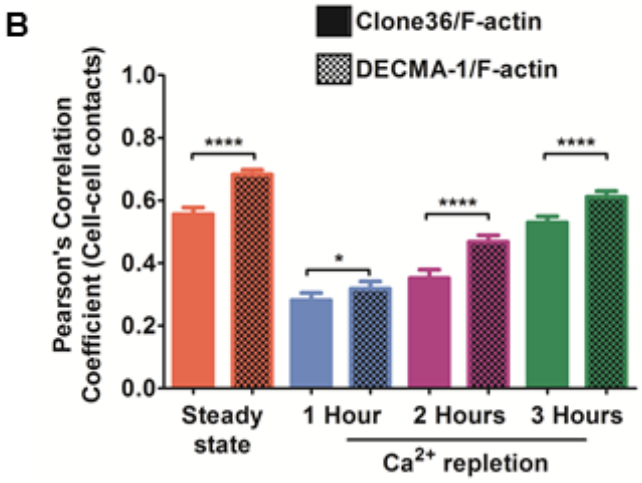
B
Clone36/F-actin
DECMA-1/F-actin
Pearson's Correlation Coefficient (Cell-cell contacts)
1.0
0.8
0.6
0.4
0.2
0.0
****
*
****
****
Steady state
1 Hour
2 Hours
3 Hours
Ca2+ repletion

Figure 9: Detection of adhesion activated E-cadherin during *de novo* adherens junction assembly. (**A**) **Left to right:** Optical sections representing MDCK cells in steady state; and 1 hour, 2 hours and 3 hours after calcium repletion. **Top to bottom:** Immunostaining with clone 36 mouse monoclonal antibody, DECMA-1 rat monoclonal antibody, and F-actin. (**A′**) +PDM maps for images shown in (**A**). **Top panel:** clone 36 and F-actin; **Bottom panel:** DECMA-1 and F-actin. White arrows point to areas with low signal for clone 36, and correspondingly a low covariance with F-actin compared to covariance between DECMA-1 and F-actin. (**B**) Changes in PCC values at cell-cell contacts for E-cadherin and F-actin during a calcium switch experiment. **Solid bars:** Clone 36 and F-actin; **Patterned bars:** DECMA-1 and F-actin. N (sample size) values: Steady state = 123, 1 hour = 113, 2 hours = 115 and 3 hours = 120. Independent student's t-test with Welch's correction was performed for individual pairs of data (* $p < 0.05$, **** $p < 0.0001$). Error bars represent mean ± 95% CI. I would like to acknowledge Lissette Cruz for help with organizing the images shown in panel **A** and **A′**.

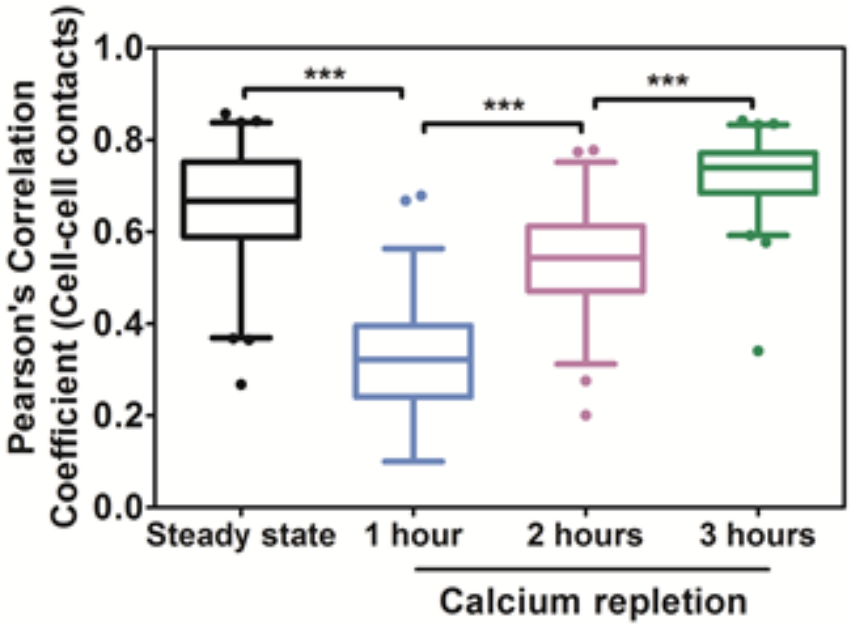
Pearson's Correlation
Coefficient (Cell-cell contacts)
1.0
0.8
0.6
0.4
0.2
0.0
***
***
***
Steady state
1 hour
2 hours
3 hours
Calcium repletion

Figure 10: Correlation analysis between adhesion activated and total E-cadherin at cell-cell contacts during *de novo* adherens junction assembly. Pearson's Correlation Coefficients for E-cadherin stained with clone 36 and DECMA-1 following calcium repletion. A Kruskal-Wallis test gave $p < 0.0001$. Dunn's post-hoc multiple comparison test results with *** $p < 0.001$ are indicated on the graph. N (sample size) values: steady state = 123, 1 hour = 113, 2 hours = 115 and 3 hours = 120.

Fluorescence covariance analysis quantifies minimal cadherin-catenin complex assembly in the perinuclear cytoplasm and subsequent accumulation at cell-cell contacts following *de novo* contact

E-cadherin binds β-catenin, which then binds α-catenin in the ER-golgi compartments prior to its trafficking to the baso-lateral surface of contacting epithelial cells (Chen et al., 1999; Curtis et al., 2008; van Roy and Berx, 2008). A significant proportion of E-cadherin localizes with β-catenin and α-catenin in the cytoplasm and correspondingly, positive correlations are observed in this compartment between E-cadherin and β-catenin, and E-cadherin and α-catenin, at 1 and 2 hours following calcium repletion (**Figure 11A and B**, 1 and 2 hours). Conversely, increasing co-localization between E-cadherin and β-catenin, and E-cadherin and α-catenin is observed along with increasing positive correlations for the two combinations of molecules at cell-cell contacts from 1 through 3 hours after calcium repletion (**Figure 11A, B**). Also, positive cytoplasmic correlations progressively reduced, which together with the increase in correlations at cell-cell contacts indicate trafficking of the minimal cadherin-catenin complex from the perinuclear biosynthetic compartment to sites of adherens junction assembly. Frequency distribution plots of FCI values for the cadherin-catenin complexes show a progressive increase in the accumulation of cadherin-catenin complexes at the cell-cell contacts (**Figure 11C, D**). These data indicate FCI values can be used to track the localization of pre-assembled minimal cadherin-catenin complexes from the perinuclear cytoplasm to the cell-cell contacts.

Microtubules are known to interact with adherens junction complexes with a geometry perpendicular to the actin filaments at these intercellular junctions (Bellett et

al., 2009; Harris and Tepass, 2010; Ligon et al., 2001; Shaw et al., 2007; Takeichi, 2014). The microtubule network at cell-cell contacts is significantly less dense than the cortical F-actin network (**Figure 12A**, α-tubulin staining in steady state, compare with **Figure 2B** F-actin staining). This suggests that the extent of correlation between microtubules and adherens junction components should be significantly lower than F-actin and adherens junction components. As per the prediction, MDCK cells in steady state show some positive correlations between β-catenin and α-tubulin at cell-cell contacts. However, the extent of this correlation is much lower than between E-cadherin and F-actin (**Figure 12A** compare +PDM map at steady state to **Figure 2B** +PDM map for E-cadherin and F-actin). Interestingly, 1 hour following calcium repletion, punctate positive correlations for β-catenin and α-tubulin are observed in the cytoplasm (**Figure 12A** 1 hour, arrowheads). These cytoplasmic correlations decrease 2 and 3-hours after calcium repletion (**Figure 12A, B**). Given cadherin-catenin complexes are assembled in the perinuclear cytoplasm following translation (Chen et al., 1999; Curtis et al., 2008), the positive correlation of β-catenin with α-tubulin in the cytoplasm 1 hour following calcium repletion likely represents cadherin-catenin complexes being trafficked along microtubules. Most cells show little positive correlation between α-tubulin and β-catenin at cell-cell contact sites through the course of calcium repletion for 3 hours (**Figure 12C**). Some punctate positive correlations were observed at a few cell-cell contacts 3 hours after calcium repletion (**Figure 12A,** 3 hour), but the overall correlation coefficients were low (**Figure 12B, C**). Lastly, frequency distribution plots of FCI values for β-catenin and α-tubulin fit normal distributions centered at zero for low calcium, 1, 2 and 3-hours after calcium repletion. A small positive mean FCI value for steady state distribution demonstrates microtubules

associate with adherens junctions, albeit on a slower time scale and to a lesser extent than actin filaments (**Figure 12D**). The following four conclusions can be drawn from these results. First, microtubule and adherens junction interactions require longer time scales than adherens junctions anchoring to actin. Second, the extent of microtubule and adherens junction interaction is lower than F-actin and adherens junction interaction at cell-cell contacts. Third, the minimal cadherin-catenin complex assembles in the perinuclear cytoplasm, and likely traffics on microtubules before reaching the cell-cell contact. Lastly, given the frequency distributions of FCI values for α-tubulin and β-catenin are all almost perfectly centered at zero, the right shift seen in the frequencies of FCI values for the cadherin-catenin complexes represents a biologically significant accumulation of these complexes at the cell-cell contacts, in spite of the very low frequency of high FCI values (**Figure 11C, D**).

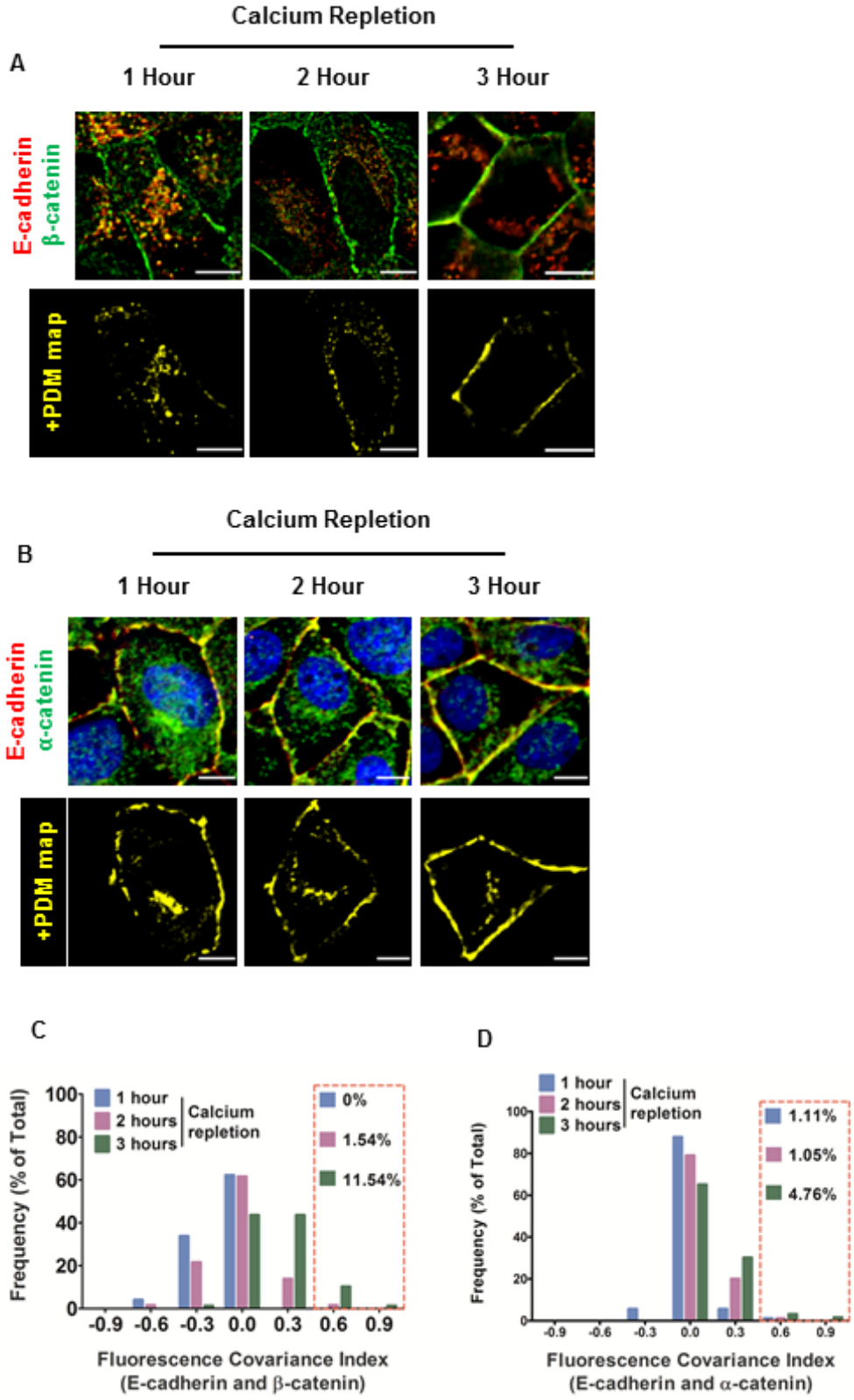
Calcium Repletion
A
1 Hour
2 Hour
3 Hour
E-cadherin
β-catenin
+PDM map
Calcium Repletion
B
1 Hour
2 Hour
3 Hour
E-cadherin
α-catenin
+PDM map
C
Frequency (% of Total)
100
80
60
40
20
0
1 hour
2 hours
3 hours
Calcium repletion
0%
1.54%
11.54%
-0.9 -0.6 -0.3 0.0 0.3 0.6 0.9
Fluorescence Covariance Index
(E-cadherin and β-catenin)
D
Frequency (% of Total)
1 hour
2 hours
3 hours
Calcium repletion
1.11%
1.05%
4.76%
Fluorescence Covariance Index
(E-cadherin and α-catenin)

Figure 11: Quantifying perinuclear association and subsequent cell-cell contact localization of the minimal cadherin-catenin complex (E-cadherin, β-catenin and α-catenin). (**A**) **Top panel:** Optical sections of MDCK cells in 1 hour, 2 hours and 3 hours after calcium repletion immunostained for E-cadherin (red) and β-catenin (green); **Bottom panel:** +PDM maps for the images shown in the **top panel**. (**B**) **Top panel:** Optical sections of MDCK cells in 1 hour, 2 hours and 3 hours after calcium repletion immunostained for E-cadherin (red) and α-catenin (green); **Bottom panel:** +PDM maps for the images shown in the **top panel**. Scale bar = 10μm. (**C**) Frequency plots of FCI values for E-cadherin and β-catenin at 1 hour (N = 74), 2 hours (N = 65) and 3 hours (N = 78) after calcium repletion. (**D**) Frequency plots of FCI values for E-cadherin and α-catenin at 1 (N = 90), 2 hours (N = 95) and 3 hours (N = 63 cells) after calcium repletion. Bin width = 0.3. Red boxes indicate the percentage of high FCI values (0.5 – 1.0) for each case. I would like to acknowledge Lissette Cruz for acquiring the images shown in panel **A** and calculating PCC values for the same.

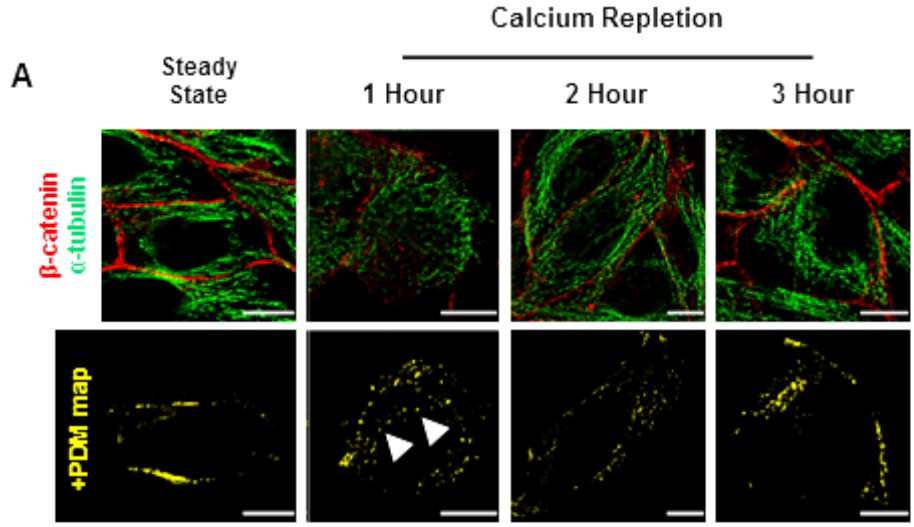
A
Calcium Repletion
Steady State
1 Hour
2 Hour
3 Hour
β-catenin
α-tubulin
+PDM map

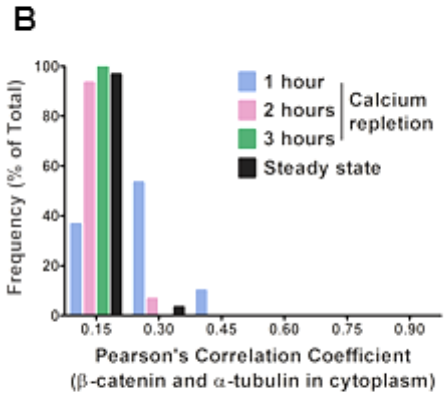
B
Frequency (% of Total)
1 hour
2 hours
3 hours
Steady state
Calcium repletion
Pearson's Correlation Coefficient
(β-catenin and α-tubulin in cytoplasm)

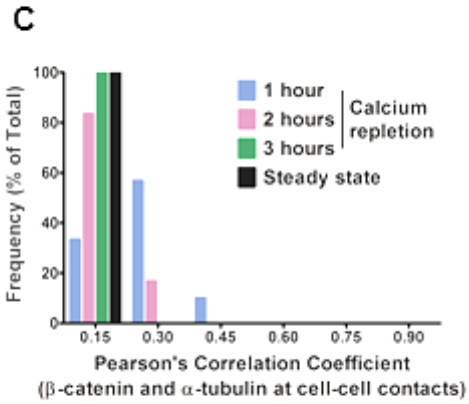
C
Frequency (% of Total)
1 hour
2 hours
3 hours
Steady state
Calcium repletion
Pearson's Correlation Coefficient
(β-catenin and α-tubulin at cell-cell contacts)

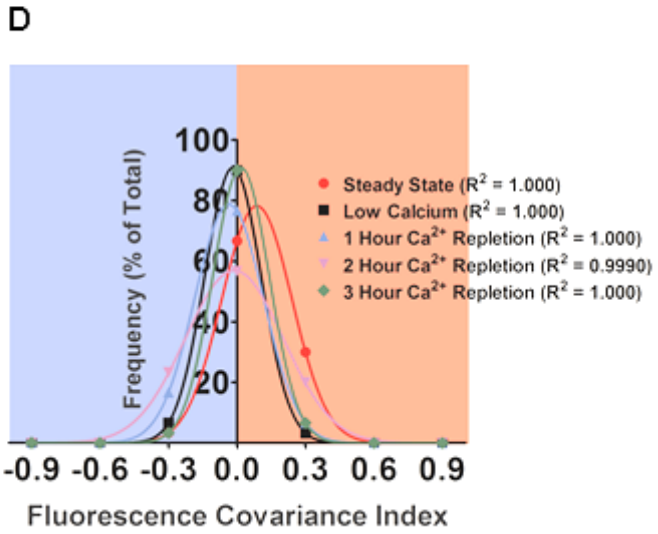
D
Frequency (% of Total)
Steady State (R² = 1.000)
Low Calcium (R² = 1.000)
1 Hour Ca²⁺ Repletion (R² = 1.000)
2 Hour Ca²⁺ Repletion (R² = 0.9990)
3 Hour Ca²⁺ Repletion (R² = 1.000)
Fluorescence Covariance Index

Figure 12: Quantifying α-tubulin and β-catenin interactions during adherens junction assembly. (**A**) **Top panel:** Optical sections of MDCK cells in steady state, 1, 2 and 3 hours after calcium repletion immunostained for α-tubulin (green) and β-catenin (red). Scale bar = 10μm. **Bottom panel:** +PDM maps for the images shown in the top panel. Arrowheads in 1 hour calcium repletion indicate punctate positive correlations in the cytoplasm. (**B, C**) Frequency distributions of PCC values for β-catenin and α-tubulin in: (**B**) cytoplasm and (**C**) cell-cell contact, during a calcium repletion experiment. Bin width = 0.15. (**D**) Gaussian best fit plots of FCI frequency distributions for α-tubulin and β-catenin during a calcium switch. Bin width = 0.3. N (sample size) value for each time point was 30. I would like to acknowledge Lissette Cruz for acquiring the images shown in panel **A** and calculating PCC values.

FCI analysis of α-catenin and F-actin correlates with established tissue tension profile during assembly and maturation of adherens junctions

α-catenin is a tension sensitive component of two intercellular adhesion systems: adherens junctions and tight junctions (Buckley et al., 2014; Rajasekaran et al., 1996; Rajasekaran and Rajasekaran, 2003; Takeichi, 2014; Yonemura et al., 2010). In a polarized epithelial tissue, adherens junctions are subject to a circumferential myosin IIB dependent tension restricted to the apical region (Yonemura et al., 2010) and myosin IIA dependent tension along the baso-lateral membrane (Wu et al., 2014). As a result, the baso-lateral plasma membranes develop protrusions which contain what appear as lateral/*en face* adherens junctions (Wu et al., 2015; Yonemura et al., 1995). On the other h, and during the initial phases of adherens junction assembly, cells form lamellar overlaps which contain adherens junction components. These nascent adhesion complexes are then trafficked in a basal-to-apical manner as cells lift and polarize (Hong et al., 2010; Kametani and Takeichi, 2007). Atomic force microscopic measurements in an assembling epithelial monolayer have shown that myosin II dependent tension peaks between 2 and 3 hours following calcium repletion (Harris et al., 2014). The two tension profiles, myosin IIB dependent apical and myosin IIA dependent baso-lateral tension components balance each other resulting in the formation of a polarized columnar epithelium. In view of these findings and evidence that α-catenin binding to F-actin is tension sensitive, cells were co-stained for α-catenin and F-actin and FCI analysis was carried out to determine the dynamics of interactions between these two molecules during *de novo* adherens junction assembly. Positive correlations in the cytoplasm are observed at steady state, 1 and 3 hours after calcium repletion, which appear as contributions from

lamellar overlaps and lateral adhesions, respectively (**Figure 13A** arrowheads in +PDM maps). However, 2 hours after calcium repletion cells show significantly less cytoplasmic correlations (**Figure 13A**, 2 hours). Additionally, calcium chelation results in loss of high frequency FCI values (≈ 36% at steady state compared to 0% in low calcium) indicating disassembly of adherens junction complexes results in decoupling of α-catenin and F-actin interaction (**Figure 13B**). The proportion of cells with high FCI values for α-catenin and F-actin is greatest at 2 hours following calcium repletion (**Figure 13C**, ≈ 40% at 2 hours compared to ≈ 12% and ≈ 28% at 1 and 3 hours, respectively). This increase is due to a corresponding decrease (left shift in frequency plot) in cytoplasmic PCC values (**Figure 13D**). Although PCC values at cell-cell contacts during steady state and 3 hours after calcium repletion are slightly right shifted compared to 2 hours after calcium repletion (**Figure 13E**), the contribution from lateral adhesions appearing in the cytoplasmic compartment following polarization decrease the corresponding FCI values. These data demonstrate FCI values of α-catenin and F-actin correlate with established tension profiles during the assembly and maturation of adherens junctions (**Figure 13F, G**).

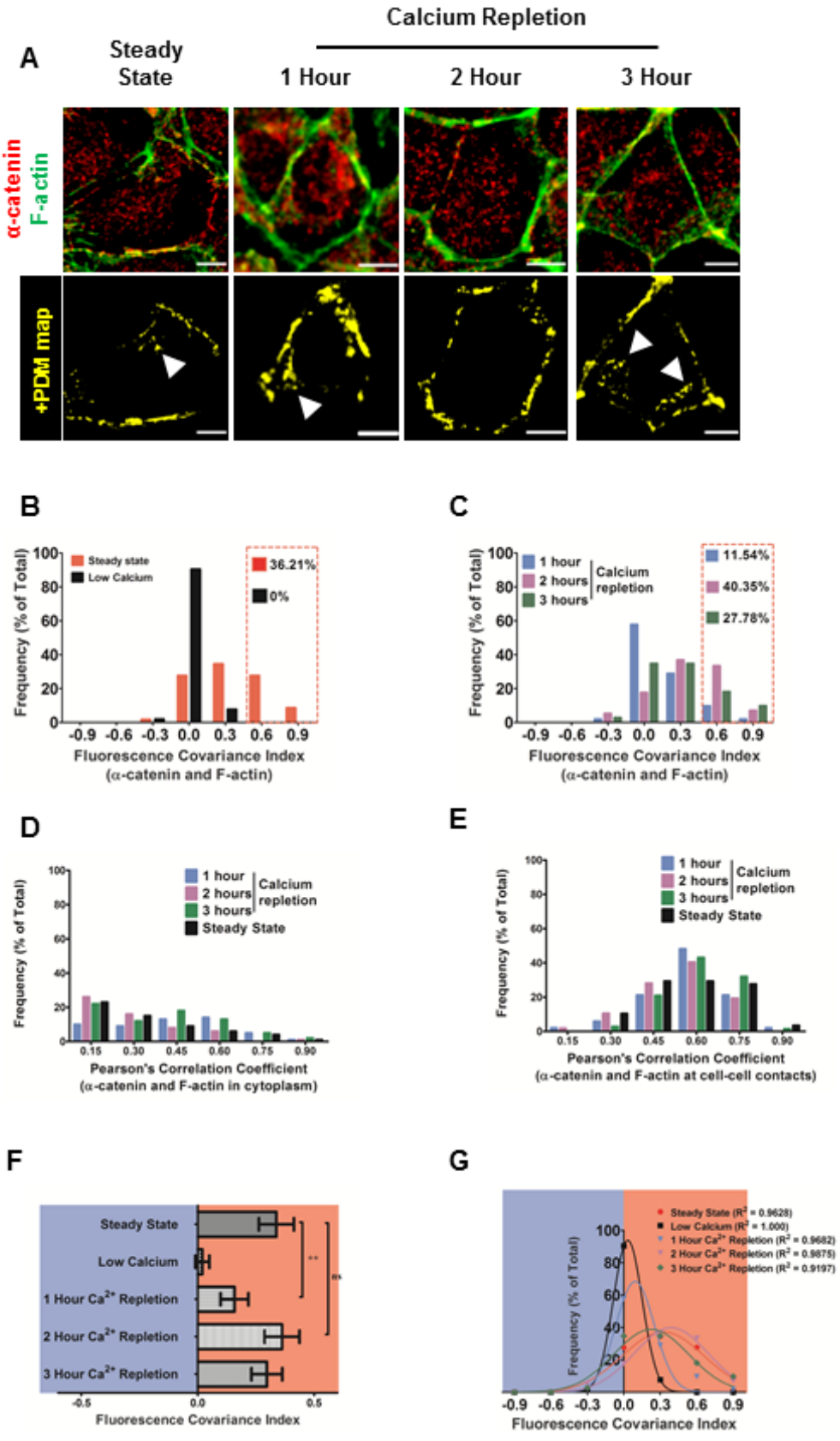
A
Steady State
Calcium Repletion
1 Hour
2 Hour
3 Hour
α-catenin
F-actin
+PDM map
B
Steady state
Low Calcium
36.21%
0%
Frequency (% of Total)
Fluorescence Covariance Index
(α-catenin and F-actin)
C
1 hour
2 hours
3 hours
Calcium repletion
11.54%
40.35%
27.78%
Frequency (% of Total)
Fluorescence Covariance Index
(α-catenin and F-actin)
D
1 hour
2 hours
3 hours
Calcium repletion
Steady State
Frequency (% of Total)
Pearson's Correlation Coefficient
(α-catenin and F-actin in cytoplasm)
E
1 hour
2 hours
3 hours
Calcium repletion
Steady State
Frequency (% of Total)
Pearson's Correlation Coefficient
(α-catenin and F-actin at cell-cell contacts)
F
Steady State
Low Calcium
1 Hour Ca2+ Repletion
2 Hour Ca2+ Repletion
3 Hour Ca2+ Repletion
Fluorescence Covariance Index
G
Steady State (R2 = 0.9628)
Low Calcium (R2 = 1.000)
1 Hour Ca2+ Repletion (R2 = 0.9682)
2 Hour Ca2+ Repletion (R2 = 0.9875)
3 Hour Ca2+ Repletion (R2 = 0.9197)
Frequency (% of Total)
Fluorescence Covariance Index

Figure 13: Quantifying α-catenin and F-actin interactions during *de novo* adherens junction assembly. (**A**) **Top panel:** Optical section of MDCK cells in steady state, 1 hour, 2 hours and 3 hours after calcium repletion immunostained for F-actin (green) and α-catenin (red). **Bottom panel:** +PDM maps for the images shown in **top panel**. Scale bar = 10μm. (**B, C**) Frequency plots for FCI values of α-catenin and F-actin: (**B**) steady state and low calcium; (**C**) 1 hour, 2 hours and 3 hours after calcium repletion. Bin width = 0.3. Red boxes indicate the percentage of cell with high FCI values (0.5 – 1.0). (**D, E**) Frequency distributions of PCC values for α-catenin and F-actin: (**D**) in the cytoplasm and (**E**) at cell-cell contacts, during a calcium repletion experiment. Bin width = 0.15. N (sample size) values: steady state = 58, low calcium = 52, 1 hour = 52, 2 hours = 57 and 3 hours = 72. (**F**) Changes in FCI values for α-catenin and F-actin during a calcium repletion experiment. Error bars represent mean ± 95% CI. The result of a non-parametric Kruskal-Wallis test (excluding low calcium data set) gives a p value = 0.0003. The results of Dunn's post-hoc multiple comparison test are indicated on the graph (*** $p < 0.001$, *ns*: not significant). (**G**) Gaussian best fits for the frequency distributions for FCI values in **B and C**.

Live cell FCI analysis tracks adherens junction assembly/disassembly dynamics with a 5-minute temporal resolution

Expressing fluorescently tagged proteins allows high temporal resolution analysis of single cells within a living tissue. Using MDCK cells expressing E-cadherin-RFP and β-actin-eGFP, adherens junction assembly was tracked in live epithelial monolayers during calcium repletion experiments. β-actin was chosen since it is required for adherens junction assembly and is enriched at the cell-cell contact zone (Baranwal et al., 2012). The molecular mechanism of actin enrichment at cell-cell contacts involves localized β-actin translation (Gutierrez et al., 2014). This synthesis event provides sufficient local concentration of monomers to drive barbed end filament polymerization to assemble linear actin filaments. These filaments in turn are required to anchor nascent adherens junction complexes (Gutierrez et al., 2014; Rodriguez et al., 2006). Immediately following calcium repletion, three optical sections were acquired using widefield microscopy with an inter-plane distance of 3μm. Nearest neighbor de-blurring was used to reduce out of focus light in each optical section. The number of optical planes was limited by acquisition speed and phototoxicity. Five minute intervals between successive acquisitions provided good temporal resolution without any evidence of phototoxicity. Consistent with the data obtained using fixed cells, 2 to 3-hours after calcium repletion, +PDM maps show positive correlations between E-cadherin and β-actin at cell-cell contact zones (**Figure 14A**). Interestingly, positive correlations for E-cadherin and β-actin are observed in the cytoplasm for the first 6-hours after calcium repletion. These cytoplasmic correlations likely arise from the non-filamentous globular actin (G-actin) and perinuclear E-cadherin, both present in the perinuclear cytoplasm. This G-actin

population is thought to function as a storage compartment for monomers, which are incorporated into spatially localized dynamic filament populations (Cao et al., 1993). Plotting FCI values as a function of time shows an inflection point between 2 and 3-hours after calcium repletion (**Figure 14B** yellow arrow). This shift from negative to positive FCI values coincides with the appearance of cell-cell contact zone localized positive correlations consistent with the spatio-temporal dynamics of adherens junction assembly (**Figure 14A′**). During the transition from negative to positive FCI values, measurements were made every 5 minutes to determine adherens junction assembly kinetics with the highest possible temporal resolution for the experimental settings used. A smooth increase in positive correlation in the +PDM maps at cell-cell contact zones is observed during the course of 2 to 2.5 hours following calcium repletion (**Figure 14A′ and B′**). Importantly, this smooth increase in positive correlations is perturbed and delayed by adding E-cadherin function blocking antibody during calcium repletion (**Figure 15A**). Upon addition of E-cadherin function blocking antibodies, FCI values show a fluctuating trend for the first 4.5 hours after calcium repletion indicating, cycles of adherens junction assembly and disassembly without significant anchoring and maturation (**Figure 15B**). Additionally, PCC values at cell-cell contact zone and the cytoplasm are substantially reduced for the first 4.5 hours after calcium repletion with E-cadherin function blocking antibody (**Figure 15B′, B′′**). These results demonstrate live cell FCI analysis quantitates the dynamics of protein-protein interaction within 2 different subcellular compartments with high spatial and temporal resolution.

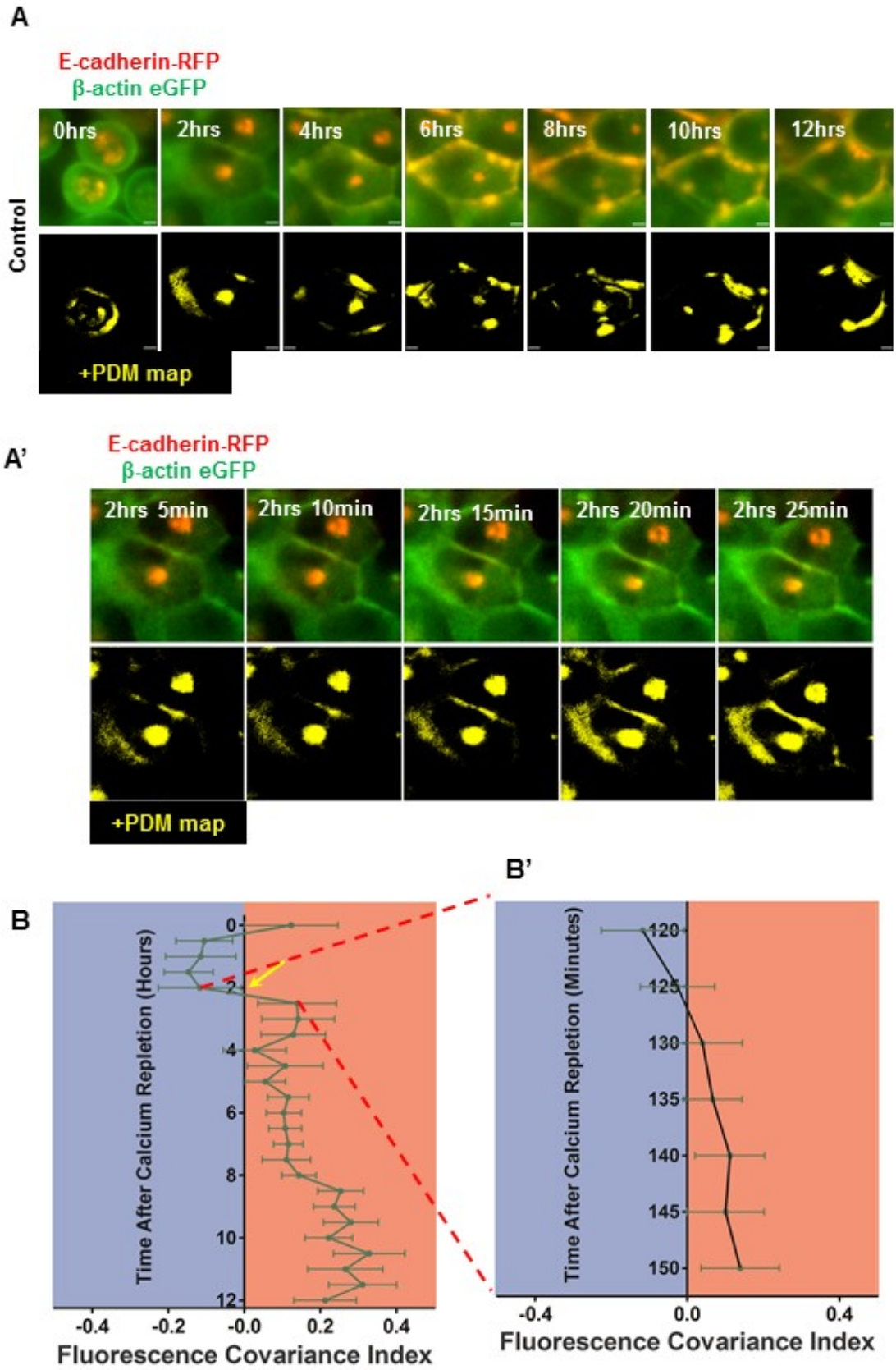
A
E-cadherin-RFP
β-actin eGFP
0hrs
2hrs
4hrs
6hrs
8hrs
10hrs
12hrs
Control
+PDM map
A'
E-cadherin-RFP
β-actin eGFP
2hrs 5min
2hrs 10min
2hrs 15min
2hrs 20min
2hrs 25min
+PDM map
B
B'
Time After Calcium Repletion (Hours)
0
2
4
6
8
10
12
-0.4
-0.2
-0.0
0.2
0.4
Fluorescence Covariance Index
Time After Calcium Repletion (Minutes)
120
125
130
135
140
145
150
-0.4
0.0
0.4
Fluorescence Covariance Index

Figure 14: Live cell FCI analysis of adherens junction assembly using fluorescent fusion tags. (**A**) **Top panel:** Montage of optical sections from a live cell movie (0 hour – 12 hours) showing MDCK cells expressing E-cadherin-RFP (red) and β-actin-eGFP (green) after calcium repletion. **Bottom panel:** +PDM maps of images from the **top panel**. **(A′) Top panel:** Montage of optical sections from a live cell movie (2 hours – 2.5 hours) showing MDCK cells expressing E-cadherin-RFP (red) and β-actin-eGFP (green) after calcium repletion. **Bottom panel:** +PDM maps of images from the **top panel**. (**B**) FCI values for E-cadherin-RFP and β-actin-eGFP plotted every 30 minutes after calcium repletion (N = 9). Arrow indicates the time at which FCI values shift from negative to positive. (**B′**) FCI values plotted every 5 minutes for E-cadherin-RFP and β-actin-eGFP between 2 and 2.5 hours after calcium repletion. Error bars indicate mean ± s.e.m. I would like to acknowledge Lissette Cruz for calculating PCC values.

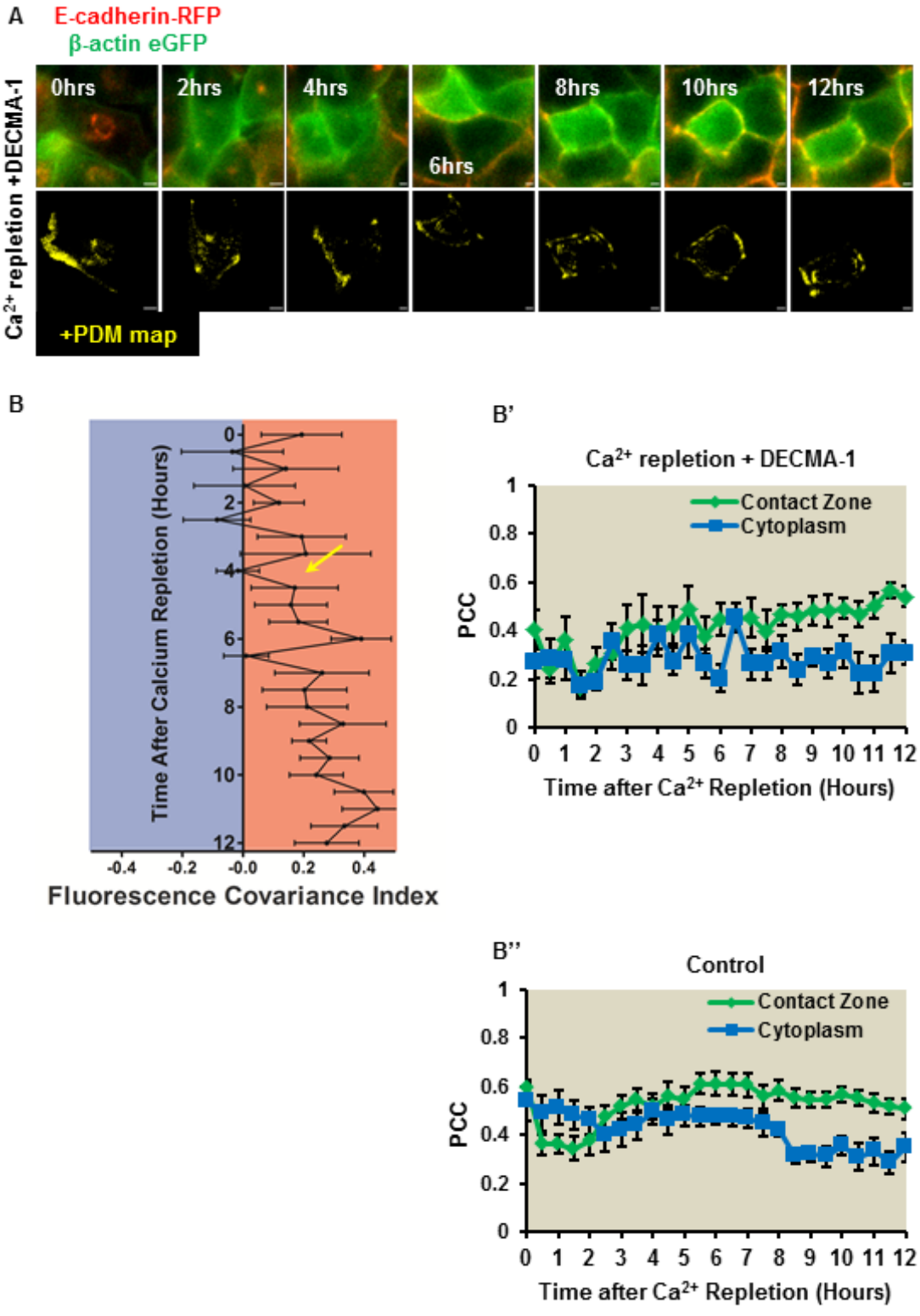
A
E-cadherin-RFP
β-actin eGFP
Ca2+ repletion +DECMA-1
0hrs
2hrs
4hrs
6hrs
8hrs
10hrs
12hrs
+PDM map
B
Time After Calcium Repletion (Hours)
Fluorescence Covariance Index
B'
Ca2+ repletion + DECMA-1
Contact Zone
Cytoplasm
PCC
Time after Ca2+ Repletion (Hours)
B''
Control
Contact Zone
Cytoplasm
PCC
Time after Ca2+ Repletion (Hours)

Figure 15: Effect of E-cadherin function on live cell FCI measurements. (**A**) **Top panel:** Montage of optical sections from a live cell movie (0 hour – 12 hours) showing MDCK cells expressing E-cadherin-RFP (red) and β-actin-eGFP (green) treated with DECMA-1 antibody after calcium repletion. **Bottom panel:** +PDM maps of images from the top panel. (**B**) FCI values plotted every 30 minutes for E-cadherin-RFP and β-actin-eGFP after calcium repletion (N = 6). Arrow indicates the time at which FCI is positive and remains positive through the rest of the experiment. Error bars indicate mean ± s.e.m. (**B′, B′′**) PCCs for β-actin-eGFP and E-cadherin-RFP in the contact zone (green curve) and cytoplasm (blue curve) plotted every 0.5 hours for: (**B′**) calcium repletion with E-cadherin function blocking antibody (DECMA-1), and (**B′′**) calcium repletion (Control). Error bars represent mean ± s.e.m. I would like to acknowledge Lissette Cruz for calculating PCC values in panels **B′** and **B′′**.

DISCUSSION

Why chose a Pearson's Correlation Coefficient based method to study macromolecular complex dynamics?

Analysis of subcellular co-localization to study the formation of protein complexes and protein-protein interactions is riddled with caveats and footnotes (Adler and Parmryd, 2010; Barlow et al., 2010; Bolte and Cordelieres, 2006; Zinchuk et al., 2013). In this thesis, a method based on Pearson's Correlation Coefficients is used to demonstrate various aspects of multi-protein complex assembly dynamics pertaining to the assembly of the adherens junction complex in epithelial cells. While, E-cadherin clustering and dynamics at adherens junctions have been studied using super-resolution light microscopy and FRAP analysis (de Beco et al., 2009; Wu et al., 2015), there have been few analysis tools to robustly study the spatial and temporal dynamics of macromolecular complexes such as adherens junctions. To date, the only available methods to study multi-protein complexes are those in a biochemists toolbox: immunoprecipitation, sub-cellular fractionation, protein cross-linking and pull down experiments. While the utility of these biochemical approaches is not discounted, they are not without their own technical caveats. Alternatively, Spatial Intensity Distribution Analysis (SpIDA) (Godin et al., 2011) can be utilized to assess clustering of transmembrane receptors such as E-cadherin during adherens junction assembly. However, the goal of the PCC based method presented here is to determine the dynamics of association of various components of a multi-protein complex during assembly, and not to quantitate the clustering aspect of a single component of such a complex. PCC

measurements offer a simple yet robust method to carry out "biochemical analysis on a microscope", thus having the advantage of being able to provide quantitative spatio-temporal data regarding macromolecular complexes. Fluorescence Covariance Index provides a quantitation of the asymmetry in correlation between two signals within two user defined sub-cellular compartments. The assumption is that the multi-protein complex which includes the two molecular components being studied forms preferentially in one of the sub-cellular compartments. While defining these two distinct sub-cellular compartments, one needs to bear in mind that the compartment with no protein complex assembly should have a very weak correlation. For instance, FCI analysis of β-catenin and F-actin during a calcium repletion assay, using the cytoplasm and cell-cell contact as the two compartments in the analysis violates this assumption. This is due to the fact that during later phases of adherens junction assembly, β-catenin is sequestered at the cell-cell contact zone by E-cadherin. F-actin is also predominantly present at the cell-cell interface in a polarized epithelium. As a result both signals in the cytoplasm are very low, causing the PCC in cytoplasm to be high (**Equation 3**). Consequently FCI is very low with a frequency distribution resembling the null hypothesis, where there is no preferred asymmetry in correlation in either compartment (data not shown). However, with the right choice of two proteins and sub-cellular compartments, several behaviors of the adherens junction complex have been quantitated using the FCI analysis. (1) extent of anchoring of the adherens junction complex to the actin cytoskeleton (for example, **Figures 7 and 8**); (2) tracking the extent of changes in activation of components of the complex over time (for example, **Figures 9 and 10**); (3) tracking the localization of minimal cadherin-catenin complexes from biosynthetic

compartment to sites of cell-cell adhesions (for example, **Figures 11 and 12**), (4) correlating the interactions of components of the complex which are tension sensitive to tissue tension profiles (for example, **Figure 13**); and (5) correlating the extent of anchoring of the adherens junction to the actin cytoskeleton with tissue barrier function (Cruz et al., 2015) (**See also, Chapter 3**).

Extending the utility of the fluorescence covariance analysis to other biologically important multi-protein complexes

The adherens junction complex has a mechano-transduction module: α-catenin and F-actin. Polarized epithelia demonstrate apico-lateral and baso-lateral acto-myosin tension profiles mediated by myosin IIB and myosin IIA, respectively (Smutny et al., 2010; Wu et al., 2014). The balance between these two tension profiles determines whether cells form a functional epithelial tissue (Smutny et al., 2010) or extrude out of the tissue (Behrndt and Heisenberg, 2014). Acto-myosin tension in the basolateral compartment results in the appearance of lateral/*en face* adhesions or protrusions, while the apico-lateral tension acts to keep the apical zonula adherens intact. FCI analysis is a viable and simple method to study the relative contributions of these two tension components by assessing the interaction of α-catenin and F-actin in these two sub-cellular compartments, using the antibody which recognizes the conformational change in α-catenin which occurs due to acto-myosin tension (Yonemura et al., 2010).

E-cadherin exists in multiple conformational states (Chen and Chen, 2009; Petrova et al., 2012). Adhesion activated E-cadherin is only a subset of E-cadherin present at the cell-cell contacts (**Figure 10**). Given, E-cadherin function is subject to

regulation and can potentially regulate epithelial tissue fate without any marked changes in its transcriptional regulation (Chen and Chen, 2009; Najy et al., 2008; Thiery, 2003), a correlation analysis of adhesion activated E-cadherin and its other conformational states could potentially be used as a diagnostic tool to determine the extent of functional E-cadherin mediated adhesions in epithelial cancers. Further, adhesion activated E-cadherin is a scaffold for several signaling molecules including Src family of kinases (McLachlan and Yap, 2011). It would be interesting to determine whether other conformational states of E-cadherin can function as a scaffold for these signaling molecules. These questions can be tested using the FCI method to analyze the covariance of various E-cadherin conformational states with the appropriate signaling molecules believed to be associated with functional E-cadherin.

This novel technique provides a cost effective, reliable and robust method to assess the extent to which proteins are part of a complex in specific sub-cellular compartments within the resolution limit of a light microscope. The technique facilitates quantitative comparison of the extent of inhibition/stimulation of protein complex assembly by perturbing different nodes along intracellular signaling pathways. One such example using the formation of the good old adherens junction complex is: the effect of E-cadherin function on adherens junctions (see **Figures 7 and 15**). Another novel node in the formation of adherens junctions is localization of β-actin translation to cell-cell contacts (Cruz et al., 2015; Gutierrez et al., 2014). Such experiments with other multi-protein complexes like the tight junctions (McNeil et al., 2006), apico-basal polarity determinants (Baum and Georgiou, 2011), to name a couple, will answer key questions regarding the dynamics of assembly/disassembly of these complexes.

Live cell FCI analysis: a utilitarian approach to study multi-protein complex dynamics in living cells

Studying protein-protein interactions in living cells is typically carried out using *F*luorescence *R*esonance *E*nergy *T*ransfer (FRET) or *F*luorescence *C*orrelation *S*pectroscopy (FCS) (Aoki et al., 2013; Trepat et al., 2007). However, these techniques require that the two proteins have direct interaction (effective distance for FRET imaging is 5-10nm). Proteins that do not directly interact, but are part of large multi-protein complexes with several components cannot be studied using either FRET or FCS approaches. Live cell FCI analysis provides a high temporal resolution picture of protein-protein interactions in live tissues without the limitations of FRET experiments (for example, **Figure 14**). Using the appropriate fluorescent fusion proteins, this analysis can be easily extended to study for instance, focal adhesion complex assembly dynamics at the leading edge of motile cells, or tight junction assembly in epithelial cells. In conclusion, the FCI analysis is a simple, robust and reliable tool to quantitate the dynamics of assembly of multi-protein complexes within specific sub-cellular compartments. Since our publication of this technique, collaborators in Mexico (Dr. L González Mariscal), and at Rutgers University, Newark (Dr. Nan Gao) have used variations of this approach to study protein interactions such as 14-3-3 isoforms and ZO-1, and Rab8a and Gpr177, respectively. Since a custom code in MATLab is used to carry out parts of the analysis, I invoke the equivalent of a "beerware license" for anyone wishing to use this script in the future. If you are wondering what a beerware license is, here is the Wikipedia definition "Should the user of the product meet the author and

consider the software useful, they are encouraged to either buy the author a beer "in return" or drink one themselves.”

MATERIALS AND METHODS

Cell culture

MDCK (Madin-Darby Canine Kidney, ATCC# CCL - 34) cells were cultured in DMEM (Corning Cellgro®) containing 10% FBS (Life Technologies, Gibco), penicillin (100 I.U./mL) and streptomycin (100µg/mL) (Corning Cellgro®). For calcium switch experiments, cells were seeded at a density of 250,000 cells per well in a 6-well plate on glass coverslips (22 X 22 mm) for fixed cell experiments, and 35 mm dishes with glass bottom dishes (MatTek Corp.) for live cell experiments. Cells were grown for 2 d at 37 °C, 95% humidity and 5% CO_2 to form a monolayer.

Transfection and generation of stable cell lines

MDCK cells stably expressing E-cadherin-RFP (a gift from Dr. James Nelson, Stanford) were transfected with the plasmid TC-eGFP-β-actin full length (Addgene ID: 27123) using Lipofectamine 2000 (Life Technologies) according to manufacturer guidelines. Cells co-expressing eGFP-β-actin and E-cadherin-RFP were sorted using FACS and used for live-cell experiments. These cells were cultured in regular growth medium along with 500µg/ml final concentration of G418 to maintain the expression of the reporter genes.

Calcium switch

To disassemble the adherens junctions in monolayers, the cells were incubated with DMEM (no serum or antibiotics) containing 4 mM EGTA for 1 hour at 37 °C, 95%

humidity and 5% CO_2. Cells were then returned to regular growth media (calcium repletion) and fixed at various time points of the calcium switch experiment (steady state, low calcium, 1, 2 and 3 hours after calcium repletion). For live-cell microscopy, imaging was performed after returning the cells to regular growth media composed of: FluoroBrite DMEM (Life Technologies), FBS (10% v/v), penicillin (100 I.U./mL), streptomycin (100μg/mL), OxyFluor (1% v/v, Oxyrase) and Sodium dl – Lactate (20mM, Sigma Aldrich). For fixed cells and live cell imaging E-cadherin function blocking antibody (100 μg/ml, DECMA-1, Sigma Aldrich) was added during calcium repletion.

Antibodies

The following primary antibodies were used for indirect immunofluorescence staining: mouse anti-E-cadherin (1:250, clone 36, BD Biosciences), rat anti-E-cadherin (1:250, DECMA-1 from Sigma Aldrich was used for immunofluorescence staining in Figure 9 and 11), rabbit anti-β-catenin (1:400, abcam), mouse anti-β-catenin (clone 14, 1:250, BD Biosciences), rabbit anti-Transferrin Receptor (1:100, abcam), rabbit anti-α-catenin (1:250, BD Sigma), mouse anti-α-tubulin (1:500, Sigma Aldrich). The following secondary antibodies were used for indirect immunofluorescence staining: Alexa Fluor 488 conjugated goat anti-rabbit (1:500, Life Technologies), Cy5 conjugated goat anti-rabbit (1:500, Life Technologies), Cy3 conjugated goat anti-mouse (1:500, Life Technologies), CF640 conjugated goat anti-rat (1:500, Life Technologies). Additionally, for staining F-actin either Alex Fluor 488 or Rhodamine conjugated Phalloidin (1:150, Life Technologies) was used.

Indirect immunofluorescence

All steps were performed at room temperature unless specified. Cells were fixed with 4% (w/v) paraformaldehyde (Sigma Aldrich) for 20 min and then permeabilized with 0.5% (v/v) Triton (Bio-Rad) for 1 min. 1% (w/v) BSA was used to block for 1 h, following which samples were incubated with primary antibodies overnight at 4 ºC. Samples were then incubated with secondary antibodies, Hoechst (1:10,000, GE Healthcare) and Phalloidin for 1.5 h in the dark. Coverslips were mounted onto slides using ProLong Gold (Life Technologies) mounting media and incubated for 24 h at 4 ºC in the dark.

Image acquisition and processing

For indirect immunofluorescence, images were taken on AxioObservor Z1 (Zeiss) using Axiovision 4.8.2 software (Zeiss) equipped with a Plan-Apo 63X oil immersion objective with NA 1.4. 35 z-stacks with a step size of 0.240µm were acquired for each field. Binning was set to 2x2 using a CoolSNAP HQ^2 (Photometrics). Filter cube sets used were: Blue Channel: 49 (Zeiss), Green Channel: 38HE (Zeiss), Red Channel: Ex:560/40, Em:630/75, and Far-red Channel: 50 (Zeiss). The following deconvolution parameters were used: theoretical PSF, constrained iterative algorithm, autolinear normalization (See **Equation 1** below) and strength setting of medium (or as mentioned in the figure legend) for all fixed images.

$$I_N = (I - I_{min})\frac{(2^n-1)-0}{I_{max}-I_{min}} + 0 \quad \text{… Equation (1)}$$

Where I_N is the normalized intensity, I_{min} and I_{max} are the lowest and highest gray values of the acquired image and n is the bit size of the camera used.

For live cell experiments, images were acquired on AxioObservor Z1 (Zeiss), using a 63X water immersion objective with NA 1.3. The stage was equipped with an incubator chamber (37 ºC, 95% humidity and 5% CO_2). QuantEM 512SC camera (Photometrics) was used with no binning. Time-lapse images were taken in 5 minutes intervals for 12 hours, in both RFP (Ex: 560/40 and Em: 630/75) and GFP (Filter Set 38HE, Zeiss) channels. A stack of 3-5 images with a step size of 1μm was acquired for each time point and nearest neighbor deblurring algorithm was used to process the images. Images were imported to Volocity (Perkin-Elmer) and their brightness adjusted before being exported as a TIF.

Fluorescence Covariance analyses

Deconvolved images were imported into Volocity 6.0.1 (PerkinElmer) to calculate the PCC values at the cell-cell contact sites and in the cytoplasm. Regions of interest (ROIs) were defined using the Free Hand tool at cell-cell contact and cytoplasm for each cell in an image stack. The PCC values were exported in a comma separated value (.csv) format. A custom written script in MATLAB (MathWorks) was used to extract the PCCs and compute FCI values (**See Appendix**).

The following equations define MOC (**Equation 2**) and PCC (**Equation 3**):

$$Mander's\ Overlap\ Coefficient = \frac{\sum(I_R)(I_G)}{\sqrt{\sum(I_R)^2(I_G)^2}} \quad \text{… Equation (2)}$$

$$Pearson's\ Correlation\ Coefficient = \frac{\sum(I_R - I_{R,Mean})(I_G - I_{G,Mean})}{\sqrt{\sum(I_R - I_{R,Mean})^2(I_G - I_{G,Mean})^2}} \quad \text{… Equation (3)}$$

Derivation of Fluorescence Covariance Index:

$$Fluorescence\ Covariance\ Index = Log_{10}\ \frac{PCC\ in\ Periphery}{PCC\ in\ Cytoplasm} \quad \ldots \text{Equation } (\mathbf{4})$$

Statistical Analyses

A parametric ANOVA or non-parametric Kruskal-Wallis test was followed by appropriate post-hoc multiple comparisons tests was performed as indicated in the figure legends. GraphPad Prism 5 (GraphPad Software) was used for all statistical analyses. Frequency distributions were plotted for PCC values and FCI values with bin widths of 0.15 and 0.3 respectively. Bin sizes were determined by using the Sturges' rule (See **Equation 5** below). Gaussian best fits of the frequency distributions for FCI values were obtained with the standard deviation parameter set to be positive.

$$k = [\log_2 N + 1] \quad \ldots \text{Equation } (\mathbf{5})$$

Where k is number of bins and N is sample size. According to this rule, the number of bins will vary depending on sample size. However, it should be noted that while this rule works very well for data with > 30 samples, it assumes the population is normally distributed. More importantly, this is still an empirical rule and hence varying bin size could reveal different features of the data. This could become especially important with biologically distinct populations being present which could be falsely grouped into large bins. Conversely, populations that do not arise from different distributions could be split using smaller bins. However, for the sake of the current analysis, the lowest available sample size was about 32, which gives a bin number of 6. This was set as the standard for all frequency plots for FCI values and PCC values (with thresholds).

CHAPTER 3: SPATIALLY REGULATED β-ACTIN TRANSLATION INTEGRATES SEVERAL SIGNALING PATHWAYS TO DETERMINE EPITHELIAL STRUCTURE AND TISSUE FUNCTION

INTRODUCTION

Adherens junctions are a major class of cell adhesion complexes observed in epithelial tissues (Nagafuchi, 2001; Takeichi, 2014). These complexes contain E-cadherin, a classical cell-cell adhesion molecule, and the adaptor proteins β-catenin and α-catenin. Dynamic interactions between cadherin-catenin complexes and linear actin filaments regulate epithelial homeostasis (Cavey et al., 2008; van Roy and Berx, 2008). For instance, in several epithelial cancers, reduced E-cadherin expression correlates with increased metastatic potential (Blanco et al., 2002; Rosivatz et al., 2002). In addition to methylation of the E-cadherin promoter (Lombaerts et al., 2006) and down-regulation by transcriptional repression (Blanco et al., 2002; Cano et al., 2000; Korpal et al., 2008), post-translational control of E-cadherin regulates epithelial-to-mesenchymal transition and cancer cell invasion (Thiery, 2003). Phosphorylation decreases the residence time of cadherin-catenin complexes at the cell surface reducing cell-cell adhesion strength and barrier integrity (Bertocchi et al., 2012). Additionally, activation of the Src oncogene or growth factors, such as TGF-β or HGF, cause targeted E-cadherin degradation in lysosomes which drives tumor and metastasis progression (Fujita et al., 2002; Janda et al., 2006; Kimura et al., 2006; Shen et al., 2008), as reviewed in (de Beco et al., 2012; Mosesson et al., 2008). Conversely, blocking E-cadherin recycling at the cell surface by

inhibiting endocytosis increases E-cadherin *trans*-dimer formation (Troyanovsky et al., 2006) and F-actin anchoring thereby stabilizing adherens junction complexes (Harris and Tepass, 2010). The contribution of E-cadherin endocytosis to the maintenance of mature adherens junctions in epithelia has been well studied (de Beco et al., 2009). However, its role in balancing F-actin anchoring of cadherin-catenin complexes during *de novo* adherens junction formation has yet to be explored. Results in the following sections demonstrate that dynamin mediated endocytosis opposes F-actin anchoring of cadherin-catenin complexes, thus negatively regulating adherens junction assembly.

Epithelial cell-cell contact stimulates E-cadherin clustering causing a local increase in α-catenin levels driving actin filament remodeling from branched networks to linear bundles (Drees et al., 2005; Yamada et al., 2005). Linear actin bundles anchor cadherin-catenin complexes to positively regulate adherens junction assembly (Gloushankova et al., 1997; Krendel and Bonder, 1999; Vasioukhin et al., 2000; Wu et al., 2015). E-cadherin clustering on the cell surface and actin filament remodeling, following *de novo* epithelial cell-cell contact, are interdependent processes driving adherens junction assembly/disassembly dynamics. Actin cytoskeleton remodeling required for adherens junction assembly is driven by a local increase in β-actin monomer concentration (Gutierrez et al 2014). Localizing β-actin mRNA translation governs monomer concentration at epithelial cell-cell contacts and regulates actin filament polymerization (Gutierrez et al., 2014; Mingle et al., 2005; Rodriguez et al., 2006). β-actin knock-down (Baranwal et al., 2012) or mislocalizing its synthesis (Gutierrez et al., 2014; Kislauskis et al., 1994) specifically impairs adherens junction assembly. Additionally, expressing β-actin mRNA lacking its 3′UTR (Δ3′UTR), and thus the

mRNA zipcode, impairs actin filament remodeling at the cell periphery (Lyubimova et al., 1999), which results in reduced cadherin clustering at cell-cell contacts (Rodriguez et al., 2006).

In this thesis, Dynamin inhibitors: dynasore (Macia et al., 2006) and hydroxy-dynasore (McCluskey et al., 2013), are used to block endocytosis in MDCK cells with partial mislocalization of β-actin translation in order to increase cadherin clustering at the cell surface (Troyanovsky et al., 2006). This tips the balance towards actin anchoring of cadherin-catenin complexes and rescues adherens junction assembly defects in cells with partial mislocalization of β-actin translation. In addition, epithelial monolayer barrier integrity is shown to correlate with adherens junction assembly, as quantified with FCI analysis developed in **Chapter 2**. Also, a more complete mislocalization of β-actin translation is sufficient to prevent the rescue of adherens junction assembly by inhibiting endocytosis in cells. Finally, the rescue of adherens junction assembly in monolayers composed of epithelial cells, which have partial mislocalization of β-actin translation, requires E-cadherin function as determined by using a function blocking antibody (Vestweber and Kemler, 1985).

Utilizing calcium repletion experiments is an excellent tool to study some of the molecular underpinnings of adherens junction assembly. However, it is not a very physiologically relevant model system. 3-dimensional Matrigel embedded MDCK cultures provide a better physiologically relevant model system to study the factors influencing *de novo* lumen formation and epithelial morphogenesis. The cells can be manipulated using molecular tools to disrupt β-actin mRNA spatial regulation prior to embedding allowing for the study of long term effects of the manipulation on lumen

formation. Additionally, once embedded, the cultures are amenable to treatment with inhibitors of the zipcode pathway to allow for the study of short term effects of mislocalizing β-actin translation in a 3-dimensional culture setting. Previous work from Keith Mostov's group shows that proper spatio-temporal localization of PI3K/PTEN signaling, apico-lateral sorting machinery, and key apical polarity determinants – Par3, aPKC, Occludin and Cdc42, dictate epithelial morphogenesis in MDCK cysts (Bryant et al., 2010; Martin-Belmonte et al., 2007). Mathematical models of cyst formation from *in vitro* data indicate that three factors influence the morphogenesis of epithelia: signaling from distinctly polarized apical, basal and lateral surfaces, acto-myosin contractility, and cell division (Cerruti et al., 2013). However, little is known the role of spatially regulated β-actin translation on cyst formation.

Utilizing MDCK cyst cultures in Matrigel as model for epithelial morphogenesis, spatially regulated β-actin translation is shown to regulate epithelial structure. Cells with partially mislocalized β-actin translation form smaller cysts with a reduced number of proliferating cells per cyst. Additionally, these cysts have "wavy" tight junctional architecture likely resulting from disorganized myosin IIA along cell-cell adhesions. Newly translated β-actin was seen to accumulate at apical and lateral cell-cell interfaces in mature cysts, implicating a role for the newly synthesized monomer in regulating acto-myosin mediated tension in these sub-cellular compartments and thereby controlling cyst homeostasis. Finally, acutely mislocalizing β-actin translation in mature cyst cultures causes a loss of typical epithelial single layer single lumen organization, resulting instead in multiple layers with cells extruding into the luminal cavity. Changes in cell shape, size and number have been known to relay mechanical signals which are then translated to

gene expression changes via the Hippo and/or YAP/TAZ pathways (Yu and Guan, 2013) to control organ size (Low et al., 2014). The results with MDCK cysts demonstrate that spatially regulated β-actin translation controls typical epithelial morphogenesis. The work indicates a potentially novel role for compartmentalized β-actin translation in regulating acto-myosin tension at cell-cell adhesions and thus affecting the Hippo and/or YAP/TAZ mechano-transduction pathways. Thus, spatially regulated β-actin translation acts as an integrator of several signal transduction pathways: from 2D calcium repletion assays, where it is shown to balance dynamin mediated endocytosis of E-cadherin to 3D cyst cultures, where it potentially regulates mechano-transduction signals.

RESULTS

Partially mislocalizing β-actin translation in MDCK cells impairs their ability to assemble functional epithelial monolayers

The β-actin mRNA zipcode is a 28 nucleotide sequence present in the 3′UTR. Exogenously expressing 3′UTR deleted β-actin downstream from a human β-actin promoter in cells causes significant morphological perturbations to epithelial monolayer structure. Interestingly, total actin expression in epithelial monolayers assembled from cells expressing either full length or Δ3′UTR β-actin mRNA was similar (Ballestrem et al., 1998; Gutierrez et al., 2014). Importantly, expressing zipcode deleted β-actin mRNA causes mislocalization of β-actin translation (Gutierrez et al., 2014; Rodriguez et al., 2006). MDCK monolayers assembled from cells that properly localize β-actin translation to cell-cell contacts exhibit strong E-cadherin and F-actin co-localization at cell-cell contact sites. These cells also contain stress fibers in the basal cytoplasm (**Figure 16A**, Full length β-actin mRNA expressing cells). In contrast, few stress fibers are observed in the cytoplasm of MDCK monolayers composed of cells with partially mislocalized β-actin translation. However, these cells still show significant, albeit weaker, E-cadherin and F-actin co-localization at cell-cell contacts. Importantly, these cells also exhibit extensive lamellar protrusions that are largely absent in confluent monolayers assembled from MDCK cells that properly localize β-actin translation to cell-cell contacts (**Figure 16B**, Δ3′UTR β-actin mRNA expressing cells). During adherens junction assembly, E-cadherin clustering at cell-cell contact sites increases α-catenin recruitment, which is required for inhibiting lamellar protrusions (Drees et al., 2005). However, cells impaired

in their ability to locally synthesize monomers exhibit reduced cadherin localization at the cell-cell contacts (Rodriguez et al., 2006). Thus epithelial monolayers composed of cells with partially mislocalized β-actin translation are unable to recruit and anchor α-catenin to cell-cell contacts and turn off lamellar protrusions following *de novo* contact.

Actin anchored cadherin-catenin complexes induce a myosin II dependent feed forward loop driving additional cadherin-catenin/actin filament anchoring (Biswas et al., 2015). The resulting expansion and maturation of adherens junctions is required for epithelial structure and function (Smutny et al., 2010; Yonemura et al., 2010). Conversely, E-cadherin that is not anchored at the cell surface is internalized by dynamin mediated endocytosis, and is either recycled or degraded (Cavey et al., 2008; Harris and Tepass, 2010). To quantify the extent of E-cadherin anchoring to F-actin, FCI analysis developed in Chapter 2 was utilized. MDCK monolayers impaired in their ability to localize β-actin translation have fewer cells with high FCI values (0.5 – 1.0) compared to monolayers composed of cells that properly localize β-actin translation (**Figure 17A**, ≈ 52% for full length β-actin mRNA expressing cells compared to ≈ 25% for Δ3′UTR expressing cells). Cells with partially mislocalized β-actin translation have high cytoplasmic correlations between E-cadherin and F-actin, generating low FCI values. These cytoplasmic correlations arise from overlap of lamellar protrusions, which are inhibited in cells that properly localize β-actin translation. Additionally, monolayers assembled from cells partially impaired in their ability localize β-actin translation are only ≈ 66% the height of monolayers assembled from cells that have no defects in localizing β-actin translation (**Figure 16A and B**, ΔZ values). These results indicate partial impairment in localizing β-actin translation causes defects in epithelial adherens

junction maturation. Additionally, the *in vitro* permeability to fluorescent dextran is ≈ 4 fold higher in confluent monolayers assembled from cells with partially mislocalized β-actin translation (**Figure 17B**). Importantly, low FCI values correlate with reduced barrier integrity demonstrating this metric has value in quantifying gain or loss of epithelial monolayer function.

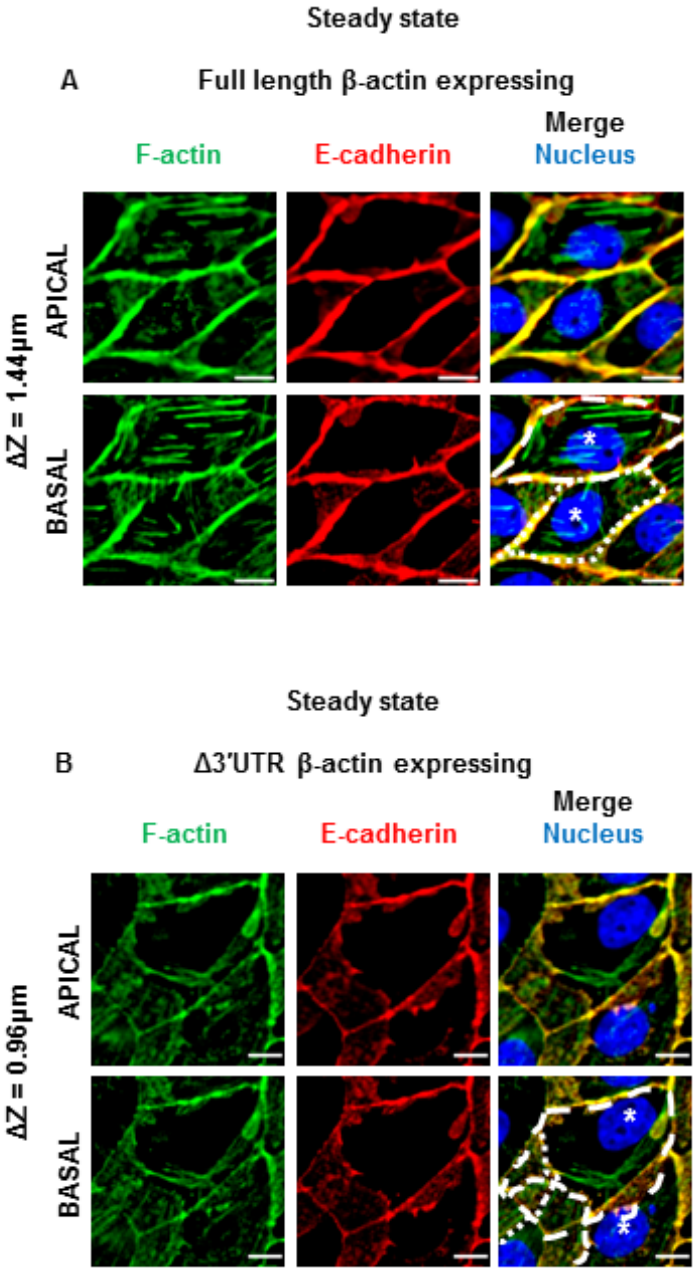
Steady state
A
Full length β-actin expressing
F-actin
E-cadherin
Merge
Nucleus
APICAL
BASAL
ΔZ = 1.44µm
Steady state
B
Δ3'UTR β-actin expressing
F-actin
E-cadherin
Merge
Nucleus
APICAL
BASAL
ΔZ = 0.96µm

Figure 16: MDCK cells with partially mislocalized β-actin translation show extensive lamellipodial overlap. (**A**) MDCK cells with proper localization of β-actin translation (expressing full length β-actin mRNA) fixed at steady state and immunostained for F-actin (Green), E-cadherin (Red), and Nucleus (Blue). Stress fibers are visible in the basal compartment; E-cadherin and F-actin co-stain cell-cell interfaces in the apical and basal compartments. (**B**) MDCK cells with partially mislocalized β-actin translation (expressing Δ3′UTR β-actin mRNA) fixed at steady state and stained for F-actin (Green), E-cadherin (Red) and Nucleus (Blue). Scale bars = 10μm. Dotted lines indicate cell boundaries and * indicates nucleus of individual cells. ΔZ represents the distance between the apical and basal planes in μm.

A

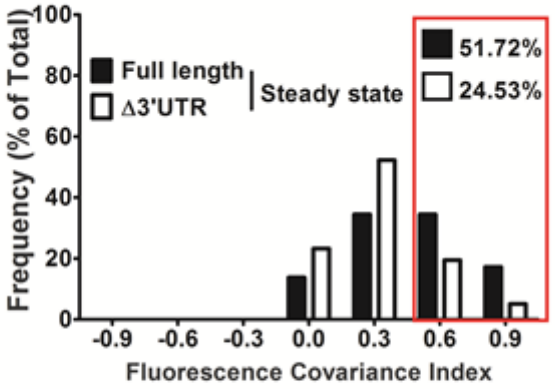
Frequency (% of Total)
100
80
60
40
20
0
Full length
Δ3'UTR
Steady state
51.72%
24.53%
-0.9
-0.6
-0.3
0.0
0.3
0.6
0.9
Fluorescence Covariance Index

B

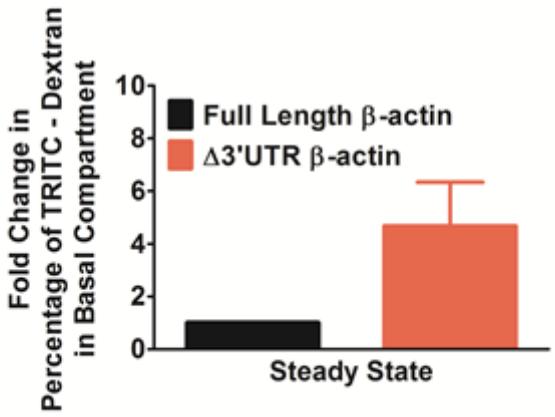
Fold Change in Percentage of TRITC - Dextran in Basal Compartment
10
8
6
4
2
0
Full Length β-actin
Δ3'UTR β-actin
Steady State

Figure 17: FCI values of E-cadherin and F-actin correlate with epithelial barrier function. (**A**) Frequency distributions of FCI values for E-cadherin and F-actin in cells fixed at steady state. Cells were either expressing full length β-actin mRNA (Black bars; N = 29) or Δ3′UTR β-actin mRNA (White bars; N = 314). Bin size = 0.3. Red box indicates the proportion of cells with high FCI values. (**B**) Fold change in percentage of TRITC-Dextran in the bottom compartment measured in an *in vitro* permeability assay for MDCK cells in steady state with and without partial defects in localizing β-actin translation. Bars represent mean ± s.e.m.

Inhibiting Dynamin mediated endocytosis rescues the epithelial adherens junction assembly defect caused by partially mislocalizing β-actin translation

Adherens junction assembly dynamics in epithelial MDCK monolayers composed of cells with partially mislocalized β-actin translation was studied using calcium repletion experiments and FCI analysis of E-cadherin and F-actin (Volberg et al., 1986) (See **Chapter 2**). Epithelial adherens junction assembly *in vitro* is known to occur in three phases – contact initiation, contact expansion and junction maturation (Adams et al., 1998; Baum and Georgiou, 2011; Kovacs et al., 2002). Following calcium repletion, cells with partially mislocalized β-actin translation form initial contact within 1 hour and expand these contacts within 2 hours (**Figure 18A**, co-localization of E-cadherin and F-actin at cell-cell contacts 1 and 2 hours after calcium repletion). However, significant lamellar protrusions are observed 3 hours after calcium repletion (**Figure 18A**, cellular overlaps 3 hours after calcium repletion). In addition, these cells fail to reach the height of monolayers assembled from cells which have no defects in localizing β-actin translation (**Figure 18A,** ΔZ values compared to **Figure 16A** ΔZ value). PCC values for E-cadherin and F-actin at cell-cell contacts increase between 1 and 2 hours after calcium repletion, indicating initial cell-cell contact is followed by contact expansion phase in these cells. However, between 2 and 3 hours after calcium repletion, PCC values for E-cadherin and F-actin increase in the cytoplasm, while PCC values at the periphery remain unchanged (**Figure 18B**). Correspondingly, changes in FCI values correlate with morphological changes, increasing between 1 hour and 2 hours after calcium repletion and decreasing significantly 3 hours after calcium repletion (**Figure 18C**). These results indicate that following contact expansion, these cells form extensive lamellar protrusions,

which contain nascent cadherin-catenin complexes anchored to F-actin (*en face* adhesions). Thus, cells with partial mislocalization of β-actin translation undergo contact expansion, but fail to progress to junction maturation unlike wild type MDCK cells (See **Chapter 2, Figure 7**). Mislocalizing β-actin translation from the cell-cell contact zone reduces actin filament polymerization (Gutierrez et al., 2014), reducing cadherin anchoring to F-actin (Rodriguez et al., 2006). Concomitantly, it was hypothesized that E-cadherin endocytosis is increased during adherens junction assembly in cells with partial mislocalization of β-actin translation.

In order to test the hypothesis, dynasore, a small molecule inhibitor of Dynamin's GTPase function (Macia et al., 2006), was used to inhibit Dynamin mediated endocytosis. At 80μM dynasore, the initial phases of adherens junction assembly: cell-cell contact formation and contact expansion are unaffected (**Figure 19A**, E-cadherin and F-actin co-localization at cell-cell contacts 1 and 2 hours following calcium repletion). Importantly, E-cadherin and F-actin co-localize at cell-cell contacts, along with few lamellar protrusions 3 hours after calcium repletion with 80μM dynasore (**Figure 19A**, 3 hours following calcium repletion compare with **Figure 18A**, 3 hours following calcium repletion). Additionally, these cells are as tall as cells in monolayers assembled from cells with no defects in localizing β-actin translation (**Figure 19A**, ΔZ value compare with **Figure 16A**, ΔZ value). PCC values for E-cadherin and F-actin remain low in the cytoplasm, while correlations at cell-cell contacts progressively increase from 1 to 3 hours after calcium repletion with 80μM dynasore (**Figure 19B**). Consequently, FCI values remain high 3 hours after calcium repletion, indicating these cells successfully

complete adherens junction maturation upon inhibition of dynamin mediated endocytosis (**Figure 19C**).

To further validate the specificity of dynasore inhibition, Hydroxy-Dynasore aka Dyngo 4a, a new generation Dynamin inhibitor (McCluskey et al., 2013), was used. The results obtained are similar to those observed following dynasore treatment. Contact initiation and contact expansion are observed 1 and 2 hours following calcium repletion with 80μM hydroxy-dynasore in cells with partially mislocalized β-actin translation (**Figure 20A**). Additionally, cells have few lamellar protrusions 3 hours after calcium repletion with 80μM hydroxy-dynasore, and reach a height similar to cells without defects in localization of β-actin translation (**Figure 20A**, compare ΔZ values with **Figures 16A** and **19A**, ΔZ values). PCC values for E-cadherin and F-actin remain low in the cytoplasm, while correlations at the cell-cell contact increase during calcium repletion with hydroxy-dynasore (**Figure 20B**). Consequently, FCI values progressively increase between 1, 2 and 3 hours after calcium repletion with hydroxy-dynasore (**Figure 20C**).

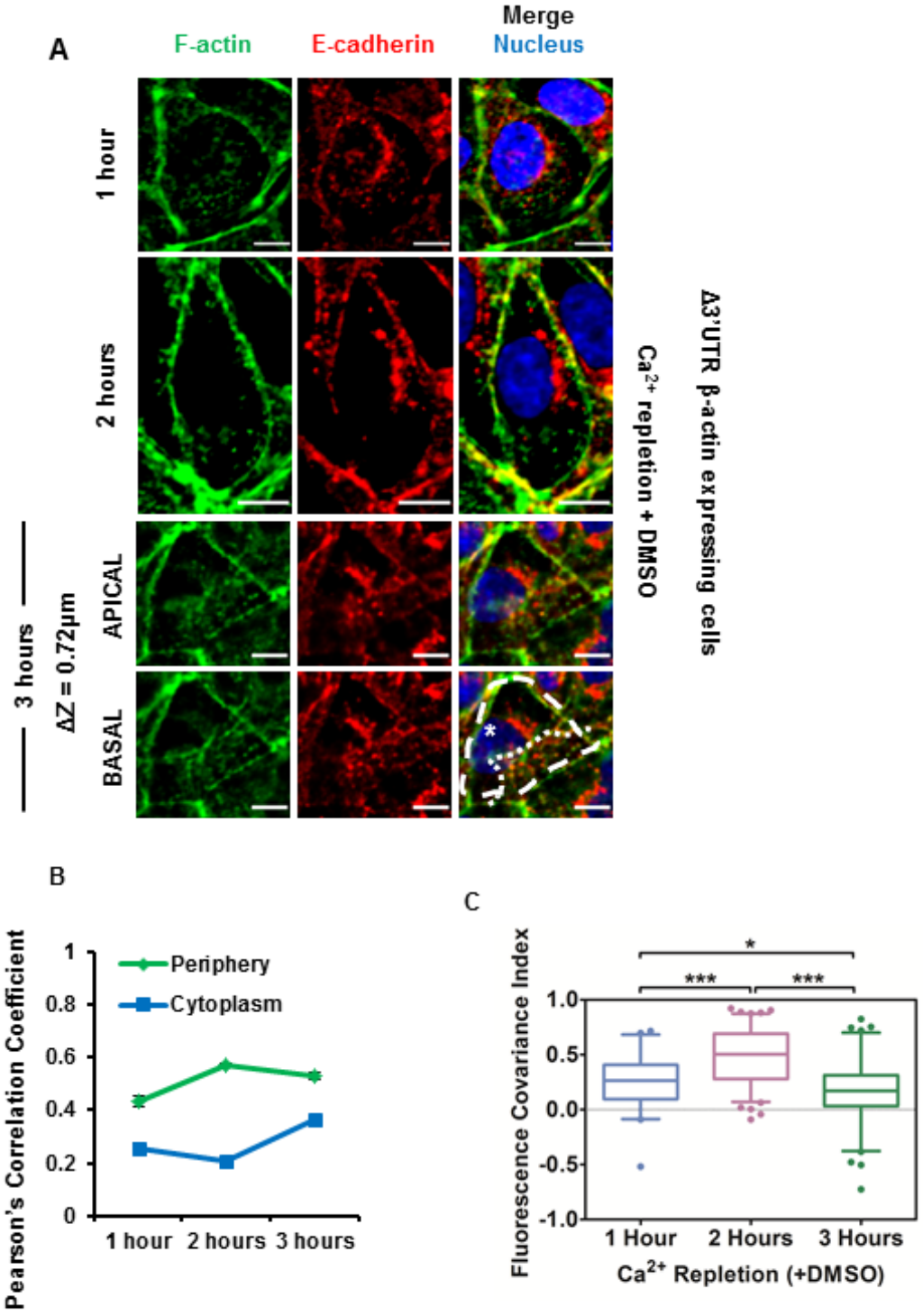
A
F-actin
E-cadherin
Merge
Nucleus
1 hour
2 hours
3 hours
ΔZ = 0.72μm
APICAL
BASAL
Ca2+ repletion + DMSO
Δ3'UTR β-actin expressing cells
B
Pearson's Correlation Coefficient
Periphery
Cytoplasm
1 hour 2 hours 3 hours
C
Fluorescence Covariance Index
*
***
***
1 Hour
2 Hours
3 Hours
Ca2+ Repletion (+DMSO)

Figure 18: Partial mislocalization of β-actin translation causes extensive lamellipodial overlap following contact expansion during adherens junction assembly. (**A**) MDCK cells with partially mislocalized β-actin translation (expressing Δ3′UTR β-actin mRNA) fixed: Top to bottom: 1 hour, 2 hours and 3 hours after calcium repletion with DMSO (0.5% v/v) and immunostained for F-actin (Green), E-cadherin (Red), and Nucleus (Blue). (**B**) Change in PCC values for F-actin and E-cadherin in the periphery and the cytoplasm measured for cells with partially mislocalized β-actin translation (expressing Δ3′UTR β-actin mRNA) fixed 1, 2 and 3 hours after calcium repletion with DMSO (0.5% v/v). Points represent Mean ± S.E.M. Note 3 hours after calcium repletion PCC values in the periphery do not increase while PCC values in the cytoplasm increase due to extensive lamellar overlap from neighboring cells (dotted lines in bottom panel in **A**). Dotted lines indicate cell boundaries and * indicates nucleus of individual cells. ΔZ represents the distance between the apical and basal planes in μm. Note the lamellar overlap 3 hours following calcium repletion in cells treated with 0.5% v/v DMSO. (**C**) Box and whiskers plot for FCI values. Whiskers represent 2.5 to 97.5 percentiles. 1 hour (N = 97); 2 hours (N = 229); 3 hours (N = 192). One-way ANOVA result: p value < 0.0001. Tukey's post-hoc multiple comparison test results with * $p < 0.05$, *** $p < 0.001$ are indicated on the graph.

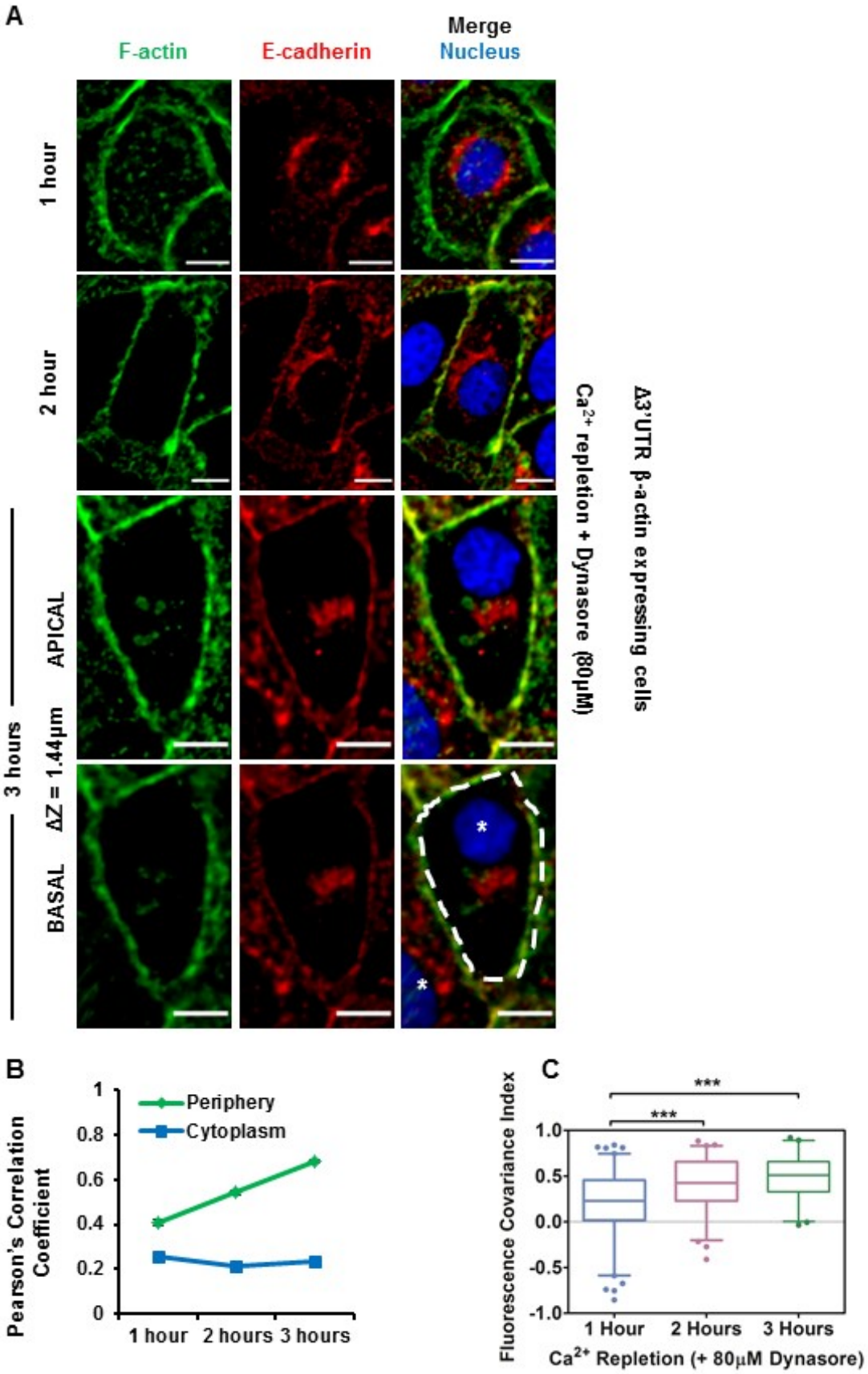
A
F-actin
E-cadherin
Merge
Nucleus
1 hour
2 hour
3 hours
APICAL
ΔZ = 1.44µm
BASAL
Ca2+ repletion + Dynasore (80µM)
Δ3'UTR β-actin expressing cells
B
Pearson's Correlation Coefficient
Periphery
Cytoplasm
1 hour
2 hours
3 hours
C
Fluorescence Covariance Index
***
***
1 Hour
2 Hours
3 Hours
Ca2+ Repletion (+ 80µM Dynasore)

Figure 19: Inhibiting dynamin mediated endocytosis with 80μM dynasore rescues the adherens junction assembly defects caused by partially mislocalizing β-actin translation. (**A**) MDCK cells with partially mislocalized β-actin translation (expressing Δ3′UTR β-actin mRNA) fixed: Top to bottom: 1 hour, 2 hours and 3 hours after calcium repletion with 80μM dynasore and immunostained for F-actin (Green), E-cadherin (Red), and Nucleus (Blue). Scale bars = 10μm. Dotted lines indicate cell boundaries and * indicates nucleus of individual cells. ΔZ represents the distance between the apical and basal planes in μm. Note cells treated with 80μM dynasore show little lamellar overlap 3 hours following calcium repletion. (**B**) Change in PCC values for F-actin and E-cadherin in the periphery and the cytoplasm measured for cells with partially mislocalized β-actin translation (expressing Δ3′UTR β-actin mRNA) fixed 1, 2 and 3 hours after calcium repletion with 80μM dynasore. Points represent Mean ± S.E.M. Note 3 hours after calcium repletion PCC values in the periphery increase while PCC values in the cytoplasm remain low. (**C**) Box and whiskers plot for FCI values. Whiskers represent 2.5 to 97.5 percentiles. 1 hour (N = 201); 2 hours (N = 147); 3 hours (N = 112). One-way ANOVA result: p value < 0.0001. Tukey's post-hoc multiple comparison test results with *** $p < 0.001$ are indicated on the graph. I would like to acknowledge Lissette Cruz for acquiring the images shown in panel **A** and calculating PCC values for the same.

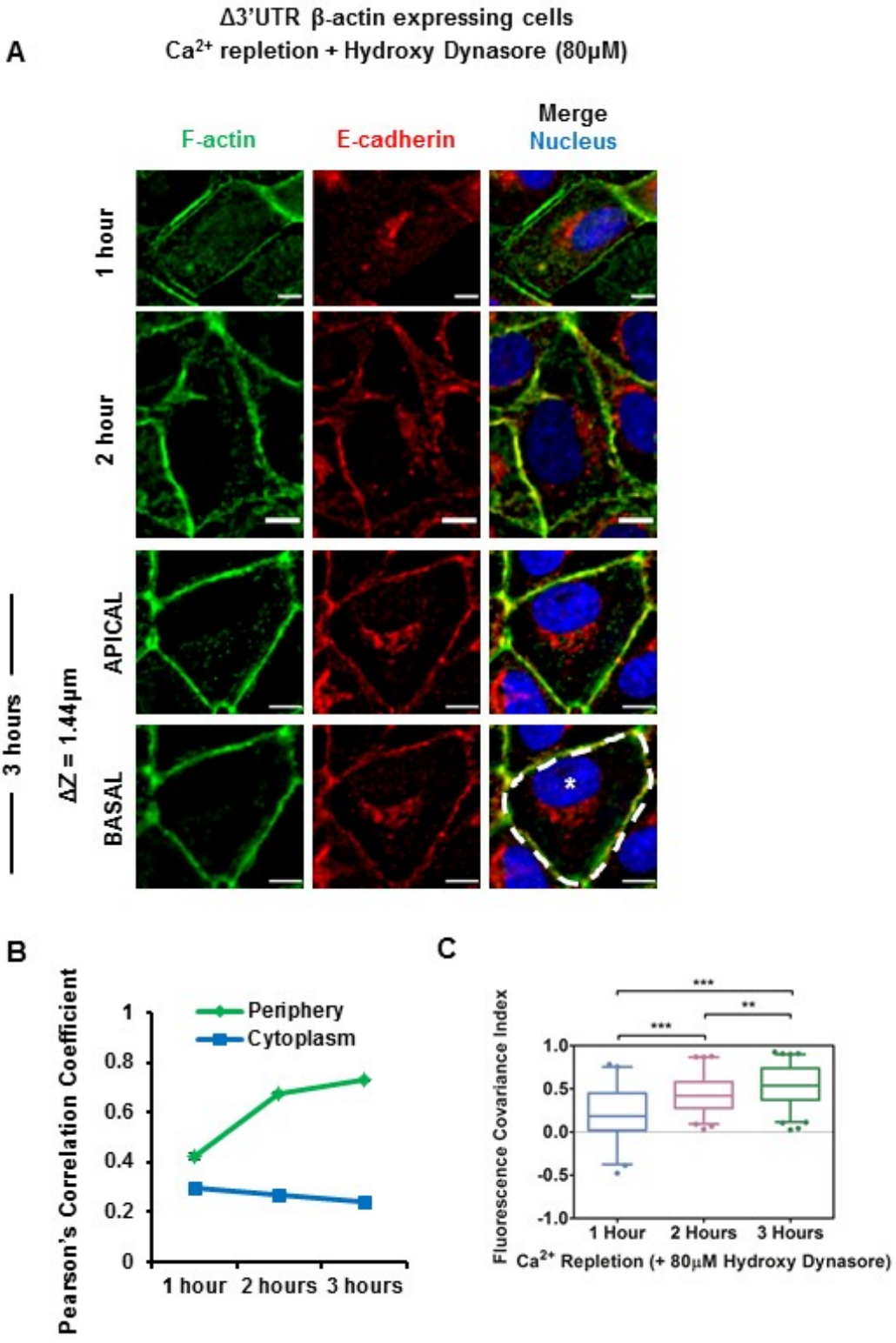
A
Δ3'UTR β-actin expressing cells
Ca2+ repletion + Hydroxy Dynasore (80μM)
F-actin
E-cadherin
Merge
Nucleus
1 hour
2 hour
APICAL
BASAL
ΔZ = 1.44μm
3 hours
B
Pearson's Correlation Coefficient
Periphery
Cytoplasm
1 hour 2 hours 3 hours
C
Fluorescence Covariance Index
1 Hour
2 Hours
3 Hours
Ca2+ Repletion (+ 80μM Hydroxy Dynasore)

Figure 20: Hydroxy-Dynasore (Dyngo 4a), a new generation of dynamin inhibitor also rescues of adherens junction assembly in MDCK cells with partially mislocalized β-actin translation. (**A**) MDCK cells with partially mislocalized β-actin translation (expressing Δ3′UTR β-actin mRNA) fixed: Top to bottom: 1 hour, 2 hours and 3 hours after calcium repletion with 80μM hydroxy-dynasore and immunostained for F-actin (Green), E-cadherin (Red), and Nucleus (Blue). Scale bars = 10μm. Dotted lines indicate cell boundaries and * indicates nucleus of individual cells. Note cells 3 hours after calcium repletion with 80μM hydroxyl-dynasore display no lamellar overlap. ΔZ represents the distance between the apical and basal planes in μm. (**B**) Change in PCC values for E-cadherin and F-actin in the periphery and the cytoplasm measured for cells with partially mislocalized β-actin translation (expressing Δ3′UTR β-actin mRNA) fixed 1 hour, 2 hours and 3 hours after calcium repletion with 80μM hydroxy-dynasore. Points represent Mean ± S.E.M. Note 3 hours after calcium repletion PCC values in the periphery increase while PCC values in the cytoplasm remain low. (**C**) Box and whiskers plot for FCI values. Whiskers represent 2.5 to 97.5 percentiles; 1 hour (N = 93); 2 hours (N = 156); 3 hours (N = 168). Bars represent Mean ± 95% C.I. One-way ANOVA result: p value < 0.0001. Tukey's post-hoc multiple comparison test results with ** $p < 0.01$ *** $p < 0.001$ are indicated on the graph.

Spatially regulated β-actin translation and Dynamin mediated endocytosis balance each other to drive adherens junction maturation

Previously it was shown that exogenous expression of the 3′UTR deleted β-actin contributes to approximately 20% of the total β-actin content in the cells (Gutierrez et al., 2014). Consequently, 80% of β-actin mRNA in these cells is endogenous and contains the zipcode. The endogenous β-actin mRNA localizes to cell-cell contacts to produce actin monomer. However, reduced actin monomer at cell-cell contacts compared to cells without any defects in β-actin mRNA localization, decreases the extent of cadherin-catenin complexes anchoring to actin filaments. Reduced anchoring, combined with increased endocytosis of cadherin-catenin complexes, causes defects in adherens junction maturation. Inhibiting endocytosis in these cells tips the balance towards increased anchoring of cadherin-catenin complexes, rescuing adherens junction maturation defects. If however, the endogenous β-actin mRNA is also mislocalized, adherens junction assembly should remain perturbed even upon inhibiting dynamin mediated endocytosis. In order to achieve mislocalization of endogenous β-actin mRNA, antisense oligonucleotides that mask the β-actin mRNA zipcode were used (Gutierrez et al., 2014; Shestakova et al., 2001) (**Figure 21A**). Pretreating MDCK cells with β-actin mRNA zipcode antisense oligonucleotides does not affect E-cadherin or IMP-1 levels in cells during calcium repletion (**Figure 21B**). However, pretreating MDCK cells partially defective in localizing β-actin translation with β-actin mRNA zipcode antisense oligonucleotides results in significant lamellar protrusive activity 3 hours after calcium repletion (**Figure 22A**). Adding dynasore to cells treated with antisense oligonucleotides results in taller cells, but lamellar protrusive activity is still present 3 hours after calcium

repletion (**Figure 22B**). Concomitantly, FCI values remain low after calcium repletion even in the presence of 80μM dynasore (**Figure 22C**). These results demonstrate that zipcode dependent spatial regulation of endogenous β-actin translation is required to balance endocytosis in cells with partial defects in β-actin mRNA localization. Inhibiting endocytosis in cells with completely mislocalized β-actin translation cannot rescue adherens junction maturation defects because these cells fail to produce sufficient monomer to be able to anchor cadherin-catenin complexes.

A

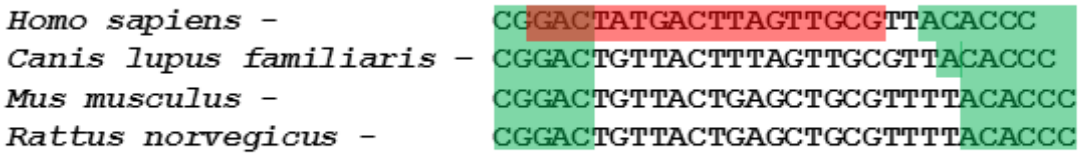
Homo sapiens -
Canis lupus familiaris -
Mus musculus -
Rattus norvegicus -
CGGACTATGACTTAGTTGCGTTACACCC
CGGACTGTTACTTTAGTTGCGTTACACCC
CGGACTGTTACTGAGCTGCGTTTTACACCC
CGGACTGTTACTGAGCTGCGTTTTACACCC

B

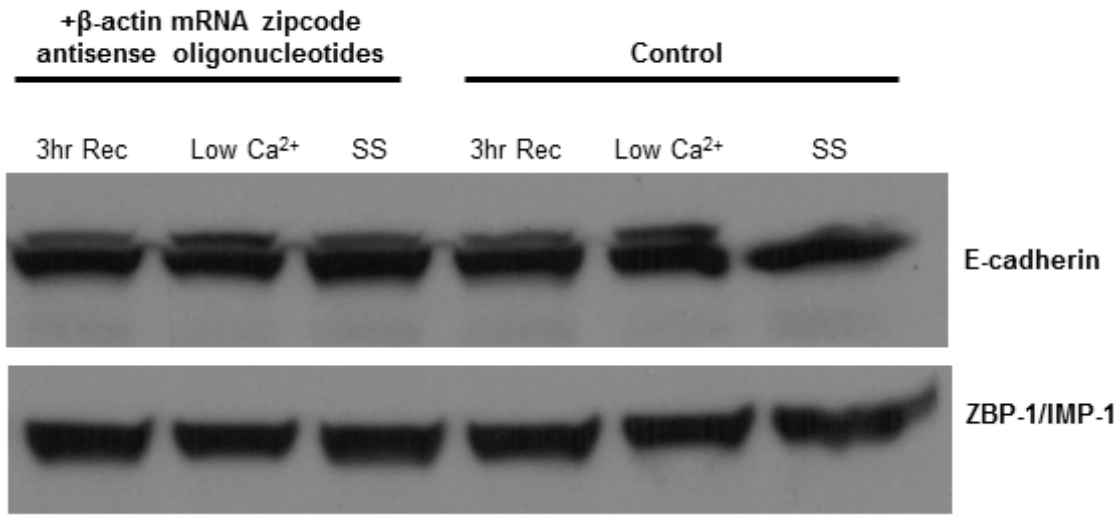
+β-actin mRNA zipcode antisense oligonucleotides
Control
3hr Rec
Low Ca2+
SS
3hr Rec
Low Ca2+
SS
E-cadherin
ZBP-1/IMP-1

Figure 21: Design of β-actin mRNA zipcode antisense oligonucleotides and their effect on ZBP-1/IMP-1 expression. (**A**) β-actin mRNA zipcode sequences in mammalian model systems: humans, dogs, mouse and rats. Green shaded sequences are consensus ZBP-1/IMP-1 binding sequences. Red shaded sequence corresponds to the antisense oligonucleotides used in this study. (**B**) Immunoblot for E-cadherin and ZBP-1 in MDCK cells untreated or following 8 hour pretreatment with β-actin mRNA zipcode antisense oligonucleotides during a calcium switch assay. 3hr Rec indicates 3 hours post calcium repletion.

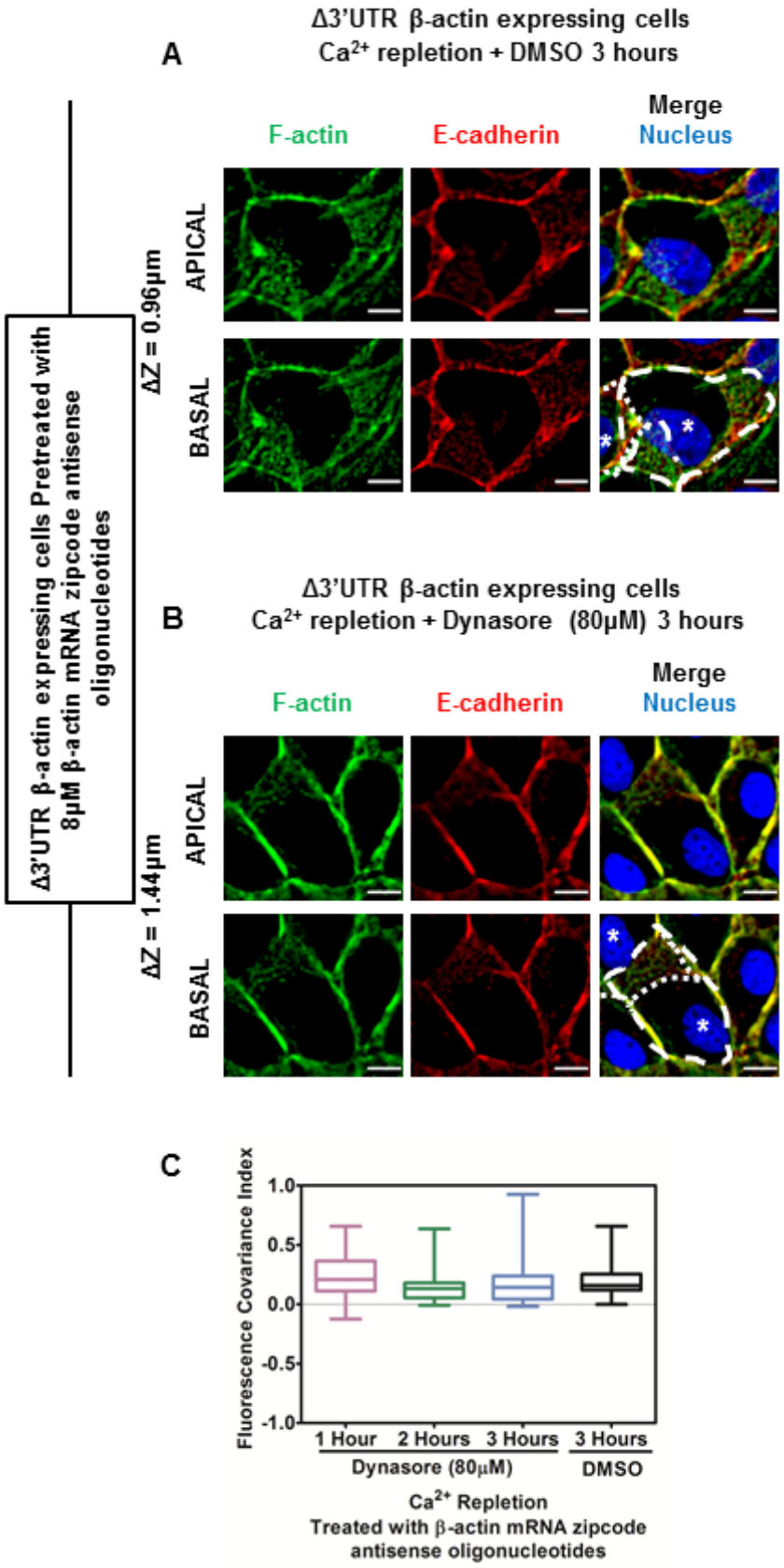
A
Δ3'UTR β-actin expressing cells
Ca2+ repletion + DMSO 3 hours
F-actin
E-cadherin
Merge
Nucleus
APICAL
BASAL
ΔZ = 0.96μm
Δ3'UTR β-actin expressing cells Pretreated with 8μM β-actin mRNA zipcode antisense oligonucleotides
B
Δ3'UTR β-actin expressing cells
Ca2+ repletion + Dynasore (80μM) 3 hours
F-actin
E-cadherin
Merge
Nucleus
APICAL
BASAL
ΔZ = 1.44μm
C
Fluorescence Covariance Index
1.0
0.5
0.0
-0.5
-1.0
1 Hour
2 Hours
3 Hours
3 Hours
Dynasore (80μM)
DMSO
Ca2+ Repletion
Treated with β-actin mRNA zipcode antisense oligonucleotides

Figure 22: Completely mislocalizing β-actin translation blocks adherens junction assembly even with endocytosis inhibition. MDCK cells with partially mislocalized β-actin translation (expressing Δ3′UTR β-actin mRNA) were pretreated with β-actin mRNA zipcode antisense oligonucleotides and fixed 3 hours after calcium repletion with: (**A**) DMSO (0.5% v/v) or (**B**) 80μM dynasore; and immunostained for F-actin (Green), E-cadherin (Red), and Nucleus (Blue). Scale bars = 10μm. Dotted lines indicate cell boundaries and * indicates nucleus of individual cells. ΔZ represents the distance between the apical and basal planes in μm. Note the lamellar overlap in the cells seen in the basal compartment. (**C**) Box and whiskers plot for FCI values. Whiskers represent 2.5 to 97.5 percentiles. Dynasore treatment: 1 hour (N = 29); 2 hours (N = 29); 3 hours (N = 28) or DMSO treatment: 3 hours (N = 22). One-way ANOVA results for Dynasore with β-actin mRNA zipcode antisense oligonucleotides treatment indicates no significant difference with time in FCI values. Unpaired Student *t* test indicates no significant variation between Dynasore with antisense oligonucleotides and DMSO with antisense oligonucleotides treatment 3 hours following calcium repletion.

Inhibiting dynamin mediated endocytosis rescues barrier permeability defects in cells with partially mislocalized β-actin translation

As seen in Chapter 2, a population of cells with ≥ 45% frequency of high FCI values (0.5 – 1.0) for E-cadherin and F-actin, represents mature adherens junctions (**Figure 7**). Additionally, such cell populations form a functional barrier measured by the extent of fluorescent dextran permeability (**Figure 17A, B**). Along the same line of analysis, frequency plots of FCI values for E-cadherin and F-actin in cells with partially mislocalized β-actin translation treated with DMSO following calcium repletion were plotted. The results show an increase in frequency of FCI values between 1 and 2 hours (≈ 19% at 1 hour to ≈ 56% at 2 hours) followed by a decrease 3 hours (≈ 14%) after calcium repletion (**Figure 23A**). However, upon treating these cells with dynasore, a progressive increase in the frequency of cells with high FCI values is observed (**Figure 23B**, ≈ 26% at 1 hour; ≈ 48% at 2 hours and ≈ 49% at 3 hours after calcium repletion). Results with dyngo4a also show a progressive increase in frequency of high FCI values (**Figure 23C**, ≈ 25% at 1 hour; ≈ 43% at 2 hours and ≈ 56% at 3 hours after calcium repletion). These results confirm inhibiting Dynamin mediated endocytosis rescues adherens junction assembly defects caused by partially mislocalizing β-actin translation. Additionally, a more complete mislocalization of β-actin mRNA using β-actin mRNA antisense oligonucleotides results in a significant reduction in the frequency of cells in high FCI range (**Figure 23D**).

To assess the barrier functionality of assembling epithelial monolayers composed of cells without defects in localizing β-actin translation, these monolayers were subjected to a calcium repletion assay on transwell permeability inserts. The extent of barrier

function increased as the cells assembled and matured adherens junctions (**Figure 24A**). In comparison, cells with partial defects in localizing β-actin mRNA showed an inability to form a functional barrier exhibiting ≈ 6 fold higher permeability to fluorescent dextran 4 hours after calcium repletion. This defect in barrier function was however, rescued by treating these cells with dynamin inhibitor during calcium repletion (**Figure 24B**). A more complete mislocalization of β-actin translation using β-actin mRNA zipcode antisense oligonucleotides abolished the rescue of barrier integrity observed by inhibiting endocytosis (**Figure 24C**). These results show partial mislocalization of β-actin translation can be compensated by inhibiting endocytosis, whereas a complete mislocalization of β-actin translation blocks the rescue of adherens junction assembly and epithelial function. Lastly, validating results seen in Chapter 2, the frequency of FCI values in 0.5 – 1.0 range correlates with epithelial barrier function.

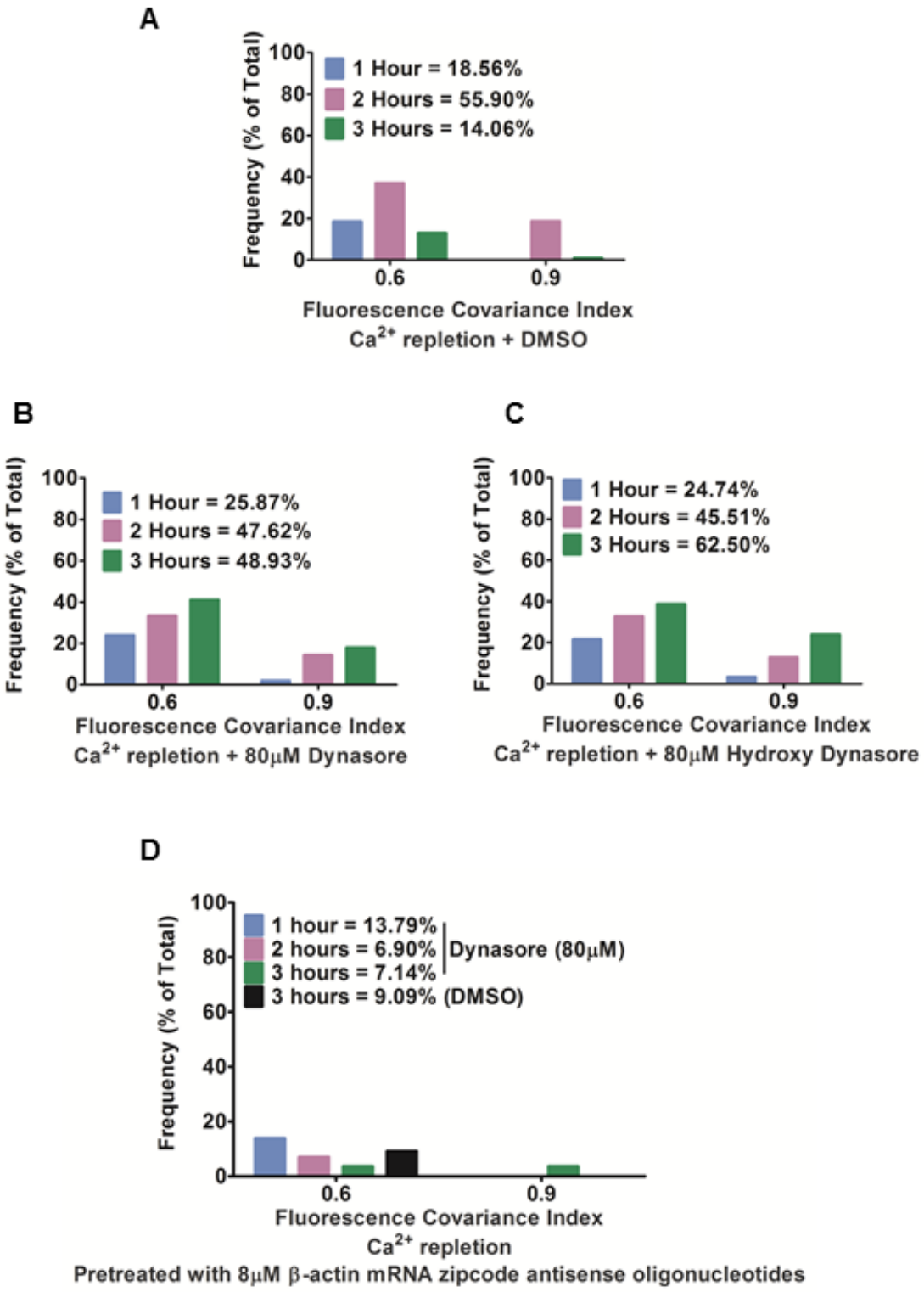
A
Frequency (% of Total)
100
80
60
40
20
0
1 Hour = 18.56%
2 Hours = 55.90%
3 Hours = 14.06%
0.6
0.9
Fluorescence Covariance Index
Ca2+ repletion + DMSO
B
Frequency (% of Total)
1 Hour = 25.87%
2 Hours = 47.62%
3 Hours = 48.93%
Fluorescence Covariance Index
Ca2+ repletion + 80μM Dynasore
C
Frequency (% of Total)
1 Hour = 24.74%
2 Hours = 45.51%
3 Hours = 62.50%
Fluorescence Covariance Index
Ca2+ repletion + 80μM Hydroxy Dynasore
D
Frequency (% of Total)
1 hour = 13.79%
2 hours = 6.90%
3 hours = 7.14%
Dynasore (80μM)
3 hours = 9.09% (DMSO)
Fluorescence Covariance Index
Ca2+ repletion
Pretreated with 8μM β-actin mRNA zipcode antisense oligonucleotides

Figure 23: Frequency of high FCI values for E-cadherin and F-actin correlate with adherens junction maturation observed with dynamin inhibition in cells with partially mislocalized β-actin translation. Frequency plots for high FCI values (0.5 – 1.0) of F-actin and E-cadherin in cells with partially mislocalized β-actin translation (expressing Δ3′UTR β-actin mRNA) following: (**A**) calcium repletion with DMSO (0.5% v/v); (**B**) calcium repletion with 80μM dynasore; (**C**) calcium repletion with 80μM hydroxy-dynasore; and (**D**) pretreatment with β-actin mRNA zipcode antisense oligonucleotides as well as 80μM Dynasore or DMSO (0.5% v/v, black bars) following calcium repletion. Bin size = 0.3. Note 3 hours after calcium repletion with DMSO the proportion of cells with high FCI values decreases, while calcium repletion with 80μM dynasore or hydroxy-dynasore results in a progressive increase in the proportion of cells with high FCI values indicating adherens junction recovery. This progressive increase is completely blocked by pretreatment with β-actin mRNA zipcode antisense oligonucleotides indicating the dynamin inhibition mediated rescue of adherens junction assembly in cells with partially mislocalized β-actin translation is dependent on endogenous β-actin mRNA zipcode function.

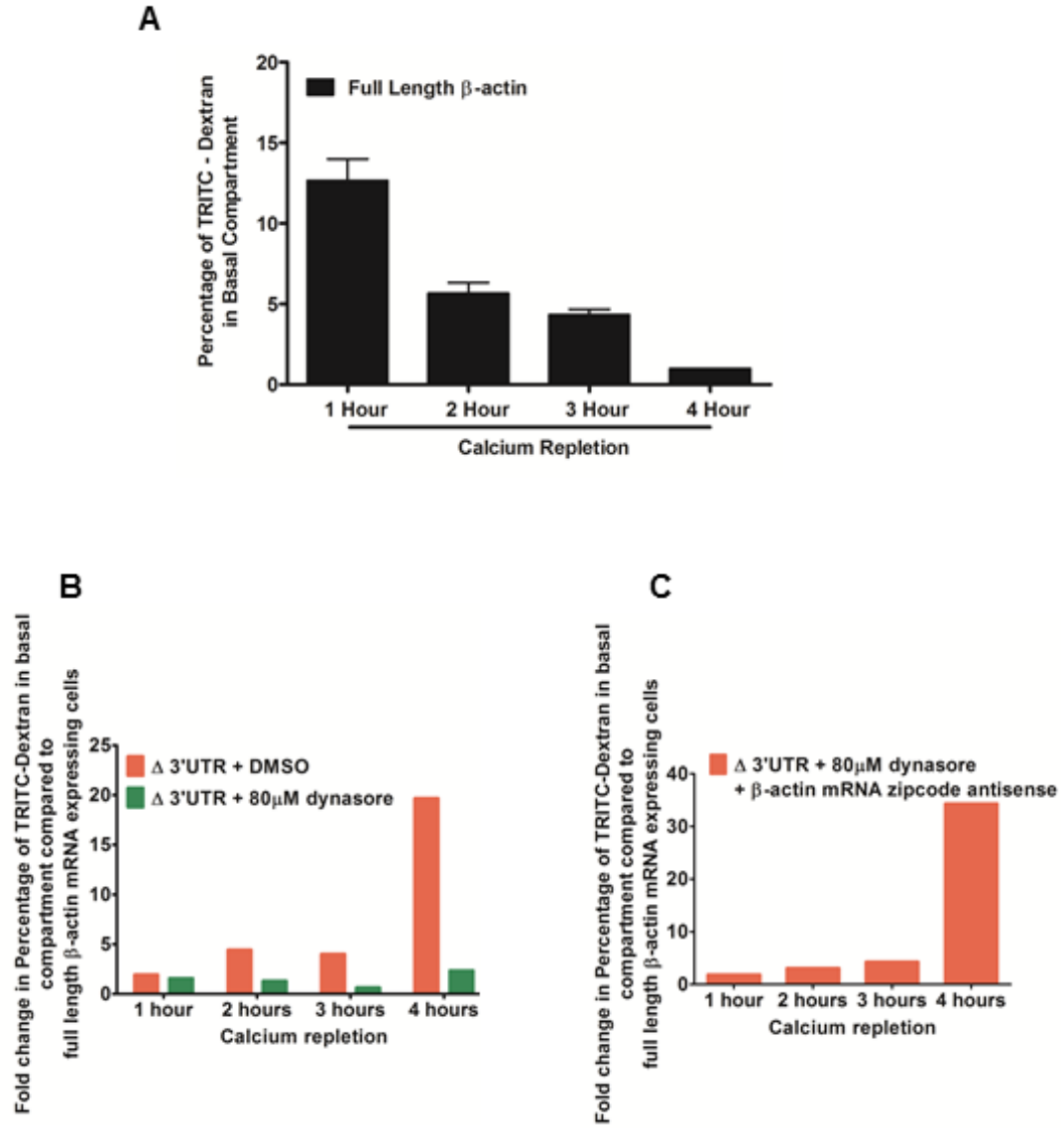
A
Full Length β-actin
Percentage of TRITC - Dextran in Basal Compartment
20
15
10
5
0
1 Hour
2 Hour
3 Hour
4 Hour
Calcium Repletion
B
Fold change in Percentage of TRITC-Dextran in basal compartment compared to full length β-actin mRNA expressing cells
Δ 3'UTR + DMSO
Δ 3'UTR + 80μM dynasore
25
20
15
10
5
0
1 hour
2 hours
3 hours
4 hours
Calcium repletion
C
Fold change in Percentage of TRITC-Dextran in basal compartment compared to full length β-actin mRNA expressing cells
Δ 3'UTR + 80μM dynasore
+ β-actin mRNA zipcode antisense
40
30
20
10
0
1 hour
2 hours
3 hours
4 hours
Calcium repletion

Figure 24: Inhibition of dynamin mediated endocytosis in cells with partially mislocalized β-actin translation rescues epithelial barrier function. (**A**) Graph representing the percentage of TRITC-dextran in the bottom compartment in an in vitro permeability experiment following a calcium switch in cells with proper localization of β-actin translation (expressing full length β-actin mRNA). Note that the percentage of TRITC-dextran reduces in the bottom compartment progressively decreases following calcium repletion. Bars represent Mean ± S.E.M. (**B, C**) Fold change in percentage of TRITC-Dextran in the bottom compartment of MDCK cells with partially mislocalized β-actin translation relative to cells with proper localization of β-actin translation: (**B**) following calcium repletion with DMSO (orange bars) or 80μM dynasore (green bars); (**C**) pretreated with β-actin mRNA zipcode antisense oligonucleotides followed by calcium repletion with 80μM dynasore. Note treating cells with partially mislocalized β-actin translation with 80μM dynasore rescues the barrier integrity defect. Also, barrier integrity fails to recover following calcium repletion upon a more complete mislocalization of β-actin translation with zipcode antisense oligonucleotides.

Dynasore dependent rescue of adherens junction assembly in cells with partially mislocalized β-actin translation requires functional E-cadherin

Dynamin inhibitors block recycling of several transmembrane proteins including E-cadherin. To test whether global inhibition of dynamin mediated endocytosis or more specifically, E-cadherin function at the cell surface, was required for rescuing adherens junction assembly in cells with partial defects in localizing β-actin translation, DECMA-1, an E-cadherin function blocking antibody was used (Vestweber and Kemler, 1985). Following calcium repletion in cells expressing Δ3′UTR β-actin mRNA that encodes β-actin with an eGFP –fusion tag, live cell imaging experiments were performed. In cells treated with vehicle alone, contact initiation followed by contact expansion is observed as an increase in distance between cell-cell vertices (**Figure 25A**, arrows). However, soon after this phase, cells continue to overlap contacting neighbors and fail to reach the junction maturation phase (**Figure 25A**). Cells treated with 80μM dynasore during calcium repletion, also exhibit normal contact initiation followed by contact expansion. However, this is followed by junction maturation seen as the accumulation of linear actin cables running along the cell-cell interface. Additionally, lamellar protrusive activity is shut off as the cells proceed through junction maturation stage 3 hours after calcium repletion (**Figure 25B**). By contrast, treating cells with DECMA-1 and 80μM of dynasore during calcium repletion not only abolishes the rescue of junction maturation, but also inhibits contact expansion (**Figure 25C**). These data show that inhibiting Dynamin mediated endocytosis requires E-cadherin function to rescue adherens junction assembly in cells with partially mislocalized β-actin translation.

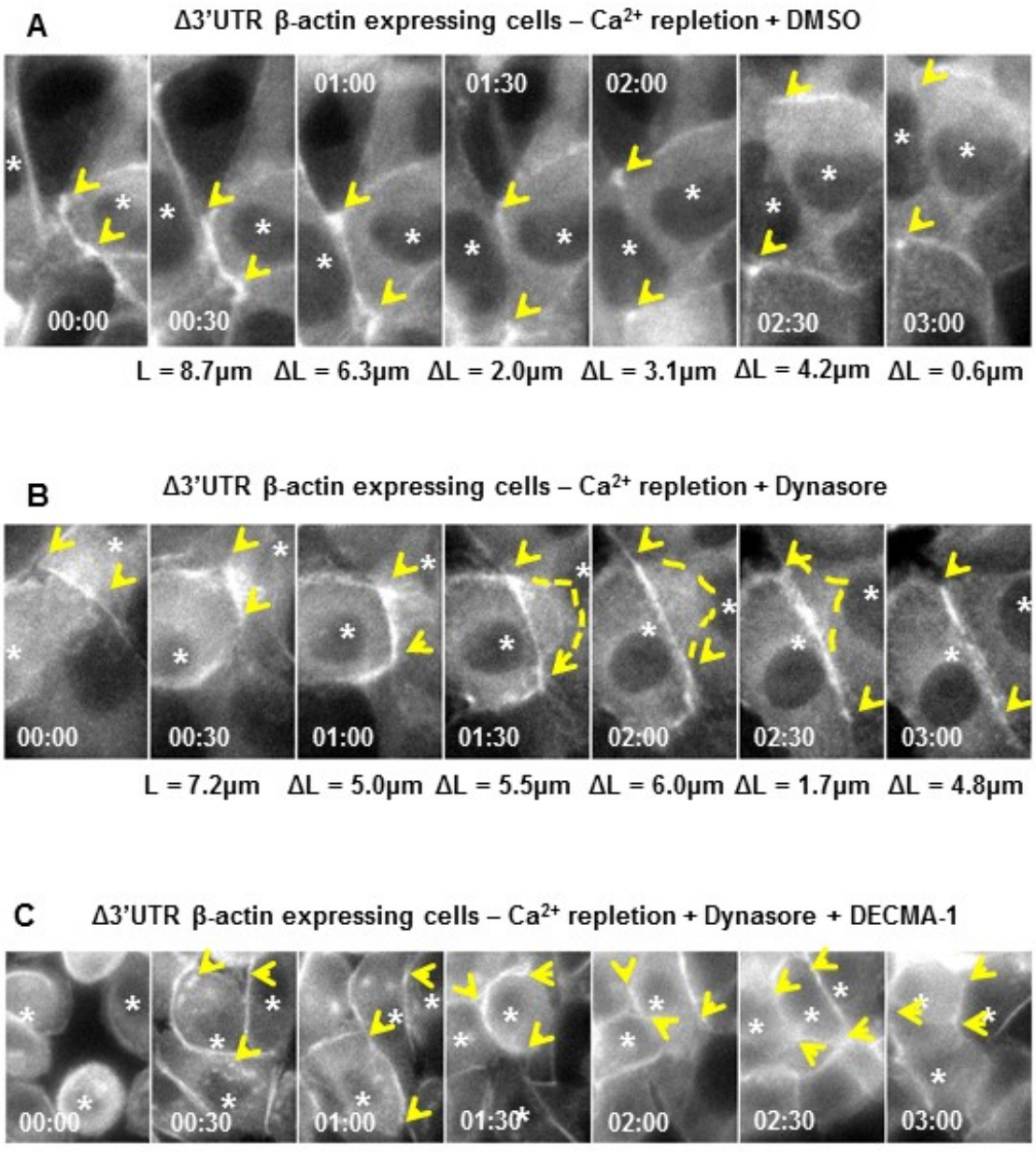
A
Δ3'UTR β-actin expressing cells – Ca2+ repletion + DMSO
00:00
00:30
01:00
01:30
02:00
02:30
03:00
L = 8.7μm ΔL = 6.3μm ΔL = 2.0μm ΔL = 3.1μm ΔL = 4.2μm ΔL = 0.6μm
B
Δ3'UTR β-actin expressing cells – Ca2+ repletion + Dynasore
00:00
00:30
01:00
01:30
02:00
02:30
03:00
L = 7.2μm ΔL = 5.0μm ΔL = 5.5μm ΔL = 6.0μm ΔL = 1.7μm ΔL = 4.8μm
C
Δ3'UTR β-actin expressing cells – Ca2+ repletion + Dynasore + DECMA-1
00:00
00:30
01:00
01:30
02:00
02:30
03:00

Figure 25: E-cadherin function in conjunction with endocytosis inhibition is required for rescuing adherens junction assembly in cells with partially mislocalized β-actin translation. Montage of MDCK cells with partially mislocalized β-actin translation (expressing Δ3′UTR β-actin mRNA that encodes an eGFP-fusion tag), following calcium repletion. Cells were treated with: (**A**) 0.5% (v/v) DMSO or (**B**) 80μM Dynasore or (**C**) 80μM DMSO + 100μg/mL DECMA-1, following calcium repletion. Time is indicated as duration post initial contact (**hh:mm**). **L** is an estimate of contact length and **ΔL** represents the increase in length with respect to the previous frame. Arrows point to expanding contacts. Note in cells treated with DMSO, there is overlap of neighboring cells while in cells treated with 80μM dynasore, contact expansion is followed by retraction of the protrusion (dotted line). Treating cells with DECMA-1 completely abolishes contact expansion as seen by the lack of continued expansion of the filamentous actin along the cell-cell interface. The data represents qualitative assessment of retraction followed by contact expansion upon inhibition of endocytosis in cells expressing Δ3′UTR β-actin mRNA following calcium repletion. Three independent experiments were performed for each condition in **A, B** and two independent experiments for **C**.

Spatial localization of β-actin translation regulates epithelial morphogenesis in 3 dimensional cyst cultures

Single MDCK cells embedded in Matrigel form 3 dimensional cysts with a single layer and single fluid filled lumen over a period of 6-14 days. The sub-cellular localization of newly synthesized β-actin protein in cyst cultures has not been determined. To this end, MDCK cells expressing full length β-actin mRNA with a tetracysteine coding tag were grown into cysts for 8 days. A pulse chase experiment using the biarsenical dyes: FlAsH and ReAsH (Gutierrez et al., 2014; Hoffmann et al., 2010; Martin et al., 2005; Rodriguez et al., 2006) was performed to determine the localization of newly synthesized β-actin monomer. After a 4.5 hour chase period, ReAsH, which stains newly synthesized β-actin monomer within this period, is asymmetrically distributed (**Figure 26**, ReAsH panel). Most of the newly synthesized β-actin monomer appears at the apical membrane while a slightly lesser, but still substantial accumulation is observed at cell-cell interfaces (**Figure 26**, yellow and white arrows). While it is yet to be determined whether β-actin mRNA is also asymmetrically localized in epithelial cysts, the preliminary result indicates that β-actin protein is asymmetrically incorporated in different sub-cellular compartments in 3 dimensional epithelial cysts.

To determine the extent to which spatial regulation of β-actin translation controls epithelial morphogenesis, single cell suspensions of MDCK cells with either no defects in localizing β-actin translation or those with partially mislocalized β-actin translation were cultured in Matrigel for 6 days. The following morphometric measurements were made: percentage of cysts with “normal morphology” – single layer single lumen (SLSL), mean lumen diameter, and mean height of cells in SLSL cysts. While the cysts derived from

cells with partially mislocalized β-actin translation have a slightly higher percentage of SLSL cysts, the mean lumen diameter and the mean cell height are both significantly lower compared to the controls (**Figure 27A-C and C′**). These results indicate that spatial regulation of β-actin translation controls cell shape and size during epithelial morphogenesis.

In view of the above described observations with cysts derived from cells with partially mislocalized β-actin translation, it was hypothesized that acto-myosin organization is perturbed upon partially mislocalizing β-actin translation. This could then result in cell shape and size changes and ultimately gene expression changes by impinging on mechano-transduction pathways. Additionally, experiments carried out in 2-dimensional calcium repletion assays indicated that cells with partially mislocalized β-actin translation took a longer time to achieve confluence in culture, indicating a possible defect in cell proliferation (**Materials and Methods, Calclium Repletion Experiments**). In addition to changes in cell shape and size, cysts derived from cells with partially mislocalized β-actin translation have fewer cells (**Figure 27A**, see number of nuclei). There are two possibilities to explain these observations: (1) there is reduced proliferation, or (2) there is increased apoptosis during cyst development. In order to test which of these two plausible mechanisms could explain the size variation in cysts due to mislocalization of β-actin translation, 6 day old cyst cultures were labelled with the cell proliferation marker, EdU. Cysts derived from cells with partially mislocalized β-actin translation have significantly fewer EdU positive cells per cyst than the controls indicating that proliferation in these cysts is indeed reduced (**Figure 28**).

Since, acto-myosin mediated tension in a cell lies at the core of any mechano-transduction module, F-actin and Non-muscle Myosin IIA (NMIIA) organization was evaluated in cysts derived from cells with either no defects in localizing β-actin translation or with partially mislocalized β-actin translation. While control cysts show well defined NMIIA and F-actin localized to cell-cell interfaces, cysts derived from cells with partially mislocalized β-actin translation show a disorganized NMIIA, F-actin network (**Figure 29A**). Additionally, tight junctions indicated by ZO-1 appear "wavy" in cysts derived from cells with partially mislocalized β-actin translation, rather than the polygonal appearance in control cysts (**Figure 29B**). These data together indicate that cells with partially mislocalized β-actin translation exhibit defects in acto-myosin organization that potentially contributes to a disruption of tight junction architecture and results in cell shape and size changes. Recent reports shed light on Hippo and/or Yap/TAZ pathways as regulators of gene expression changes by integrating acto-myosin tension dependent mechano-transduction signals (Low et al., 2014; Yu and Guan, 2013). One of the read outs of downregulated Hippo and/or YAP/TAZ pathways, is reduced cell proliferation. Thus it is plausible that spatially regulated β-actin translation controls this novel mechano-transduction module during epithelial morphogenesis.

Lastly, in order to explore the effect of acutely mislocalizing all β-actin mRNA following normal epithelial morphogenesis, β-actin mRNA zipcode antisense or scrambled oligonucleotides were added to 6 day old cysts derived from control cells. Cysts treated with scrambled oligonucleotides display SLSL organization and no morphological defects (**Figure 30A**). However, cysts treated with antisense oligonucleotides show multiple layers of cells (**Figure 30B**). Additionally, 7.5 hours after

treatment with β-actin mRNA zipcode antisense oligonucleotides cells begin to extrude into the lumen of the cyst (**Figure 30B**, arrows). Taken together these preliminary results indicate a role for spatially regulated β-actin translation in controlling cell shape, size, and number during epithelial morphogenesis.

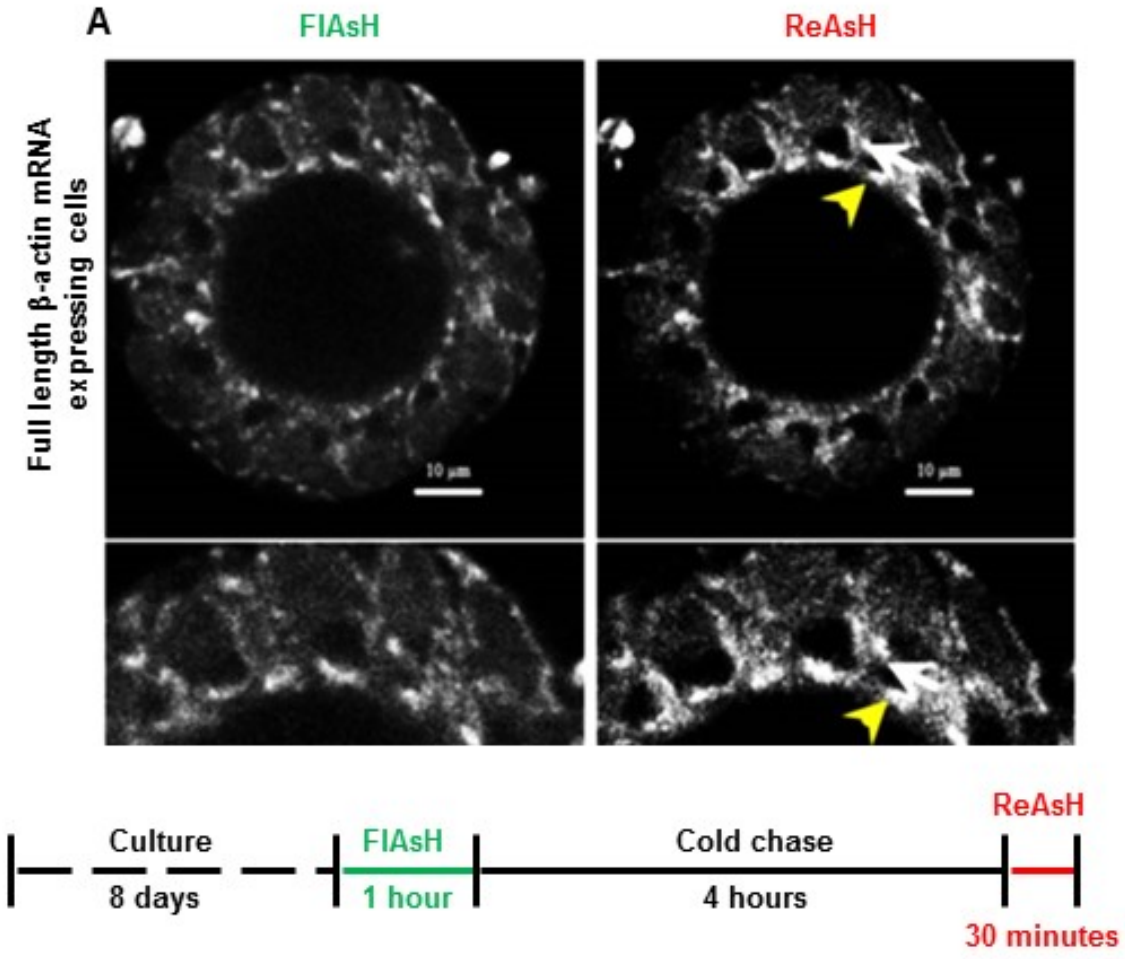
A
FlAsH
ReAsH
Full length β-actin mRNA expressing cells
10 μm
10 μm
Culture
8 days
FlAsH
1 hour
Cold chase
4 hours
ReAsH
30 minutes

Figure 26: Newly synthesized β-actin monomer localizes to the apical and lateral plasma membranes in epithelial cysts. MDCK cells expressing tetracysteine tagged β-actin were seeded as single cells in matrigel and allowed to develop into cysts for 6 days. The cultures were then pulsed with FlAsH for one hour to label all the β-actin synthesized till this point. Following a 4 hour cold chase period, cultures were labelled with ReAsH for 30 minutes to track the newly synthesized β-actin in the 4.5 hour chase window. Cultures were then fixed and imaged using a 63X/1.4 N.A. on a Zeiss CellObserver Spinning disc confocal. Note the accumulation of ReAsH signal (newly synthesized β-actin) at the apical and lateral plasma membranes (yellow arrowheads and white arrows, respectively. Scale bars = 10μm.

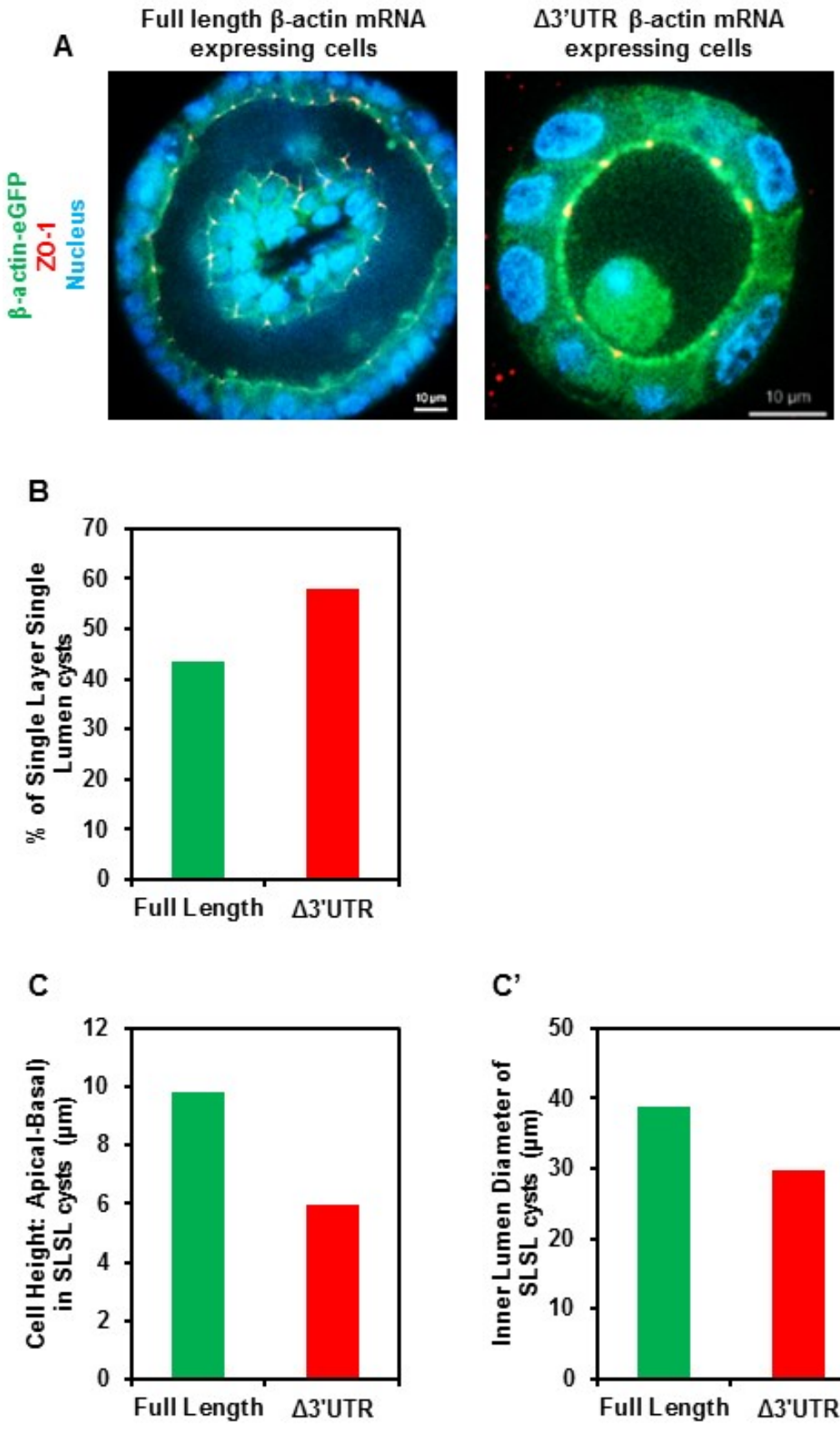
A
Full length β-actin mRNA expressing cells
Δ3'UTR β-actin mRNA expressing cells
β-actin-eGFP
ZO-1
Nucleus
10 μm
10 μm
B
% of Single Layer Single Lumen cysts
70
60
50
40
30
20
10
0
Full Length
Δ3'UTR
C
Cell Height: Apical-Basal) in SLSL cysts (μm)
12
10
8
6
4
2
0
Full Length
Δ3'UTR
C'
Inner Lumen Diameter of SLSL cysts (μm)
50
40
30
20
10
0
Full Length
Δ3'UTR

Figure 27: MDCK cysts assembled from cells with partially mislocalized β-actin translation exhibit smaller cyst diameters and have shorter cell height. (**A**) Representative images of MDCK cysts grown in matrigel for 6 days derived from control cells (Full length β-actin mRNA expressing) or cells with partially mislocalized β-actin translation (Δ3′UTR β-actin expressing). Scale bar = 10μm. Note that the control cysts are much larger than the ones derived from cells expressing Δ3′UTR β-actin mRNA. (**B-C**) Physical characteristics of cysts derived from control cells (green bars) or Δ3′UTR β-actin mRNA expressing cells (red bars). (**B**) Percentage of cysts with a single layer and single lumen (SLSL) – Normal cyst morphology. (**C**) Average height of cells in cysts with single layer and single lumen morphology. (**C′**) Mean inner lumen diameter of single layer single lumen cysts. Note that cysts derived from cells expressing Δ3′UTR β-actin mRNA have a smaller mean lumen diameter and are shorter than their control counterparts. Total number of cyst analyzed: for **A**, Full length β-actin mRNA expressing = 69 and Δ3′UTR β-actin mRNA expressing = 104; for B and C, Full length β-actin mRNA expressing = 30 and Δ3′UTR β-actin mRNA expressing = 58**.**

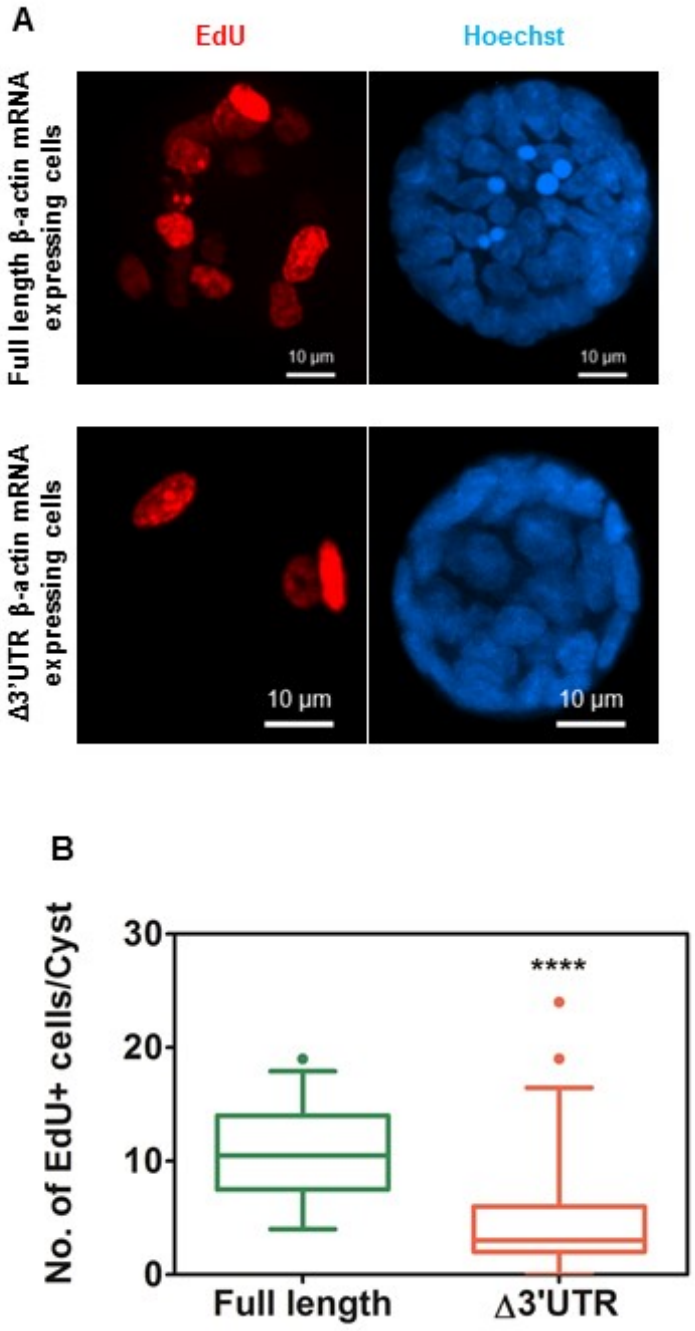
A
EdU
Hoechst
Full length β-actin mRNA expressing cells
Δ3'UTR β-actin mRNA expressing cells
10 μm
B
No. of EdU+ cells/Cyst
30
20
10
0
****
Full length
Δ3'UTR

Figure 28: Cysts from cells with partial mislocalization of β-actin translation have fewer proliferating cells. (A) 6 day old epithelial cysts derived from control cells (top panel) and cells with partially mislocalized β-actin translation (Bottom panel) were pluse labelled with EdU for 0.5 hours and stained with Alexa Fluor 555 conjugated azide using click chemistry. Note the presence of higher number of EdU positive cells in the control cysts. (B) Quantification of number of EdU positive (proliferating) cells per cyst. Full length β-actin mRNA expressing cysts (N = 30), Δ3′UTR β-actin mRNA expressing cysts (N = 58). An uppaired non-parametric student's t-test yielded ****$p < 0.0001$. Box plots with whiskers representing 2.5 and 97.5 percentiles.

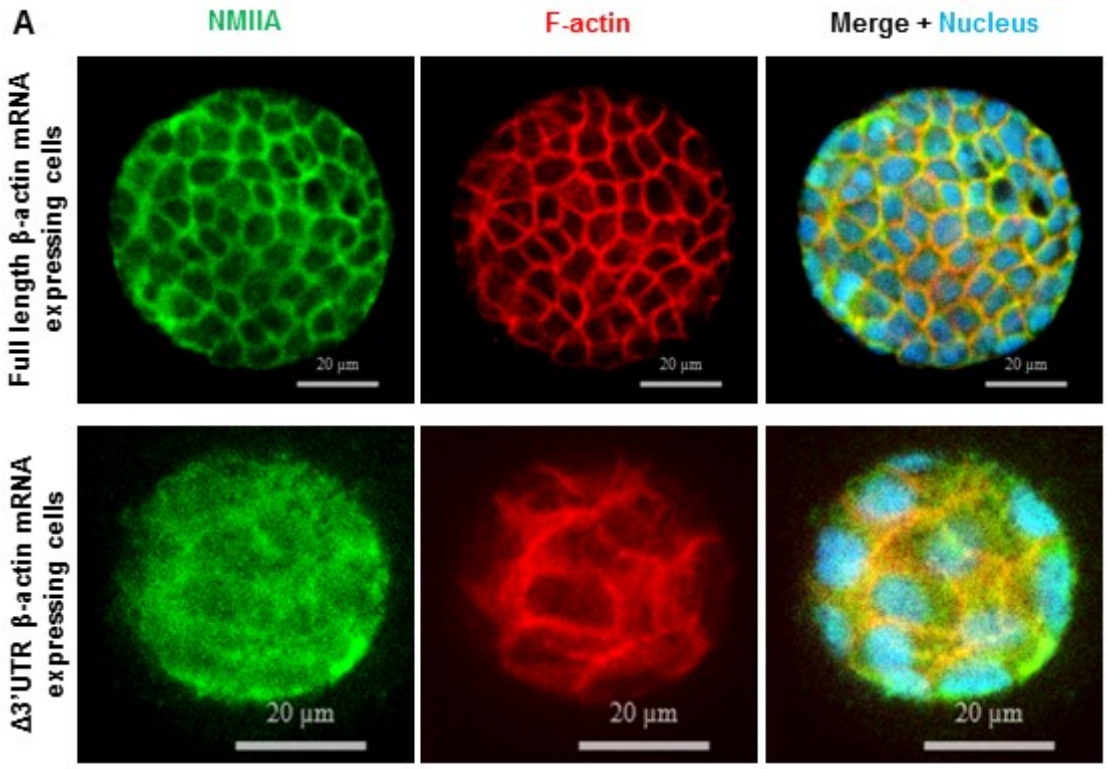
A
NMIIA
F-actin
Merge + Nucleus
Full length β-actin mRNA expressing cells
Δ3'UTR β-actin mRNA expressing cells
20 μm
20 μm
20 μm
20 μm
20 μm
20 μm

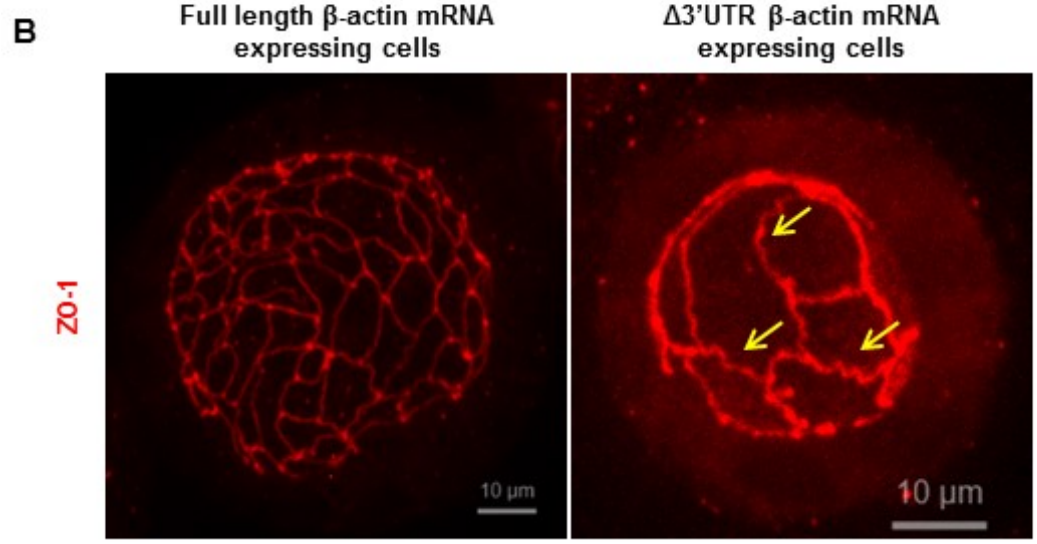
B
Full length β-actin mRNA expressing cells
Δ3'UTR β-actin mRNA expressing cells
ZO-1
10 μm
10 μm

Figure 29: Acto-myosin and tight junctional organization is disrupted in epithelial cysts derived from cells with partially mislocalized β-actin translation. (**A**) Cysts derived from control cells (Top panel) and cells with partially mislocalized β-actin translation (Bottom panel), immunostained for non-muscle myosin IIA (NMIIA, Green) and F-actin (Rhodamine Phalloidin, Red). Note the disruption in NMIIA organization in Δ3′UTR β-aactin mRNA expressing cells. (**B**) Cysts derived from control cells (left panel) and cells with partially mislocalized β-actin translation (right panel), immunostained for the tight junction marker ZO-1. Note the wavy nature of tight junction organization in cysts derived from cells with partially mislocalized β-actin translation (yellow arrows).

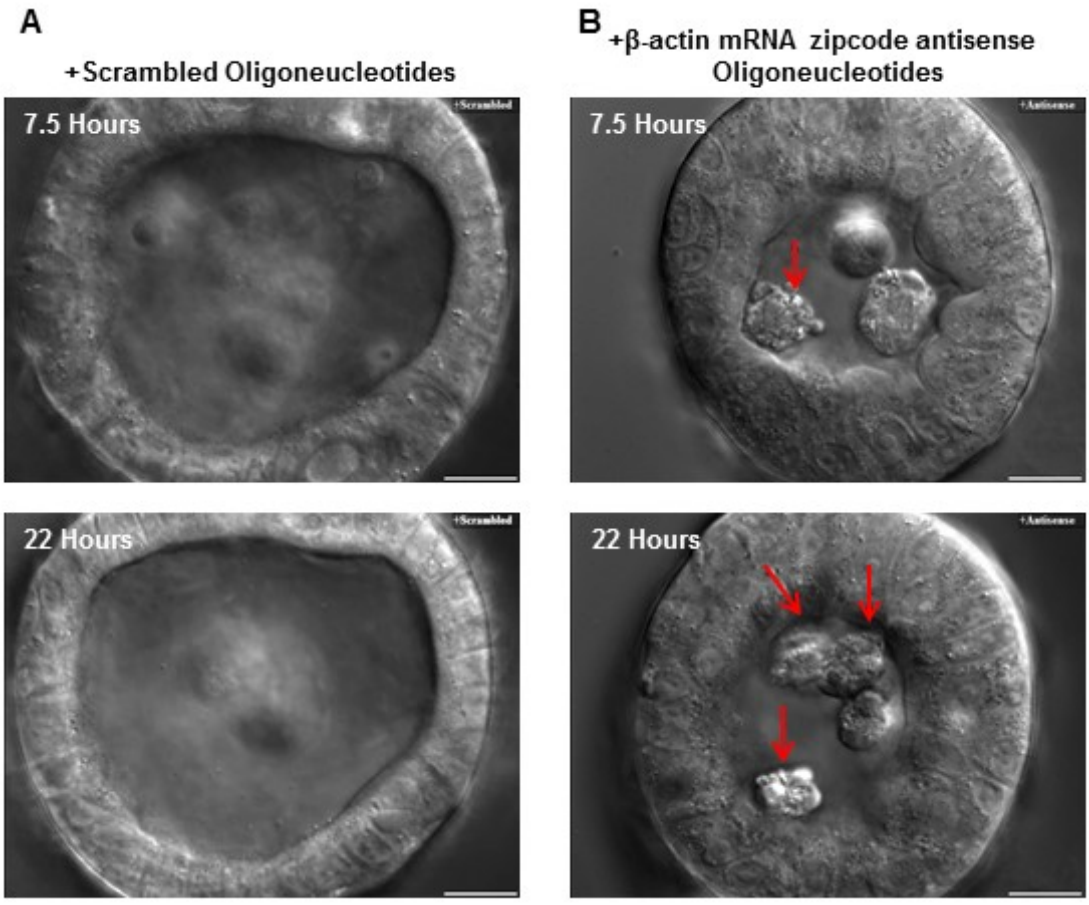
A
+Scrambled Oligoneucleotides
B
+β-actin mRNA zipcode antisense Oligoneucleotides
7.5 Hours
7.5 Hours
22 Hours
22 Hours

Figure 30: Acute and complete mislocalization of β-actin translation in epithelial cysts causes cells to extrude into cyst lumen. MDCK cells were seeded as single cells and allowed to develop into cysts for 6 days. Cultures were then treated with 8μM (**A**) scrambled oligonucleotides or (**B**) β-actin mRNA antisense oligonucleotides. Single cysts were imaged using a 63X/1.33 N.A. water immersion objective on a Zeiss AxioObserverZ1 widefiled microscope. DIC images were obtained. Top panel shows individual cysts 7.5 hours after oligonucleotide treatment and bottom panel shows 22 hours after treatment. Note that the cyst treated with β-actin mRNA zipcode antisense oligonucleotides has cells extruding into the lumen (red arrows).

DISCUSSION

Actin-anchoring and endocytosis: The Yin and Yang of adherens junction complex assembly

E-cadherin endocytosis contributes significantly to the dynamics of adherens junctions (Kowalczyk and Nanes, 2012; Troyanovsky et al., 2006). While endocytosis is required for redistributing E-cadherin at mature junctions (de Beco et al., 2009), constitutively active Rac1 depletes E-cadherin from cell-cell contacts by increasing its internalization (Akhtar and Hotchin, 2001), suggesting two roles for E-cadherin endocytosis. The first is a rapid turnover during the initial phase of adherens junction assembly following cell-cell contact where Rac1 activity is high, and the second is to recycle E-cadherin at mature junctions following disassembly of *trans* dimers (**Figure 31**). In fact, non-*trans* interacting E-cadherin is preferentially internalized (Izumi et al., 2004). Based on the evidence from literature and observations presented in this thesis, a model of adherens junction assembly is proposed (**Figure 31**). This model suggests β-actin translation dependent actin filament remodeling drives E-cadherin clustering at the cell surface to oppose the negative contributor, endocytosis of E-cadherin, and drives adherens junction assembly in epithelial cells (**Figure 31**). The balance tips towards reduced anchoring of the cadherin-catenin complex if actin filament assembly and remodeling is blocked. This is shown by the use of pharmacological agents such as Latrunculin A (Wu et al., 2015) and Cytochalasin B (Krendel and Bonder, 1999) or by inhibiting cell-cell contact localized β-actin monomer synthesis (Gutierrez et al., 2014). The result is that cells are unable to transition from contact initiation to contact

maturation owing to endocytosis of cadherin-catenin complexes, which now dominates actin anchoring of these complexes.

In Chapter 2, FCI analysis was developed as a tool to quantitate the extent of protein complex assembly and it was shown that frequency of FCI values for E-cadherin and F-actin serves as a measure of adherens junction assembly and maturation. Utilizing this analysis in Chapter 3, it was shown that in epithelial cells that have partially mislocalized β-actin translation, inhibiting dynamin mediated endocytosis results in a rescue of adherens junction assembly/maturation. These results were in fact reproducible with two different dynamin inhibitors – dynasore and a new generation of modified dynasore, Dyngo4a, which has greater specificity for dynamin inhibition (Macia et al., 2006; McCluskey et al., 2013). Cells that have partially mislocalized β-actin translation have reduced frequencies of cells with high FCI measures during adherens junction assembly unlike their wild type counterparts (compare **Chapter 2, Figure 9** and **Chapter 3, Figure 18**). However, treating cells that have partially mislocalized β-actin translation with the dynamin inhibitors, results in a rescue of adherens junction assembly defects. This is quantified by FCI analysis for E-cadherin and F-actin during a calcium repletion assay (**Figures 19-21**). Importantly, this aforementioned rescue of adherens junction assembly is dependent on the function of the endogenously expressed β-actin mRNA, which contains a functioning zipcode (**Figure 22**). Last but not least, high FCI values which represent adherens junction assembly/maturation following *de novo* cell-cell contact correlate with barrier integrity (**Figures 23 and 24**), and therefore are a useful measure of epithelial functionality.

β-actin zipcode functions as an integrator of several key signal transduction pathways to control epithelial structure and function

Signal transduction by RhoA family of small GTPases – RhoA, Rac1, Cdc42, and the Src family of kinases regulate epithelial adherens junction dynamics (Calautti et al., 1998; Manser, 2005; McLachlan and Yap, 2011; Menke and Giehl, 2012; Takahashi et al., 2005). While each of the signaling molecules mentioned has a wide range of roles in regulating epithelial cell-cell adhesion, their effect on F-actin dynamics at adhesions serves as a convergence point to determine the adhesive fate of the cell and tissue. For instance, Rac1 and RhoA show reciprocal spatio-temporal activation at cell-cell contacts during adherens junction assembly. During the initial phases of cell-cell contact formation, Rac1 activity at the cell periphery drives lamellipodia formation causing cellular overlap and facilitating E-cadherin homophillic ligation (Yamada and Nelson, 2007). This is followed by a downregulation of Rac1 activity and an upregulation of RhoA activity at cell-cell contacts (**Figure 32**). RhoA activity is maintained though contact expansion phase with the highest activity localized to the expanding cell-cell contact (**Figure 32**) (Yamada and Nelson, 2007). The RhoA activity at cell-cell contacts serves as a signal for β-actin mRNA to be localized to this compartment (Gutierrez et al., 2014; Latham et al., 2001). Localization and anchoring of cadherin-catenin complexes at cell-cell contacts provides a scaffold for signaling molecules such as Src (McLachlan and Yap, 2011). Src in turn acts to phosphorylate ZBP-1/IMP-1 resulting in the translation of cell-cell contact localized β-actin (Gutierrez et al., 2014; Huttelmaier et al., 2005). In addition, Rac1 activity increases E-cadherin recycling at the cell surface (Akhtar and Hotchin, 2001). Thus a failure to downregulate Rac1 activity at cell-cell contact

following contact initiation causes continued lamellipodail overlap. The resulting reduction in E-cadherin clustering causes reduced Src activity and ultimately junction maturation defects. Cell-cell contact localized β-actin translation thus acts as a key node in the feedforward loop (**Figure 31**), wherein it integrates Rho family of GTPase signaling, Src family of kinase signaling and E-cadherin recycling to ultimately control epithelial adherens junction assembly and maturation.

In addition to the lessons learned from 2-dimensional cultures using the calcium repletion assay, experiments carried out with 3-dimensional MDCK cyst cultures demonstrate a crucial role for spatially regulated β-actin translation in epithelial morphogenesis. First, preliminary evidence suggests that newly synthesized β-actin monomer is asymmetrically local in mature cysts indicating a role for spatially regulated translation. Next, upon partial mislocalization of β-actin translation, the cell size and cyst size are significantly reduced along with fewer proliferating cells per cyst. Additionally, the acto-myosin organization is perturbed plausibly causing a disrupted tight junction organization. All these observations point to an altered gene regulatory pathway owing to disrupted mechano-transduction apparatus. The most likely candidate for such an effect seen on cell proliferation is the Hippo and/or YAP/TAZ pathway. It would be interesting to test the total levels of phosphorylated YAP and or Hippo to determine whether this pathway is indeed downstream of a mechano-transduction cascade with spatially regulated β-actin translation at the top of the pathway. Further experiments along this line of reasoning would shed light on a novel function for spatially regulated β-actin translation in 3-dimensional epithelial morphogenesis as a key integrator of mechano-transduction signaling cascades.

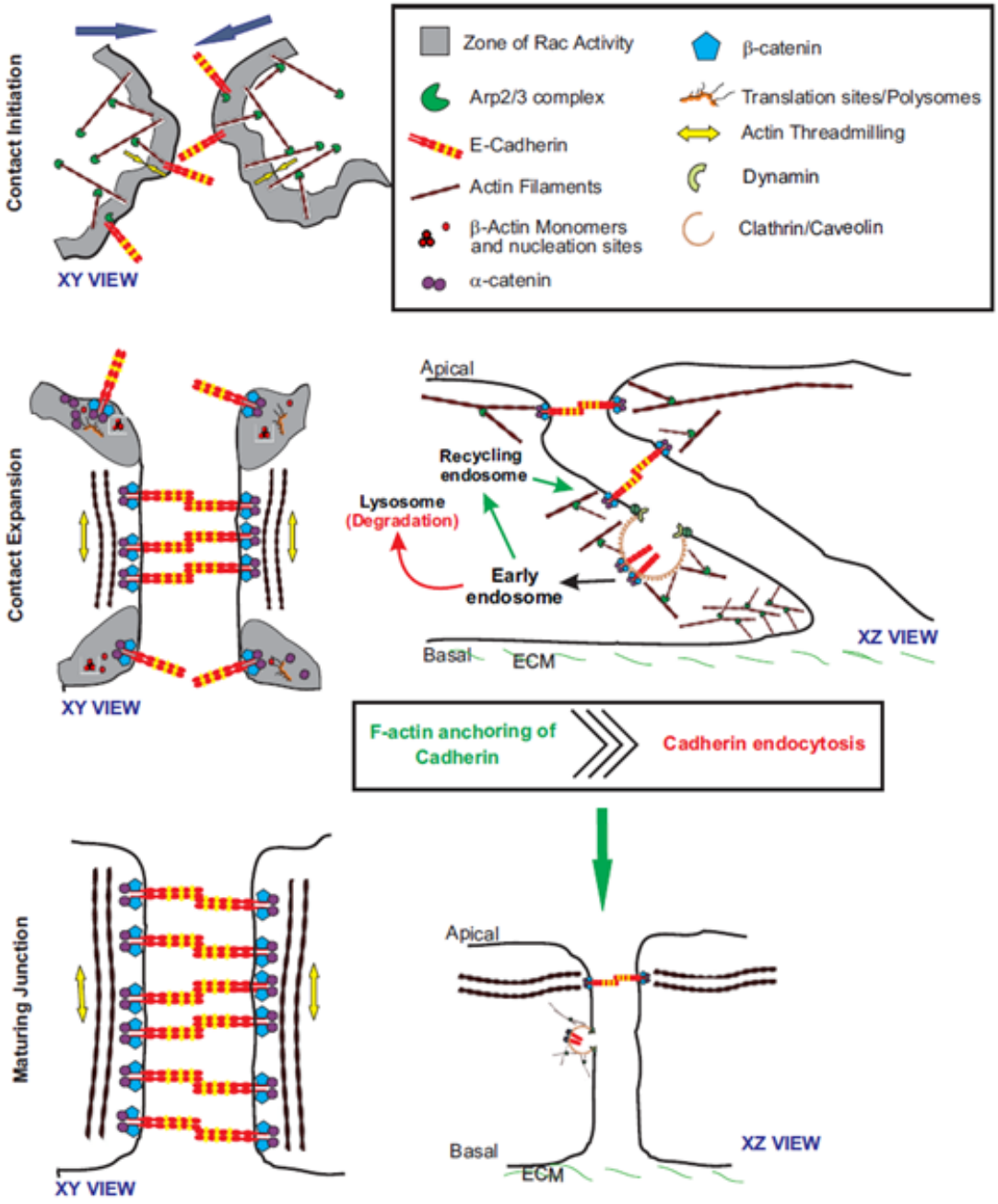
Contact Initiation
XY VIEW
Zone of Rac Activity
Arp2/3 complex
E-Cadherin
Actin Filaments
β-Actin Monomers and nucleation sites
α-catenin
β-catenin
Translation sites/Polysomes
Actin Threadmilling
Dynamin
Clathrin/Caveolin
Contact Expansion
XY VIEW
Apical
Recycling endosome
Lysosome (Degradation)
Early endosome
Basal
ECM
XZ VIEW
F-actin anchoring of Cadherin
Cadherin endocytosis
Maturing Junction
XY VIEW
Apical
Basal
ECM
XZ VIEW

Figure 31: Actin filament remodeling mediated E-cadherin clustering and E-cadherin endocytosis balance each other during adherens junction assembly. Schematic showing the three stages of *de novo* adherens junction assembly – contact initiation, contact expansion and junction maturation. Contact initiation is characterized by branched actin network at the leading edge of the cells. E-cadherin clustering mediates actin filament remodeling from branched array to linear filaments which anchor adherens junctions complexes, leading to the contact expansion phase. This is followed by an inhibition of protrusive activity and junction maturation. Endocytosis acts to remove E-cadherin-catenin complexes that are not actin anchored during contact expansion thus contributing negatively to contact expansion. The actin driven clustering supersedes endocytosis mediated removal of E-cadherin at the cell surface to drive adherens junction assembly.

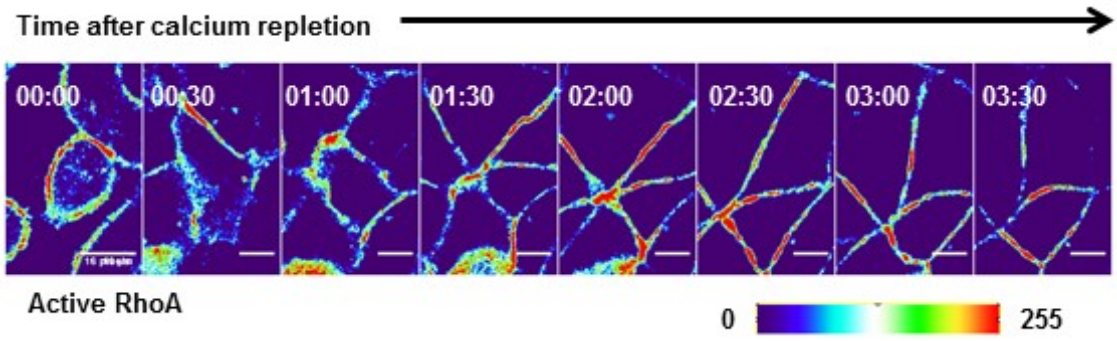
Time after calcium repletion
00:00
00:30
01:00
01:30
02:00
02:30
03:00
03:30
Active RhoA
0
255

Figure 32: RhoA is activated at cell-cell contacts following *de novo* epithelial cell-cell contact. Active RhoA was imaged using a Raichu RhoA FRET biosensor in MDCK cells following calcium repletion. Zones of RhoA activity are seen on the heat map at the areas of contact expansion.

MATERIALS AND METHODS

Cell culture and stable cell lines

MDCK – NBL2 cells (ATCC® CCL-34™) were cultured in DMEM supplemented with 10% (v/v) FBS and 100 I.U./mL Penicillin and 100µg/mL Streptomycin. Transfection of these cells with eTC GFP β-actin full length and eTC GFP β-actin ΔZip – (Δ3'UTR) (Addgene Plasmid #27123, #27124 and (Rodriguez et al., 2006)) was carried out using Lipofectamine® 2000 (Life Technologies) as per manufacturer's specifications. Transfected cells were selected using 500µg/mL G418 (Sigma-Aldrich). Flow cytometry was used to sort cells and obtain a homogeneous population of cells expressing GFP-β-actin.

Calcium switch experiments

Cells were plated at a density of 250,000 cells (for full length β-actin mRNA expressing cells) or 300,000 cells (for Δ3′UTR β-actin expressing cells) per well in a 6 well plate onto a 22X22mm No.1 coverslip (Fisher Scientific) and grown 48 hours. Cells washed with 1XPBS and medium without serum and supplemented with 4mM EGTA was added for 1 hour. Regular growth medium was added to initiate *de novo* adherens junction assembly. Additionally, either DMSO (0.5% v/v) (Sigma-Aldrich) or Dynasore (Sigma-Aldrich) at a concentration of 40µM/80µM/160µM or 4-Hydroxy Dynasore at a concentration of 80µM (Sigma-Aldrich) was added.

Pretreatment of cells with β-actin mRNA zipcode antisense oligonucleotide treatment was carried out in regular growth medium with 8µM of oligonucleotides for 12

hours prior to start of the experiment with fresh oligonucleotides being added every 4 hours. This was followed by a calcium switch as described above, maintaining oligonucleotides in the medium throughout the course of the experiment.

Live cell imaging

Cells were seeded at a density of 250,000 in 35mm MatTek dishes with glass cover bottom (MatTek Corp.) for 48 hours and treated subject to low calcium treatment as described above. FluorBrite DMEM (Life Technologies) supplemented with 10% FBS and OxyFluor (Oxyrase) at 1% (v/v) was used as calcium repletion medium to minimize photoxicity and photobleaching. Images were acquired on an inverted wide field Zeiss microscope (Zeiss AxioObserver.Z1) equipped with an incubator chamber (37 ºC and 5% CO_2) was used. A 63X water immersion objective, NA 1.33 was used. QuantEM 512SC camera (Photometrics) was used with no binning. Time-lapse images were taken in GFP channel (Filter Set 38HE, item number 489038-9901-000, Carl Zeiss, Inc) at 5 minute intervals for 12 hours. DECMA-1 antibody (Sigma-Aldrich) was used at 100µg/mL following calcium repletion.

Matrigel cultures

Single cell suspensions of MDCK cells expressing either full length or Δ3′UTR β-actin mRNA were seeded at a density of 4000-5000 cells in 100% Matrigel per well of an 8-well multi-chamber slide (MatTek). Once the Matrigel polymerized, DMEM containing 5% (v/v) FBS, 100 I.U./mL Penicillin and 100µg/mL Streptomycin was added. Cysts were allowed to develop from single cells over a period of 6-8 days.

Immunofluorescence and imaging

Cells were fixed at room temperature in 4% (w/v) paraformaldehyde in 1XPBS (pH 7.2) for 20 minutes. 0.5% (v/v) Triton-X was used to permeablize the cells for 1 minute at room temperature. Followed by blocking in 1% (w/v) BSA, cells were incubated in mouse monoclonal anti-E-cadherin primary antibody (1:200 dilution in blocking solution, BD Biosciences, #610181) overnight at 4°C. Cells were then incubated with goat anti-mouse Cy5 (Life Technologies) conjugated secondary antibody (1:1000 dilution in blocking solution for 1½ hours at room temperature. Rhodamine-Phalloidin (1:40 dilution in 1X PBS, Life technologies) was used to stain F-actin for 40 minutes at room temperature. DAPI or Hoechst 33342 was used to stain the nucleus following which coverslips were mounted using Prolong® Gold (Life Technologies). Images were acquired using a Zeiss AxioObserver.Z1 microscope and a 63X oil immersion lens (NA 1.4). Z-stacks were acquired using QuantEM 512SC camera (Photometrics) or Cool Snap HQ^2 (Photometrics) at a Z-depth of 240μm per slice.

Cyst cultures grown in 8-well chamber slides were fixed at room temperature in 4% (w/v) paraformaldehyde in 1XPBS (pH 7.2) for 30 minutes. 0.5% (v/v) Triton-X was used to permeablize the cells for 10 minutes at 4°C. Fixed and permeablized cultures were then washed in 100mM PBS-Glycine. This was followed by blocking with 10% (v/v) normal goat serum, 0.1% (w/v) BSA, 0.2% (v/v) Triton-X 100 and 0.04% (v/v) Tween-20 in 1XPBS for 1 hour at room temperature. The cysts were then incubated with primary antibody diluted in blocking solution (anti-ZO-1, mouse monoclonal, Sigma Aldrich 1:200) overnight at 4°C. The chamber-slide was then allowed to equilibrate to room temperature and cysts were washed with 0.1% (w/v) BSA, 0.2% (v/v) Triton-X 100

and 0.04% (v/v) Tween-20 in 1XPBS. Cysts were then incubated with goat anti-mouse Cy5 (Life Technologies) conjugated secondary antibody (1:200 dilution), Rhodamine-Phalloidin (Life Technologies) (1:200 dilution), Hoechst 33342 (1:10,000) in blocking solution at room temperature for 2 hours. Images were acquired using a Zeiss CellObserver Spinning Disc confocal microscope fitted with a 40X oil immersion objective (N.A. 1.0). Z-stacks were acquired using Evolve EMCCD camera (Photometrics).

EdU labelling of Matrigel cyst cultures

MDCK cells expressing either full length or Δ3′UTR β-actin mRNA were seeded into Matrigel as described above and allowed to develop into cysts for 6 days. Cysts were then incubated for 45 minutes with 10μM EdU solution diluted in growth medium. The cysts were then fixed with 4% (w/v) paraformaldehyde for 20 minutes at room temperature. This was followed by permeablization with 0.5% (v/v) Triton-X 100 for 10 minutes at 4°C. The cysts were then washed twice with 100mM PBS-Glycine followed by by two washes (3 minutes each) with 3% (w/v) BSA at room temperature. The click-iT reaction cocktail (For ≈ 500μL; 450μL of 1X reaction buffer diluted in water + 20μL CuSO4 + 1.25μL AlexFluor conjugated Azide + 50μL additive. The order in which the solutions are added must be the same as the list above) is added to the cysts and allowed to incubate for 30 minutes at room temperature. The cysts were then washed with 3% (w/v) BSA and the cysts were immunostained starting with blocking as described above. EdU labelling kit was purchased from Life Technologies.

Image processing and quantitative analysis

Images were processed using the Zeiss AxioVision 4.8.2 Deconvolution algorithm with the following parameters – Autolinear normalization, Noise regularization: Manual Strength – 6 and Constrained Iterative deconvolution. Processed images were exported into Volocity® 6.1 (PerkinElmer). Two distinct cellular compartments – cell periphery and the cytoplasm (interior of the cell excluding the periphery and the nucleus) were defined using the ROI tool and the Pearson's Correlation Coefficient (for E-cadherin and F-actin) was computed using the object co-localization tool. The data for all the cells was analyzed using MATLAB and graphed using GraphPad Prism 5 software. For more details on image processing and analysis, see Chapter 2.

***In vitro* permeability assay**

MDCK cells expressing Δ3′UTR β-actin were plated at 700,000 cells per Transwell® support (0.4μm pore size, Corning) in a 6 well plate and incubated for 48 hours. A calcium switch was performed as described above and 5mg/mL of 3000MW TRICT-dextran was added in 1, 2, 3 or 4 hours after calcium repletion in the top compartment for 2 hours. 200μl samples were taken from the top and bottom compartments and fluorescence intensity was measured using a GloMax plate reader (Promega). The ratio of the fluorescence intensities in the bottom and top compartments was taken. The contribution of TRITC-dextran in the bottom chamber was used as a proxy to assess the barrier functionality of a monolayer.

CHAPTER 4: SPATIALLY REGULATED β-ACTIN TRANSLATION CONTROLS EPITHELIAL COLLECTIVE CELL MIGRATION BY MODULATING ACTIN DYNAMICS AT LEADER-FOLLOWER CELL-CELL ADHESIONS

INTRODUCTION

Collective cell migration is a hallmark of several key developmental processes (Friedl and Gilmour, 2009). Some examples which have been studied include: border cell migration in *Drosophila melanogaster* oogenesis (Montell, 2003), branching morphogenesis in mammary epithelia (Ewald et al., 2008), and migration of neural crest cells – a key feature in vertebrate development (Mayor and Theveneau, 2013; Theveneau and Mayor, 2012). Several modes of migration based on the morphology of protrusions in the migrating cells have been proposed: amoeboid migration driven by pseudopodia, mesenchymal migration driven by lamellipodia and novel lobopodia in 3D matrices, collective or chain migration driven by lamellipodia in leader-follower pairs, and cell streaming directed by a combination of the above mentioned types of protrusive activity (Friedl and Wolf, 2010; Petrie et al., 2014; Rorth, 2009; Roussos et al., 2011). Omelchenko and colleagues described the formation of "leader cells" following wounding in epithelial sheets, which were characterized by loss of marginal actin bundles aligned parallel to the wound edge followed by the formation of large lamellipodia in these cells (Omelchenko et al., 2003). Follower cells to either side of the leaders still maintain actin bundles parallel to the wound edge and appear to follow suit after the

leaders (Omelchenko et al., 2003; Poujade et al., 2007). This results in a collective sheet migration in epithelial cells, unlike mesenchymal cells which behave as individual migrating cells. While the dysfunction of epithelial collective behavior is essential for neural crest migration and development, it is detrimental in epithelial cancers. A loss of epithelial phenotype and gain of mesenchymal phenotype – Epithelial-to-Mesenchymal Transition (EMT) – precedes the development of metastases in epithelial tumors (Bravo-Cordero et al., 2012; Revenu and Gilmour, 2009).

Many signaling molecules play an important role in collective cell migratory behavior (Ilina and Friedl, 2009). Some of the players that have been subject to extensive studies in this context are: Rho family of small GTPases mediating cytoskeletal rearrangements (Zegers and Friedl, 2014), Integrin family of transmembrane receptors mediating cell-matrix adhesions during migration (Huttenlocher and Horwitz, 2011), and Cadherin family of transmembrane receptors mediating cell-cell interactions during collective migration (Friedl and Gilmour, 2009). While the role of mRNA localization is being extensively studied in single cell migratory behavior (Liao et al., 2015; Mili and Macara, 2009; Mili et al., 2008), its role in collective cell migration in epithelia is still poorly understood. A non-exhaustive list of mRNAs that exhibit differential localization in a ZBP-1/IMP-1 dependent manner within single migrating cells include: β-actin (Lawrence and Singer, 1986), members of the Arp2/3 complex sub-units (Mingle et al., 2005), and more recently cofilin (Maizels et al., 2015). On the whole ≈ 3% of the transcriptome in Human Embryonic Kidney 293 (HEK293) cells was found to be associated with IMP-1, which is about 372 transcripts (Jonson et al., 2007). The underlying common theme connecting many of the mRNAs localized to protrusions is the

ability of their protein products to affect cytoskeletal dynamics and thus regulate cell migratory behavior.

The goal of this chapter is to elucidate the role of spatially regulated β-actin translation on the migratory behavior of wounded epithelial sheets. Work from Rob Singer and colleagues has shown that spatially regulated β-actin translation is essential for directional cell migration in fibroblasts (Latham et al., 2001; Shestakova et al., 2001). Work presented in this thesis and previous publications from the lab have demonstrated a role for spatially regulated β-actin translation in the formation of cell-cell adhesions (Cruz et al., 2015; Gutierrez et al., 2014; Rodriguez et al., 2006). However, the extent to which spatially regulated β-actin translation regulates collective epithelial cell migration involving dynamic rearrangements of cell-cell adhesions and migration of cells is yet to be explored. Results in this chapter indicate partial mislocalization of β-actin translation leads to increased protrusion dynamics in leader cells. However, the increased activity of the leading edge fails to translate to tissue level migration, where in fact cells with partially mislocalized β-actin translation migrate at slower rates than tissues composed of cells with no defects in localizing β-actin translation. Finally, FRAP experiments demonstrate that spatially regulated β-actin translation controls actin dynamics at leader-follower cell-cell adhesions to determine epithelial collective cell migratory behavior.

RESULTS

Partial mislocalization of β-actin translation increases protrusive activity in leader cells during epithelial collective cell migration

In order to determine the role of spatially regulated β-actin translation in epithelial collective cell migration, MDCK cells without any defects in localization of β-actin translation (Full length β-actin mRNA expressing) or partially mislocalized β-actin translation (Δ3′UTR β-actin mRNA expressing) were grown into monolayers and an infinite scratch wound was made. The exogenous β-actin expressed as an eGFP fusion was used to track the dynamics of lamellipodial protrusions in leader cells following an initial 2 hour refractory period (**Figure 33**). Radial velocities vectors were obtained and plotted as a function of angle with respect to a fixed centroid (Dubin-Thaler et al., 2004; Ryan et al., 2013). Vector maps show protrusions and retractions along various points on the lamellipodium in leader cells with or without partial defects in localizing β-actin translation (**Figure 34A, 35A**, red areas indicate protrusions, blue areas indicate retractions). In order to measure the net velocity of the entire leading edge, an instantaneous vector sum of the velocities was plotted for each time step. Both cells show 0 net velocities over a minute of analysis, with intermittent net protrusive and retractile activity (**Figure 34B, 35B**, green and red arrows). These results are consistent with the fact that protrusions have a half-life on the order of tens of seconds and over the minute time scale of analysis the net protrusive activity is centered around 0 (Ryan et al., 2013). The activity of the leading edge regardless of the direction of velocity i.e., protrusion or retraction, can be measured by the root mean squared velocity (V_{RMS}) at each time step. While control cells have a $V_{RMS} \approx 100$nm/s (**Figure 34C**), leader cells with partially

mislocalized β-actin translation have 1.5 fold higher V_{RMS} (**Figure 35C**, ≈ 150nm/s). These results taken together indicate that leader cells with partially mislocalized β-actin translation have a more active leading edge than control cells.

Partial mislocalization of β-actin translation reduces rate of collective migration in epithelial sheets

To determine how the leading edge activity translates to rate of collective tissue migration, wounded monolayers were imaged at low magnification to measure tissue migration rates. Surprisingly, the rate of migration was about three times faster in control cells as compared to cells with partially mislocalized β-actin translation **(Figure 36A-C)**. Additionally, epithelial sheets composed of cells with partially mislocalized β-actin translation had overlapping cells 1.5 hours after wounding while control epithelial sheets moved as a single sheet without significant overlap of cells **(Figure 36A, B)**. The controls cells had a relatively normal refractory period of about 10 – 15 minutes following wounding, similar to wild type MDCK monolayers following wounding (Matsubayashi et al., 2011). These results indicate although the leading edge of cells with partially mislocalized β-actin translation is more active, these cells are less efficient in translating the leading edge activity to tissue level migratory behavior.

Collective cell migration in epithelial sheets can be modeled by a physical system that maintains a continual stretch with the following assumptions about the underlying cell mechanics: first, cell-cell contacts transmit forces across the monolayer acting as springs (Weber et al., 2012), and second, the cytoskeleton has a threshold strain value beyond which it first reinforces and then fluidizes away from the source of the strain

(Hamilton et al., 2013; Serra-Picamal et al., 2012). Trepat and colleagues showed that pharmacological agents that stabilize the actin cytoskeleton, such as jasplakinolide, tend to bring about the greatest fluidization in cells to stretch. On the contrary, lantranculin A, which depolymerizes actin cytoskeleton, elicits a reduced fluidization of the cell to stretch. Additionally, a more stable cytoskeleton causes a faster recovery to a solid-like state (Trepat et al., 2007). The role of spatially regulated β-actin translation in collective cell migratory behavior can be explained by superimposing the model of cell mechanics described by Trepat and colleagues onto observations presented in this thesis. First, cells with partially mislocalized β-actin exhibit defects in establishing and stabilizing cadherin mediated cell-cell contacts (Cruz et al., 2015), which plausibly translate to the inability of these cells to transmit sufficient forces via cell-cell adhesions during collective cell migration. Second, partially mislocalizing β-actin translation results in a less stable cytoskeleton, mimicking the effect of actin depolymerizing drugs such as latrunculin A. The combined effect of the above two phenomenon, is lower migration rates of tissues owing to lack of sufficient force transmission across the tissue and additionally, an inability to efficiently stabilize the cytoskeleton to achieve cycles of fluidization and re-solidification.

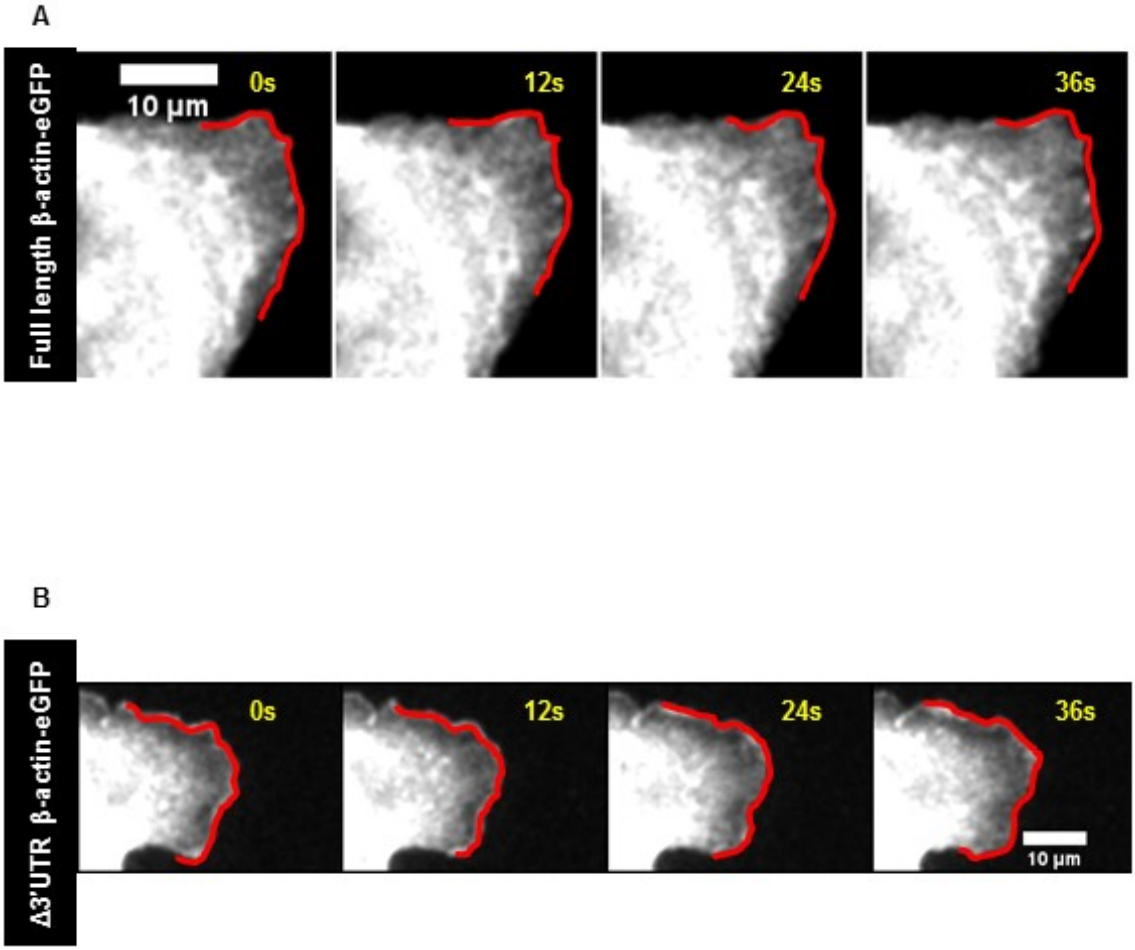
A
Full length β-actin-eGFP
10 µm
0s
12s
24s
36s
B
Δ3'UTR β-actin-eGFP
0s
12s
24s
36s
10 µm

Figure 33: Tracking leading edge protrusions in leader cells following model wounds. MDCK cells expressing (**A**) full length and (**B**) Δ3′UTR β-actin mRNA with an eGFP fusion tag were grown into monolayers and an infinite scratch wound was made to stimulate collective cell migration. Live cell imaging was performed on leader cells and images were acquired at an interval of 800ms. Using JFilament plugin for ImageJ, the protrusions were tracked (Red curves in **A** and **B**). Time is indicated in seconds for the montages shown in **A** and **B**. Scale bar = 10μm.

A

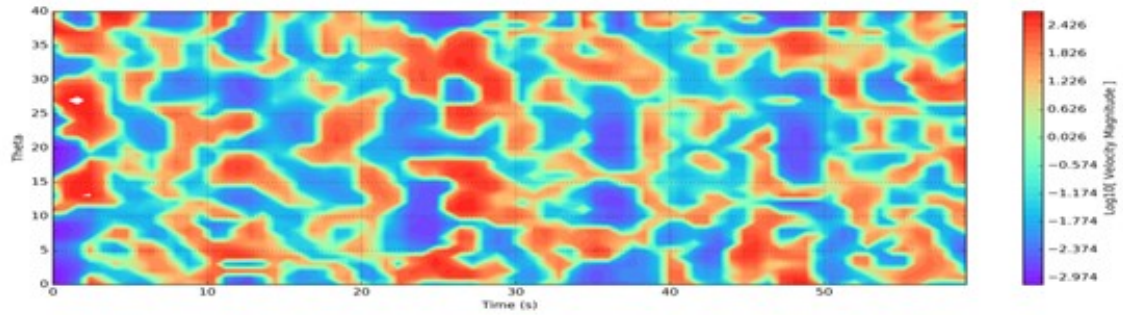
Theta
Time (s)
Log[10] Velocity Magnitude]
2.426
1.826
1.226
0.626
0.026
−0.574
−1.174
−1.774
−2.374
−2.974

B

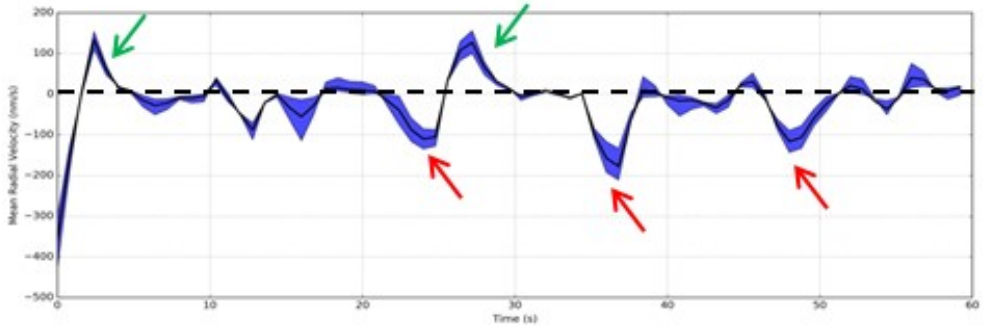
Mean Radial Velocity (mm/s)
Time (s)

C

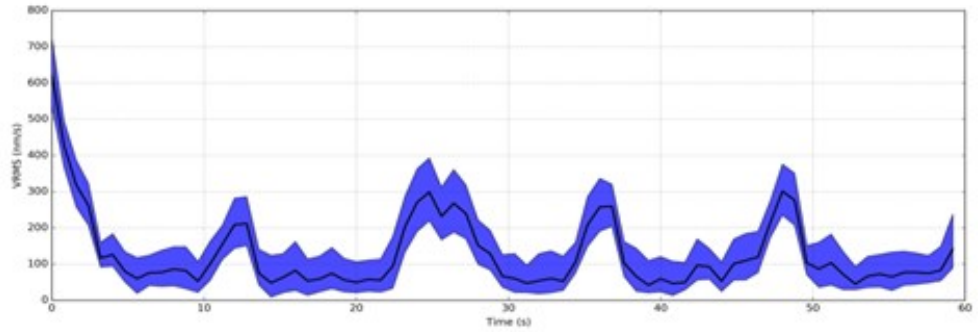
VRMS (mm/s)
Time (s)

Figure 34: Leader cells without any defects in localizing β-actin translation display protrusive dynamics on the order of 100nm/s. (**A**) Radial velocity vector maps for leader cells following model wound in monolayers composed of MDCK cells expressing full length β-actin mRNA. Y-axis represents the angle with respect to the fixed centroid of the protrusion. X-axis represents time in seconds. The heat map scale defines: retractions (Blue to Green: Negative velocities) and protrusions (Green to Red: Positive velocities). (**B**) Instantaneous mean radial velocity of the leading edge. The graph represents a vector sum of the velocities at each time step shown in **A**. Black line indicates 0nm/s. Red arrows indicate a net retraction of the leading edge while Green arrows indicate a net protrusion. (**C**) Root mean squared velocities (V_{RMS}) of the leading edge at any given time. Note the V_{RMS} fluctuates around 100nm/s. The solid black lines in **B** and **C** indicate the calculated mean radial velocity and V_{RMS}, respectively. The blue bands in **B** and **C** represent the uncertainty in measurement.

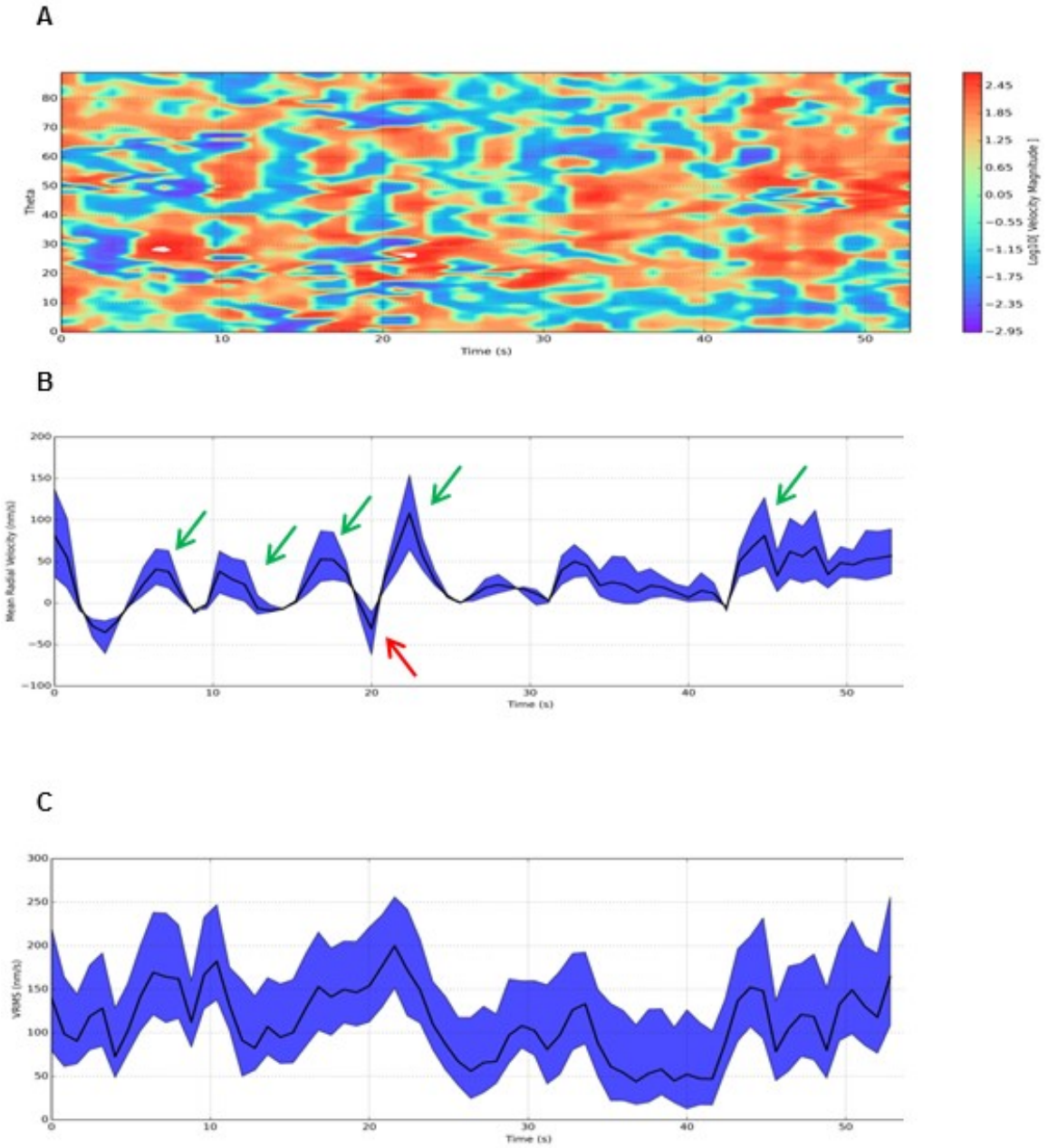
A
Theta
Time (s)
Log10[Velocity Magnitude]
B
Mean Radial Velocity (nm/s)
Time (s)
C
VRMS (nm/s)
Time (s)

Figure 35: Leader cells with partially mislocalized β-actin translation display protrusive dynamics on the order of 150nm/s. (**A**) Radial velocity vector maps for leader cells following model wound in monolayers composed of MDCK cells expressing Δ3′UTR β-actin. The Y-axis represents the angle with respect to the fixed centroid of protrusion. X-axis represents time in seconds. The heat map scale defines: retractions (Blue – Green: Negative velocities) and protrusions (Green – Red: Positive velocities). (**B**) Instantaneous mean radial velocity of the leading edge. The graph represents a vector sum of the velocities shown in **A**. Black line indicates 0nm/s. Red arrows indicate a net retraction of the leading edge while Green arrows indicate a net protrusion. (**C**) Root mean squared velocities (V_{RMS}) of the leading edge at any given time. Note that the V_{RMS} fluctuates around 150nm/s. The solid black lines in **B** and **C** indicate the calculated mean radial velocity and V_{RMS}, respectively. The blue bands in **B** and **C** represent the uncertainty in measurement.

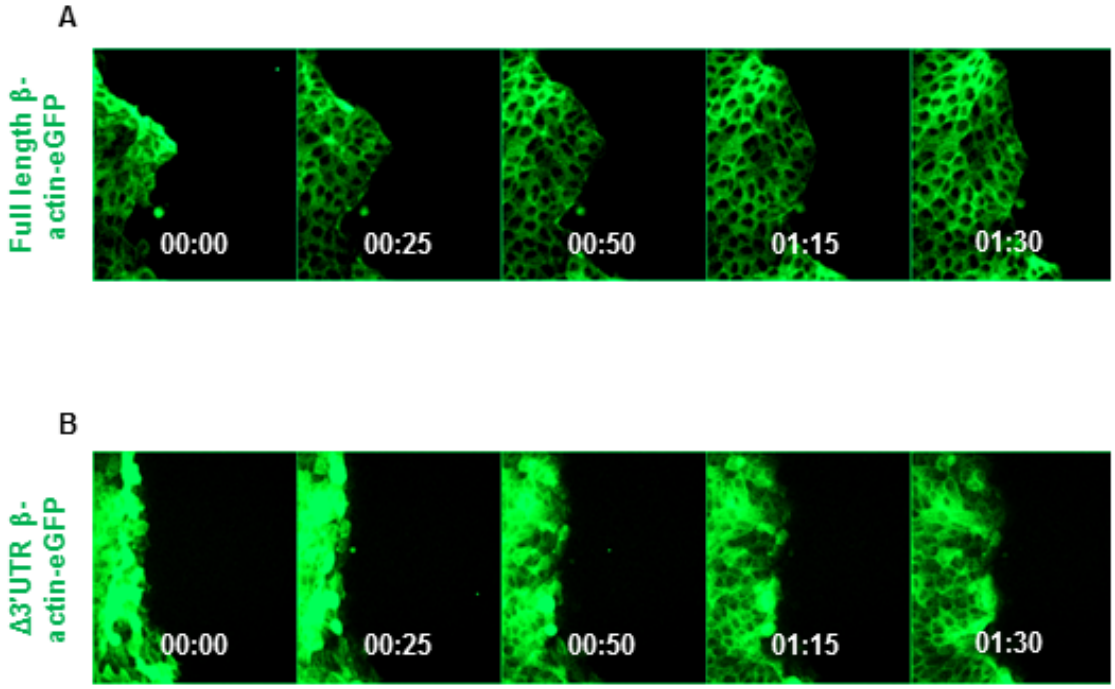
A
Full length β-actin-eGFP
00:00
00:25
00:50
01:15
01:30
B
Δ3'UTR β-actin-eGFP
00:00
00:25
00:50
01:15
01:30

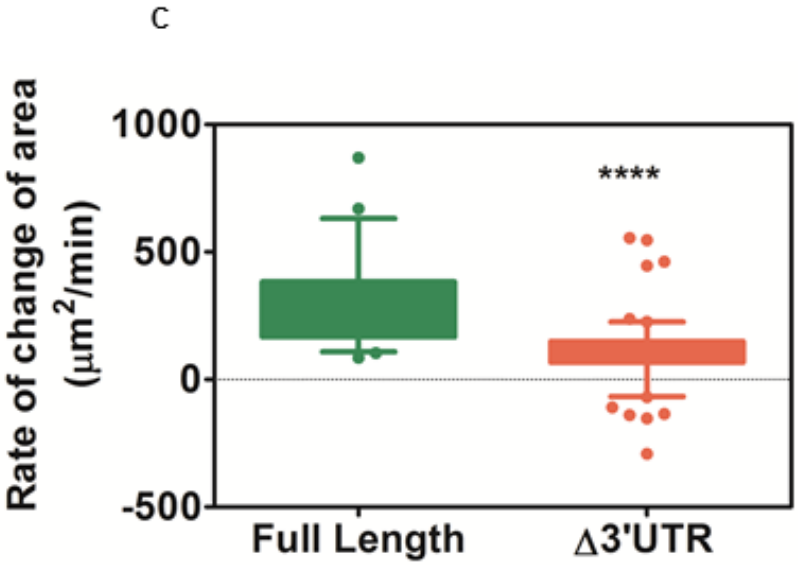
C
Rate of change of area (μm²/min)
1000
500
0
-500
****
Full Length
Δ3'UTR

Figure 36: MDCK monolayers composed of cells with partially mislocalized β-actin translation exhibit 3 fold lower migration rates. Montages of MDCK monolayers composed of (**A**) cells expressing full length β-actin-eGFP or (**B**) cells expressing Δ3′UTR β-actin-eGFP, stimulated to collective migrate following model wound. Time is indicated as hh:mm. Time gap between wounding and acquisition of first frame ≈ 15 minutes. (C) Rate of migration into wound area represented as rate of change of area following wounding (μm^2/min). Frames were acquired at 5 minute intervals and points represent the rate of change on area every 5 minutes. Box plots with whiskers representing 2.5 and 97.5 percentiles. Non-parametric Mann-Whitney test gave a significance with ****$p < 0.0001$. Note that the cells expressing Δ3′UTR β-actin have negative rates of migration which were observed as the monolayer retracted during the initial phase following wounding. Also note that tissues with partially mislocalized β-actin translation displayed significant cell-cell overlap which was largely absent from the control cells.

Actin dynamics at leader-follower cell-cell adhesions is controlled by spatially regulated β-actin translation

In order to assess the dynamics of β-actin at the cell-cell adhesions between leader-follower cell pairs, Fluorescence Recovery After Photobleaching (FRAP) experiments were performed. MDCK monolayers, assembled from control cells or cells with partially mislocalized β-actin translation, were stimulated to undergo collective cell migration into an infinite scratch wound. 2 hours following the scratch, FRAP analysis was carried out on β-actin-eGFP at cell-cell interfaces of leader-follower pairs (**Figure 37A, B, Red boxes**). The normalized fluorescence intensities were fit to a one phase association curve to obtain half times ($t_{1/2}$) of fluorescence recovery. Control cells show higher $t_{1/2}$ values compared to cells with partially mislocalized β-actin translation (**Figure 37A′, B′,** Control ≈ 31s compared to Δ3′UTR β-actin mRNA expressing cells ≈ 10s).

As a control, the dynamics of β-actin at cell-cell adhesions in steady state was analyzed. Interestingly, the $t_{1/2}$ of fluorescence recoveries shows little variation between cells that properly localize β-actin translation and cells with partially mislocalized β-actin translation (**Figure 38A, A′ and B, B′**). These results indicate that upon stimulation of collective migratory behavior epithelial cells establish a new dynamic equilibrium for β-actin at cell-cell adhesions in leader-follower pairs. Importantly, this new equilibrium is dependent the spatial regulation of β-actin translation (**Figure 39A**). Although the $t_{1/2}$ of fluorescence recovery times was similar in monolayers of cells with and without partially mislocalized β-actin translation, an estimation of the immobile fraction of β-actin-eGFP at cell-cell contacts in steady state is significantly higher in cells with partially mislocalized β-actin translation (**Figure 39B, C**). These results indicate a more stable β-

actin pool at cell-cell adhesions in monolayers assembled from cells with partial defects in β-actin translation. However, upon stimulation of collective cell migration, partial mislocalization of β-actin translation results in a faster turnover of β-actin at cell-cell interfaces of leader-follower cell pairs. These seemingly contradictory results can be reconciled by the following logical argument. In steady state conditions, partial mislocalization of β-actin translation leads to an inability to synthesize a local pool of β-actin to drive filament polymerization at cell-cell adhesions (Gutierrez et al., 2014), causing a lower turnover of actin filaments. Upon stimulation of collective cell migration, the same defect in β-actin translation leads to an inability to stabilize and maintain filament populations leading to increased turnover of actin during the dynamic rearrangements which occur in a migrating tissue.

Together, with observations from collective tissue migratory behavior (**Figure 36**), the FRAP experiments support the hypothesis that spatially regulated β-actin translation controls actin dynamics during collective cell migration to bring about cycles of fluidization and reinforcement. Partial mislocalization of β-actin translation causes the actin filaments to be less stable; resulting in increased turnover and concomitantly suppresses collective cell migratory behavior. These results point to a fundamental role for spatially regulated β-actin translation in governing cell mechanics during collective cell migration,

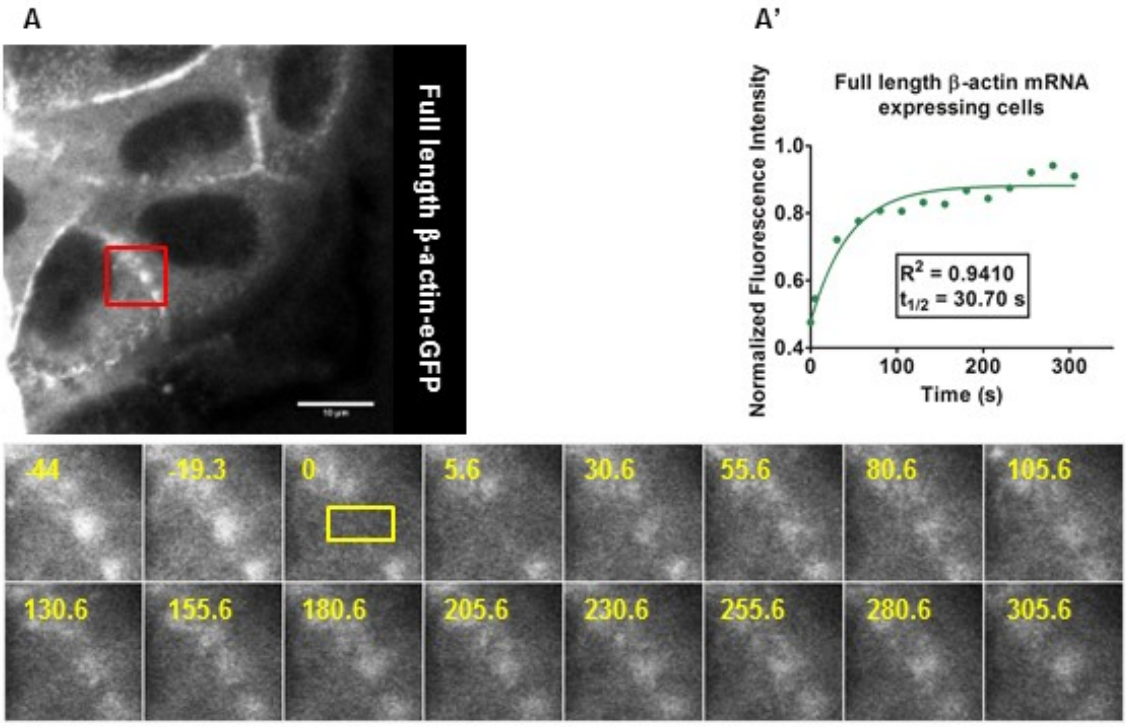
A
A'
Full length β-actin-eGFP
Full length β-actin mRNA expressing cells
Normalized Fluorescence Intensity
1.0
0.8
0.6
0.4
0
100
200
300
Time (s)
R² = 0.9410
t1/2 = 30.70 s
-44
-19.3
0
5.6
30.6
55.6
80.6
105.6
130.6
155.6
180.6
205.6
230.6
255.6
280.6
305.6

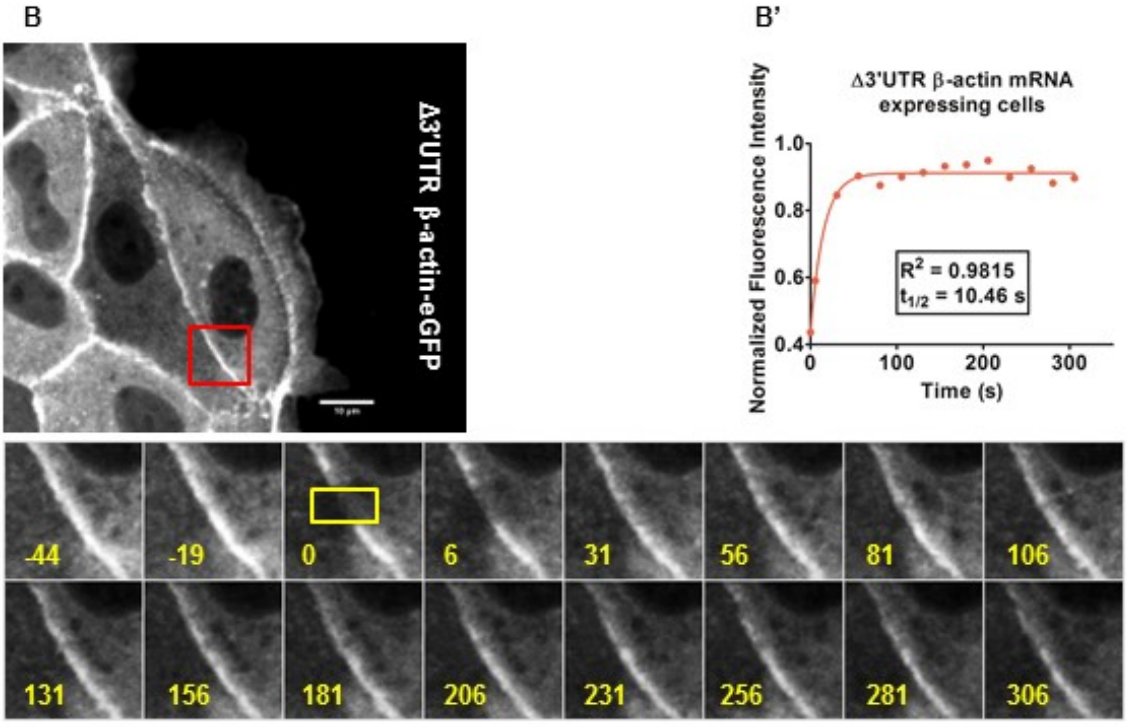
B
B'
Δ3'UTR β-actin-eGFP
Δ3'UTR β-actin mRNA expressing cells
Normalized Fluorescence Intensity
1.0
0.8
0.6
0.4
0
100
200
300
Time (s)
R² = 0.9815
t1/2 = 10.46 s
-44
-19
0
6
31
56
81
106
131
156
181
206
231
256
281
306

Figure 37: β-actin displays increased dynamics at leader-follower cell-cell adhesions in cells with partially mislocalized β-actin translation. (**A, A′**) MDCK cells expressing full length β-actin-eGFP. (**B, B′**) MDCK cells expressing Δ3′UTR β-actin-eGFP. (**A, B**) Top panels: Confocal images of leader cells. Scale bar = 10μm. Bottom Panels: Area shown by the Red box in **A or B** and displayed as a montage for representative FRAP experiments. Time is indicated in seconds and time 0 represents image acquired immediately following photobleaching of the yellow boxed area. (**A′, B′**) Graphs showing Normalized Fluorescence Intensity as a function of time following photobleaching. (**A′**) Green and (**B′**) Red curves represent the one phase association best fit for the data points shown by (**A′**) green and (**B′**) red solid circles. Insets indicate R^2 for the best fit curve and the corresponding $t_{1/2}$ of fluorescence recovery. Note that the $t_{1/2}$ of fluorescence recovery is about 3 times higher in control compared to cells with partially mislocalized β-actin translation.

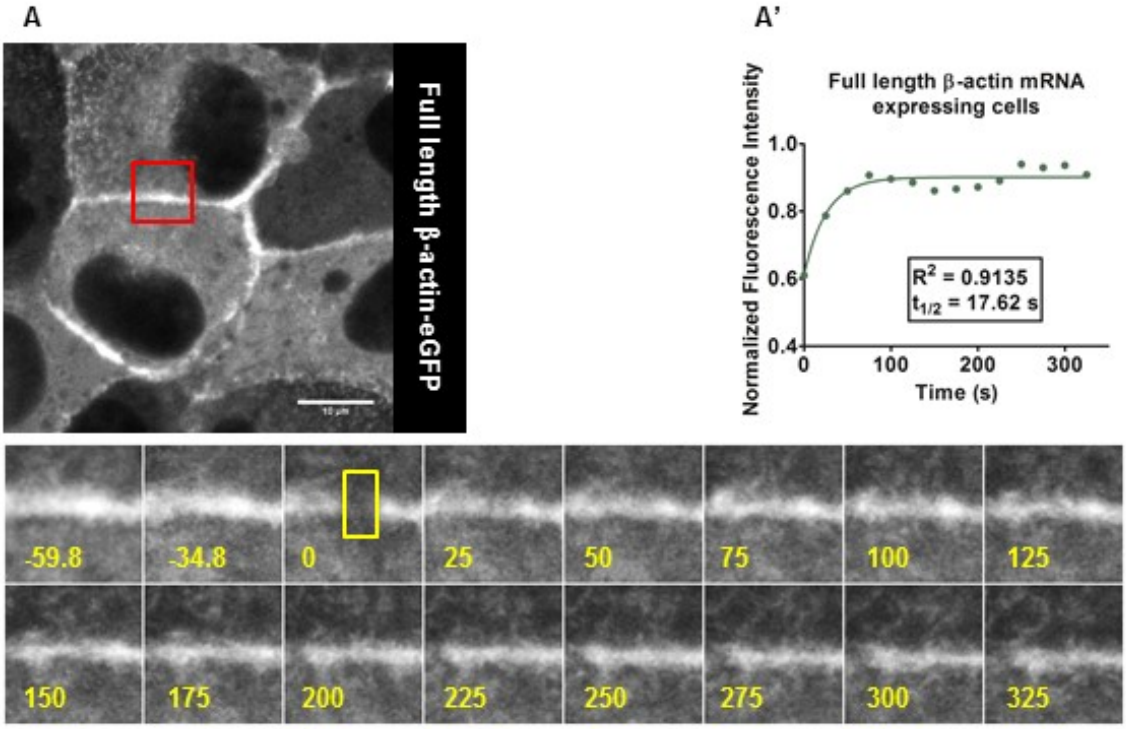
A
Full length β-actin-eGFP
A'
Full length β-actin mRNA expressing cells
Normalized Fluorescence Intensity
1.0
0.8
0.6
0.4
0
100
200
300
Time (s)
R² = 0.9135
t1/2 = 17.62 s
-59.8
-34.8
0
25
50
75
100
125
150
175
200
225
250
275
300
325

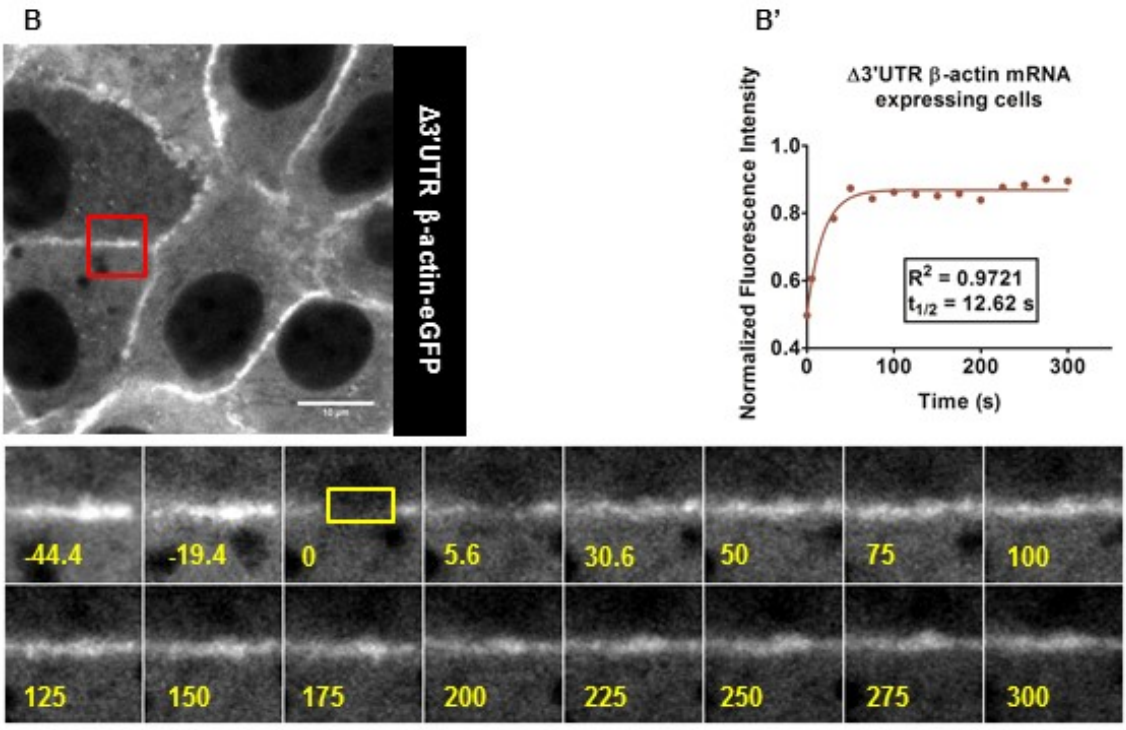
B
Δ3'UTR β-actin-eGFP
B'
Δ3'UTR β-actin mRNA expressing cells
Normalized Fluorescence Intensity
1.0
0.8
0.6
0.4
0
100
200
300
Time (s)
R² = 0.9721
t1/2 = 12.62 s
-44.4
-19.4
0
5.6
30.6
50
75
100
125
150
175
200
225
250
275
300

Figure 38: β-actin dynamics at cell-cell adhesions in steady state monolayers is unaffected by spatially regulated β-actin translation. (**A, A′**) MDCK cells expressing full length β-actin-eGFP. (**B, B′**) MDCK cells expressing Δ3′UTR β-actin-eGFP. (**A, B**) Top panels: Confocal images of cells in steady state. Scale bar = 10μm. Bottom Panels: Area shown by the Red box in **A or B** and displayed as a montage for representative FRAP experiments. Time is indicated in seconds and time 0 represents image acquired immediately following photobleaching of the yellow boxed area. (**A′, B′**) Graphs showing Normalized Fluorescence Intensity as a function of time following photobleaching. (**A′**) Green and (**B′**) Red curves represent the one phase association best fit for the data points shown by (**A′**) green and (**B′**) red solid circles. Insets indicate R^2 for the best fit curve and the corresponding $t_{1/2}$ of fluorescence recovery. Note that the $t_{1/2}$ of fluorescence recovery in control cells is of the same order as in cells with partially mislocalized β-actin translation.

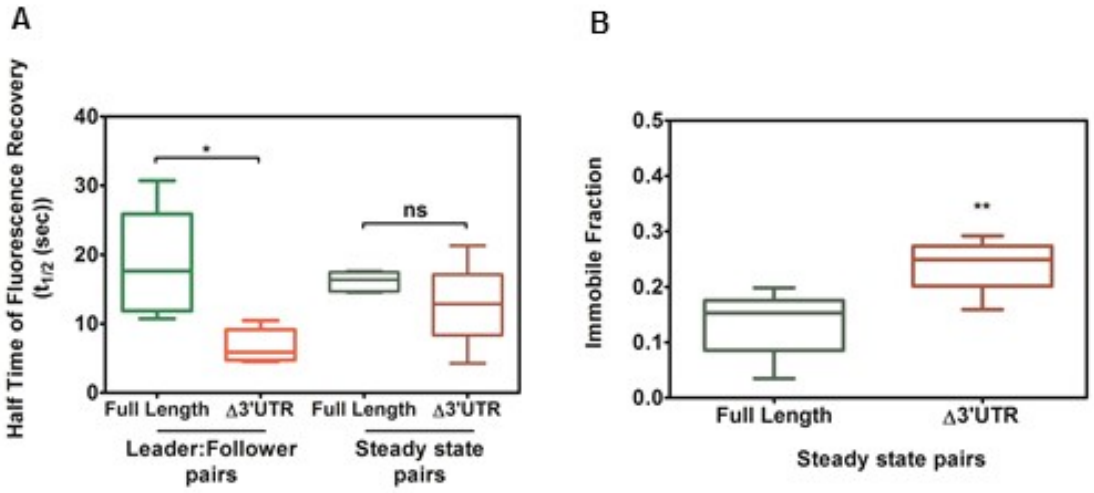
A
Half Time of Fluorescence Recovery ($t_{1/2}$ (sec))
40
30
20
10
0
*
ns
Full Length
Δ3'UTR
Full Length
Δ3'UTR
Leader:Follower pairs
Steady state pairs
B
Immobile Fraction
0.5
0.4
0.3
0.2
0.1
0.0
**
Full Length
Δ3'UTR
Steady state pairs

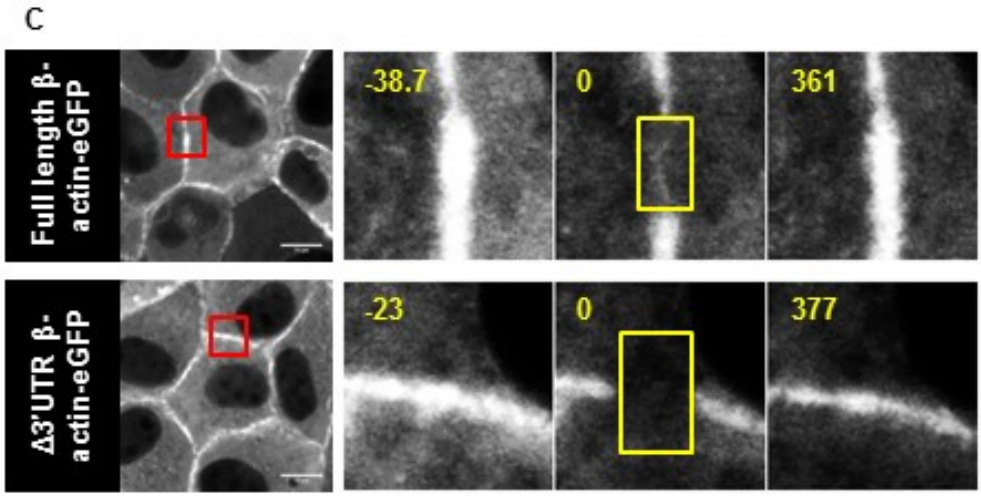
C
Full length β-actin-eGFP
-38.7
0
361
Δ3'UTR β-actin-eGFP
-23
0
377

Figure 39: Cells with partially mislocalized β-actin translation display faster actin turnover at cell-cell adhesions in leader follower pairs and decreased recovery at cell-cell adhesions in steady state. (**A**) Box plots representing t1/2 of fluorescence recoveries for β-actin-eGFP at cell-cell contacts in leader-follower cell pairs and at steady state. Whiskers indicate 2.5 and 97.5 percentiles. Individual non-parametric unpaired student's t-test with Welch's correction was carried out for leader-follower pairs and steady state pairs. * p = 0.0296. (**B**) Box plots representing the immobile fractions from independent experiments on steady state cell-cell adhesions. Whiskers indicate 2.5 and 97.5 percentiles. Unpaired student's t test gave a p value of 0.0021. (**C**) Representative FRAP experiments to calculate the immobile fraction of β-actin eGFP at cell-cell adhesions in steady state monolayers. Top panel: Cells expressing full length β-actin-eGFP; Bottom panel: Cells expressing Δ3′UTR β-actin-eGFP. Scale bar = 10μm Red boxes indicate the zoomed in view used for the montages shown on the right indicating the photobleached area (yellow box) and fluorescence recovery. Time is indicated in seconds and 0 represents image acquired immediately following photobleaching.

DISCUSSION

Spatially regulated β-actin translation governs actin dynamics influencing collective cell migratory behavior

MDCK monolayers have been extensively used to study the behavior of collective cell migration in epithelial cells following wounding (Farooqui and Fenteany, 2005; Fenteany et al., 2000; Matsubayashi et al., 2011; Poujade et al., 2007). Results presented in this chapter shed light on the role of the spatially regulated β-actin translation in collective epithelial migration. First, partial mislocalization of β-actin translation results in a more dynamic leading edge (**Figure 34, 35**). However, these cells migrate at a rate about three times slower than control cells with no defects in localizing β-actin translation (**Figure 36**). Interestingly, cells with partially mislocalized β-actin translation showed a more dynamic actin population from FRAP experiments at leader-follower cell-cell adhesions during collective migration (**Figure 37, 39A**). Additionally, actin at cell-cell adhesions in steady state monolayers showed similar kinetics of recovery independent of the status of spatially regulated β-actin translation in these cells (**Figure 39A**). However, the extent of fluorescence recovery is significantly lower in steady state monolayers composed of cells with partially mislocalized β-actin translation (**Figure 39B**). Taken together, a model can be deduced for epithelial collective cell migratory behavior incorporating the role of spatially regulated β-actin translation. First, spatially regulated β-actin synthesis controls the pool of available actin at cell-cell adhesions in steady state monolayers, but not the overall rate of filament turnover. Second, upon induction of collective cell migratory behavior, spatially regulated β-actin synthesis acts

to keep the filament populations at cell-cell adhesions between leader and follower cells more stable by reducing the rate of filament turnover. This suggests that the dynamic rearrangement of cell-cell adhesions that occur due to mechanical stimuli during collective cell migration result in a relatively stable actin filament population. The slow turnover of these filaments is in turn controlled by spatially regulated β-actin translation. Partially mislocalized β-actin translation results in increased filament turnover, and as a result cells fail to undergo cycles of fluidization and re-solidification. As a consequence cells with partially mislocalized β-actin translation migrate at a slower pace than cells with properly localized β-actin translation.

Epithelial collective cell migration is an emergent property of single cell behavior and cell-cell interactions

Collective cell migration in epithelia is a result of balancing forces exerted by: cell-matrix and cell-cell adhesions (Weber et al., 2012). The latter, cell-cell adhesions, is the main subject of this discussion and is mediated by cadherins. E-cadherin mediated adherens junctions are important players in transducing mechanical forces across the migrating tissue and are required for cohesion during migration. A tugging force on the cadherin adhesions as result of migrating leader cells can do one of the following: reinforce the adhesions, resulting in cohesive epithelial migration or cause cells to dissociate, leading to mesenchymal transition of epithelia seen in metastasis. In normal epithelial cells, a tugging force on cadherin mediated junctions results in a RhoA dependent Myosin II feedback loop which acts to reinforce the junctions (le Duc et al., 2010; Lecuit and Yap, 2015). In fact, E-cadherin dependent RhoA activation and

subsequent Myosin II activity at the apical junctions is essential for junctional integrity and barrier function (Priya et al., 2013; Twiss et al., 2012). In addition to regulating Myosin II activity, RhoA, activates LIM-kinase 1 which acts to inhibit the activity of cofilin, an actin filament severing protein. Par-3, a component of the apical polarity complex, has also been shown to regulate tight junction assembly and barrier integrity by decreasing cofilin activity at the zonula adherens (Chen and Macara, 2006).

Life at the leading edge of an epithelial leader cell is, however, very different from the biochemical and mechanical cues governing the dynamics of cell-cell adhesions in a migrating tissue (**Figure 40**). The front and rear end of cells during collective cell migration are polarized with different effectors (Mayor and Etienne-Manneville, 2016). While an actin driven cadherin tread-milling is observed (Peglion et al., 2014), it is known that E-cadherin adhesions increase with increasing intercellular tension forces (Bazellieres et al., 2015). Additionally, the activity of signaling molecules such as Rho family of small GTPases is tightly controlled both at the leading edge and at cell-cell adhesions. While Rac and Arp2/3 activity is high at the lamellipodia driving branched actin filament polymerization, RhoA activity dominates at the cell-cell adhesions increasing contractility and reinforcing the actin cytoskeleton. The net result of this differential signaling is the cohesive migration of the epithelial tissue (**Figure 40**) (Omelchenko et al., 2003; Zegers and Friedl, 2014). In addition to the Arp2/3 complex, other actin binding proteins, notably cofilin – an actin severing protein, are also differentially localized to the leading edge (Bamburg, 1999). Cofilin activity increases free barbed ends promoting polymerization. Its activity is regulated by several mechanisms: cofilin mRNA localizes to the leading edge (Maizels et al., 2015), PIP2

hydrolysis mediated cofilin release from the plasma membrane (Mouneimne et al., 2004), and global LIMK1 activity acts to phosphorylate and inhibit cofilin activity (Wang et al., 2007). Another important node of the complex signaling that occurs at the basal surface of cells during collective cell migration comes from Integrinβ1 mediated cell-matrix adhesions. These adhesions regulate Rac activity downstream of a PI3K signaling cascade in leader cells (Yamaguchi et al., 2015). Rac activation and Arp2/3 mediated branched actin filament assembly aid lamellar protrusive activity in leader cells, as well as in basal surface of follower cells which form cryptic lamellipodia extending beneath multiple rows of cells (Farooqui and Fenteany, 2005). Also, cofilin and Arp2/3 have been shown to synergistically regulate the actin dynamics at the leading edge resulting in protrusive activity (DesMarais et al., 2004). The net result of this complex regulatory mechanism is lamellipodium localized cofilin activity which then promotes directional cell migration (Bravo-Cordero et al., 2012; Sidani et al., 2007; Zhang et al., 2011). Collective cell migratory behavior is thus a consequence of biochemical and mechanical coupling of cell-cell adhesion mediated interactions at the apical surface and cell-matrix mediated interaction on the basal surface (**Figure 40**).

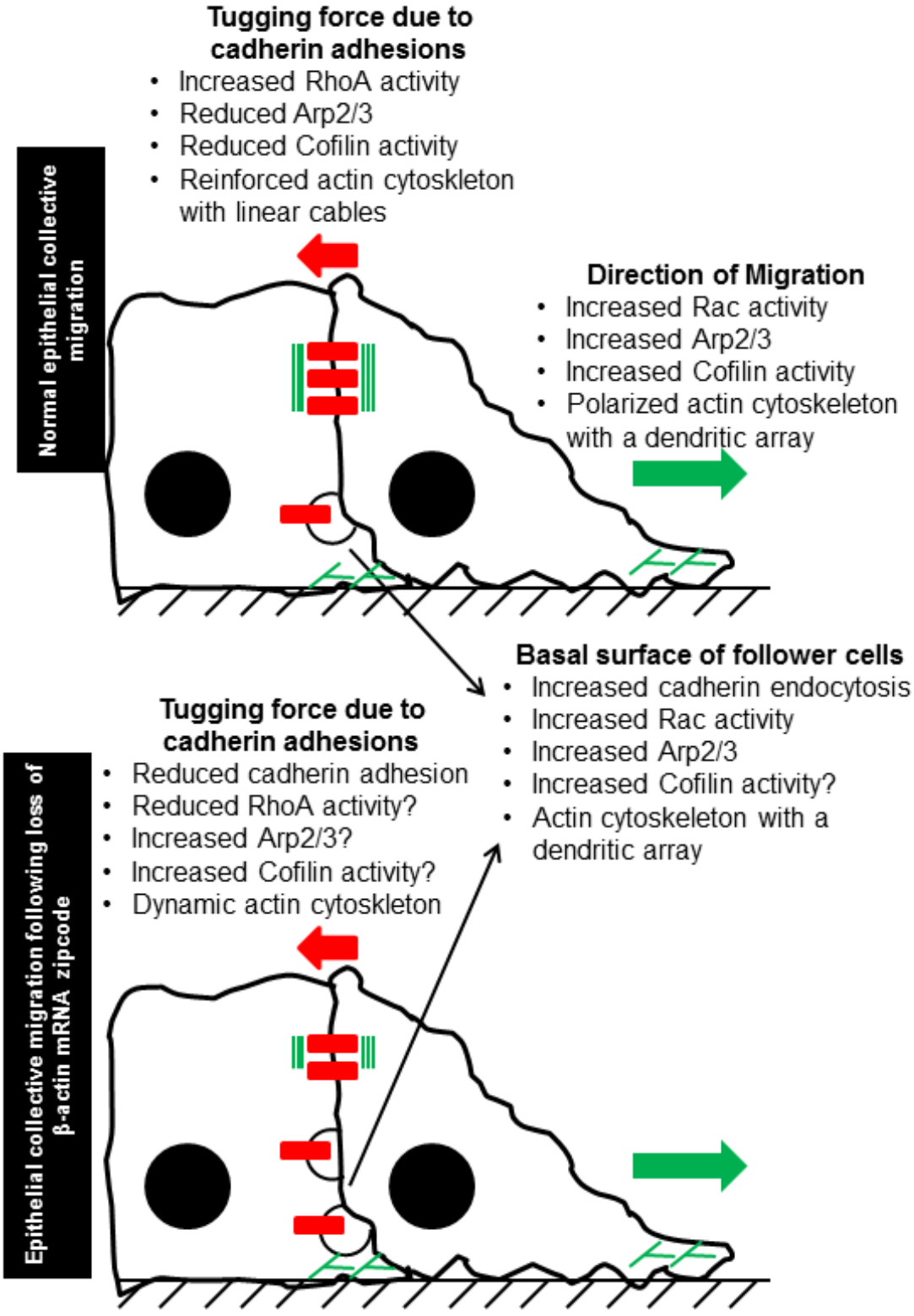
Tugging force due to cadherin adhesions
• Increased RhoA activity
• Reduced Arp2/3
• Reduced Cofilin activity
• Reinforced actin cytoskleton with linear cables
Normal epithelial collective migration
Direction of Migration
• Increased Rac activity
• Increased Arp2/3
• Increased Cofilin activity
• Polarized actin cytoskeleton with a dendritic array
Basal surface of follower cells
• Increased cadherin endocytosis
• Increased Rac activity
• Increased Arp2/3
• Increased Cofilin activity?
• Actin cytoskeleton with a dendritic array
Tugging force due to cadherin adhesions
• Reduced cadherin adhesion
• Reduced RhoA activity?
• Increased Arp2/3?
• Increased Cofilin activity?
• Dynamic actin cytoskleton
Epithelial collective migration following loss of β-actin mRNA zipcode

Figure 40: Schematic representing role of spatially regulated β-actin translation in epithelial collective cell migration. Collective cell migration in epithelial sheets is characterized by tugging forces on cells due to cadherin mediated cell-cell adhesions. These forces tend to activate signaling cascades, notably increased RhoA activity, reduced Arp2/3 actvity, and reduced cofilin activity, all of which act to reinforce the cell-cell adhesion. Conversely the afore mentioned signaling cascades act in the opposite direction at the leading edge in a leader/follower cell, i.e., decreased RhoA activity, increased Rac activity, increased cofilin activity, all which act to mediate a dendritic actin array and push the cell forward. Additionally, cadherin endocytosis at the basal surface of cell-cell contacts in a migrating epithelium acts to render protrusive activity to the basal surface resulting in cryptic lamellipodial protrusions in follower cells which also contribute to tissue migration. The bottom portion of the schematic shows derailed endocytosis in cells with partial mislocalization of β-actin translation resulting in reduced cadherin anchoring to the actin cytoskeleton. This causes a decrease in the biochemical signals that would otherwise act to reinforce cell-cell adhesions. Also, I propose that there a corollary increase in the biochemical signaling, namely cofilin activity and Arp2/3 activity at cell-cell adhesions as a result of mislocalizing β-actin translation leading to a more dynamic actin cytoskeleton at cell-cell adhesions in these cells.

MATERIALS AND METHODS

Cell culture and wounding to stimulate collective cell migration

MDCK – NBL2 cells (ATCC® CCL-34™) were cultured in DMEM supplemented with 10% (v/v) FBS and 100 I.U./mL Penicillin and 100µg/mL Streptomycin. Transfection of these cells with eTC GFP β-actin full length and eTC GFP β-actin ΔZip – (Δ3'UTR) (Addgene Plasmid #27123, #27124 and (Rodriguez et al., 2006)) was carried out using Lipofectamine® 2000 (Life Technologies) as per manufacturer's specifications. Transfected cells were selected using 500µg/mL G418 (Sigma-Aldrich). Flow cytometry was used to sort cells and obtain a homogeneous population of cells expressing GFP-β-actin. Monolayers assembled from MDCK cells in glass bottom dishes (Mattek Corp.) were scratched to make an infinite wound and stimulate collective cells migration. FluorBrite DMEM (Life Technologies) supplemented with 10% FBS (Gibco), 100 I.U./mL Penicillin, 100µg/mL Streptomycin and 1% OxyFluor (Oxyrase) along with 100mM Sodium-dl-lactate as substrate was used for live imaging cell experiments.

Measuring rate of tissue migration

Wounded monolayers were imaged using a 20X objective at 5 minute intervals following wound generation. ImageJ was used to determine the area covered by the wound within successive time frames. Statistical analysis was performed using GraphPad Prism software. An unpaired student's t-test was performed and significance was reported by p values.

FRAP experiments

MDCK monolayers were scratched to make an infinite wound and allowed an initial 2 hour refractory period for the migration to reach equilibrium. β-actin-eGFP was imaged on a cLSM510 Meta microscope using a 63X/1.4 N.A. oil immersion objective and a 488nm argon laser. A pinhole diameter equivalent to 2.0 airy units and a 3X zoom factor was used to image cell-cell adhesion in steady state or leader-follower pairs. A bleach ROI was demarcated for the actin at the cell-cell contacts and a 100% Laser power with 100 bleach iterations was used to perform photobleaching following acquisition of two initial pre-bleach frames. Following bleaching, images were acquired at 25s intervals for a period of 300 seconds. Acquisition was done at 50% laser intensity with 50% laser output and 12 bit images were acquired at 1024X1024 resolution. StackReg plugin in ImageJ was used to account for drift in cells during acquisition. Multiple unbleached ROIs was defined for actin at cell-cell adhesions within the acquisition frames and background values were subtracted for bleach ROIs and unbleached ROIs. Bleach ROI intensities were normalized to intensities in unbleached ROIs. Normalized fluorescence intensities were plotted as a function of time in GrpahPad Prism software and fit to a one phase association curve using non-linear regression analysis. The obtained $t_{1/2}$ of fluorescence recoveries were tested for statistical significance using unpaired student's t-test. $t_{/12}$ values within 2.5 standard deviations from the mean were used for statistical analysis.

For measurement of immobile fractions, the experiments were setup as detailed above with the following variations: post bleach acquisition was done at times 0s and 325s. The immobile fractions were estimated as:

$$IMF = 1 - \frac{F_\infty}{F_0}$$ …Equation (**6**)

Where IMF is the immobile fraction; F_∞: fluorescence intensity in bleach ROI at the final acquisition and; F_0: fluorescence intensity in bleach ROI pre-bleach.

Statistical analysis was carried out using unpaired student's t-test and significance was reported by *p* values.

Leading edge tracking and velocity measurements

Following a 2 hour refractory period post generation of wound, leader cells expressing β-actin-eGFP were chosen and imaged using a 100X/1.46 N.A. on a Zeiss Cell Observer Spinning Disc confocal microscope equipped with an 488nm Argon laser. Laser intensity was set to 15%, with a 400ms exposure time and images were acquired every 800ms for a period of 5 minutes. The images were contrast adjusted and smoothed in ImageJ to show the leading edge of the cells. The leading edge was tracked using JFilament plugin for ImageJ (Li et al., 2009; Smith et al., 2010). Leading edge velocity estimates were then determined using the Leading Edge Position Velocity plugin for ImageJ (Ryan et al., 2012; Ryan et al., 2013). Custom script written in Python was used to plot the radial velocity vectors. Mean radial velocity was then calculated by carrying out a vector sum of the radial velocities for each point along the leading edge for any given time. Root mean squared velocities were obtained using the following formula:

$$V_{RMS} = \sqrt{\frac{1}{n}\sum_{i=1}^{n} V_i^2}$$ …Equation (**7**)

Where *n* = integral number of degrees in the arc subtended by the protrusion.

Uncertainty in velocity measurements were calculated as a function of image resolution according to the following equation:

$$Uncertainty\ in\ Volocity\ = \frac{\sqrt{2}}{2} * \frac{Image\ resolution}{time\ interval\ between\ images}$$ …Equation (**8**)

CHAPTER 5: CONCLUSIONS AND FUTURE DIRECTIONS

Work presented so far in this thesis and elsewhere has explored the role of spatially regulated β-actin translation in cellular processes such as cell migration (Shestakova et al., 2001), cell-cell adhesion (Cruz et al., 2015; Gutierrez et al., 2014; Rodriguez et al., 2006), cell-matrix adhesion (Katz et al., 2012), and growth cone guidance in neurons (Welshhans and Bassell, 2011). The underlying common theme in all these studies is that they focus on fundamental cellular behavior typically in a simple single cell context or at most multiple cells of the same type growing in culture. Working on principles gleaned from the above mentioned studies, it is important to understand how the spatial regulation of β-actin translation is important at the organ and organismal levels.

Furthermore, dysregulation of IMP-1 in the context of disease such as cancer has been the subject of some studies in the recent past (Bell et al., 2013; Gu et al., 2009; Hamilton et al., 2013; Wang et al., 2004; Wang et al., 2002). While some studies have found IMP-1 to be an oncogene, others have concluded that it is a tumor suppressor. How then does one reconcile this dichotomy? The focus of these studies has been on the RNA binding protein – IMP-1, and the phenotype of a cell with gain/loss of function of an RNA binding protein (RBP) would be dictated by the transcriptome of the cell which is capable of being regulated by the said RBP. Thus any conclusions about the effect of the RBP on the phenotype that do not take into account the expression of all the mRNAs being regulated by the RBP should be re-evaluated critically. One approach to this complex question regarding the role of IMP-1 in diseases such as cancer is to explore the

expression pattern of transcripts, which are regulated by IMP-1 and carry out opposing functions in a cell – such as those of oncogenes and tumor suppressors, epithelial and mesenchymal genes, proliferative and apoptotic genes.

Mini guts: an *ex vivo* model system of small intestinal crypt homeostasis to study the role of spatially regulated β-actin translation in epithelial morphogenesis

The small intestine is one of the fastest regenerating epithelium with a characteristic replenishment rate of 4-5 days for the entire epithelium. This makes the small intestine an excellent model system to study the role of spatial regulation of β-actin expression in epithelial homeostasis. ZBP-1/IMP-1 – the RNA binding protein required for β-actin mRNA localization and translational regulation, is essential for normal development of the small intestine. *Imp1*$^{-/-}$ mice show gross histological defects in the small intestine and exhibit dwarfism phenotype plausibly due to intestinal dysfunction (Hansen et al., 2004). Although the total expression level of β-actin mRNA and protein remain unchanged in *Imp1*$^{-/-}$ mice, the spatial distribution of β-actin gene expression has not been evaluated. It is plausible that the abnormal small intestinal development and dwarfism phenotype observed in *Imp1* null mice is due to the dysfunction of spatial regulation of β-actin translation as seen in MDCK cyst cultures (**Chapter 3**). However, it is more likely that the phenotype associated with the loss of *Imp1* is due to the deregulation of post-transcriptional control of several mRNA targets of the RNA binding protein. In order to determine the role of spatially regulated β-actin translation specifically on small intestinal homeostasis, an organotypic culture model developed by the Hans Clevers group was adopted in this thesis. The model involves isolation of small

intestinal crypts (stem cell and proliferative compartment of the small intestine) and their *ex vivo* culture. The crypts develop into epithelial organoids or "mini guts" when embedded in Matrigel (Sato and Clevers, 2013; Sato et al., 2009). These cultures provide an excellent model system to study the role of spatially regulated β-actin translation in the context of a complex, self-renewing epithelial tissue. They are amenable to manipulations such as adding β-actin mRNA zipcode antisense oligonucleotides, which then mask IMP-1/β-actin mRNA interaction. Additionally, the β-actin protein and mRNA can be tracked in live mini-guts using crypts isolated from transgenic mice expressing GFP-tagged β-actin (Gurniak and Witke, 2007), and MCP (MS2 bacteriophage capsid protein) x β-actin MBS (MS2 binding site) (Park et al., 2014), respectively.

Cancer and ZBP-1/IMP-1: Does spatially regulated translation take center stage in disease progression?

Previous studies have shown that ZBP-1/IMP-1 dependent mRNA localization pathway is disrupted in cancer cells. Specifically, metastatic breast cancer cells showed a marked down regulation of ZBP-1 expression and the extent of downregulation was correlated to metastatic potential (Wang et al., 2002). Also, the ZBP-1 promoter was found to be methylated in metastatic cancer cells compared to non-metastatic cancer cells (Gu et al., 2009). These data suggest that the ZBP-1/IMP-1 dependent post-transcriptional gene regulation is an important and yet, underappreciated mechanism controlling tumor cell invasion and disease progression. It is hypothesized a loss of ZBP-1/IMP-1 expression results in metastatic phenotype owing to a less polarized cytoskeleton which causes more efficient chemotaxis (Wang et al., 2004). However, in

addition to promoter methylation, another mode of ZBP-1/IMP-1 regulation in cancer and metastasis is the alternative polyadenylation and cleavage of its 3′UTR resulting in increased stability of the IMP-1 transcript. This aberrant expression profile of IMP-1 has been shown to promote transformation (Mayr and Bartel, 2009). Additionally, some studies also point to an oncogenic role of IMP-1, from promoting tumor growth, dissemination to upregulation of metastatic genes like LEF1 and SLUG (Bunnell and Ervasti, 2011; Zirkel et al., 2013). These seemingly contradictory hypotheses regarding the role of IMP-1 in cancer progression, arise from the complexity of the phenotype resulting from gain or loss of function of an RNA binding protein with about 300 mRNA targets (Jonson et al., 2007). Thus, in order to ascertain the role of IMP-1 in cancer progression, it is imperative to determine the transcriptional state of the "zipcode containing" genes.

PRELIMINARY RESULTS

ZBP-1/IMP1 is localized to the stem cell compartment in intestinal epithelia

ZBP-1/IMP-1 is expressed during mouse development, increasing at embryonic day 12.5 followed by a marked downregulation of expression in most organs, expect for the intestinal epithelium (Hansen et al., 2004; Zinchuk et al., 2007). IMP-1 expression in the small intestinal epithelium of the adult mouse is localized to the crypt compartment. More specifically, cells in the +4 position from the crypt base show a strong positive signal for the presence of IMP-1 (**Figure 41**). These findings were confirmed from Kathryn Hamilton's work in Anil Rustgi's group looking at the role of IMP-1 in

regulating autophagy related transcripts in the intestine (Personal communication from Kathryn Hamilton). Additionally, IMP-1 is localized to the crypt compartment in the large intestine (**Figure 42**). These results indicate a role for IMP-1 in maintaining intestinal homeostasis by post-transcriptional gene regulation in the stem cell compartments of both the small and large intestines in the adult mouse.

Spatially regulated β-actin translation is required for the maintenance of small intestinal crypt architecture

In order to observe the spatial expression pattern of β-actin protein during epithelial homeostasis in the small intestine, crypts were isolated from human GFP-actin expressing (huGE) mouse (Gurniak and Witke, 2007) and grown in Matrigel as *ex vivo* cultures. β-actin-GFP localizes largely to the apical membrane composed of microvilli and the zonula adherens. β-actin-GFP is also observed to localize to the lateral cell-cell adhesions and almost completely absent from the basal plasma membrane (**Figure 43**). The asymmetric localization pattern of β-actin remained unchanged as the crypt cultures expanded to form mini-guts over a period of 5 days. These results along with the localization of IMP-1 to the crypt compartment suggest spatially regulated β-actin translation plausibly plays a role in the asymmetric localization of β-actin in small intestinal crypts.

In order to test the above hypothesis, small intestinal organoids were treated with β-actin mRNA zipcode antisense oligonucleotides. Interestingly, the crypts treated with β-actin mRNA antisense oligonucleotides show marked disruption in epithelial organization followed by a complete loss of crypt morphology. Control crypts either

untreated or treated with scrambled oligonucleotides show normal organization and expansion (**Figure 44**). These preliminary findings, taken together with the localization of IMP-1 to the crypt compartment suggest a role for spatially regulated β-actin translation in the maintenance of small intestinal epithelium.

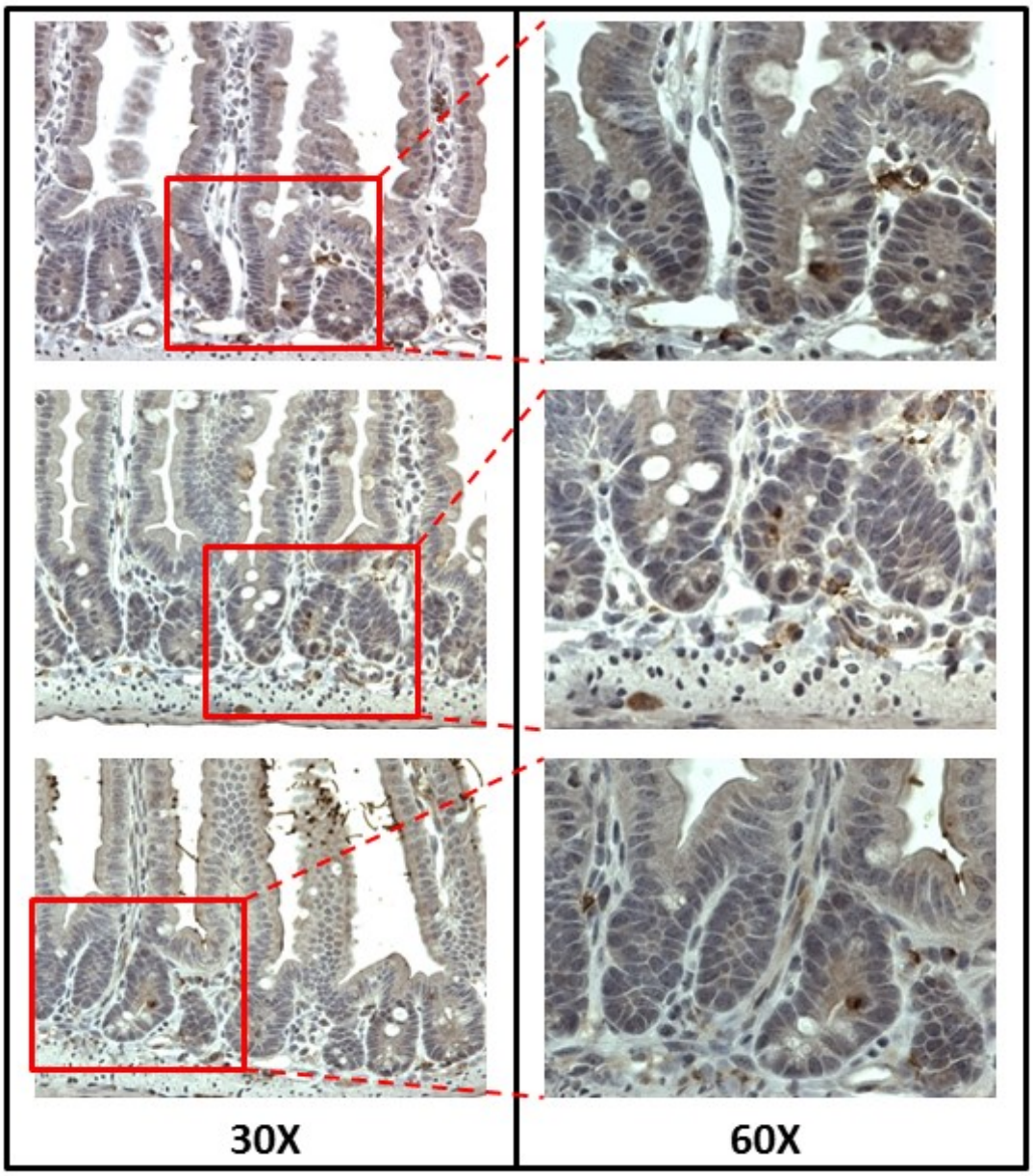
30X
60X

Figure 41: IMP-1 localizes to the proliferative compartment in mouse small intestinal crypts. Paraffin embedded mouse small intestinal sections were stained for IMP-1 using immunohistochemistry. Left Panel: Representative photomicrographs of small intestinal sections acquired at 30X magnification. Right Panels: 60X magnification images of red boxed areas in the left panels. Dark brown staining at the crypt base indicates the presence of IMP-1 positive cells.

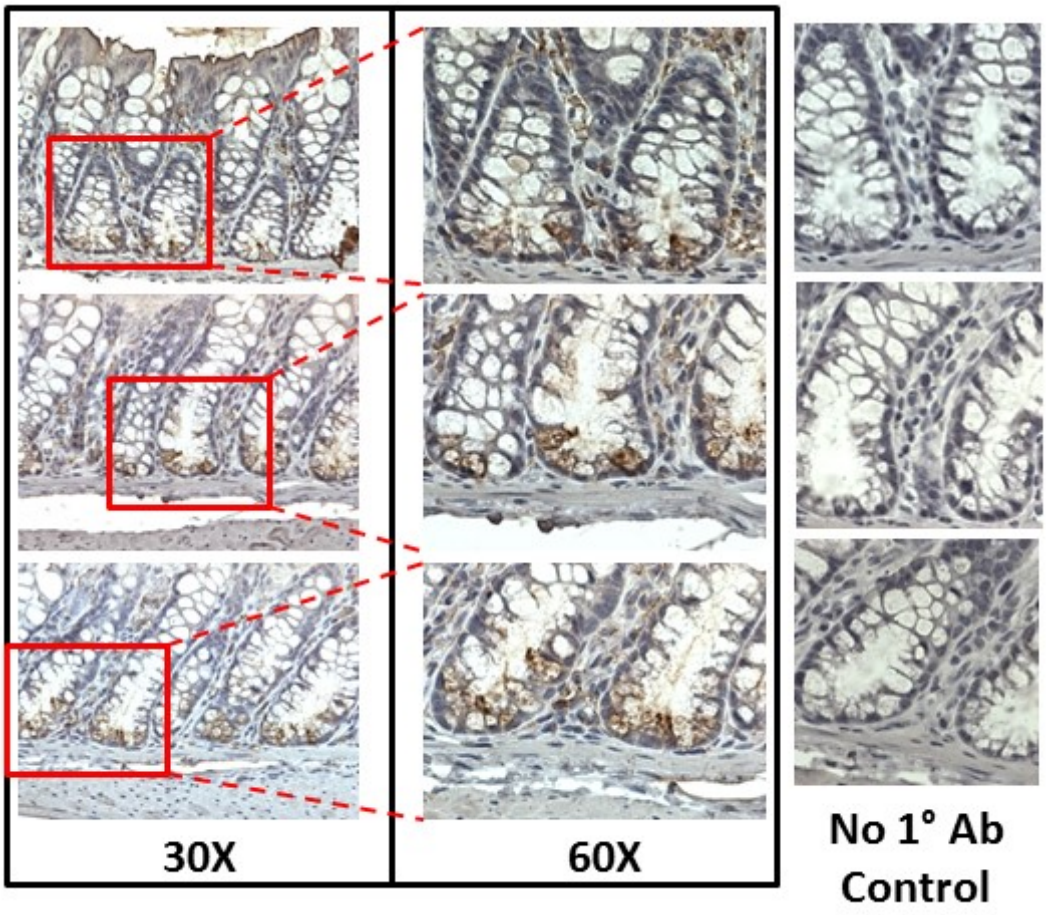
30X
60X
No 1° Ab
Control

Figure 42: IMP-1 localizes to proliferative compartment in the mouse colonic epithelium. Paraffin embedded mouse large intestinal sections were stained for IMP-1 using immunohistochemistry. Left Panel: Representative photomicrographs of small intestinal sections acquired at 30X magnification. Right Panels: 60X magnification images of red boxed areas in the left panels. Dark brown staining at the crypt base indicates the presence of IMP-1 positive cells.

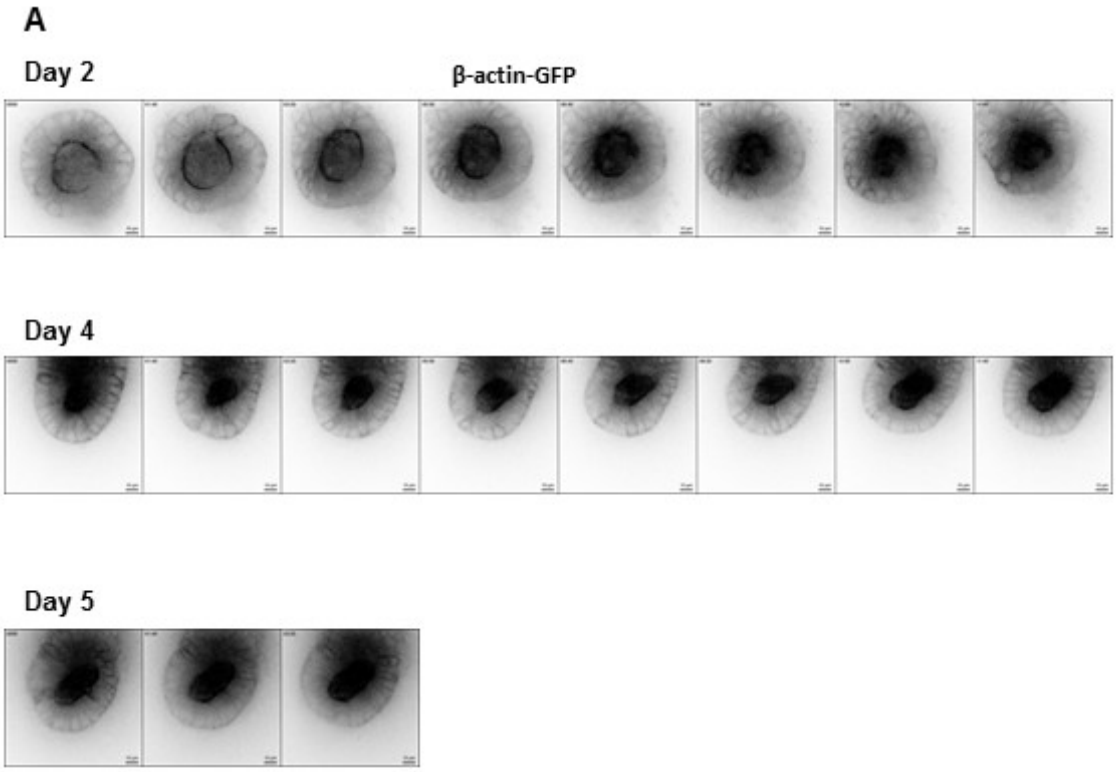
A
Day 2
β-actin-GFP
Day 4
Day 5

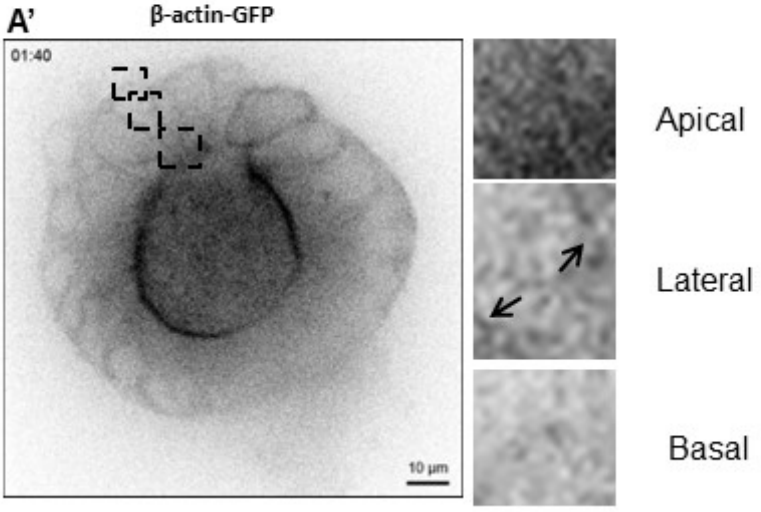
A'
β-actin-GFP
01:40
10 µm
Apical
Lateral
Basal

Figure 43: The mouse small intestinal crypt display an asymmetric localization of β-actin protein expression. Grey scale images of GFP fluorescence inverted to better observe the signal. (**A**) Small intestinal crypts from human GFP-β-actin expressing mouse imaged on day 2 (top panel), day 4 (middle panel) and day5 (bottom panel). The images were acquired at 20 minute intervals over a period of 12 hours each day. Time is indicated in hh:mm. (**A′**) Magnified images of apical, lateral and basal surface of the crypt. Magnified panels on the right indicate GFP localization for the boxed areas on the left panel. Note the apical and cell-cell interface localized β-actin-GFP.

Untreated

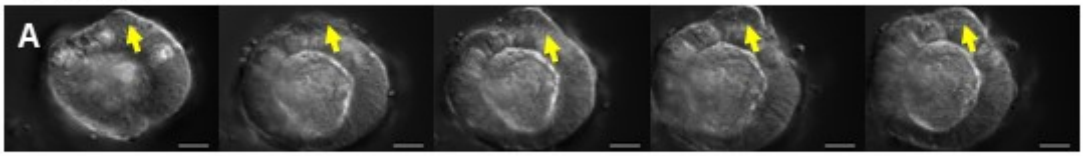

+β-actin mRNA antisense Oligoneucleotides

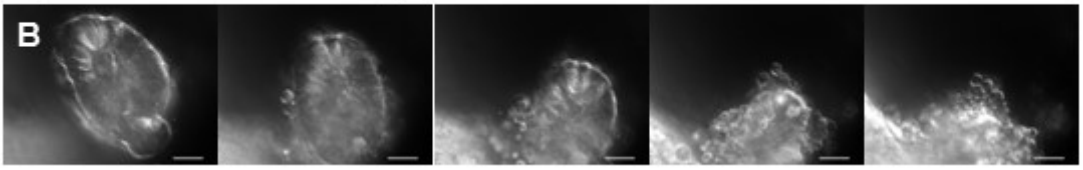

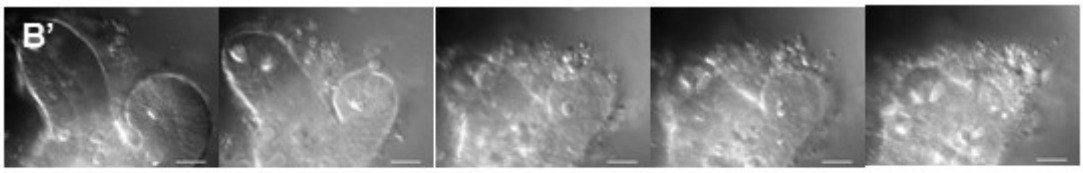

+Scrambled Oligoneucleotides

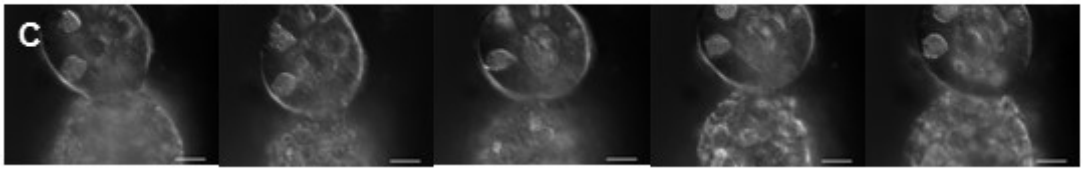

Figure 44: Spatially regulated β-actin translation modulates small intestinal crypt homeostasis. Mouse small intestinal crypts were isolated and cultured in Matrigel and (**A**) untreated, (**B, B′**) treated with 8μM β-actin mRNA zipcode antisense oligonucleotides and (**C**) scrambled oligonucleotides and imaged. Montages show images acquired over a period of 12 hours from left to right. The crypts show either normal growth (**A, C**) with "buds" indicating proliferation and growth (see yellow arrows in **A**), or complete disruption of crypt architecture upon treatment with β-actin mRNA zipcode antisense oligonucleotides (**B. B′**).

Colon cancer cells are insensitive to perturbation of β-actin mRNA zipcode/IMP-1 interaction

The expression of IMP-1 and its role in driving tumor progression remains poorly understood. While in certain cases, IMP-1 expression is downregulated in metastatic cells, in other studies, IMP-1 is shown to be an onco-fetal protein driving tumor progression (Bell et al., 2013; Bunnell and Ervasti, 2011; Gu et al., 2009; Wang et al., 2004; Wang et al., 2002; Zirkel et al., 2013). Given its role in intestinal development and post-natal expression pattern in the intestinal epithelium, colon carcinoma was chosen as a model to study the role of IMP-1 in cancer progression. Seven different colon carcinoma cell lines of varying origins (Zhang et al., 2009) were probed for IMP-1 expression. Interestingly, 5 out of the seven cell lines showed no detectable levels of IMP-1. Also, one of these five cell lines, Lim 2551 showed no E-cadherin expression, indicating these cells had undergone EMT (**Figure 45A**). Indeed Lim 2551 cells exhibit minimal cell-cell adhesions and have a rounded morphology (Zhang et al., 2009). IMP-1 has 3 paralogs in humans: IMP-1, IMP-2 and IMP-3, each known to perform different roles. IMP-1/3 are known to have an onco-fetal pattern of expression, playing roles in development and tumor progression (Findeis-Hosey and Xu, 2011; Findeis-Hosey and Xu, 2012; Zirkel et al., 2013). The third member of the family, IMP-2 is expressed in non-neoplastic adult tissue and it role is poorly understood. To determine the expression of these paralogs in the seven colon carcinoma cell lines, RT-PCR was carried out. Paralog specific primers confirm the absence of IMP-1 specifically from three of the five cell lines that showed no protein expression (**Figure 45B**). Lim 2550 and to a lesser extent Lim 1215 express IMP-1 mRNA although the protein was not detectable in these

cells. This indicates that IMP-1 is post-transcriptionally silenced in these cells. All seven cell lines tested are positive for the expression of IMP-2 mRNA. IMP-3 mRNA is also detected in all cells except Lim 1899 (**Figure 45B**). These results also confirm that the paralog detected in the western blot analysis was indeed IMP-1.

The absence of IMP-1 expression in some of the colon carcinoma cells suggests that the spatial regulation of β-actin translation through IMP-1 is no longer functional in these cells. To confirm the same, β-actin mRNA zipcode antisense oligonucleotides were added to Lim 1863 colon carcinoma cells that grow as floating organoids in culture. The cells show no apparent change in morphology even upon adding β-actin mRNA zipcode antisense oligonucleotides (**Figure 46A, A′**). On the other h, and Caco-2 colon cancer cells express IMP-1, E-cadherin, and display adherens junctions (Kovacs et al., 2011). To test the extent to which spatial regulation of β-actin translation via IMP-1 is functional in these cells and determine its role in adherens junction assembly, calcium repletion experiment was carried out (**Chapters 2, 3**). Pre-treating Caco-2 cells with β-actin mRNA zipcode antisense oligonucleotides has little observable effect during the phases of cell-cell contact formation and contact expansion. However, in both untreated control cells as well as those pre-treated with β-actin mRNA zipcode antisense oligonucleotides the contact expansion phase is followed by cells continuing to have lamellipodial overlaps (**Figure 46B, B′**). Thus unlike typical epithelial adherens junction assembly, Caco-2 cells are unable to restrict lamellipodial overlaps during junction maturation phase. This defect is independent of spatially regulated β-actin translation unlike typical epithelia. These preliminary results suggest that IMP-1/β-actin mRNA zipcode pathway is dysfunctional in colon cells despite the expression of IMP-1.

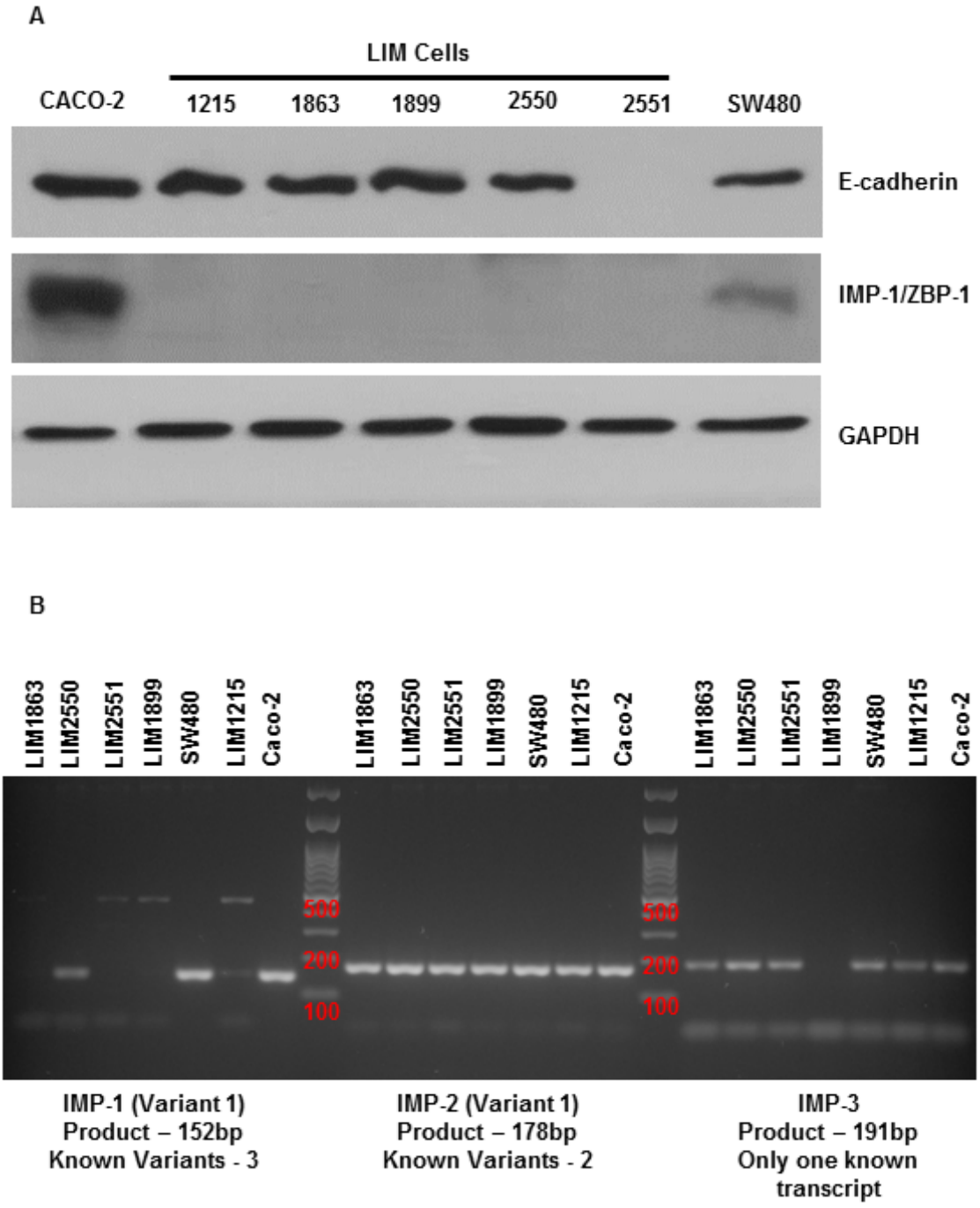
A
LIM Cells
CACO-2
1215
1863
1899
2550
2551
SW480
E-cadherin
IMP-1/ZBP-1
GAPDH
B
LIM1863
LIM2550
LIM2551
LIM1899
SW480
LIM1215
Caco-2
500
200
100
IMP-1 (Variant 1)
Product – 152bp
Known Variants - 3
IMP-2 (Variant 1)
Product – 178bp
Known Variants - 2
IMP-3
Product – 191bp
Only one known
transcript

Figure 45: IMP-1 is transcriptionally/translationally down-regulated in several colon cancer cell lines. (**A**) Western blot of cell lysates made from different colon cancer cell lines. The top panel shows a blot for E-cadherin, middle panel for IMP1 and bottom panel for GAPDH (loading control). (**B**) RT-PCR for IMP-1, IMP-2 and IMP-3 for cDNA extracted from the seven colon cancer cell line shown in **A**. Red numbers indicate the base pair size of the DNA ladder. The expected product size is indicated below the respective parts of the gel. The higher base pair bands seen for IMP-1 in Lim2551, Lim1899 and Lim1215 were sequenced. These are non-specific genomic DNA amplicons (data not shown).

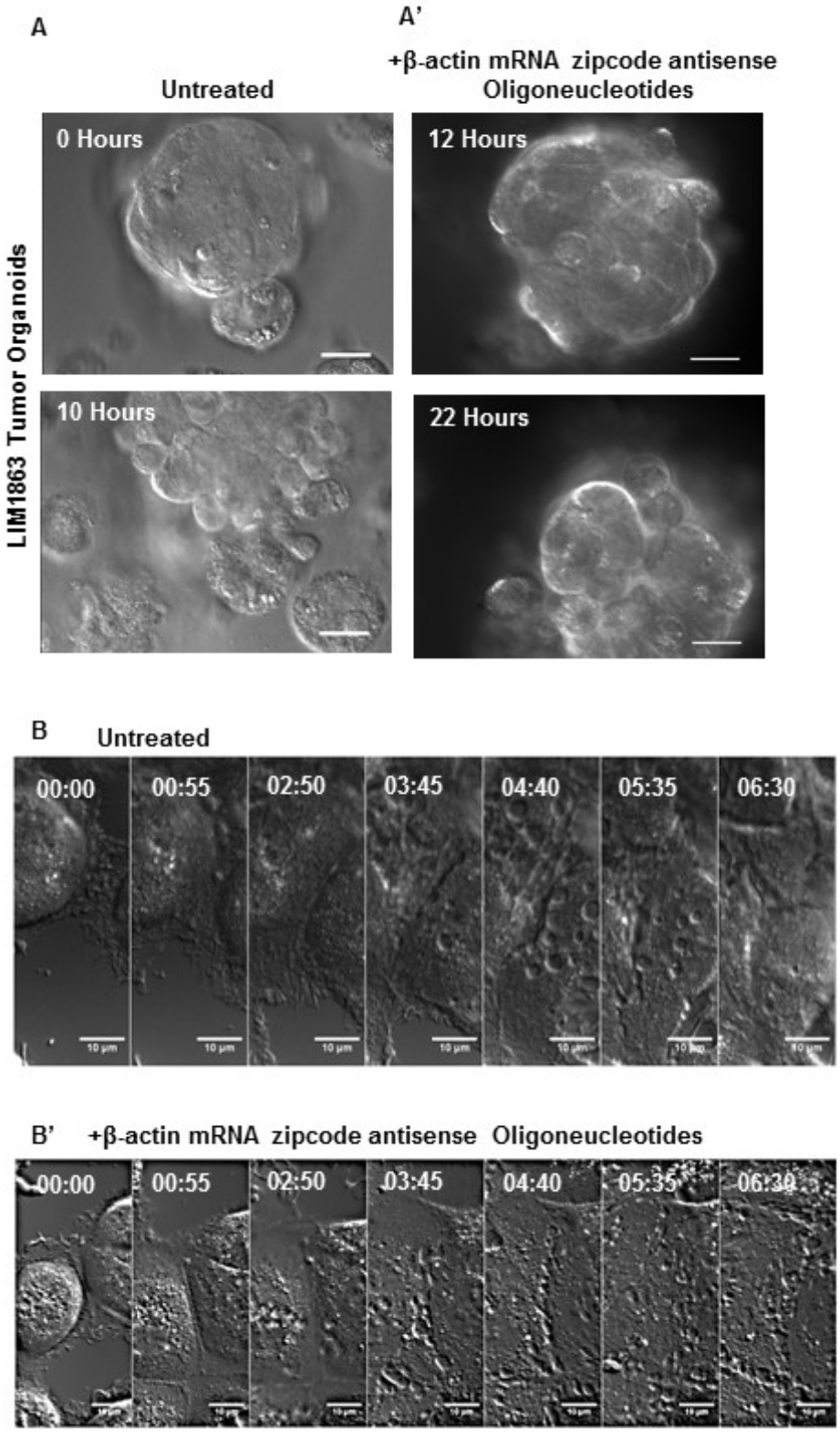
A
A'
+β-actin mRNA zipcode antisense Oligoneucleotides
Untreated
LIM1863 Tumor Organoids
0 Hours
12 Hours
10 Hours
22 Hours
B
Untreated
00:00
00:55
02:50
03:45
04:40
05:35
06:30
B'
+β-actin mRNA zipcode antisense Oligoneucleotides
00:00
00:55
02:50
03:45
04:40
05:35
06:30

Figure 46: Dysfunction of IMP-1 mediated spatial regulation of β-actin translation in colon cancer. DIC images of Lim 1863 tumor cell aggregates (**A**) untreated, or (**A′**) treated with β-actin mRNA zipcode antisense oligonucleotides. (**A**) Top and bottom panel show images acquired at 0 hours and 10 hours, respectively. (**A′**) Top and bottom panels show images acquired 12 hours and 22 hours following treatment with β-actin mRNA zipcode antisense oligonucleotides. Caco-2 cells (**B**) untreated, or (**B′**) treated with β-actin mRNA zipcode antisense oligonucleotides for 12 hours prior to a calcium repletion experiment. Following calcium repletion, cells were imaged for 6.5 hours. Time is indicated in hh:mm following calcium repletion. Scale bars = 10μm. Note that treatment with β-actin mRNA zipcode antisense oligonucleotides had no appreciable effect on cell morphology of Lim1863 tumor organoids. Caco-2 cells show extensive lamellar overlaps following contact expansion phase of adherens junction assembly.

FUTURE DIRECTIONS

A complex gene regulatory network with IMP-1 at the center stage controls epithelial cell fate

The preliminary results presented above point to a role for spatially regulated β-actin translation in intestinal epithelial homeostasis. Experiments designed to observe the localization of β-actin mRNA in the crypt compartment, would answer whether the asymmetric distribution of β-actin protein (**Figure 44**) arises from an mRNA localization which is also asymmetric. To this end, utilizing mini gut cultures derived from MCP (MS2 bacteriophage capsid protein) x β-actin MBS (MS2 binding site) mouse could be used to track β-actin mRNA localization during intestinal homeostasis (Park et al., 2014). Besides β-actin, it is plausible that a number of other mRNAs also regulated by IMP-1 play a crucial role in intestinal homeostasis, given IMP-1 is localized to the stem cell and proliferative compartment of the epithelium (**Figure 42, 43**). It would be interesting to determine whether genes that determine stem cell fate and/or differentiation status are regulated post-transcriptionally by IMP-1. These experiments will reveal the extent to which translational regulation by IMP-1 controls epithelial morphogenesis *ex vivo*.

Besides a role for IMP-1 mediated spatio-temporal translational control in small intestinal homeostasis, its role in promoting or suppressing colon cancer is also very poorly understood. Given its expression is down-regulated in several of the colon cancer cells tested above (**Figure 45**), it will be interesting to investigate the promoter methylation status of IMP-1 in those cell lines where the mRNA is absent. In addition, in

some instances, there appears to be a post-transcriptional silencing of the gene. This could plausibly be due to miRNA mediated regulation in these cells (Mayr and Bartel, 2009). However, besides regulation at the level of IMP-1 expression, the presence of the protein still seems to not affect the spatial regulation of β-actin translation in certain colon cancer cells (**Figure 46**). One plausible explanation for the ability of cancer cells to bypass translational control mediated by IMP-1, is the widespread alternative polyadenylation during transformation (Mayr and Bartel, 2009). However, very little is currently known about the phenomenon when it comes to how APA affects gene regulation by RNA binding proteins.

IMP-1 is an important RNA binding protein with several mRNA interacting partners (Jonson et al., 2007). Some of the mRNA produce proteins regulating cell-cell adhesion, others control cell migration, while still others are implicated in cell survival and proliferation (Zirkel et al., 2013). Given the complexity of the network (**Figure 47**), experiments involving re-expression of IMP-1 in cancer cells that have downregulated its expression can be tricky to interpret. Cancer cell fate is determined in part by its transcriptome and hence it is vital to analyze the gene expression signatures to determine what role IMP-1 may play in a given cancer cell type. One very inviting alternative is to first determine the gene expression signature followed by masking the mRNA *cis* acting elements specifically for those mRNAs that drive a mesenchymal fate. The re-expression of IMP1 in this scenario will push the cell towards an adhesive cell fate thus preventing metastasis.

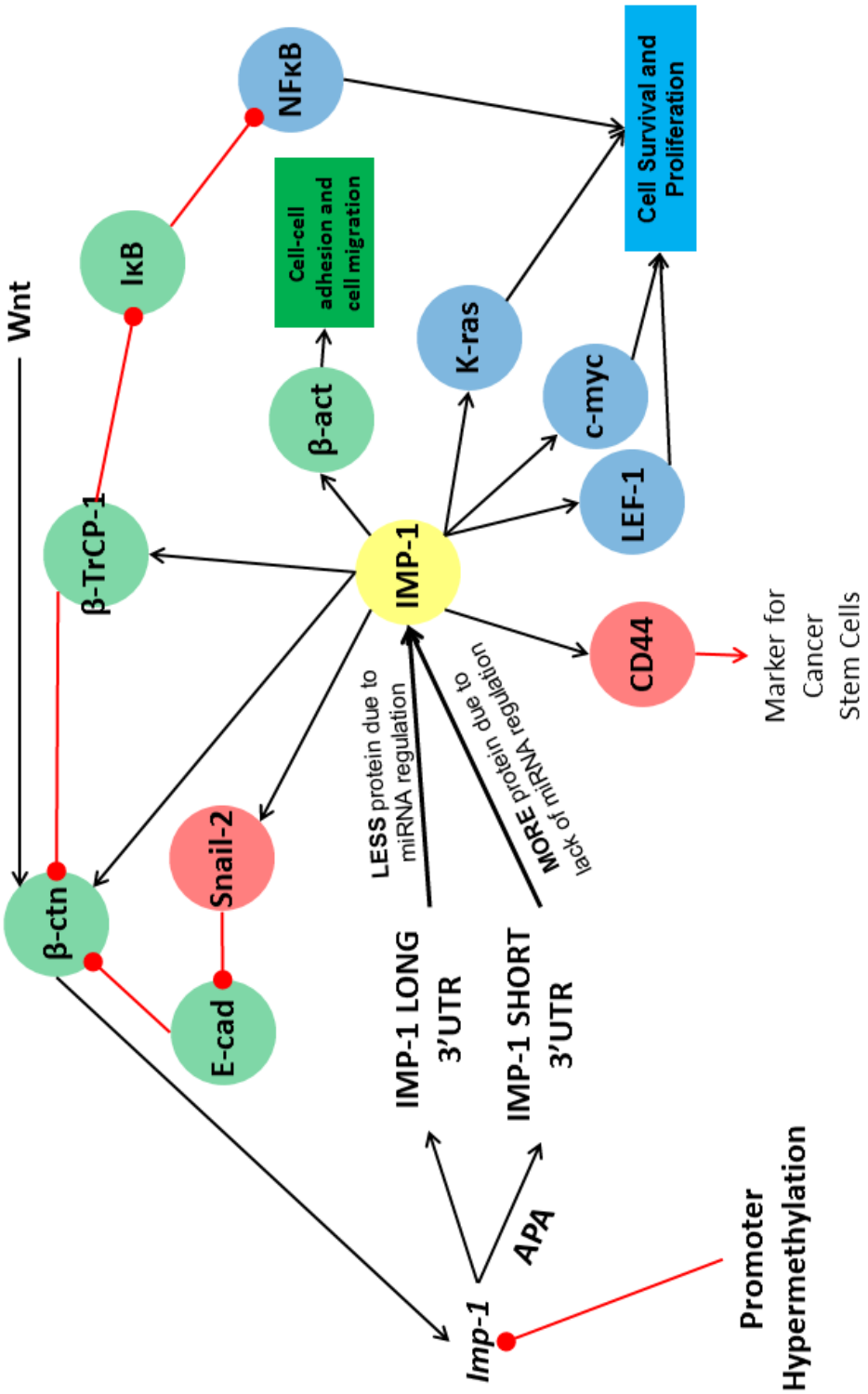
Wnt
IκB
NFκB
β-TrCP-1
β-act
Cell-cell adhesion and cell migration
K-ras
Cell Survival and Proliferation
c-myc
LEF-1
IMP-1
CD44
Marker for Cancer Stem Cells
LESS protein due to miRNA regulation
MORE protein due to lack of miRNA regulation
Snail-2
β-ctn
E-cad
IMP-1 LONG 3'UTR
IMP-1 SHORT 3'UTR
APA
Imp-1
Promoter Hypermethylation

Figure 47: A complex IMP-1 dependent gene regulatory network determines cell fate specification. Schematic representing a cell fate regulatory gene network with IMP1 at the center stage. Some of the several mRNAs that are regulated by IMP1 expression are highlighted in the schematic: LEF-1, c-myc and K-ras (Blue circles) regulate cell survival and proliferation and are upregulated in several cancers; Snail-2 (Red circle) represses E-cadherin expression during EMT and promotes tumorigenesis; CD44 is expressed in putative cancer stem cells; and β-actin, β-catenin and E-cadherin (Green circles) regulate cell-cell adhesion and cell motility. In addition, β-Trcp regulates β-catenin localization to the nucleus to control Wnt signaling. Also, β-catenin regulates IMP-1 expression directly by binding to its promoter region. Lastly, IMP1 is subject to transcriptional and post transcriptional control by promoter methylation and miRNA mediated mechanisms, respectively.

CONCLUSIONS

Fluorescence Covariance Index: A simple, robust and reliable tool to assess adherens junction dynamics and more

As part of the thesis, a fluorescence microscopy based method, which utilizes Pearson's Correlation Coefficients, was developed to estimate protein complex assembly in fixed and living cells. The analysis is simple in terms of instrumentation costs: requires an epifluorescence microscope, and image processing software to carry out deconvolution. It is to be noted that while in this thesis, a proprietary software from Zeiss (AxioVision) was used to carry out the deconvolution, open source plugins for ImageJ can also be used to carry out image processing (Bruce and Butte, 2013; Preibisch et al., 2014). In addition, since the technique runs a custom MATLAB script (**See Appendix**) for compiling data, it is ideal for large data sets, which may be required to determine minor variations in the extent of protein complexes assembly. The analysis was validated by measuring: adherens junction complex anchoring (E-cadherin anchoring to F-actin) and trafficking of minimal cadherin-catenin complex from the biosynthetic ER-golgi compartment to sites adherens junction assembly (E-cadherin association with β-actenin and α-catenin). Additionally, FCI analysis was shown to be useful in estimating protein interactions that are mechanosensitive, such as α-catenin and F-actin interaction. The technique was then applied to study the effect of partially mislocalized β-actin translation on the extent of adherens junction assembly. Additionally, the FCI measures were correlated with tissue barrier function, demonstrating the structural and morphological changes assessed by the method indeed correlate with tissue function (Cruz et al., 2015).

Several key signaling pathways impinge upon actin dynamics to regulate epithelial structure and function

Work presented in this thesis points to spatially regulated β-actin translation as a key node for processing several signaling pathways which effect epithelial structure and function.

First, experiments in chapter 3, point to a model of adherens junction assembly that is governed by a balance between β-actin translation mediated cadherin anchoring at cell-cell contacts and E-cadherin endocytosis. Mislocalizing β-actin translation results in shifting the balance towards E-cadherin endocytosis and as a result cells fail to undergo adherens junction maturation. Inhibiting endocytosis in cells with partially mislocalized β-actin translation shifts the balance back towards actin mediated cadherin anchoring rescuing adherens junction maturation.

Second, cyst culture models of MDCK cells demonstrate a role for spatially regulated β-actin translation in 3-dimensional epithelial morphogenesis. Acto-myosin contractility governs cell shape changes and epithelial tissue morphogenesis by impinging on several determinants of epithelial morphology including adherens junction, tight junctions and cell proliferation pathways such as Hippo and/or YAP/TAZ. Results presented in this thesis indicate a role for spatially regulated β-actin translation in integrating the mechano-transduction signals from acto-myosin contractility to control epithelial morphogenesis. In cultures derived from cells with partially mislocalized β-actin translation, NMIIA organization and tight junction organization were both

disrupted. The resultant phenotype was reduced cell proliferation, cell shape and size changes plausibly due to a down-regulation of the Hippo and/or YAP/TAZ pathways.

Third, results in this thesis provide evidence for a role of spatially regulated β-actin translation in governing collective cell migratory behavior of epithelial sheets. Partially mislocalizing β-actin translation increases rate of actin dynamics at cell-cell adhesions between leader-follower cell pairs during collective migration. While these cells show a more dynamic lamellipodium, the overall rate of migration of the tissue is lower. Thus by playing a role in cell-cell adhesion dynamics and leading edge protrusion dynamics, spatially regulated β-actin translation governs epithelial collective cell migratory behavior.

Why is compartmentalized translation of β-actin important?

When looking at eukaryotic cells, typically vertebrate cells, one should realize that there is abundant amounts of actin. Muscle cells for instance contain about 10% actin by weight, while non-muscle cells have anywhere between 1-5% actin by weight (Lodish, 2000). In addition to the abundant expression of actin in cells, the 6 different vertebrate isoforms exhibit remarkable conservation across species (Bulinski, 2006). The focus of this thesis is on compartmentalized translation of the β-actin isoform. In view of the fact that actin is so abundant in the cell that its concentration sometimes reaches mM levels, why indeed is it important to study the cell compartmentalized translation of β-actin? First, although β-actin and another isoform, γ-actin only differ by 4 amino acids (≈ 1% of the aa sequence), γ-actin mRNA does not get compartmentalized in cells (Hill and Gunning, 1993; Lawrence and Singer, 1986). Second, compartmentalized translation can

increase the local concentration of β-actin well above the critical concentration required for polymerization (Condeelis and Singer, 2005; Gutierrez et al., 2014). Third, locally synthesized β-actin can be subject to post-translational modification such as arginylation (Saha et al., 2010), which confer different properties to the dynamics of the local filament populations. Fourth, β-actin and γ-actin have different rates of translation regulated by coding sequence variation, co-translational and post-translational targeting for degradation (Zhang et al., 2010). Last, but not least, the post-translational modifications conferred to β-actin result in differential binding to actin binding proteins such as capping proteins modulating polymer levels in cells (Saha et al., 2010). Given the complexity of regulation of actin isoforms at various levels post-transcriptionally, one could postulate that the cell has evolved numerous stratified mechanisms to regulate the spatial and temporal expression of specific actin isoforms. It is thus important to study how each of the above mentioned regulatory modules: localization of mRNA, post-translational modification, co-translational and post-translational degradation, and differential association with binding partners operates to bring about complex cellular processes. The work presented in this thesis helps shed light on how the first step in post-transcriptional gene regulation of β-actin, its mRNA localization, plays an important role in epithelial tissue structure and function.

APPENDICES

Isolation and culture of mouse small intestinal crypts

1. Take the proximal third of the small intestine, flush it with PBS (18 gauge syringe) and cut open.
2. Divide into three or more 1cm long pieces.
3. Wash with 1XPBS three times (3minutes each wash) by inverting in a 15mL conical tube.
4. Transfer the pieces into 10mL of PBS-EDTA (2mM) and wash twice by rotating very gently at 4°C (5minutes first wash; 40minutes second wash).
5. Shake the tube very hard 15-20 times until the solution becomes very cloudy.
6. Pour the solution into 40mL pre-cooled (standing on ice) PBS through a 70µm filter.
7. Spin the tube at 200g for 3-5 minutes at 4°C. Repeat spin, if necessary, to see a clear supernatant.
8. Decant the supernatant and resuspend the pellet in about 20 mL of pre-chilled PBS and repeat the centrifugation step.
9. Decant supernatant and this time resuspend the pellet in 1mL of ice cold PBS.
10. Count the crypts using a hemocytometer at this stage.
11. Centrifuge the crypts in a 1mL microfuge tube at 4°C for 3-5 minutes.
12. Resuspend the crypts in an appropriate volume of crypt culture medium and add to Matrigel.

13. See the appropriate number of crypts into 8-well chamber slides and allow the Matrigel to polymerize.
14. Add crypt culture medium (See recipe below).

Crypt culture Medium

Basal culture medium: 50mL Advanced DMEM/F12; 5mL Pencillin/Streptavadin (10,000units/mL and 10,000µg/mL, respectively); 5mL 1M HEPES buffer; 5mL GlutaMax.

To make up crypt culture medium: 50mL of basal culture medium; 1mL of 100X N2; 500µL of B27; 100µL of 500mM N-Acetyl Cysteine; 5µL of 500µg/mL EGF; 50µL of 100µg/mL Noggin and 50µg vial of R-Spondin resuspended in BCM. Filter the medium through a 0.22µm filter and aliquot. Store aliquots at -20°C till use. Thaw and store at 4°C for up to a week.

Immunohistochemistry for IMP-1 in mouse small intestinal and colonic tissue sections embedded in paraffin

1. Dewax the slides at 55°C for 30 minutes.
2. Immerse slides in Xylene – 2X (15 minutes and 10 minutes each).
3. Immerse slides in 0.3% (v/v) H_2O_2 (prepared in 100% (v/v) methanol) for 20 minutes.
4. Wash the slides under running water for 5 minutes.
5. Wash the slides with 1X PBS for 5 minutes.
6. Antigen retrieval: Partially boil 800mL of citric acid buffer for 5 minutes. Immerse slides and boil for additional 15 minutes.

7. Let the slides cool for 20 minutes in the citric acid buffer.
8. Wash the slides under running water for 5 minutes.
9. Wash slides quickly with 1X PBS.
10. Block slides with 1X animal free blocking solution for 1 hour – 2 hours at room temperature.
11. Dilute primary antibody in 1X animal free blocking solution (1:50 dilution) and incubate slide with primary antibody at 4°C overnight.
12. Wash slides with 1X PBS – 3X (5 minutes each at room temperature).
13. Add secondary antibody (1:200) dilutes in 1X animal free blocking solution and incubate at room temperature for 1 – 1.5 hours.
14. Wash slides with 1X PBS – 3X (5 minutes each at room temperature).
15. Prepare HRP conjugated ABC reagent (Vector Shield):

    Reagent A – 20µL

    Reagent B – 20µL

    Blocking solution – 1mL
16. Incubate slides with ABC reagent for 2 hours at room temperature.
17. Wash slides with 1X PBS – 3X (10 minutes each at room temperature).
18. Developing color: Prepare the DAB reagent

    Buffer – 1 drop

    DAB – 2 drops

    H_2O_2 – 1 drop

    Water – 2.5 mL

Add the DAB reagent to the slides (2-4 drops) and observe under light microscope for color development. Typically the development times for IMP-1 are 1-1.5 minutes. Optimize time as necessary. Stop reactin by immersing the slide in water.

19. Wash the slides under running water for 5 minutes.

Nuclear staining with Hematoxylin

1. Add Hematoxylin to the slide and incubate for 8 minutes.
2. Wash the slides under running water for 5 minutes.
3. Immerse slides in 1% (v/v) Acetic acid prepared in MilliQ water for 3 minutes.
4. Wash the slides under running water for 5 minutes.
5. Immerse slides in 0.3% (v/v) ammonia for 8 minutes.
6. Wash the slides under running water for 5 minutes.
7. Immerse the slides in increasing concentration of Ethanol – 70% (v/v), 80% (v/v), 90% (v/v), 95% (v/v) – 2 minutes in each solution.
8. Immerse the slides in 100% Ethanol – 2X (2 minutes each).
9. Immerse the slides in Xylene – 2X (5 minute and 10 minutes each).
10. Mount the slides without letting them dry.
11. Images were acquired using Nikon TE2000 microscope equipped with a color camera. Images were acquired at 30X and 60X magnification

Primer Sequences for RT-PCR

The following primer pairs were used to carry out paralog specific RT-PCR for IMP-1. Annealing temperature used was 60°C.

IMP1 V1 F	GTGAGCAAGTGAACACCGAGA
IMP1 V1 R	TGCTATCTGCTCATCGGGGA
IMP2 V1 F	AGCGCACTTGGCATCTTTTC
IMP2 V1 R	CCTGCTCTGGATAAGAGTGATGA
IMP3 V1 F	CGGTCCCAAAAAGGCAAAGG
IMP3 V1 R	TAGTGCTTGTCTAGCTTGGTCC

Custom Script for FCI analysis

```
Reading .csv files and storing the measurement values in an array.
function [mystruct1] = readData(filename)
% Make the folder containing the .csv files to be analyzed the filepath
for MATLab. Execute this script from the MATLab command prompt by
typing readData('filename.csv'). Note that the input argument contains
'' marks to enclose the filename. The filenames must not contain these
characters. The filename can be the name of the first csv file in the
dataset folder.

    NumCols = 27;

% Input the right number of columns present in the .csv files to be
read.
% Note that the number of columns in all the files in a data set should
be the same for the script to execute. If the dataset consists of
batches of files with different numbers of columns, separate them into
different folder and run the script on different folders with the
appropriate number of columns in each subset of the data.
```

```
    fid = fopen(filename,'r');
    InputText = textscan(fid,'%s',NumCols,'delimiter',',');
% Reads header line.
    HeaderLines = InputText{1};
% Inputs header line into a new array called InputText.
    HeaderLines = regexprep(HeaderLines, '[-/\s()."µm³]', '');
% Searches header lines for the following expressions: [-/\s()."µm³],
and delete them. These characters are not compatible with running the
script.
    FormatString = repmat('%s', 1, NumCols);
% Creates format string based on parameter
    InputText = textscan(fid,FormatString, ...          % Read data
                         'delimiter',',');
      for i = 1:27

% Input the right number of columns present in the .csv files to be
read.
        InputText{i} = str2double(regexprep(InputText{i}, '["]', ''));
      end

% The original data has all values enclosed with "". The enclosing
quotation marks ("") are manually removed to convert strings to
floating point numbers.

    Data = cell2mat(InputText);
% Converts to numerical array from cell

     mystruct1 = struct(HeaderLines{1, 1}, Data(:, 1)');
```

```
% The following loop writes all the values from the .csv files into an
array with the headerlines taken from the first row.

      for j = 2:NumCols
         name = HeaderLines{j, 1};
         newName = regexprep(name,'[-/\s().]','');
         mystruct1.(newName) = Data(:, j)';
      end


     fclose(fid);
end

Reading measurement values stored in an array using the above script
and computing FCI values or returning PCC values for a dataset in a
folder.
function [myExps, out1, out2, out3] = combineExps()

 fileList = dir('*.csv');
 myExps = [];
% The following loop reads over all the .csv files in the folder and
writes them to arrays by running the above readData function for each
file.

for i = 1: length(fileList)
  myData = readData(fileList(i).name);
  myExps = [myExps myData];
 end
```

```
% The following loop sets a lower threshold on PCC values. Using 0.1 as
the lower threshold, the loop will reassign any PCC values below this
threshold to 0.1. The lower threshold can be modified if setting a
different value or the whole loop can be eliminated if this is not
desired.

for k = 1:1:length(fileList)
   a = myExps(k).PearsonsCorrelation; %Storing all PCCs in a matrix.
    for j = 1:1:length(a) %Defining the the number of cells
                          %("length(a)") to be checked for PCC values.
     if 0 > a(j);         %Checking for any negative PC.
         a(j) = 0.1;      %Input Least Possible PC to set for all
                          %PCC(s) that are negative.
     elseif a(j) < 0.1; %Checking for all PCCs that are positive
                          %and below the Least Possible PC.
         a(j) = 0.1;      %Input Least Possible PCC to set for all PCC(s)
                          %positive and below the Least Possible PCC.
     end %End the checking loop for a single cell.
    myExps(k).PearsonsCorrelation = a; %Store all the corrected PCC(s)
in the original array.
    end %End the checking loop for one file.
 end

% The following loop runs from the User defined value of k for j times.
The value of k should be set to the number of the first .csv file that
is part of the same time point/condition, for instance steady state.
The value of j depends on how many experimental repeats are contained
```

```
for the particular time point/condition. The array into which the
required PCC values are stored is also initialized by the User in the
first line. So use appropriate names. If there are multiple
combinations of PCCs within a particular data set, check the proper
increments in k.


 SS = [];
  k = 1;
  for j = 1: 20
   out1 =
myExps(k+3).PearsonsCorrelation./myExps(k).PearsonsCorrelation;
   out2 =
myExps(k+4).PearsonsCorrelation./myExps(k+1).PearsonsCorrelation;
   out3 =
myExps(k+5).PearsonsCorrelation./myExps(k+2).PearsonsCorrelation;
   SS = [SS; out1' out2' out3'];
   k = k+6;
  end


% Log transform the data obtained.
SSL = log10 (SS);


% Write the log transformed data to a text file.


dlmwrite('B-ctn2_FF_RG_FCI.txt', SSL)
```

References

Adams, C.L., Y.T. Chen, S.J. Smith, and W.J. Nelson. 1998. Mechanisms of epithelial cell-cell adhesion and cell compaction revealed by high-resolution tracking of E-cadherin-green fluorescent protein. *The Journal of cell biology*. 142:1105-1119.

Adler, J., and I. Parmryd. 2010. Quantifying colocalization by correlation: the Pearson correlation coefficient is superior to the Mander's overlap coefficient. *Cytometry. Part A : the journal of the International Society for Analytical Cytology*. 77:733-742.

Akhtar, N., and N.A. Hotchin. 2001. RAC1 regulates adherens junctions through endocytosis of E-cadherin. *Mol Biol Cell*. 12:847-862.

Alberts, B., J.H. Wilson, and T. Hunt. 2008. Molecular biology of the cell. Garland Science, New York. xxxiii, 1601, 1690 p. pp.

Aoki, K., Y. Kamioka, and M. Matsuda. 2013. Fluorescence resonance energy transfer imaging of cell signaling from in vitro to in vivo: basis of biosensor construction, live imaging, and image processing. *Development, growth & differentiation*. 55:515-522.

Baj, G., E. Leone, M.V. Chao, and E. Tongiorgi. 2011. Spatial segregation of BDNF transcripts enables BDNF to differentially shape distinct dendritic compartments.

Proceedings of the National Academy of Sciences of the United States of America. 108:16813-16818.

Ballestrem, C., B. Wehrle-Haller, and B.A. Imhof. 1998. Actin dynamics in living mammalian cells. *Journal of cell science*. 111 (Pt 12):1649-1658.

Bamburg, J.R. 1999. Proteins of the ADF/cofilin family: essential regulators of actin dynamics. *Annual review of cell and developmental biology*. 15:185-230.

Baranwal, S., N.G. Naydenov, G. Harris, V. Dugina, K.G. Morgan, C. Chaponnier, and A.I. Ivanov. 2012. Nonredundant roles of cytoplasmic beta- and gamma-actin isoforms in regulation of epithelial apical junctions. *Mol Biol Cell*. 23:3542-3553.

Barlow, A.L., A. Macleod, S. Noppen, J. Sanderson, and C.J. Guerin. 2010. Colocalization analysis in fluorescence micrographs: verification of a more accurate calculation of pearson's correlation coefficient. *Microscopy and microanalysis : the official journal of Microscopy Society of America, Microbeam Analysis Society, Microscopical Society of Canada*. 16:710-724.

Baum, B., and M. Georgiou. 2011. Dynamics of adherens junctions in epithelial establishment, maintenance, and remodeling. *The Journal of cell biology*. 192:907-917.

Bazellieres, E., V. Conte, A. Elosegui-Artola, X. Serra-Picamal, M. Bintanel-Morcillo, P. Roca-Cusachs, J.J. Munoz, M. Sales-Pardo, R. Guimera, and X. Trepat. 2015. Control of cell-cell forces and collective cell dynamics by the intercellular adhesome. *Nature cell biology*. 17:409-420.

Beach, R.L., and W.R. Jeffery. 1990. Temporal and spatial expression of a cytoskeletal actin gene in the ascidian Styela clava. *Developmental genetics*. 11:2-14.

Behrndt, M., and C.P. Heisenberg. 2014. Lateral junction dynamics lead the way out. *Nature cell biology*. 16:127-129.

Bell, J.L., K. Wachter, B. Muhleck, N. Pazaitis, M. Kohn, M. Lederer, and S. Huttelmaier. 2013. Insulin-like growth factor 2 mRNA-binding proteins (IGF2BPs): post-transcriptional drivers of cancer progression? *Cellular and molecular life sciences : CMLS*. 70:2657-2675.

Bellett, G., J.M. Carter, J. Keynton, D. Goldspink, C. James, D.K. Moss, and M.M. Mogensen. 2009. Microtubule plus-end and minus-end capture at adherens junctions is involved in the assembly of apico-basal arrays in polarised epithelial cells. *Cell motility and the cytoskeleton*. 66:893-908.

Bertocchi, C., M. Vaman Rao, and R. Zaidel-Bar. 2012. Regulation of adherens junction dynamics by phosphorylation switches. *Journal of signal transduction*. 2012:125295.

Biswas, K.H., K.L. Hartman, C.H. Yu, O.J. Harrison, H. Song, A.W. Smith, W.Y. Huang, W.C. Lin, Z. Guo, A. Padmanabhan, S.M. Troyanovsky, M.L. Dustin, L. Shapiro, B. Honig, R. Zaidel-Bar, and J.T. Groves. 2015. E-cadherin junction formation involves an active kinetic nucleation process. *Proceedings of the National Academy of Sciences of the United States of America*. 112:10932-10937.

Blanco, M.J., G. Moreno-Bueno, D. Sarrio, A. Locascio, A. Cano, J. Palacios, and M.A. Nieto. 2002. Correlation of Snail expression with histological grade and lymph node status in breast carcinomas. *Oncogene*. 21:3241-3246.

Bolte, S., and F.P. Cordelieres. 2006. A guided tour into subcellular colocalization analysis in light microscopy. *Journal of microscopy*. 224:213-232.

Bouget, F.Y., S. Gerttula, S.L. Shaw, and R.S. Quatrano. 1996. Localization of Actin mRNA during the Establishment of Cell Polarity and Early Cell Divisions in Fucus Embryos. *The Plant cell*. 8:189-201.

Bravo-Cordero, J.J., L. Hodgson, and J. Condeelis. 2012. Directed cell invasion and migration during metastasis. *Current opinion in cell biology*. 24:277-283.

Bruce, M.A., and M.J. Butte. 2013. Real-time GPU-based 3D Deconvolution. *Optics express*. 21:4766-4773.

Bryant, D.M., A. Datta, A.E. Rodriguez-Fraticelli, J. Peranen, F. Martin-Belmonte, and K.E. Mostov. 2010. A molecular network for de novo generation of the apical surface and lumen. *Nature cell biology*. 12:1035-1045.

Bryant, D.M., and J.L. Stow. 2004. The ins and outs of E-cadherin trafficking. *Trends in cell biology*. 14:427-434.

Buckley, C.D., J. Tan, K.L. Anderson, D. Hanein, N. Volkmann, W.I. Weis, W.J. Nelson, and A.R. Dunn. 2014. Cell adhesion. The minimal cadherin-catenin complex binds to actin filaments under force. *Science*. 346:1254211.

Bulinski, J.C. 2006. Cell biology. Actin discrimination. *Science*. 313:180-181.

Bunnell, T.M., and J.M. Ervasti. 2011. Structural and functional properties of the actin gene family. *Critical reviews in eukaryotic gene expression*. 21:255-266.

Buxbaum, A.R., G. Haimovich, and R.H. Singer. 2015. In the right place at the right time: visualizing and understanding mRNA localization. *Nat Rev Mol Cell Biol*. 16:95-109.

Cailliez, F., and R. Lavery. 2005. Cadherin mechanics and complexation: the importance of calcium binding. *Biophys J*. 89:3895-3903.

Calautti, E., S. Cabodi, P.L. Stein, M. Hatzfeld, N. Kedersha, and G. Paolo Dotto. 1998. Tyrosine phosphorylation and src family kinases control keratinocyte cell-cell adhesion. *The Journal of cell biology*. 141:1449-1465.

Cano, A., M.A. Perez-Moreno, I. Rodrigo, A. Locascio, M.J. Blanco, M.G. del Barrio, F. Portillo, and M.A. Nieto. 2000. The transcription factor snail controls epithelial-mesenchymal transitions by repressing E-cadherin expression. *Nature cell biology*. 2:76-83.

Cao, L.G., D.J. Fishkind, and Y.L. Wang. 1993. Localization and dynamics of nonfilamentous actin in cultured cells. *The Journal of cell biology*. 123:173-181.

Cavey, M., M. Rauzi, P.F. Lenne, and T. Lecuit. 2008. A two-tiered mechanism for stabilization and immobilization of E-cadherin. *Nature*. 453:751-756.

Cerruti, B., A. Puliafito, A.M. Shewan, W. Yu, A.N. Combes, M.H. Little, F. Chianale, L. Primo, G. Serini, K.E. Mostov, A. Celani, and A. Gamba. 2013. Polarity, cell division, and out-of-equilibrium dynamics control the growth of epithelial structures. *The Journal of cell biology*. 203:359-372.

Chao, J.A., Y. Patskovsky, V. Patel, M. Levy, S.C. Almo, and R.H. Singer. 2010. ZBP1 recognition of beta-actin zipcode induces RNA looping. *Genes & development*. 24:148-158.

Chen, C.L., and H.C. Chen. 2009. Functional suppression of E-cadherin by protein kinase Cdelta. *Journal of cell science*. 122:513-523.

Chen, X., and I.G. Macara. 2006. Par-3 mediates the inhibition of LIM kinase 2 to regulate cofilin phosphorylation and tight junction assembly. *The Journal of cell biology*. 172:671-678.

Chen, Y.T., D.B. Stewart, and W.J. Nelson. 1999. Coupling assembly of the E-cadherin/beta-catenin complex to efficient endoplasmic reticulum exit and basal-lateral membrane targeting of E-cadherin in polarized MDCK cells. *The Journal of cell biology*. 144:687-699.

Condeelis, J., and R.H. Singer. 2005. How and why does beta-actin mRNA target? *Biology of the cell / under the auspices of the European Cell Biology Organization*. 97:97-110.

Costes, S.V., D. Daelemans, E.H. Cho, Z. Dobbin, G. Pavlakis, and S. Lockett. 2004. Automatic and quantitative measurement of protein-protein colocalization in live cells. *Biophys J*. 86:3993-4003.

Cruz, L.A., P. Vedula, N. Gutierrez, N. Shah, S. Rodriguez, B. Ayee, J. Davis, and A.J. Rodriguez. 2015. Balancing spatially regulated beta-actin translation and dynamin mediated endocytosis is required to assemble functional epithelial monolayers. *Cytoskeleton*.

Curtis, M.W., K.R. Johnson, and M.J. Wheelock. 2008. E-cadherin/catenin complexes are formed cotranslationally in the endoplasmic reticulum/Golgi compartments. *Cell communication & adhesion*. 15:365-378.

de Beco, S., F. Amblard, and S. Coscoy. 2012. New insights into the regulation of E-cadherin distribution by endocytosis. *International review of cell and molecular biology*. 295:63-108.

de Beco, S., C. Gueudry, F. Amblard, and S. Coscoy. 2009. Endocytosis is required for E-cadherin redistribution at mature adherens junctions. *Proceedings of the National Academy of Sciences of the United States of America*. 106:7010-7015.

DesMarais, V., F. Macaluso, J. Condeelis, and M. Bailly. 2004. Synergistic interaction between the Arp2/3 complex and cofilin drives stimulated lamellipod extension. *Journal of cell science*. 117:3499-3510.

Drees, F., S. Pokutta, S. Yamada, W.J. Nelson, and W.I. Weis. 2005. Alpha-catenin is a molecular switch that binds E-cadherin-beta-catenin and regulates actin-filament assembly. *Cell*. 123:903-915.

Dubin-Thaler, B.J., G. Giannone, H.G. Dobereiner, and M.P. Sheetz. 2004. Nanometer analysis of cell spreading on matrix-coated surfaces reveals two distinct cell states and STEPs. *Biophys J*. 86:1794-1806.

Dunn, K.W., M.M. Kamocka, and J.H. McDonald. 2011. A practical guide to evaluating colocalization in biological microscopy. *American journal of physiology. Cell physiology*. 300:C723-742.

Eliscovich, C., A.R. Buxbaum, Z.B. Katz, and R.H. Singer. 2013. mRNA on the move: the road to its biological destiny. *The Journal of biological chemistry*. 288:20361-20368.

Ewald, A.J., A. Brenot, M. Duong, B.S. Chan, and Z. Werb. 2008. Collective epithelial migration and cell rearrangements drive mammary branching morphogenesis. *Developmental cell*. 14:570-581.

Farooqui, R., and G. Fenteany. 2005. Multiple rows of cells behind an epithelial wound edge extend cryptic lamellipodia to collectively drive cell-sheet movement. *Journal of cell science*. 118:51-63.

Fenteany, G., P.A. Janmey, and T.P. Stossel. 2000. Signaling pathways and cell mechanics involved in wound closure by epithelial cell sheets. *Current biology : CB*. 10:831-838.

Findeis-Hosey, J.J., and H. Xu. 2011. The use of insulin like-growth factor II messenger RNA binding protein-3 in diagnostic pathology. *Human pathology*. 42:303-314.

Findeis-Hosey, J.J., and H. Xu. 2012. Insulin-like growth factor II-messenger RNA-binding protein-3 and lung cancer. *Biotechnic & histochemistry : official publication of the Biological Stain Commission*. 87:24-29.

Friedl, P., and D. Gilmour. 2009. Collective cell migration in morphogenesis, regeneration and cancer. *Nat Rev Mol Cell Biol*. 10:445-457.

Friedl, P., and K. Wolf. 2010. Plasticity of cell migration: a multiscale tuning model. *The Journal of cell biology*. 188:11-19.

Fujita, Y., G. Krause, M. Scheffner, D. Zechner, H.E. Leddy, J. Behrens, T. Sommer, and W. Birchmeier. 2002. Hakai, a c-Cbl-like protein, ubiquitinates and induces endocytosis of the E-cadherin complex. *Nature cell biology*. 4:222-231.

Gloushankova, N.A., N.A. Alieva, M.F. Krendel, E.M. Bonder, H.H. Feder, J.M. Vasiliev, and I.M. Gelfand. 1997. Cell-cell contact changes the dynamics of lamellar activity in nontransformed epitheliocytes but not in their ras-transformed descendants. *Proceedings of the National Academy of Sciences of the United States of America*. 94:879-883.

Godin, A.G., S. Costantino, L.E. Lorenzo, J.L. Swift, M. Sergeev, A. Ribeiro-da-Silva, Y. De Koninck, and P.W. Wiseman. 2011. Revealing protein oligomerization and densities in situ using spatial intensity distribution analysis. *Proceedings of the National Academy of Sciences of the United States of America*. 108:7010-7015.

Gu, W., F. Pan, and R.H. Singer. 2009. Blocking beta-catenin binding to the ZBP1 promoter represses ZBP1 expression, leading to increased proliferation and migration of metastatic breast-cancer cells. *Journal of cell science*. 122:1895-1905.

Gurniak, C.B., and W. Witke. 2007. HuGE, a novel GFP-actin-expressing mouse line for studying cytoskeletal dynamics. *European journal of cell biology*. 86:3-12.

Gutierrez, N., I. Eromobor, R.J. Petrie, P. Vedula, L. Cruz, and A.J. Rodriguez. 2014. The beta-actin mRNA zipcode regulates epithelial adherens junction assembly but not maintenance. *Rna*. 20:689-701.

Hamilton, K.E., F.K. Noubissi, P.S. Katti, C.M. Hahn, S.R. Davey, E.T. Lundsmith, A.J. Klein-Szanto, A.D. Rhim, V.S. Spiegelman, and A.K. Rustgi. 2013. IMP1 promotes tumor growth, dissemination and a tumor-initiating cell phenotype in colorectal cancer cell xenografts. *Carcinogenesis*. 34:2647-2654.

Hansen, T.V., N.A. Hammer, J. Nielsen, M. Madsen, C. Dalbaeck, U.M. Wewer, J. Christiansen, and F.C. Nielsen. 2004. Dwarfism and impaired gut development in insulin-like growth factor II mRNA-binding protein 1-deficient mice. *Molecular and cellular biology*. 24:4448-4464.

Harris, A.R., A. Daeden, and G.T. Charras. 2014. Formation of adherens junctions leads to the emergence of a tissue-level tension in epithelial monolayers. *Journal of cell science*. 127:2507-2517.

Harris, T.J., and U. Tepass. 2010. Adherens junctions: from molecules to morphogenesis. *Nat Rev Mol Cell Biol*. 11:502-514.

Hill, M.A., and P. Gunning. 1993. Beta and gamma actin mRNAs are differentially located within myoblasts. *The Journal of cell biology*. 122:825-832.

Hinck, L., I.S. Nathke, J. Papkoff, and W.J. Nelson. 1994. Dynamics of cadherin/catenin complex formation: novel protein interactions and pathways of complex assembly. *The Journal of cell biology*. 125:1327-1340.

Hoffmann, C., G. Gaietta, A. Zurn, S.R. Adams, S. Terrillon, M.H. Ellisman, R.Y. Tsien, and M.J. Lohse. 2010. Fluorescent labeling of tetracysteine-tagged proteins in intact cells. *Nature protocols*. 5:1666-1677.

Hong, S., R.B. Troyanovsky, and S.M. Troyanovsky. 2010. Spontaneous assembly and active disassembly balance adherens junction homeostasis. *Proceedings of the National Academy of Sciences of the United States of America*. 107:3528-3533.

Huttelmaier, S., D. Zenklusen, M. Lederer, J. Dictenberg, M. Lorenz, X. Meng, G.J. Bassell, J. Condeelis, and R.H. Singer. 2005. Spatial regulation of beta-actin translation by Src-dependent phosphorylation of ZBP1. *Nature*. 438:512-515.

Huttenlocher, A., and A.R. Horwitz. 2011. Integrins in cell migration. *Cold Spring Harbor perspectives in biology*. 3:a005074.

Ilina, O., and P. Friedl. 2009. Mechanisms of collective cell migration at a glance. *Journal of cell science*. 122:3203-3208.

Ishiyama, N., and M. Ikura. 2012. The three-dimensional structure of the cadherin-catenin complex. *Sub-cellular biochemistry*. 60:39-62.

Ivanov, A.I., M. Bachar, B.A. Babbin, R.S. Adelstein, A. Nusrat, and C.A. Parkos. 2007. A unique role for nonmuscle myosin heavy chain IIA in regulation of epithelial apical junctions. *PLoS One*. 2:e658.

Ivanov, A.I., D. Hunt, M. Utech, A. Nusrat, and C.A. Parkos. 2005. Differential roles for actin polymerization and a myosin II motor in assembly of the epithelial apical junctional complex. *Mol Biol Cell*. 16:2636-2650.

Izumi, G., T. Sakisaka, T. Baba, S. Tanaka, K. Morimoto, and Y. Takai. 2004. Endocytosis of E-cadherin regulated by Rac and Cdc42 small G proteins through IQGAP1 and actin filaments. *The Journal of cell biology*. 166:237-248.

Janda, E., M. Nevolo, K. Lehmann, J. Downward, H. Beug, and M. Grieco. 2006. Raf plus TGFbeta-dependent EMT is initiated by endocytosis and lysosomal degradation of E-cadherin. *Oncogene*. 25:7117-7130.

Jeffery, W.R., C.R. Tomlinson, and R.D. Brodeur. 1983. Localization of actin messenger RNA during early ascidian development. *Developmental biology*. 99:408-417.

Jonson, L., J. Vikesaa, A. Krogh, L.K. Nielsen, T. Hansen, R. Borup, A.H. Johnsen, J. Christiansen, and F.C. Nielsen. 2007. Molecular composition of IMP1 ribonucleoprotein granules. *Molecular & cellular proteomics : MCP*. 6:798-811.

Jung, H., B.C. Yoon, and C.E. Holt. 2012. Axonal mRNA localization and local protein synthesis in nervous system assembly, maintenance and repair. *Nat Rev Neurosci*. 13:308-324.

Kametani, Y., and M. Takeichi. 2007. Basal-to-apical cadherin flow at cell junctions. *Nature cell biology*. 9:92-98.

Katz, Z.B., A.L. Wells, H.Y. Park, B. Wu, S.M. Shenoy, and R.H. Singer. 2012. beta-Actin mRNA compartmentalization enhances focal adhesion stability and directs cell migration. *Genes & development*. 26:1885-1890.

Kimura, T., T. Sakisaka, T. Baba, T. Yamada, and Y. Takai. 2006. Involvement of the Ras-Ras-activated Rab5 guanine nucleotide exchange factor RIN2-Rab5 pathway

in the hepatocyte growth factor-induced endocytosis of E-cadherin. *The Journal of biological chemistry*. 281:10598-10609.

Kislauskis, E.H., X. Zhu, and R.H. Singer. 1994. Sequences responsible for intracellular localization of beta-actin messenger RNA also affect cell phenotype. *The Journal of cell biology*. 127:441-451.

Kissinger, J.C., J.H. Hahn, and R.A. Raff. 1997. Rapid evolution in a conserved gene family. Evolution of the actin gene family in the sea urchin genus Heliocidaris and related genera. *Molecular biology and evolution*. 14:654-665.

Kobielak, A., and E. Fuchs. 2004. Alpha-catenin: at the junction of intercellular adhesion and actin dynamics. *Nat Rev Mol Cell Biol*. 5:614-625.

Korpal, M., E.S. Lee, G. Hu, and Y. Kang. 2008. The miR-200 family inhibits epithelial-mesenchymal transition and cancer cell migration by direct targeting of E-cadherin transcriptional repressors ZEB1 and ZEB2. *The Journal of biological chemistry*. 283:14910-14914.

Kovacs, E.M., R.G. Ali, A.J. McCormack, and A.S. Yap. 2002. E-cadherin homophilic ligation directly signals through Rac and phosphatidylinositol 3-kinase to regulate adhesive contacts. *The Journal of biological chemistry*. 277:6708-6718.

Kovacs, E.M., S. Verma, R.G. Ali, A. Ratheesh, N.A. Hamilton, A. Akhmanova, and A.S. Yap. 2011. N-WASP regulates the epithelial junctional actin cytoskeleton through a non-canonical post-nucleation pathway. *Nature cell biology*. 13:934-943.

Kowalczyk, A.P., and B.A. Nanes. 2012. Adherens junction turnover: regulating adhesion through cadherin endocytosis, degradation, and recycling. *Sub-cellular biochemistry*. 60:197-222.

Krendel, M.F., and E.M. Bonder. 1999. Analysis of actin filament bundle dynamics during contact formation in live epithelial cells. *Cell motility and the cytoskeleton*. 43:296-309.

Kusakabe, T. 1997. Ascidian actin genes: developmental regulation of gene expression and molecular evolution. *Zoological science*. 14:707-718.

Kusakabe, T., I. Araki, N. Satoh, and W.R. Jeffery. 1997. Evolution of chordate actin genes: evidence from genomic organization and amino acid sequences. *Journal of molecular evolution*. 44:289-298.

Ladoux, B., W.J. Nelson, J. Yan, and R.M. Mege. 2015. The mechanotransduction machinery at work at adherens junctions. *Integrative biology : quantitative biosciences from nano to macro*.

Latham, V.M., E.H. Yu, A.N. Tullio, R.S. Adelstein, and R.H. Singer. 2001. A Rho-dependent signaling pathway operating through myosin localizes beta-actin mRNA in fibroblasts. *Current biology : CB*. 11:1010-1016.

Lawrence, J.B., and R.H. Singer. 1986. Intracellular localization of messenger RNAs for cytoskeletal proteins. *Cell*. 45:407-415.

le Duc, Q., Q. Shi, I. Blonk, A. Sonnenberg, N. Wang, D. Leckband, and J. de Rooij. 2010. Vinculin potentiates E-cadherin mechanosensing and is recruited to actin-anchored sites within adherens junctions in a myosin II-dependent manner. *The Journal of cell biology*. 189:1107-1115.

Lecuit, T., and A.S. Yap. 2015. E-cadherin junctions as active mechanical integrators in tissue dynamics. *Nature cell biology*. 17:533-539.

Lembo, A., F. Di Cunto, and P. Provero. 2012. Shortening of 3'UTRs correlates with poor prognosis in breast and lung cancer. *PLoS One*. 7:e31129.

Li, H., T. Shen, M.B. Smith, I. Fujiwara, D. Vavylonis, and X. Huang. 2009. Automated Actin Filament Segmentation, Tracking and Tip Elongation Measurements Based on Open Active Contour Models. *Proceedings / IEEE International Symposium on Biomedical Imaging: from nano to macro. IEEE International Symposium on Biomedical Imaging*. 2009:1302-1305.

Liao, G., L. Mingle, L. Van De Water, and G. Liu. 2015. Control of cell migration through mRNA localization and local translation. *Wiley interdisciplinary reviews. RNA*. 6:1-15.

Ligon, L.A., S. Karki, M. Tokito, and E.L. Holzbaur. 2001. Dynein binds to beta-catenin and may tether microtubules at adherens junctions. *Nature cell biology*. 3:913-917.

Lodish, H.F. 2000. Molecular cell biology. W.H. Freeman, New York. xxxvi, 1084, G-1017, I-1036 p. pp.

Lombaerts, M., T. van Wezel, K. Philippo, J.W. Dierssen, R.M. Zimmerman, J. Oosting, R. van Eijk, P.H. Eilers, B. van de Water, C.J. Cornelisse, and A.M. Cleton-Jansen. 2006. E-cadherin transcriptional downregulation by promoter methylation but not mutation is related to epithelial-to-mesenchymal transition in breast cancer cell lines. *British journal of cancer*. 94:661-671.

Low, B.C., C.Q. Pan, G.V. Shivashankar, A. Bershadsky, M. Sudol, and M. Sheetz. 2014. YAP/TAZ as mechanosensors and mechanotransducers in regulating organ size and tumor growth. *FEBS letters*. 588:2663-2670.

Lyubimova, A., A.D. Bershadsky, and A. Ben-Ze'ev. 1999. Autoregulation of actin synthesis requires the 3'-UTR of actin mRNA and protects cells from actin overproduction. *Journal of cellular biochemistry*. 76:1-12.

Macia, E., M. Ehrlich, R. Massol, E. Boucrot, C. Brunner, and T. Kirchhausen. 2006. Dynasore, a cell-permeable inhibitor of dynamin. *Developmental cell*. 10:839-850.

Maizels, Y., F. Oberman, R. Miloslavski, N. Ginzach, M. Berman, and J.K. Yisraeli. 2015. Localization of cofilin mRNA to the leading edge of migrating cells promotes directed cell migration. *Journal of cell science*. 128:1922-1933.

Manders, E.M.M., F.J. Verbeek, and J.A. Aten. 1993. Measurement of Colocalization of Objects in Dual-Color Confocal Images. *J Microsc-Oxford*. 169:375-382.

Manser, E. 2005. RHO family GTPases. Springer, Dordrecht ; Great Britain. xiii, 296 p. pp.

Martin-Belmonte, F., A. Gassama, A. Datta, W. Yu, U. Rescher, V. Gerke, and K. Mostov. 2007. PTEN-mediated apical segregation of phosphoinositides controls epithelial morphogenesis through Cdc42. *Cell*. 128:383-397.

Martin, B.R., B.N. Giepmans, S.R. Adams, and R.Y. Tsien. 2005. Mammalian cell-based optimization of the biarsenical-binding tetracysteine motif for improved fluorescence and affinity. *Nature biotechnology*. 23:1308-1314.

Martin, K.C., and A. Ephrussi. 2009. mRNA localization: gene expression in the spatial dimension. *Cell*. 136:719-730.

Matsubayashi, Y., W. Razzell, and P. Martin. 2011. 'White wave' analysis of epithelial scratch wound healing reveals how cells mobilise back from the leading edge in a myosin-II-dependent fashion. *Journal of cell science*. 124:1017-1021.

Mayor, R., and S. Etienne-Manneville. 2016. The front and rear of collective cell migration. *Nat Rev Mol Cell Biol*.

Mayor, R., and E. Theveneau. 2013. The neural crest. *Development*. 140:2247-2251.

Mayr, C., and D.P. Bartel. 2009. Widespread shortening of 3'UTRs by alternative cleavage and polyadenylation activates oncogenes in cancer cells. *Cell*. 138:673-684.

McCluskey, A., J.A. Daniel, G. Hadzic, N. Chau, E.L. Clayton, A. Mariana, A. Whiting, N.N. Gorgani, J. Lloyd, A. Quan, L. Moshkanbaryans, S. Krishnan, S. Perera, M. Chircop, L. von Kleist, A.B. McGeachie, M.T. Howes, R.G. Parton, M. Campbell, J.A. Sakoff, X. Wang, J.Y. Sun, M.J. Robertson, F.M. Deane, T.H. Nguyen, F.A. Meunier, M.A. Cousin, and P.J. Robinson. 2013. Building a better dynasore: the dyngo compounds potently inhibit dynamin and endocytosis. *Traffic*. 14:1272-1289.

McLachlan, R.W., A. Kraemer, F.M. Helwani, E.M. Kovacs, and A.S. Yap. 2007. E-cadherin adhesion activates c-Src signaling at cell-cell contacts. *Mol Biol Cell*. 18:3214-3223.

McLachlan, R.W., and A.S. Yap. 2011. Protein tyrosine phosphatase activity is necessary for E-cadherin-activated Src signaling. *Cytoskeleton*. 68:32-43.

McNeil, E., C.T. Capaldo, and I.G. Macara. 2006. Zonula occludens-1 function in the assembly of tight junctions in Madin-Darby canine kidney epithelial cells. *Mol Biol Cell*. 17:1922-1932.

Medioni, C., K. Mowry, and F. Besse. 2012. Principles and roles of mRNA localization in animal development. *Development*. 139:3263-3276.

Mellman, I., and W.J. Nelson. 2008. Coordinated protein sorting, targeting and distribution in polarized cells. *Nat Rev Mol Cell Biol*. 9:833-845.

Menke, A., and K. Giehl. 2012. Regulation of adherens junctions by Rho GTPases and p120-catenin. *Archives of biochemistry and biophysics*. 524:48-55.

Mili, S., and I.G. Macara. 2009. RNA localization and polarity: from A(PC) to Z(BP). *Trends in cell biology*. 19:156-164.

Mili, S., K. Moissoglu, and I.G. Macara. 2008. Genome-wide screen reveals APC-associated RNAs enriched in cell protrusions. *Nature*. 453:115-119.

Mingle, L.A., N.N. Okuhama, J. Shi, R.H. Singer, J. Condeelis, and G. Liu. 2005. Localization of all seven messenger RNAs for the actin-polymerization nucleator

Arp2/3 complex in the protrusions of fibroblasts. *Journal of cell science*. 118:2425-2433.

Montell, D.J. 2003. Border-cell migration: the race is on. *Nat Rev Mol Cell Biol*. 4:13-24.

Mosesson, Y., G.B. Mills, and Y. Yarden. 2008. Derailed endocytosis: an emerging feature of cancer. *Nature reviews. Cancer*. 8:835-850.

Mouneimne, G., L. Soon, V. DesMarais, M. Sidani, X. Song, S.C. Yip, M. Ghosh, R. Eddy, J.M. Backer, and J. Condeelis. 2004. Phospholipase C and cofilin are required for carcinoma cell directionality in response to EGF stimulation. *The Journal of cell biology*. 166:697-708.

Nagafuchi, A. 2001. Molecular architecture of adherens junctions. *Current opinion in cell biology*. 13:600-603.

Nagaoka, K., T. Udagawa, and J.D. Richter. 2012. CPEB-mediated ZO-1 mRNA localization is required for epithelial tight-junction assembly and cell polarity. *Nat Commun*. 3:675.

Najy, A.J., K.C. Day, and M.L. Day. 2008. The ectodomain shedding of E-cadherin by ADAM15 supports ErbB receptor activation. *The Journal of biological chemistry*. 283:18393-18401.

Oleynikov, Y., and R.H. Singer. 2003. Real-time visualization of ZBP1 association with beta-actin mRNA during transcription and localization. *Current biology : CB*. 13:199-207.

Omelchenko, T., J.M. Vasiliev, I.M. Gelfand, H.H. Feder, and E.M. Bonder. 2003. Rho-dependent formation of epithelial "leader" cells during wound healing. *Proceedings of the National Academy of Sciences of the United States of America*. 100:10788-10793.

Pan, F., S. Huttelmaier, R.H. Singer, and W. Gu. 2007. ZBP2 facilitates binding of ZBP1 to beta-actin mRNA during transcription. *Molecular and cellular biology*. 27:8340-8351.

Park, H.Y., H. Lim, Y.J. Yoon, A. Follenzi, C. Nwokafor, M. Lopez-Jones, X. Meng, and R.H. Singer. 2014. Visualization of dynamics of single endogenous mRNA labeled in live mouse. *Science*. 343:422-424.

Patel, V.L., S. Mitra, R. Harris, A.R. Buxbaum, T. Lionnet, M. Brenowitz, M. Girvin, M. Levy, S.C. Almo, R.H. Singer, and J.A. Chao. 2012. Spatial arrangement of an RNA zipcode identifies mRNAs under post-transcriptional control. *Genes & development*. 26:43-53.

Pearson, K. 1896. Contributions to the mathematical theory of evolution, n. p.,. v. pp.

Peglion, F., F. Llense, and S. Etienne-Manneville. 2014. Adherens junction treadmilling during collective migration. *Nature cell biology*. 16:639-651.

Petrie, R.J., H. Koo, and K.M. Yamada. 2014. Generation of compartmentalized pressure by a nuclear piston governs cell motility in a 3D matrix. *Science*. 345:1062-1065.

Petrova, Y.I., M.M. Spano, and B.M. Gumbiner. 2012. Conformational epitopes at cadherin calcium-binding sites and p120-catenin phosphorylation regulate cell adhesion. *Mol Biol Cell*. 23:2092-2108.

Poujade, M., E. Grasland-Mongrain, A. Hertzog, J. Jouanneau, P. Chavrier, B. Ladoux, A. Buguin, and P. Silberzan. 2007. Collective migration of an epithelial monolayer in response to a model wound. *Proceedings of the National Academy of Sciences of the United States of America*. 104:15988-15993.

Preibisch, S., F. Amat, E. Stamataki, M. Sarov, R.H. Singer, E. Myers, and P. Tomancak. 2014. Efficient Bayesian-based multiview deconvolution. *Nature methods*. 11:645-648.

Priya, R., A.S. Yap, and G.A. Gomez. 2013. E-cadherin supports steady-state Rho signaling at the epithelial zonula adherens. *Differentiation; research in biological diversity*. 86:133-140.

Rajasekaran, A.K., M. Hojo, T. Huima, and E. Rodriguez-Boulan. 1996. Catenins and zonula occludens-1 form a complex during early stages in the assembly of tight junctions. *The Journal of cell biology*. 132:451-463.

Rajasekaran, A.K., and S.A. Rajasekaran. 2003. Role of Na-K-ATPase in the assembly of tight junctions. *American journal of physiology. Renal physiology*. 285:F388-396.

Revenu, C., and D. Gilmour. 2009. EMT 2.0: shaping epithelia through collective migration. *Current opinion in genetics & development*. 19:338-342.

Rodriguez, A.J., S.M. Shenoy, R.H. Singer, and J. Condeelis. 2006. Visualization of mRNA translation in living cells. *The Journal of cell biology*. 175:67-76.

Rorth, P. 2009. Collective cell migration. *Annual review of cell and developmental biology*. 25:407-429.

Rosivatz, E., I. Becker, K. Specht, E. Fricke, B. Luber, R. Busch, H. Hofler, and K.F. Becker. 2002. Differential expression of the epithelial-mesenchymal transition regulators snail, SIP1, and twist in gastric cancer. *The American journal of pathology*. 161:1881-1891.

Roussos, E.T., J.S. Condeelis, and A. Patsialou. 2011. Chemotaxis in cancer. *Nature reviews. Cancer*. 11:573-587.

Ryan, G.L., H.M. Petroccia, N. Watanabe, and D. Vavylonis. 2012. Excitable actin dynamics in lamellipodial protrusion and retraction. *Biophys J*. 102:1493-1502.

Ryan, G.L., N. Watanabe, and D. Vavylonis. 2013. Image analysis tools to quantify cell shape and protein dynamics near the leading edge. *Cell structure and function*. 38:1-7.

Saha, S., M.M. Mundia, F. Zhang, R.W. Demers, F. Korobova, T. Svitkina, A.A. Perieteanu, J.F. Dawson, and A. Kashina. 2010. Arginylation regulates intracellular actin polymer level by modulating actin properties and binding of capping and severing proteins. *Mol Biol Cell*. 21:1350-1361.

Sato, T., and H. Clevers. 2013. Growing self-organizing mini-guts from a single intestinal stem cell: mechanism and applications. *Science*. 340:1190-1194.

Sato, T., R.G. Vries, H.J. Snippert, M. van de Wetering, N. Barker, D.E. Stange, J.H. van Es, A. Abo, P. Kujala, P.J. Peters, and H. Clevers. 2009. Single Lgr5 stem cells build crypt-villus structures in vitro without a mesenchymal niche. *Nature*. 459:262-265.

Schaefer, L.H., D. Schuster, and H. Herz. 2001. Generalized approach for accelerated maximum likelihood based image restoration applied to three-dimensional fluorescence microscopy. *Journal of microscopy*. 204:99-107.

Serra-Picamal, X., V. Conte, R. Vincent, E. Anon, D.T. Tambe, E. Bazellieres, J.P. Butler, J.J. Fredberg, and X. Trepat. 2012. Mechanical waves during tissue expansion. *Nat Phys*. 8:628-U666.

Shav-Tal, Y., and R.H. Singer. 2005. RNA localization. *Journal of cell science*. 118:4077-4081.

Shaw, R.M., A.J. Fay, M.A. Puthenveedu, M. von Zastrow, Y.N. Jan, and L.Y. Jan. 2007. Microtubule plus-end-tracking proteins target gap junctions directly from the cell interior to adherens junctions. *Cell*. 128:547-560.

Shen, Y., D.S. Hirsch, C.A. Sasiela, and W.J. Wu. 2008. Cdc42 regulates E-cadherin ubiquitination and degradation through an epidermal growth factor receptor to Src-mediated pathway. *The Journal of biological chemistry*. 283:5127-5137.

Shestakova, E.A., R.H. Singer, and J. Condeelis. 2001. The physiological significance of beta -actin mRNA localization in determining cell polarity and directional motility. *Proceedings of the National Academy of Sciences of the United States of America*. 98:7045-7050.

Sidani, M., D. Wessels, G. Mouneimne, M. Ghosh, S. Goswami, C. Sarmiento, W. Wang, S. Kuhl, M. El-Sibai, J.M. Backer, R. Eddy, D. Soll, and J. Condeelis. 2007. Cofilin determines the migration behavior and turning frequency of metastatic cancer cells. *The Journal of cell biology*. 179:777-791.

Smith, M.B., H. Li, T. Shen, X. Huang, E. Yusuf, and D. Vavylonis. 2010. Segmentation and tracking of cytoskeletal filaments using open active contours. *Cytoskeleton*. 67:693-705.

Smutny, M., H.L. Cox, J.M. Leerberg, E.M. Kovacs, M.A. Conti, C. Ferguson, N.A. Hamilton, R.G. Parton, R.S. Adelstein, and A.S. Yap. 2010. Myosin II isoforms identify distinct functional modules that support integrity of the epithelial zonula adherens. *Nature cell biology*. 12:696-702.

Song, T., Y. Zheng, Y. Wang, Z. Katz, X. Liu, S. Chen, R.H. Singer, and W. Gu. 2015. Specific interaction of KIF11 with ZBP1 regulates the transport of beta-actin mRNA and cell motility. *Journal of cell science*. 128:1001-1010.

Sun, Y. 2007. Three-dimensional quantitative optical microscopy imaging applied to large scale digital cell analysis system. University of Iowa. x, 121 leaves, bound.

Takahashi, M., F. Takahashi, K. Ui-Tei, T. Kojima, and K. Saigo. 2005. Requirements of genetic interactions between Src42A, armadillo and shotgun, a gene encoding E-cadherin, for normal development in Drosophila. *Development*. 132:2547-2559.

Takeichi, M. 2014. Dynamic contacts: rearranging adherens junctions to drive epithelial remodelling. *Nat Rev Mol Cell Biol*. 15:397-410.

Theveneau, E., and R. Mayor. 2012. Neural crest delamination and migration: from epithelium-to-mesenchyme transition to collective cell migration. *Developmental biology*. 366:34-54.

Thiery, J.P. 2003. Epithelial-mesenchymal transitions in development and pathologies. *Current opinion in cell biology*. 15:740-746.

Thiery, J.P., and J.P. Sleeman. 2006. Complex networks orchestrate epithelial-mesenchymal transitions. *Nat Rev Mol Cell Biol*. 7:131-142.

Trepat, X., L. Deng, S.S. An, D. Navajas, D.J. Tschumperlin, W.T. Gerthoffer, J.P. Butler, and J.J. Fredberg. 2007. Universal physical responses to stretch in the living cell. *Nature*. 447:592-595.

Troyanovsky, R.B., E.P. Sokolov, and S.M. Troyanovsky. 2006. Endocytosis of cadherin from intracellular junctions is the driving force for cadherin adhesive dimer disassembly. *Mol Biol Cell*. 17:3484-3493.

Twiss, F., Q. Le Duc, S. Van Der Horst, H. Tabdili, G. Van Der Krogt, N. Wang, H. Rehmann, S. Huveneers, D.E. Leckband, and J. De Rooij. 2012. Vinculin-dependent Cadherin mechanosensing regulates efficient epithelial barrier formation. *Biology open*. 1:1128-1140.

van Roy, F., and G. Berx. 2008. The cell-cell adhesion molecule E-cadherin. *Cellular and molecular life sciences : CMLS*. 65:3756-3788.

Vasioukhin, V., C. Bauer, M. Yin, and E. Fuchs. 2000. Directed actin polymerization is the driving force for epithelial cell-cell adhesion. *Cell*. 100:209-219.

Vestweber, D., and R. Kemler. 1985. Identification of a putative cell adhesion domain of uvomorulin. *The EMBO journal*. 4:3393-3398.

Volberg, T., B. Geiger, J. Kartenbeck, and W.W. Franke. 1986. Changes in membrane-microfilament interaction in intercellular adherens junctions upon removal of extracellular Ca2+ ions. *The Journal of cell biology*. 102:1832-1842.

Wang, W., R. Eddy, and J. Condeelis. 2007. The cofilin pathway in breast cancer invasion and metastasis. *Nature reviews. Cancer*. 7:429-440.

Wang, W., S. Goswami, K. Lapidus, A.L. Wells, J.B. Wyckoff, E. Sahai, R.H. Singer, J.E. Segall, and J.S. Condeelis. 2004. Identification and testing of a gene expression signature of invasive carcinoma cells within primary mammary tumors. *Cancer research*. 64:8585-8594.

Wang, W., J.B. Wyckoff, V.C. Frohlich, Y. Oleynikov, S. Huttelmaier, J. Zavadil, L. Cermak, E.P. Bottinger, R.H. Singer, J.G. White, J.E. Segall, and J.S. Condeelis. 2002. Single cell behavior in metastatic primary mammary tumors correlated with

gene expression patterns revealed by molecular profiling. *Cancer research*. 62:6278-6288.

Weber, G.F., M.A. Bjerke, and D.W. DeSimone. 2012. A mechanoresponsive cadherin-keratin complex directs polarized protrusive behavior and collective cell migration. *Developmental cell*. 22:104-115.

Welshhans, K., and G.J. Bassell. 2011. Netrin-1-induced local beta-actin synthesis and growth cone guidance requires zipcode binding protein 1. *The Journal of neuroscience : the official journal of the Society for Neuroscience*. 31:9800-9813.

Willett, M., M. Brocard, A. Davide, and S.J. Morley. 2011. Translation initiation factors and active sites of protein synthesis co-localize at the leading edge of migrating fibroblasts. *The Biochemical journal*. 438:217-227.

Wolpert, L. 2013. Cell polarity. *Philosophical transactions of the Royal Society of London. Series B, Biological sciences*. 368:20130419.

Wu, S.K., G.A. Gomez, M. Michael, S. Verma, H.L. Cox, J.G. Lefevre, R.G. Parton, N.A. Hamilton, Z. Neufeld, and A.S. Yap. 2014. Cortical F-actin stabilization generates apical-lateral patterns of junctional contractility that integrate cells into epithelia. *Nature cell biology*. 16:167-178.

Wu, Y., P. Kanchanawong, and R. Zaidel-Bar. 2015. Actin-delimited adhesion-independent clustering of E-cadherin forms the nanoscale building blocks of adherens junctions. *Developmental cell*. 32:139-154.

Yamada, S., and W.J. Nelson. 2007. Localized zones of Rho and Rac activities drive initiation and expansion of epithelial cell-cell adhesion. *The Journal of cell biology*. 178:517-527.

Yamada, S., S. Pokutta, F. Drees, W.I. Weis, and W.J. Nelson. 2005. Deconstructing the cadherin-catenin-actin complex. *Cell*. 123:889-901.

Yamaguchi, N., T. Mizutani, K. Kawabata, and H. Haga. 2015. Leader cells regulate collective cell migration via Rac activation in the downstream signaling of integrin beta1 and PI3K. *Scientific reports*. 5:7656.

Yap, A.S., M.S. Crampton, and J. Hardin. 2007. Making and breaking contacts: the cellular biology of cadherin regulation. *Current opinion in cell biology*. 19:508-514.

Yisraeli, J.K. 2005. VICKZ proteins: a multi-talented family of regulatory RNA-binding proteins. *Biology of the cell / under the auspices of the European Cell Biology Organization*. 97:87-96.

Yonemura, S., M. Itoh, A. Nagafuchi, and S. Tsukita. 1995. Cell-to-cell adherens junction formation and actin filament organization: similarities and differences between non-polarized fibroblasts and polarized epithelial cells. *Journal of cell science*. 108 (Pt 1):127-142.

Yonemura, S., Y. Wada, T. Watanabe, A. Nagafuchi, and M. Shibata. 2010. alpha-Catenin as a tension transducer that induces adherens junction development. *Nature cell biology*. 12:533-542.

Yu, F.X., and K.L. Guan. 2013. The Hippo pathway: regulators and regulations. *Genes & development*. 27:355-371.

Zegers, M.M., and P. Friedl. 2014. Rho GTPases in collective cell migration. *Small GTPases*. 5:e28997.

Zhang, F., S. Saha, S.A. Shabalina, and A. Kashina. 2010. Differential arginylation of actin isoforms is regulated by coding sequence-dependent degradation. *Science*. 329:1534-1537.

Zhang, H.H., F. Walker, S. Kiflemariam, R.H. Whitehead, D. Williams, W.A. Phillips, T. Mikeska, A. Dobrovic, and A.W. Burgess. 2009. Selective inhibition of proliferation in colorectal carcinoma cell lines expressing mutant APC or activated B-Raf. *International journal of cancer. Journal international du cancer*. 125:297-307.

Zhang, L., J. Luo, P. Wan, J. Wu, F. Laski, and J. Chen. 2011. Regulation of cofilin phosphorylation and asymmetry in collective cell migration during morphogenesis. *Development*. 138:455-464.

Zinchuk, V., Y. Wu, and O. Grossenbacher-Zinchuk. 2013. Bridging the gap between qualitative and quantitative colocalization results in fluorescence microscopy studies. *Scientific reports*. 3:1365.

Zinchuk, V., O. Zinchuk, and T. Okada. 2007. Quantitative colocalization analysis of multicolor confocal immunofluorescence microscopy images: pushing pixels to explore biological phenomena. *Acta histochemica et cytochemica*. 40:101-111.

Zirkel, A., M. Lederer, N. Stohr, N. Pazaitis, and S. Huttelmaier. 2013. IGF2BP1 promotes mesenchymal cell properties and migration of tumor-derived cells by enhancing the expression of LEF1 and SNAI2 (SLUG). *Nucleic acids research*. 41:6618-6636.